

TECHNISCHE UNIVERSITÄT MÜNCHEN

Lehrstuhl für Proteomik und Bioanalytik

Chemoproteomic characterization of covalent target engagement in cells

Lars Thorsten Dittus

Vollständiger Abdruck der von der Fakultät Wissenschaftszentrum Weihenstephan für Ernährung, Landnutzung und Umwelt der Technischen Universität München zur Erlangung des akademischen Grades eines

Doktors der Naturwissenschaften

genehmigten Dissertation.

Vorsitzender: Priv.-Doz. Dr. Karl Kramer

Prüfer der Dissertation: 1. Prof. Dr. Bernhard Küster
2. Prof. Dr. Andreas Pichlmair

Die Dissertation wurde am 28.05.2018 bei der Technischen Universität München eingereicht und durch die Fakultät Wissenschaftszentrum Weihenstephan für Ernährung, Landnutzung und Umwelt am 20.07.2018 angenommen.

Table of contents

Table of figures.....	V
List of tables.....	VII
Abbreviations.....	VIII
Abstract.....	XI
Zusammenfassung.....	XII
1. Introduction & objectives.....	1
1.1. Proteins as therapeutic targets in drug discovery.....	1
1.1.1. Covalent protein inhibitors.....	1
1.1.2. Protein kinases and (covalent) protein kinase inhibitors.....	2
1.2. A suitable assessment of small molecule target binding is required for reducing drug development costs.....	9
1.2.1. Chemoproteomic approaches for cellular target engagement measurements.....	10
1.2.2. Mass spectrometry-based proteomics.....	23
1.3. Objectives.....	28
2. Materials & methods.....	29
2.1. Lists of used chemicals, materials, instruments and software.....	29
2.2. Chemistry.....	34
2.3. Biochemistry and cell culture.....	66
3. Results.....	79
3.1. Chemoproteomic identification of cellular (off-)target engagement of covalent kinase inhibitors.....	79
3.1.1. BTK engagement measured in cells correlates with a functional effect but differs from lysate-based values.....	79
3.1.2. Differences in lysate- and cell based target engagement enable the identification of covalent and reversible kinase targets.....	80
3.1.3. Differential kinobeads selectivity profiling for the discrimination of covalent and reversible targets of covalent kinase inhibitors.....	83
3.1.4. Application of chemoproteomic strategies for off-target identification causing an unexpected phenotype in Ramos cells.....	93
3.2. Application of differential kinobeads selectivity profiling: characterization of covalent tool compounds enabling the analysis of intracellular target engagement of reversible inhibitors.....	110
3.2.1. Proof of concept of intracellular competition binding with reversible inhibitors.....	110
3.2.2. Evaluation of a generic strategy for synthesizing covalent probes from non-selective, reversible inhibitors.....	112
3.2.3. Application of probe 1A for measuring intracellular target engagement of the reversible MAPK9 inhibitor Tanzisertib with a kinobeads-based approach.....	125
4. Discussion.....	127
4.1. Formulated goal.....	127
4.2. Achievements.....	127

4.2.1.	Covalent binding in cells differs significantly from lysate-based measurements	127
4.2.2.	Differential kinobeads selectivity profiling enables the discrimination of covalent and reversible targets of covalent kinase inhibitors.....	129
4.2.3.	Expansion of cellular target engagement investigations with further chemoproteomic approaches: affinity enrichment using bioorthogonal probes, 2D-TPP and PROTAC-induced target degradation.....	132
4.2.4.	Assessment of a generic strategy for synthesizing covalent probes from non-selective, reversible inhibitors.....	137
4.2.5.	Evaluation of different reactive moieties for binding amino acids around the ATP-binding pocket of kinases irreversibly.....	139
4.2.6.	Proofing the concept of a intracellular competition binding assays for reversible inhibitors utilizing covalent tool compounds	140
4.3.	Outlook	142
5.	Conclusion	144
	Literature.....	147
	Acknowledgment	159
	Curriculum vitae.....	160
	Publications	161

Table of figures

Figure 1: The human kinome.....	2
Figure 2: Reaction scheme of protein inhibition by targeted covalent inhibitors.....	4
Figure 3: Reaction scheme of a Michael addition.....	4
Figure 4: B-cell receptor mediated signaling in B lymphocytes.....	5
Figure 5: Status of BTK targeting drugs in (pre-) clinical phases.....	5
Figure 6: BTK inhibitors.....	7
Figure 7: EGFR signaling pathway and EGFR inhibitors.....	7
Figure 8: Kinobeads as used in this work and mass spectrometry-based competition-binding analysis.	11
Figure 9: Mechanisms of bioorthogonal reactions used in this dissertation.....	15
Figure 10: Cellular thermal shift assay and thermal proteome profiling.....	18
Figure 11: Concept of proteasomal degradation using proteolysis-targeting chimeras.....	20
Figure 12: Workflows used for mass spectrometry-based proteomics.....	23
Figure 13: Basics of mass spectrometry as used in this dissertation.....	25
Figure 14: Relative quantification of proteome changes utilizing isobaric mass tags.....	27
Figure 15: BTK engagement of Ibrutinib, CC-292, and QL47 as determined in a lysate- and a cell- based kinobeads assay compared to a functional effect.....	80
Figure 16: Concept of differential kinobeads selectivity profiling using an optimized cellular kinobeads assay.....	81
Figure 17: Optimizing conditions of cell-based kinobeads assay utilizing saturated Ibrutinib.....	82
Figure 18: Differential kinobeads selectivity profiling for the identification of covalent and reversible kinase (off-) targets – proof-of-concept.....	84
Figure 19: Confirmation of ZAK as covalent target of Ibrutinib by two approaches.....	85
Figure 20: Differential kinobeads selectivity profiling of Ibrutinib in A549 cells and lysate.....	87
Figure 21: Differential kinobeads selectivity profiling of the BTK TCIs CC-292, CNX-774, and Acalabrutinib.....	89
Figure 22: Differential kinobeads selectivity profiling of the EGFR TCI Afatinib.....	90
Figure 23: Differential kinobeads selectivity profiling of the covalent kinase inhibitor of fungal origin 5Z- 7-Oxozeaenol.....	91
Figure 24: MS/MS spectra indicating a covalent reaction of 5Z-7-Oxozeaenol with two distinct cysteines in ZAK.....	92
Figure 25: Ramos cell viability after treatment with Ibrutinib and Afatinib.....	94
Figure 26: Intracellular competition binding using Ibrutinib and Afatinib competing for protein binding to azide analogues thereof.....	97
Figure 27: Comparison of targets of Ibrutinib and Afatinib identified with chemoproteomic affinity enrichment approaches.....	98
Figure 28: Multiplexed proteome dynamics profiling of Ramos cells upon PROTAC treatment.....	101
Figure 29: Protein abundancies in A549 cells upon treatment with different concentrations of Afatinib- lenalidomide.....	103

Figure 30: Target binding assessment of the Afatinib-lenalidomide conjugate in lysate and cells.	104
Figure 31: 2D-TPP analysis of Ibrutinib and Afatinib in Ramos cells.	106
Figure 32: Crude Ramos lysate-based 2D-TPP analysis upon incubation with Ibrutinib and Afatinib.	107
Figure 33: Comparison of targets identified for Ibrutinib and Afatinib with different chemoproteomic approaches.	108
Figure 34: Intracellular competition binding assay using TCO-Ibrutinib as enrichment probe compared to alternative cell-based assays reporting BTK engagement.	110
Figure 35: Intracellular competition binding using non-covalent BTK inhibitors CGI-1746 and saturated Ibrutinib competing the binding of TCO-Ibrutinib to BTK.	111
Figure 36: General approach to get covalent probes from promiscuous protein inhibitors.	112
Figure 37: Amine-incorporating promiscuous protein kinase inhibitor 1.	113
Figure 38: Reaction scheme for the synthesis of covalent probes from promiscuous protein inhibitors.	114
Figure 39: Covalent probes synthesized from linkable analogues of pan protein kinase inhibitor 1. .	114
Figure 40: Reduction in sample number for the assessment of covalent kinase probes by mass spectrometry.	115
Figure 41: Comparison of pIC ₅₀ values determined for probe 1A and probe 2A by estimating from 3 points dose-response approximation vs full 8 points dose-response curves.	116
Figure 42: Assessment of covalent probe set 1 using differential kinobeads selectivity profiling with estimated 3-points pIC ₅₀ values.	119
Figure 43: Assessment of covalent probe set 2 using differential kinobeads selectivity profiling with estimated 3-points pIC ₅₀ values.	120
Figure 44: Comparison of the reactive probes 1A and 2A to non-reactive analogues of both in a cell-based kinobeads assay.	121
Figure 45: MS/MS spectrum indicating a covalent reaction of probe 1A with Cys116 in MAPK9.	122
Figure 46: Direct comparison of selectivity and potency of the covalent probe 1A and its parent compound in a lysate-based kinobeads assay.	122
Figure 47: Covalent probes synthesized from amine-incorporating inhibitors of protein kinases, lipid kinases, and the non-selective HDAC inhibitor Vorinostat.	123
Figure 48: Differential kinobeads selectivity profiling of the covalent probe 3A.	124
Figure 49: Concept of intracellular competition binding of non-covalent inhibitors based on kinobeads affinity enrichment.	125
Figure 50: Kinobeads-based intracellular target engagement measurement of CC-930 / Tanzisertib using the covalent MAPK9 probe 1A established in this work.	126

List of tables

Table 1: Tabular listing of used chemicals and materials	29
Table 2: Tabular listing of used instruments.....	32
Table 3: Tabular listing of used analysis and visualization software	33
Table 4: Kinases robustly identified in differential kinobeads selectivity profiling of Ibrutinib and a saturated analogue	83
Table 5: Kinases for which a pIC ₅₀ value significantly above the used maximal compound concentration was determined only in lysate-based selectivity profiling of Ibrutinib and saturated Ibrutinib	86
Table 6: Kinases robustly identified as targets of Ibrutinib in A549 and Ramos cells.....	87
Table 7: Kinases identified as targets of Afatinib in comparison with Ibrutinib.	93
Table 8: Cell viability of different peripheral blood cell lines upon treatment with Afatinib and Ibrutinib	94

Abbreviations

Abbreviation	Name
ABPP	Activity-based protein profiling
ADP	Adenosine diphosphate
AGC	Kinase classification: protein kinase A, protein kinase G, protein kinase C related
ALL	Acute lymphoblastic leukemia
aPK	Kinase classification: atypical protein kinase
AspN	Asp-N Endopeptidase
ATP	Adenosine triphosphate
avg	Average
BCR	B-cell receptor
Boc group	tert-Butyloxycarbonyl protecting group
BRD	Bromodomain
BSA	Bovine serum albumin
C18/SCX	C18 bonded silica / strong cation exchange
Ca ²⁺	Calcium ion
CaCl ₂	Calcium chloride
CAMK	Kinase classification: Ca ²⁺ /calmodulin-dependent kinases
CETSA	Cellular thermal shift assay
CID	Collision induced dissociation
CK1	Kinase classification: casein kinase 1
CLL	Chronic lymphocytic leukemia
CMGC	Kinase classification: Cdk, MAPK, GSK, Cdk-like related
CuAAC	Copper(I)-catalyzed azide-alkyne cycloaddition
CuSO ₄	Copper(II) sulfate
Cys	Cysteine
Da	Dalton
DAG	Diacyl glycerol
DBCO	Dibenzocyclooctyne
DCM	Dichloromethane
DIPEA	N,N-Diisopropylethylamine
DMF	Dimethylformamide
DMSO	Dimethyl sulfoxide
DNA	Deoxyribonucleic acid
DP buffer	Drug pulldown buffer
DTT	Dithiothreitol
EC50	Half maximal effective concentration
EDTA	Ethylenediaminetetraacetic acid
ePK	Kinase classification: eukaryotic protein kinase
ESI	Electrospray ionization
FBS	Fetal bovine serum
Fmoc group	Fluorenylmethyloxycarbonyl protecting group
g	G-force
GluC	Endoproteinase GluC
GTP	Guanosine triphosphate
HATU	1-[Bis(dimethylamino)methylene]-1H-1,2,3-triazolo[4,5-b]pyridinium 3-oxid hexafluorophosphate
HCD	Higher-energy collisional dissociation
HCl	Hydrogen chloride
HDAC	Histone deacetylases
HEPES	4-(2-hydroxyethyl)-1-piperazineethanesulfonic acid

HPLC	High performance liquid chromatography
IC ₅₀ / pIC ₅₀	Half maximal inhibitory concentration / $-\log_{10}(\text{IC}_{50})$
ICAT	Isotope-coded affinity tag
IEDDA	Inverse electron demand Diels–Alder reaction
IP ₃	Inositol 1,4,5-trisphosphate
ITDR	Isothermal dose-response
iTRAQ	Isobaric tags for relative and absolute quantification
K _i	Dissociation constant
k _{inact}	Inactivation rate
LC-MS	Liquid chromatography–mass spectrometry
LDS	Lithium dodecyl sulfate
LysC	Endoproteinase LysC
m/z	Mass-to-charge ratio
MCL	Mantle cell lymphoma
MgCl ₂	Magnesium chloride
MM	Multiple myeloma
MOPS	3-(N-morpholino)propanesulfonic acid
MS/MS or MS ²	Tandem mass spectrometry
Na ₃ VO ₄	Sodium orthovanadate
NaCl	Sodium chloride
NaF	Sodium fluoride
NCE	New chemical entity
NH ₂ OH	Hydroxylamine
NH ₃	Ammonia
NHL	Non-Hodgkin's lymphoma
NHS	N-Hydroxysuccinimide
NMR	Nuclear magnetic resonance
IGEPAL CA 630	Nonyl phenoxypolyethoxyethanol
NSCLC	Non-small cell lung carcinoma
PBMC	Peripheral blood mononuclear cell
PBS	Phosphate-buffered saline
PCR	Polymerase chain reaction
PEG _n	n-times separated by polyethylen glycol
PIP ₂	Phospholipid phosphatidylinositol 4,5-bisphosphate
PLC γ	Phosphoinositide phospholipase C, isozyme gamma
ppm	Parts per million
PROTAC	Proteolysis-targeting chimera
PTM	Post-translational modification
PVDF	Polyvinylidene fluoride
PyBrOP	Bromotripyrrolidinophosphonium hexafluorophosphate
qupm	Quantified unique peptide matches
RGC	Receptor guanylyl cyclase
rpm	Rounds per minute
RT	Room temperature
s.e.m.	Standard error of the mean
SAHA	Suberoylanilide Hydroxamic Acid
SDS	Sodium dodecyl sulfate
SDS-PAGE	Sodium dodecyl sulfate polyacrylamide gel electrophoresis
Ser	Serine
SILAC	Stable isotope labeling by/with amino acids in cell culture
SPAAC	Strain-promoted azide-alkyne cycloaddition
STE	Kinase classification: STE20, STE11 and STE7 related

TBTA	Tris[(1-benzyl-1H-1,2,3-triazol-4-yl)methyl]amine
TCEP	Tris(2-carboxyethyl)phosphine
TCI	Targeted covalent inhibitor
TCO	Trans-cyclooctene
TEAB	Triethylammonium bicarbonate
TFA	Trifluoroacetic acid
THPTA	Tris(3-hydroxypropyltriazolylmethyl)amine
TK	Kinase classification: Tyrosine kinase
TKL	Kinase classification: Tyrosine-kinase like
T _m	Melting temperature
TMT	Tandem mass tag
TPP	Thermal proteome profiling
t _R	Retention time
Tris	Tris(hydroxymethyl)aminomethane
TSA	Thermal shift assay
Tz	Tetrazine
u	Unified atomic mass unit
U	Units of an enzyme
US FDA	United States Food and Drug Administration
VHL	Von Hippel Lindau
WM	Waldenströms macroglobulinemia

Abstract

Compound attrition is one of the main reasons for the increasing costs of drug discovery projects. Many candidate drug molecules fail because they do not reach the site of action or the target is not engaged by the compound so that binding does not result in a pharmacologically relevant phenotype. Further, adverse events are often caused by off-target activities not discovered with standard assay panels. For small molecules acting on protein targets, chemoproteomic assays combined with mass spectrometry enable the proteome-wide identification of drug targets including undesired binders. In contrast to lysate- and recombinant protein-based assays, cellular assays also interrogate if the cell membrane is crossed and the relevant compartment is accessed. Cell-based chemoproteomics assays can assess dose-dependent engagement of endogenously expressed targets under physiologically relevant conditions.

The recent clinical success of targeted covalent kinase inhibitors has led to increased interest in irreversible binding mechanisms across the pharmaceutical industry and academic research. A covalent mode of action can increase target selectivity and provide good potency at low dosing as well as reduce the risk of drug resistance development. Targeted covalent inhibitors are characterized by moderate target affinity paired with low reactivity towards very conserved nucleophilic amino acid side-chains. Concerns about off-target mediated idiosyncratic toxicity are limited since the compound should only react if precisely positioned towards a suitable amino acid present in only a small subset of the proteome. How well commonly applied lysate-based target engagement and selectivity assays reflect the intracellular compound/target binding and reactivity is less clear.

This thesis focusses on the characterization of targets and off-targets of covalent inhibitors using chemoproteomic techniques in cell extracts and in living cells.

It is demonstrated that for covalent inhibitors cell-based experiments reflect target potency and selectivity much better than lysate based experiments. Using a cell-based kinobeads assay and comparing it to a lysate-based variant displayed distinct differences in potency for covalent targets determined with both settings. This allowed establishing a differential kinobeads selectivity profiling strategy that discriminates covalent and reversible kinase targets. This approach was then applied to assess the selectivity of clinically relevant targeted covalent kinase inhibitors such as Ibrutinib and Afatinib. The outcomes were compared to alternative approaches for measuring target engagement including an intracellular competition binding strategy using bioorthogonal chemistry as well as the recently established cell-based thermal proteome profiling and multiplexed proteome dynamics profiling.

Due to non-equilibrium binding covalent probes might also represent valuable tool compounds for measuring target engagement of reversible inhibitors by competition binding experiments in live cells. In the second part of this thesis, differential kinobeads selectivity profiling was used to assess a generic strategy for the synthesis of covalent probes from promiscuous protein inhibitors. Different reactive moieties were coupled to non-selective inhibitors to bind an amino acid positioned close to the inhibitor binding site. It was evaluated if such an approach might aid the future design of targeted covalent inhibitors and if the generated probes enable intracellular competition binding assays for target engagement measurements of reversible protein inhibitors. With this strategy, a covalent MAPK9 probe was synthesized and used for demonstrating the concept of measuring intracellular target engagement of the reversible inhibitor Tanzisertib.

Zusammenfassung

Das erst späte Ausscheiden neuer Wirkstoffe während deren Erforschung ist einer der Hauptgründe steigender Medikamentenkosten. Sie scheitern, da viele Wirkstoffkandidaten ihr biologisches Zielmolekül nicht erreichen oder binden und somit keinen pharmakologisch relevanten Effekt induzieren. Zudem führen unerwartete Interaktionen des Wirkstoffes mit Biomolekülen, welche mit gängigen Testverfahren nicht entdeckt werden, oftmals zu unerwünschten Nebenwirkungen. Chemoproteomische Analysestrategien in Kombination mit massenspektrometrischen Messverfahren ermöglichen die proteomweite Identifizierung erwünschter und ungewollter Protein-Wirkstoff-Interaktionen. Im Gegensatz zu Methoden, die auf Zellysate oder rekombinanten Proteinen basieren, geben zelluläre Tests auch Auskunft darüber, ob ein Wirkstoff die Zellmembran durchdringt und seinen Wirkort erreicht. Außerdem ermöglichen sie die Analyse, welche endogen exprimierten Proteine gebunden werden.

Durch den aktuellen klinischen Erfolg kovalenter Kinaseinhibitoren hat das Interesse an irreversiblen Bindungsmechanismen in der pharmazeutischen Industrie und der akademischen Forschung zugenommen. Das kovalente Binden an ein Protein kann in gesteigerter Selektivität und hoher Bindungsstärke bei geringer Wirkstoffgabe resultieren und das Risiko für Resistenzentwicklungen verringern. Bedenken bezüglich unerwünschter Nebenwirkungen aufgrund unspezifischer Reaktivität werden durch das Konzept sogenannter „targeted covalent inhibitors“ reduziert. Diese Inhibitoren vereinen moderate Bindungsaffinität für ein Protein mit einer schwach reaktiven Gruppe, welche nach präziser Positionierung mit stark konservierten, nukleophilen Aminosäuren reagieren kann. Inwiefern die mit lysatbasierten Assays ermittelte Selektivität und Reaktivität solcher Inhibitoren mit der tatsächlichen zellulären Situation korrelieren ist unklar.

Diese Doktorarbeit widmet sich der Charakterisierung kovalenter Proteinbindungen mittels chemoproteomischer Verfahren in Zellysaten und lebenden Zellen.

Es wird gezeigt, dass zellbasierte Testverfahren die Bindungsstärke und -selektivität kovalenter Proteininhibitoren besser widerspiegeln als lysatbasierte Experimente. Unterschiede in der Stärke kovalenter Proteinbindungen, gemessen mit einem zellbasierten Kinobeads Assay und einer lysatbasierten Variante, wurden ausgenutzt, um ein Verfahren zur differentiellen Analyse kovalenter und reversibler Proteinbindungen aufzusetzen. Mit diesem Ansatz wurde die Selektivität klinisch relevanter kovalenter Kinaseinhibitoren, einschließlich Ibrutinib und Afatinib, untersucht. Die Ergebnisse werden mit alternativen Methoden zur Charakterisierung von Wirkstoff-Protein-Interaktionen basierend auf bioorthogonaler Chemie, thermischer Proteininstabilität und proteasomaler Degradierung verglichen.

Aufgrund der irreversiblen Bindung können reaktive Moleküle auch genutzt werden, um intrazelluläre Proteininteraktionen nicht-kovalenter Wirkstoffe in Competitionsexperimenten zu untersuchen. Das reversible Bindungsgleichgewicht kann dabei mit Hilfe des kovalenten Mechanismus während der Probenaufbereitung stabilisiert werden.

Im zweiten Teil dieser Dissertation wurde die Kinobeads-basierte differentielle Analyse kovalenter und reversibler Proteinbindungen angewandt, um eine Strategie für die Synthese kovalenter Moleküle auf Basis unselektiver Proteininhibitoren zu bewerten. Dazu wurden verschiedene reaktive Inhibitoranaloga synthetisiert, um mit Aminosäuren nahe der Inhibitorbindungsstelle zu reagieren. Es wurde untersucht, ob dieser Ansatz die Synthese neuer kovalenter Proteininhibitoren unterstützen kann oder ob sich die generierten Moleküle zur intrazellulären Analyse reversibler Proteinbindungen eignen. Auf Basis eines so synthetisierten kovalenten Moleküls und des MAPK9 Inhibitors Tanzisertib wird ein Konzept zur Bestimmung reversibler Proteininteraktionen in lebenden Zellen demonstriert.

1. Introduction & objectives

1.1. Proteins as therapeutic targets in drug discovery

Across different studies estimating how many potential drug targets might exist, there is no disagreement on proteins being the major class of biomolecules modulated by medicines.¹⁻⁴ Throughout all domains of life proteins are involved in essential processes including signaling and sensing, metabolism, replication, as well as growth and motility.⁵⁻⁷ Due to the importance of proteins in all these basic processes the modulation of a protein's function by drugs is a key aspect in drug discovery of the pharmaceutical industry. One approach for influencing the function of a protein, mostly inhibiting its activity, is to use small molecules binding to it. Most protein inhibitors act via a reversible mechanism but there is also an emerging class of protein inhibitors acting in an irreversible way.

1.1.1. Covalent protein inhibitors

In contrast to protein inhibitors which reversibly bind their targets via multiple non-covalent interactions, irreversible protein inhibitors form covalent bonds with their targets resulting in an inseparable complex. This covalent bond is usually formed between electrophiles incorporated in the small molecule and nucleophilic amino acid residues.⁸⁻¹¹ Depending on the protein microenvironment, cysteine, serine, tyrosine, lysine, threonine, aspartate, and glutamate can provide nucleophilic amino acid side chains.¹¹ Proteins or protein classes which are approached by covalent mechanisms include phosphoinositide-3-kinases,¹² bromodomain proteins,¹³ cysteine proteases,¹⁴ kinases,¹⁵⁻¹⁷ ATPases,¹⁸⁻¹⁹ GTPases,²⁰⁻²¹ and protein tyrosine phosphatases.²² Moreover, attempts to target protein-protein interactions are also pursued by covalent strategies.²³ Regarding their binding modality, covalent binders have to be clearly distinguished from reversible binders. Due to the reactive mechanism, binding is a time-dependent process and removal of the unbound compound from the system (e.g. by compound dilution) or alterations in the protein environment will not result in a re-equilibration of protein/compound binding. This non-equilibrium protein binding of covalently acting molecules can result in valuable properties of the drug candidate:^{9, 24-27}

1. Once covalent binding is established it cannot be competed by endogenous substrates resulting in excellent biochemical efficiency.
2. The dependency of the pharmacological effect on re-synthesis of the target protein allows for a lower and less frequent drug dosing. Consequently, systemic drug exposure is reduced.
3. Emergence of drug resistance might be reduced by continuous target suppression.
4. Shallow binding sites could be made 'druggable', i.e. capable of binding to a small molecule, by covalently binding inhibitors.

However, covalent drugs also raise concerns about polypharmacology, non-specific, irreversible protein modification and idiosyncratic toxicity.^{9, 24-26} Contrary to these legitimate concerns it might be surprising that about 30 % of the approved drugs act on their target by binding it covalently.^{25, 28}

Among others, some important approved drugs are aspirin (an irreversible COX1 and COX2 inhibitor), penicillin (the probably most famous beta-lactam antibiotic), clopidogrel (irreversible binding of ADP receptor, subtype P2Y12), and omeprazole (forms covalent adducts with gastric H⁺/K⁺-ATPase).^{11, 24-26, 29} Further, covalent inhibitors show promising results in the covalent inhibition of protein kinases malfunctioning in different types of cancer.³⁰⁻³³

1.1.2. Protein kinases and (covalent) protein kinase inhibitors

Kinases are a class of enzymes which catalyze the transfer of a phosphate group from a donor molecule to a substrate. This phosphorylation event alters the activity and/or structure of the substrate which can be sugars, lipids, nucleotides, and proteins. Thus, kinases are strongly involved in signaling pathways and regulation of physiological processes and represent promising targets for therapeutic approaches.³⁴ An important subclass of kinases is represented by 518 protein kinases encoded by the human genome (Figure 1).³⁵⁻³⁶ In this PhD work, which focuses on the research field of proteomics, in the following, the term "kinases" will in general stand for protein kinases if not specifically stated otherwise.

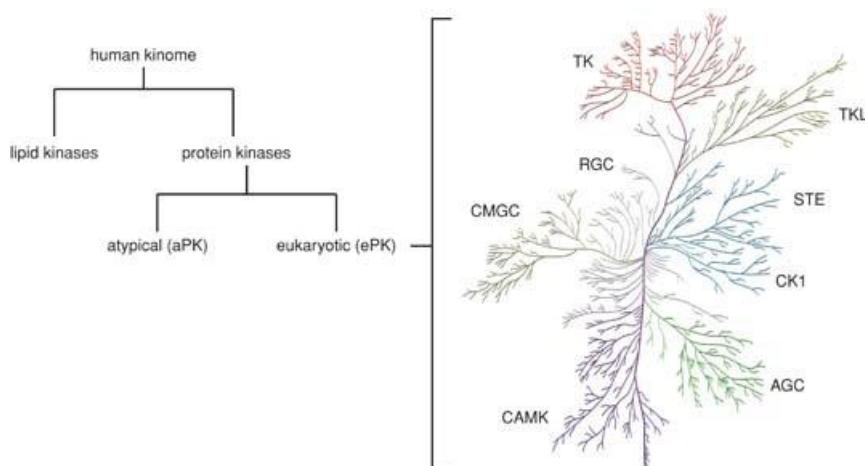


Figure 1: The human kinome. The human kinome comprises 518 protein kinases and about 20 lipid kinases. The protein kinases can be separated into 40 atypical protein kinases (aPK) and 478 enzymes with an eukaryotic protein kinase domain (ePK).³⁵ While the latter show sequence similarity for the kinase domain, the atypical protein kinases show kinase activity but lack sequence similarity. The 478 ePKs are classified into eight groups based on their similarity within the kinase domain: tyrosine kinase (TK); tyrosine-kinase like (TKL); STE20, STE11 and STE7 related (STE); casein kinase 1 (CK1); protein kinase A, protein kinase G, protein kinase C related (AGC); Ca²⁺/calmodulin-dependent kinases (CAMK); Cdk, MAPK, GSK, Cdk-like related (CMGC); and receptor guanylyl cyclase (RGC). Figure adopted from Duong-Ly, K. C. *et al.*³⁶

Protein kinases mainly phosphorylate serine, threonine, or tyrosine side chains of other proteins or of their own ('autophosphorylation') by catalyzing the transfer of a phosphate group from ATP (to a lower extent also GTP) to the hydroxyl group of these amino acid. Beyond that, also phosphorylation of other amino acids was described.³⁷⁻³⁸ The phosphorylation alters the activity of proteins in many cellular processes including proliferation, differentiation, and metabolism.³⁹ Deregulation of kinase function, either loss of function or hyperactivation, has been linked to about 400 disease indications today.⁴⁰ One strategy to target kinase dysfunction is the application of antibodies which is mainly possible for kinases with an extracellular domain. Alternatively, kinase function can be modulated by small

molecules. Small molecule kinase inhibitors are designed such to either bind to an allosteric site of the kinase (\rightarrow type III and type IV inhibitors) or to compete with ATP binding to either a catalytically active / DFG-in (\rightarrow type I inhibitors) or inactive / DFG-out (\rightarrow type II inhibitors) conformation of the enzyme.⁴¹ The strong conservation of the ATP binding site across the kinome, however, results in a hardly achievable selectivity of small molecule inhibitors. Severe side effects due to off-target binding are a common reason for drawbacks in kinase inhibition resulting in a lack of inhibitors for many clinically relevant kinases.⁴² One approach to achieve improved selectivity with retaining reasonable pharmacokinetic characteristics is, for example, to design inhibitors in such a way that binding to a target is only enabled when their three-dimensional structure appropriately accesses more kinase structures than only the ATP binding site.⁴³⁻⁴⁴ Another strategy to get more selective inhibitors is to apply covalent strategies for binding poorly conserved amino acids in the hardly divergent ATP binding sites. This rationale is realized by the concept of 'targeted covalent kinase inhibitors'.

1.1.2.1. Targeted covalent kinase inhibitors

As discussed above, irreversible inhibition is accompanied by several advantages. The fact that a reactive compound circulates through the body, though, also raises concerns about non-specific off-target reactivity and idiosyncratic toxicity.^{9, 24-26} Especially, in the case of targeting highly conserved structures by small molecule inhibitors as in kinases, worries about irreversible off-target binding are reasonable. To reduce the risk of unwanted reactions, the concept of 'targeted' covalent inhibition (TCI) was successfully applied.^{26, 31, 45-46} Inhibitors designed with this rationale combine a low-reactive electrophile with a rationally designed recognition motif for a target protein. Targeted covalent inhibition is a two-step process. In a first step, a non-covalent complex P-I is formed driven by affinity (K_i). Non-covalent binding needs to assure that a sufficient degree of selectivity is achieved and that the residence time of the molecule at the target allows for the covalent bond formation.²⁶ In a second step, the nucleophilic amino acid residue reacts with the electrophile incorporated in the inhibitor to form the irreversible complex P-I (Figure 2). The formation of this complex is defined by the rate constant k_{inact} which describes the maximal rate of covalent bond formation.²⁷ The two-step process of irreversible inactivation is influenced by diverse parameters which can significantly differ between living cells and test systems based on cell extracts or recombinant proteins: the formation of the non-covalent complex P-I is influenced by the local concentration of compound and endogenous substrates, or structural integrity of the protein including PTM patterns. As the concentration of P-I is influenced also the formation of the final covalent complex will depend on these factors. In addition, the microenvironment surrounding the amino acid⁴⁷⁻⁴⁸ including local pH,⁴⁹ and the redox environment,⁵⁰⁻⁵¹ will change the nucleophilic system and in consequence also k_{inact} . Finally, also the temperature as described by the Arrhenius equation⁵² will influence the reaction rate, and thus, the formation of the covalent complex P-I. The overall process of covalent protein inhibition by targeted covalent inhibitors can be described by a second-order rate constant defined by the ratio k_{inact}/K_i .



Figure 2: Reaction scheme of protein inhibition by targeted covalent inhibitors. The formation of a non-covalent complex P·I consisting of a protein P and an inhibitor I driven by binding affinity K_i is followed by a subsequent reaction described by the reaction rate k_{inact} to form the irreversible complex P–I. Scheme adopted from *Strelow, J. M.*²⁷

Several reactive moieties including sulfonyl fluorides,⁵³ maleimides,⁵⁴ vinyl sulfones,⁵⁵ and alkynes⁵⁶ are capable of fulfilling the task to establish covalent binding between inhibitors and proteins. To bind a target irreversibly the mechanism most commonly used by medicinal chemists is the Michael addition. For enabling this reaction an α,β -unsaturated carbonyl, such as an acrylamide, is incorporated into the small molecule inhibitor (Michael acceptor) to react with a nucleophilic amino acid residue like the sulfhydryl group of cysteine (Michael donor) (Figure 3).^{9, 30-31, 45-46, 56}

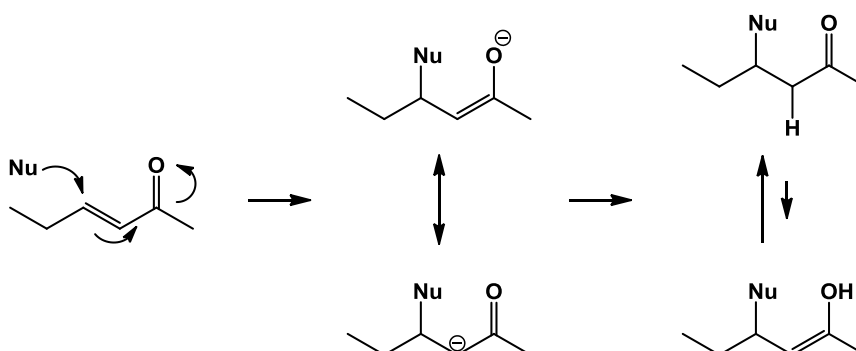


Figure 3: Reaction scheme of a Michael addition. The nucleophile attacks at the unsaturated carbonyl at the β position. The resonance stabilized structure is protonated to form the saturated nucleophile product as a keto-enol tautomer preferring the keto-form. The reactivity of intracellular nucleophiles like cysteine is influenced by the microenvironment surrounding the amino acid⁴⁷⁻⁴⁸ including local pH⁴⁹, cysteine PTMs, chemical lability and redox environment⁵⁰⁻⁵¹ and subcellular localization.⁵⁷

Due to the relatively low intrinsic reactivity of α,β -unsaturated carbonyls a covalent bond is only formed upon adequate positioning of the inhibitor with high accuracy for its target protein. This reduces non-specific cross reactivity.⁹⁻¹¹ Combining rationally designed ATP-competitive binding structures with acrylamides has yielded remarkably selective targeted covalent kinase inhibitors for the treatment of cancer.³⁰⁻³³ For example, the selective reaction with a cysteine at hinge 6 position, poorly conserved among the kinome, is realized in TCIs of Bruton's tyrosine kinase (BTK) and epidermal growth factor receptor (EGFR).

1.1.2.1.1. Targeted covalent inhibitors of Bruton's Tyrosine Kinase (BTK)

BTK is a non-receptor tyrosine kinase consisting of 659 amino acids, with a molecular weight of ~ 76 kDa. Besides BMX, ITK, TEC, and TXK/RLK, BTK is a member of the TEC kinase subfamily and is expressed predominately in hematopoietic lineage cells except for T, NK, and plasma cells.⁴⁶ BTK plays an important role in B-cell receptor (BCR) signaling. The binding of an antigen to the BCR results in a cascade of tyrosine phosphorylation events. One step in this cascade is the phosphorylation of phospholipase C (PLC γ) by BTK. After activation, PLC γ cleaves phospholipid

phosphatidylinositol 4,5-bisphosphate (PIP₂) into diacyl glycerol (DAG) and inositol 1,4,5-trisphosphate (IP₃). The latter controls the opening of Ca²⁺ channels in the smooth endoplasmic reticulum, and thus, Ca²⁺ mediated responses like survival, activation, proliferation, and differentiation of B lymphocytes (Figure 4) but also cytokine production in macrophages.⁵⁸

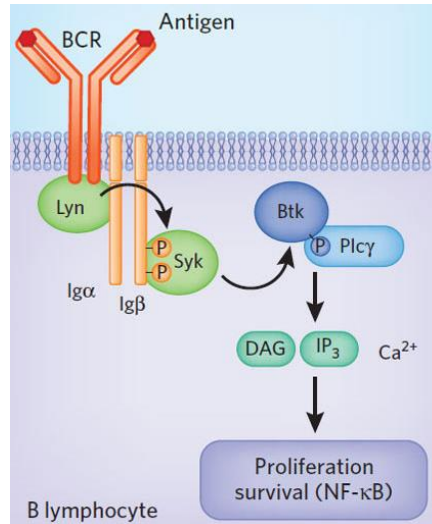


Figure 4: B-cell receptor mediated signaling in B lymphocytes. Antigen binding to the B cell receptor (BCR) leads to the activation of BTK. Further downstream signaling results in the activation of different responses like NF-κB-mediated proliferation. Figure adopted from *Hendriks, R. W.*⁵⁸

Deregulation of BTK is observed in B-cell-derived malignancies including acute lymphoblastic leukemia (ALL), chronic lymphocytic leukemia (CLL), non-Hodgkin's lymphoma (NHL), mantle cell lymphoma (MCL), Waldenstrom's macroglobunemia (WM), and multiple myeloma (MM).⁴⁶ The current knowledge about its function suggests BTK as being an interesting target for the pharmaceutical industry resulting in a continuous increase in (pre-) clinical trials over the past twelve years (Figure 5). One therapeutic approach for the treatment of B-cell derived malignancies is the inhibition of BTK using small molecule inhibitors.

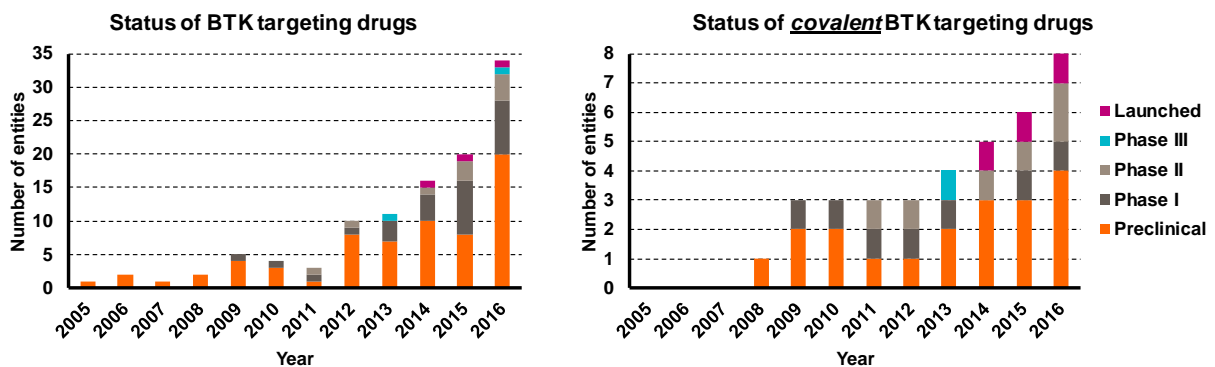


Figure 5: Status of BTK targeting drugs in (pre-) clinical phases. Data extracted from Citeline by 20th of July, 2017, 11:16 AM CET.

Up to date (April 29th, 2018), one of only two approved drugs targeting BTK is 1-[(3R)-3-[4-Amino-3-(4-phenoxyphenyl)-1H-pyrazolo[3,4-d]pyrimidin-1-yl]piperidin-1-yl]prop-2-en-1-one better known as

Ibrutinib (formerly PCI-32765) (Figure 6).³⁰ Ibrutinib is a targeted covalent inhibitor forming a covalent bond in a Michael reaction between the small molecule (Michael acceptor) and a cysteine (Cys481, Michael donor) located in the ATP binding pocket. Cys481 is poorly conserved among the kinome and can be found in only eleven kinases comprising the TEC-kinase family members BMX, BTK, ITK, TEC, and TXK/RLK as well as the kinases BLK, EGFR, ErbB2, ErbB4, JAK3, and MAP2K7.^{10, 30, 45, 59-60} Ibrutinib has been shown to inhibit autophosphorylation of BTK, and thus, modulating BTK-mediated downstream processes. In cells, Ibrutinib promotes apoptosis, inhibits proliferation, and blocks the response to survival stimuli from their environment.³⁰ Ibrutinib was approved by the US FDA for the treatment of mantle cell lymphoma in 2013 and for the treatment of chronic lymphocytic leukemia in 2014.⁶¹ The clinical success of Ibrutinib triggered renewed interest in irreversible kinase inhibitors throughout academic and industrial research.²⁶

The second just recently approved BTK TCI is (S)-4-(8-amino-3-(1-(but-2-ynoyl)pyrrolidin-2-yl)imidazo[1,5-a]pyrazin-1-yl)-N-(pyridin-2-yl)benzamide (Acalabrutinib; ACP-196) (Figure 6). It is described to be more selective than Ibrutinib^{56, 62-63} resulting in less adverse effects like diarrhea and rash potentially caused by Ibrutinib's binding to EGFR.⁶⁴ Acalabrutinib was approved for the treatment of mantle cell lymphoma and is currently undergoing promising phase III clinical trials for chronic lymphocytic leukemia (NCT02970318, NCT02477696, NCT02475681) and phase II clinical trials for several types of cancer (source: clinicaltrials.gov; accessed: 22nd of December 2017, 9.28 AM CET).

Another TCI of BTK is N-(3-(5-fluoro-2-(4-(2-methoxyethoxy)phenylamino)pyrimidin-4-ylamino)phenyl)acrylamide also known as CC-292 or AVL-292 (Figure 6).⁴⁵ This compound follows the same mechanism as Ibrutinib and is currently undergoing phase I clinical trial for the treatment of several lymphoma types (ClinicalTrials.gov Identifiers: NCT01766583, NCT01732861, NCT02031419) and completed phase II clinical trial for the treatment of rheumatoid arthritis (ClinicalTrials.gov Identifier: NCT01975610).

Another molecule published by *Wu et al*⁴⁶ is 1-(1-acryloylindolin-6-yl)-9-(1-methyl-1H-pyrazol-4-yl)benzo[h][1,6]naphthyridin-2(1H)-one (Figure 6). This compound is abbreviated as QL47 and is also described to bind its targets irreversibly by forming a covalent bond to cysteine Cys481.

4-(4-((4-((3-acrylamidophenyl)amino)-5-fluoropyrimidin-2-yl)amino)phenoxy)-N-methylpicolinamide (CNX-774) is another covalent BTK inhibitor presented by Avila Therapeutics in 2011.⁶⁵ It is described to inhibit BTK with $IC_{50} < 1$ nM in biochemical assays without any mentioned side-reactivity. CNX-774 differs from CC-292, which is described to also inhibit BLK, TEC, JAK3, and TXK, only by incorporating a methylpicolinamide instead of a methoxyethane group. CNX-774 is currently in no clinical trials (source: clinicaltrials.gov; accessed: 20th of July 2017, 10.36 AM CET).

Due to the poorly conserved cysteine Cys481 in BTK covalent inhibition of this kinase is a promising approach. However, many BTK inhibitors are also following a reversible mode-of-action. One example for such a reversible BTK inhibitor is 4-(tert-butyl)-N-(2-methyl-3-(4-methyl-6-((4-(morpholine-4-carbonyl)phenyl)amino)-5-oxo-4,5-dihydropyrazin-2-yl)phenyl)benzamide (CGI-1746) (Figure 6, blue) which was reported to be a very selective BTK inhibitor reversibly stabilizing an inactive conformation of the kinase.⁶⁶ CGI-1746 served as valuable tool to elucidate the function of BTK in rheumatoid arthritis but did not enter clinical trials.

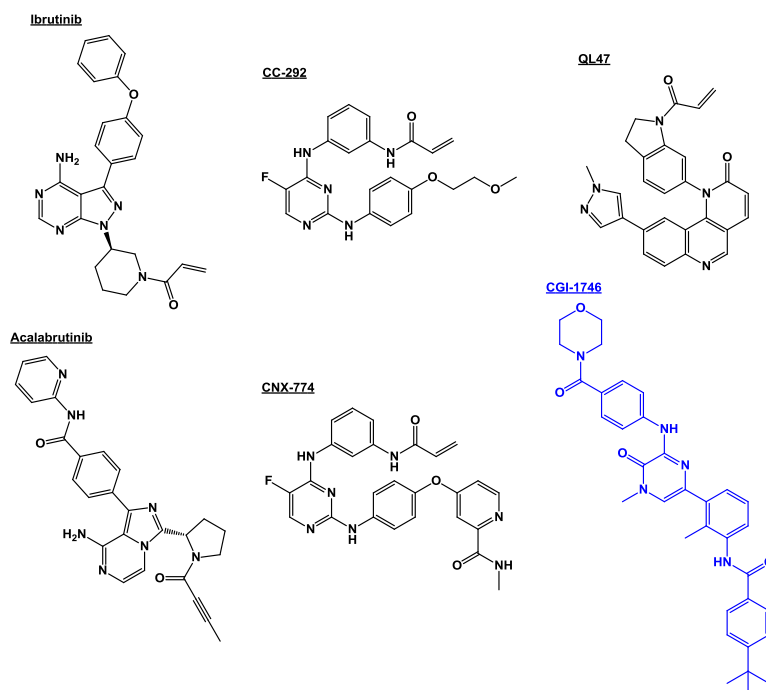


Figure 6: BTK inhibitors. Targeted covalent BTK inhibitors Ibrutinib, CC-292, QL47, Acalabrutinib, and CNX-774 (black), as well as the non-covalent BTK inhibitor CGI-1746 (blue).

1.1.2.1.2. Targeted covalent Epidermal Growth Factor Receptor (EGFR) inhibitor Afatinib

Another kinase for which the strategy of targeted covalent inhibition was successfully applied is Epidermal Growth Factor Receptor (EGFR). EGFR is a member of the ErbB receptor tyrosine kinase family with a molecular weight of ~ 134 kDa consisting of 1210 amino acids. Its activation is promoted by binding of ligands including epidermal growth factor (EGF) and transforming growth factor α (TGF α)⁶⁷ triggering the formation of homo- or heterodimers. The induced signaling cascades ultimately affect cell proliferation and other molecular effects (Figure 7).⁶⁸⁻⁷⁰ Hyperactivation can result in abnormal cell survival which is related to carcinoma formation.

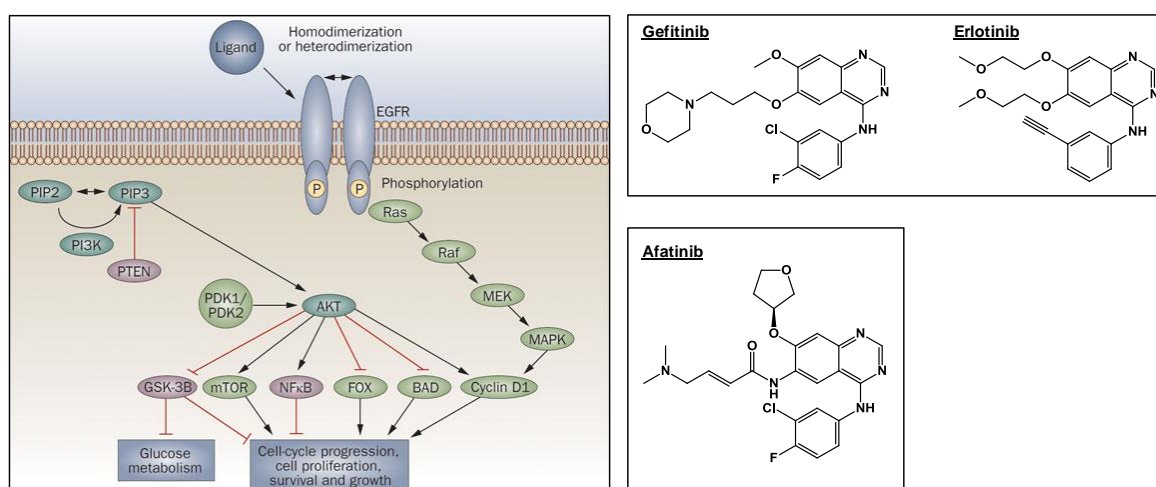


Figure 7: EGFR signaling pathway and EGFR inhibitors. The reversible inhibitors of EGFR Gefitinib and Erlotinib are shown in the upper box and the FDA-approved targeted covalent EGFR inhibitor Afatinib is shown below. Signaling pathway adopted from Okines, A. et al.⁶⁹

Inhibition of upregulated EGFR signaling represents an effective therapeutic strategy.⁷¹ One type of cancer for which EGFR inhibition using tyrosine kinase inhibitors like Gefitinib (Iressa) and Erlotinib (Tarceva) represents the therapy of choice is the non-small cell lung carcinoma (NSCLC), comprising 85 % of all lung cancers.⁷² By binding competitively to the ATP-binding site, these inhibitors downregulate EGFR's catalytic activity. However, a major resistance mechanism against these drugs developing within several months of therapy is related to a substitution of threonine by methionine at position 790 (T790M) caused by point mutations in the EGFR gene. Sterical hindrance by the bulky methionine side-chain results in decreased target affinity of the inhibitors.⁷³⁻⁷⁴ With Afatinib an irreversibly binding second-generation EGFR inhibitor was developed.³¹ Upon proper positioning, Afatinib covalently reacts with cysteine 797 at hinge 6 position of EGFR, thus, a cysteine at a homologous position to Cys481 in BTK reacting with Ibrutinib and other BTK TCIs. Compared with the first-generation EGFR inhibitors Gefitinib and Erlotinib, Afatinib has several advantages: (i) higher affinity and higher potency for the L858R and T790M mutant of EGFR, respectively, (ii) the binding to Her2 avoids dimerization of EGFR and Her2 mediating most potent signaling, and (iii) resistance develops at slower rates if used as first-line treatment agent.^{68, 72}

As every potential small molecule drug – reversibly or covalently acting – reactive compounds like the introduced targeted covalent kinase inhibitors have to be carefully analyzed for (off-)target engagement. Due to their reactive nature, which depends on the environment at the location of action, covalent compounds have to be investigated with particular suitable tools in disease relevant systems for reducing the risk of attrition at an early stage of drug development due to off-target binding mediated adverse events.

1.2.A suitable assessment of small molecule target binding is required for reducing drug development costs

The development of a new drug is a very time consuming and cost-intensive process with a high risk for failure.⁷⁵ In the year 2010, it was estimated that roughly \$ 1 billion had to be spent for getting one new drug to the market⁷⁶ and a more recent report exceeded this estimate by more than 2.5-fold.⁷⁷ It is obvious that reducing attrition and enhancing the survival of new potential medicines through the drug development process is a key objective of pharma companies.⁷⁸ A study from 2012 suggested that 43 % of the analyzed drug discovery programs failed in progressed clinical trials since the interaction between the new chemical entity (NCE) and the drug target was not adequately assessed at an early stage of the drug development process.⁷⁸ An analysis of 44 phase II programs at Pfizer yielded three key aspects for increasing the chance of clinical efficacy and reducing attrition in late drug development stages, termed the ‘three pillars of survival’.⁷⁸⁻⁷⁹

1. The unbound NCE has to reach the location of its pharmacological target (e.g. cellular compartment) and it has to reside there for a sufficient period of time.
2. The molecule has to engage the target.
3. Binding to the target has to result in a pharmacological effect.

Those three aspects are directly connected: the interaction between a target and a small molecule ligand depends on the local concentration at the target (→ pillar 1) and the binding affinity of the small molecule to its target,⁸⁰ referred as ‘target engagement’⁸¹ (→ pillar 2). The pharmacological effect (→ pillar 3) is a direct consequence from a NCE’s target engagement. Thus, the lack of a desired effect of a small molecule in a disease model could result from inappropriate binding of the drug to its target. Besides the absence of a pharmacological effect due to failed target binding, unwanted engagement of biomolecules not involved in the disease could lead to severe adverse effects. Being the decisive factor for drug efficacy but also its toxicity in a biological system,⁸⁰⁻⁸¹ detailed information about a potential drug’s target engagement is of great importance at every stage of the drug discovery process and could help reducing attrition rates and development costs.

Chemoproteomic approaches provide powerful tools to analyze binding characteristics between small molecules and proteins.⁸²⁻⁸⁵ However, routinely performed utilizing recombinant proteins and cell-extract based methods, such assays can achieve misleading results since those do not adequately address the ‘three pillars of survival’ plus a fourth requirement introduced by *Bunnage, Chekler, and Jones*⁷⁹ which is: ‘A biological assay has to capture the relevant phenotypic perturbations to avoid false positive outcomes’. Regarding the suitability of assays, a conclusion might be: the more manipulated a biological assay, the less it will generate relevant data.⁷⁹ To reduce discrepancies between assay outcomes and actual pharmacological efficacy characterization of targets/compound binding should be done under conditions preserving native protein environments including concentrations of substrates and co-factors, protein-protein interactions and protein folding.⁸⁶ This means, target engagement of small molecules to proteins should be measured directly in cells, tissues or ultimately *in vivo* to gain predictive information.

1.2.1. Chemoproteomic approaches for cellular target engagement measurements

Measuring target engagement directly in living cells has several advantages regarding the four pillars required to be fulfilled for a positive drug discovery outcome:

1. A pharmacological effect can be monitored.
2. The cellular environment mimics physiological and disease relevant parameters in a more suitable way than non-cellular assays.
3. Cellular assays allow for off-target identification beyond a limited panel of selected proteins.
4. The ability to cross natural barriers can be more reasonably addressed and active in-/efflux is considered.

The measurement of intracellular target engagement can be done in various ways all coming with some advantages but also limitations summed up in a recent review.⁸⁷

An indirect way to measure target engagement is the analysis of a functional effect downstream of the predicted target protein upon treatment with a small molecule. An example is visualizing calcium mobilization using fluorescent calcium indicators after B-cell receptor stimulation⁸⁸ as performed in this dissertation. The advantage of this kind of assay is the direct evaluation of a desired phenotype upon compound treatment. If the compound treatment should, for example, induce apoptosis of cancer cells by inhibiting hyperactive kinase signaling, cell death could be easily monitored. Moreover, a true cellular effect not biased by sample processing can be observed. This indirect approach, however, has three limitations regarding target engagement determination: (i) it does not reveal off-targets of the investigated small molecule, (ii) it can achieve misleading results in case an effect on a modulated pathway is compensated, and (iii) if no effect is observed it remains unclear if the molecule did not access the target or if binding does not result in the desired effect. Further, setting up functional assays for a certain target can be challenging and for some effects a suitable functional readout may not be available. More universal types of target engagement assessment are therefore valuable and chemoproteomics represents a suitable tool to investigate actual protein binding of small molecules in a more direct manner.⁸⁹

1.2.1.1. Measurement of intracellular target engagement of covalent kinase inhibitors using the kinobeads technology

Chemoproteomics is a powerful approach to support the process of identifying and validating molecular targets of bioactive small molecules, called 'target deconvolution',^{86, 90} on a proteome-wide scale.⁹¹⁻⁹² However, the investigation of changes on low abundant proteins is challenging due to the complexity of cellular proteomes. To address this limitation, affinity-based enrichment strategies can be applied for reducing sample complexity. A target class-specific approach to determine potency and selectivity for a small molecule is the immobilization of a number of broad-specificity protein inhibitors on a solid surface enriching many proteins of a defined target class. This concept was realized, for example, by kinobeads (Figure 8A).^{82, 93} Kinobeads represent an universal tool for profiling the selectivity of kinase inhibitors against a large portion of the kinome in one single experiment.^{82, 84, 94-95} The affinity enrichment enables investigations on the generally low abundant kinases and other purine-binding proteins. For target engagement studies, binding of kinases to the matrix is competed by the desired inhibitor under investigation. Performing such competition-binding experiments in dose-response, i.e. with increasing concentrations of free inhibitor, enables the determination of IC_{50} values derived from binding curves. Combining dose-dependent affinity enrichment of kinases with TMT-labeling allows for the selectivity profiling of kinase inhibitors against a large set of endogenous kinases (Figure 8B).^{82, 93, 96}

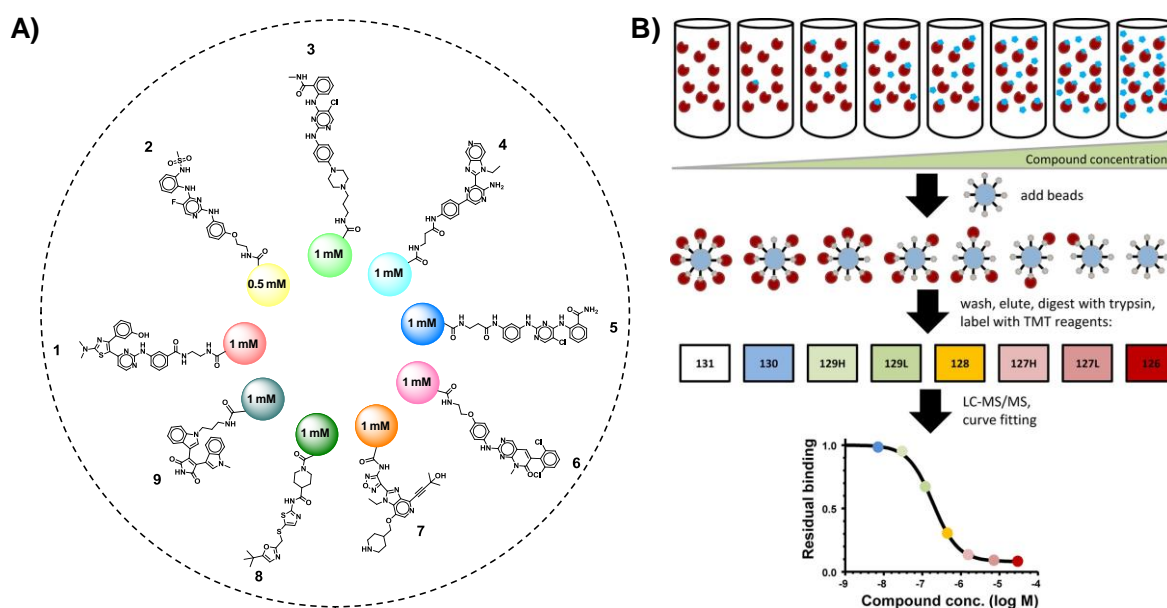


Figure 8: Kinobeads as used in this work and mass spectrometry-based competition-binding analysis. (A) Pan kinase inhibitors immobilized on sepharose beads as used in the current kinobeads mix. Compounds are immobilized on individual beads at coupling densities as given in the scheme. The master mix is achieved by mixing together equal amounts of all bead types. (B) Schematic drawing of a mass spectrometry-based competition-binding experiment as adopted from *Werner, T. et al.*⁹⁶ Protein containing samples which can be cell lysates or living cells are incubated with a soluble compound in different concentrations. Subsequently, the capturing matrix is added and proteins with affinity to the matrix are captured. For proteins in which the binding site of the affinity matrix is already occupied by the soluble compound a dose-dependent reduction of binding is expected. After processing (washing, elution, proteolytic digestion, and labeling with isobaric tags) the samples are mixed and analyzed by LC-MS/MS. IC_{50} values can be derived from binding curves representing the residual binding of the protein to the affinity matrix depending on the compound concentration.

Using this kind of assay for the determination of target engagement requires a clear distinction between reversible inhibitors and covalent compounds. When lysates are incubated with reversibly

binding small molecules and an affinity matrix, a state of equilibrium between binding and dissociation of the kinase to the free compound, the affinity matrix and endogenous ligands, like ATP, is established. Keeping the concentration of endogenous ligands and affinity matrix constant, the addition of more free compound to the sample will shift the equilibrium towards the formation of the inhibitor/protein complex P-I. Since only free protein can bind to the affinity matrix, the formation of the affinity matrix/protein complex P-A will be competed by the formation of P-I. Determining the compound concentration required to compete the binding of the protein to the affinity matrix by 50 % yields the 'IC₅₀ value' as measure for target engagement of a compound to a certain kinase.

In contrast, covalent inhibitors will form an inseparable complex P-I with a protein providing a reactive contact point. With increasing incubation time, this formation will continue until all available compound has reacted or no target protein is available anymore. Consequently, the IC₅₀ of the compound for an irreversible target will decrease with time. As discussed in the general section about covalent inhibitors, the rate of complex formation is depending on different parameters like concentration and the reactivity of the reaction partners and the environment in which the reaction takes place. It has to be noted that the kinetic aspect of irreversible, non-equilibrium binding is unaccounted in IC₅₀ values. Thus, strictly speaking an IC₅₀ can only be defined if k_{inact} is infinitely slow. IC₅₀ values measured for covalent inhibitors therefore should be considered as apparent IC₅₀ values and determined IC₅₀ values for different compounds should only be compared for equal incubation times.²⁶

These considerations about re-equilibrium binding of reversible inhibitors and non-equilibrium binding of covalent inhibitors has some consequences on target engagement measurements in living cells using kinobeads. When treating living cells or tissues with non-covalent compounds the equilibrium established inside the intact cells will be altered by sample processing like cell washing or lysis. These procedure steps will influence target engagement determination since (i) the compound itself is diluted, (ii) endogenous ligands of the target protein are diluted but also (iii) changes in target conformation due to lysis (e.g. membrane proteins which are not stable in aqueous environment) might decrease the affinity of the compound to the target. For non-covalent compounds this results in a misleading interpretation of the compound's target specific characteristics like selectivity and potency.

While intracellular target engagement measurements using kinobeads is challenging for non-covalent inhibitors and suitable assays need to be set up for this purpose, non-equilibrium binding of irreversible kinase inhibitors allows neglecting these considerations. Since covalent target engagement is irreversibly established already in the living cell, washing and lysis of the cells will not influence compound/target binding and may even prevent further reaction. Thus, kinobeads affinity enrichment can be used for measuring covalent target engagement established in living cells in an unbiased way. For potential non-covalent off-targets, re-equilibration considerations have to be kept in mind.

While an advantage of target class specific broad spectrum affinity matrices like kinobeads is their broad applicability to many kinase inhibitors without further compound design and synthesis efforts, the target class specific affinity enrichment approach has the limitation of being 'blind' for targets beyond the investigated protein class. To overcome this limitation, affinity enrichment can also be drug-centric. Here, linkable analogues of the drug of interest are synthesized by attaching reactive

handles at different positions. These analogues are immobilized on a solid matrix allowing for the enrichment of accessible target proteins of the linkable analogue and subsequent identification by, for example, mass spectrometry.⁹⁷ This drug-centric affinity enrichment approach has the advantage that it might capture target proteins not limited to a certain protein class. A limitation is the introduction of suitable handles into the small molecule which requires laborious design and synthesis efforts for every single small molecule under investigation and the reporter handle of these probes might introduce a bias towards certain binding modes.⁹⁸ To reduce the bias of the introduced handle as effectively as possible, different analogues of compounds can be synthesized incorporating handles each with a different vector for immobilization on a solid support. The incorporation of primary amines, for example, enables the immobilization of the compound on NHS-activated sepharose beads as done for generating kinobeads. However, forming this peptide bond between the amine and the activated ester requires reaction conditions not compatible with biological systems. In consequence, drug centric affinity enrichment studies can only be performed in cell extracts after pre-coupling a compound to a solid surface. To overcome this limitation, reaction mechanisms were developed allowing for the conjugation of two partners at mild conditions without reactivity towards biomolecules. These reactions are subject of bioorthogonal chemistry.

1.2.1.2. Measurement of intracellular target engagement utilizing small molecule probes combined with bioorthogonal chemistry

Significant advances in chemical probe design and synthesis were achieved by the incorporation of 'bioorthogonal' reporter groups enabling to monitor cellular processes.⁹⁹⁻¹⁰⁰ For example, target engagement studies were enabled to be done directly in living cells by combining cell-permeable probe molecules and bioorthogonal chemistry. Utilizing this approach, proteome-wide analyses identified targets and undesired binders of small molecules.^{98, 101-102}

'Bioorthogonal' refers to chemical reactions which can take place intracellularly without reacting with functional groups naturally occurring in cells, and thus, not interfering with the biological system.¹⁰³

Several requirements have to be fulfilled by bioorthogonal reaction partners limiting the number of suitable reactions to only a few.^{99-100, 104}

1. The moieties used in a bioorthogonal reaction have to be stable, in means of thermodynamics but also metabolically, inside a biological system before the reaction.
2. The molecules including reagents and products must not be toxic.
3. The reaction has to achieve stable products rapidly at high yield without byproducts at relatively low biomolecule concentrations.
4. The reaction has to be selective, i.e. the bioorthogonal partners should solely react with each other and not with amino acids / proteins and other biomolecules including nucleic acids, metabolites, lipids, and carbohydrates.
5. Physiological conditions have to allow for the formation of the product, i.e. the bioorthogonal partners have to react in aqueous solution, at a pH 6-8, at 37 °C while exposed to oxygen at atmospheric pressure.
6. The bioorthogonal groups have to be cell permeable and not too big to avoid perturbations of the tagged biomolecules.

Bioorthogonal chemistry reactions applied in this dissertation are copper(I)-catalyzed azide-alkyne cycloaddition (CuAAC),¹⁰⁵⁻¹⁰⁶ strain-promoted azide-alkyne cycloaddition (SPAAC),¹⁰⁷ and the inverse electron demand Diels–Alder reaction (IEDDA).¹⁰⁸ For a comprehensive overview beyond those selected reactions, it is referred to the work of *Lang and Chin*,¹⁰⁴ *Patterson et al*¹⁰⁹ or *Prescher and Bertozzi*.¹¹⁰

In the copper(I)-catalyzed azide-alkyne cycloaddition terminal alkynes and azides react with each other to form triazoles (Figure 9A). First described to be very slow and depending on high temperature to efficiently yield triazoles,¹¹¹ and thus, being not applicable in biological systems, this reaction was significantly improved by using copper salts as a catalyzer.¹⁰⁵⁻¹⁰⁶ This discovery increased the reaction rate by reducing the activation barrier in aqueous solution considerably, and thus, transforming it into a valuable bioorthogonal reaction.^{100, 112} While the small size of the alkyne and azide functionalities represents an advantage of these bioorthogonal reaction partners, its dependency on cell toxic copper salts is one of its major limitations. The cytotoxic effects cannot be overcome by reduction of the copper concentration since it decreases the reaction rate inversely proportional¹¹³ but it can partially

be shielded by copper(I)-stabilizing ligands like Tris[(1-benzyl-1H-1,2,3-triazol-4-yl)methyl]amine (TBTA) or Tris(3-hydroxypropyltriazolylmethyl)amine (THPTA).¹¹² CuAAC was applied in several studies identifying de novo synthesized proteins,¹¹⁴ target identification of natural products,¹¹⁵ and for the identification of cysteine residues in complex proteomes.¹¹⁶

For overcoming the limitation of using cytotoxic catalyzers but keeping the small azide which is essentially absent in biological systems¹¹⁷ another reaction was developed. Instead of using terminal alkynes, in a strain-promoted alkyne-azide cycloaddition reaction the alkyne is introduced into a strained ring (Figure 9B).¹¹⁸ This accelerates the alkyne-azide conjugation without the use of a potentially cytotoxic catalytic agent.^{100, 104} Examples for a successful application of SPAAC include studies about the dynamics and distribution of glycans¹¹⁹⁻¹²⁰ or targeted delivery of drugs to cancer cells.¹²¹

Another bioorthogonal reaction which results in desirable fast and efficient labeling is given with the inverse electron demand Diels-Alder reaction (IEDDA)^{108, 122} in which a tetrazine-functionalized molecule reacts with a strained alkene or alkyne (Figure 9C). Compared to other bioorthogonal reactions, the IEDDA reaction between a tetrazine and a transcyclooctene is very fast under physiological conditions and produces only nitrogen gas as a byproduct. Further, the reaction is of high specificity and reactivity with the proteome is not reported. The fast kinetics allows for labeling biomolecules of low abundance or monitoring fast biological processes. This bioorthogonal reaction was applied to identify drug targets¹²³⁻¹²⁴ and to validate target engagement in living cells.¹²⁵

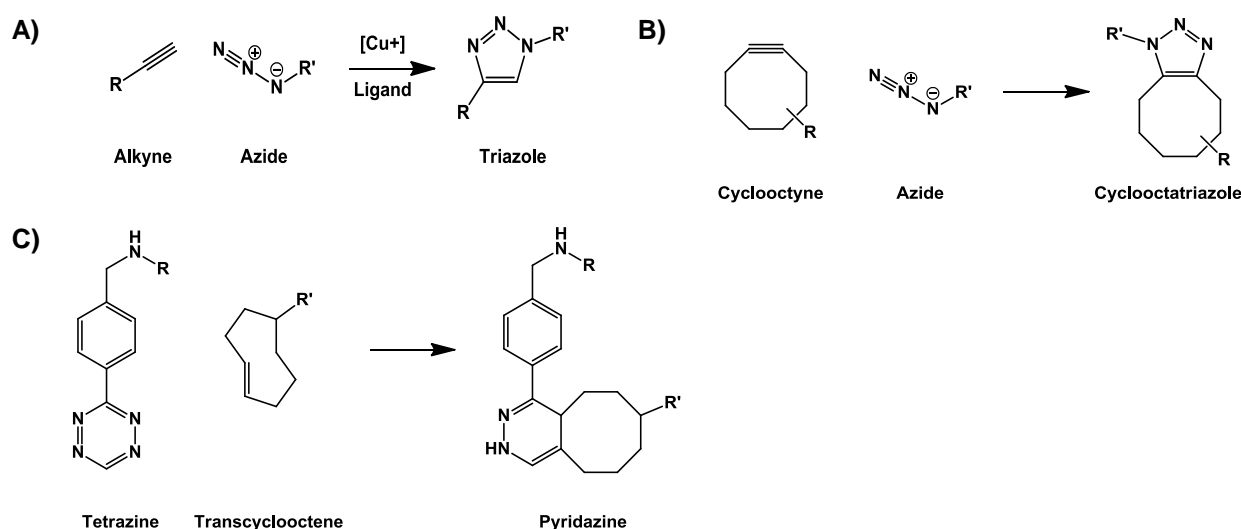


Figure 9: Mechanisms of bioorthogonal reactions used in this dissertation. (A) Mechanism of a copper(I)-catalyzed azide-alkyne cycloaddition as used in this work. A terminal alkyne reacts with an azide catalyzed by copper(I) salts and a stabilizing ligand to form a triazole (rate constant $k \sim 10\text{-}200 \text{ M}^{-1}\text{s}^{-1}$). (B) Mechanism of a strain-promoted alkyne-azide cycloaddition as used in this work. The reaction of a strained alkyne with an azide achieves a conjugated molecule by forming a cyclooctatriazole (rate constant $k \sim 0.01\text{-}1 \text{ M}^{-1}\text{s}^{-1}$). (C) Mechanism of an inverse electron demand Diels-Alder reaction as used in this work. The reaction of a tetrazine with a transcyclooctene rapidly achieves a conjugated molecule by forming a pyridazine (rate constant $k \sim 1\text{-}10000 \text{ M}^{-1}\text{s}^{-1}$).

In this work, the aforementioned reactions were applied due to advantageous characteristics of each: since the azide and alkyne functions on a molecule represent very small moieties expected to avoid negative influences on the binding modalities of the original compound, CuAAC was applied. SPAAC provides the possibility to react an azide-incorporating molecule with a reporter group containing a DBCO moiety without the need to use other reagents than the reaction partners. The

tetrazine/cyclooctene ligation was evaluated due to its superior kinetics with the goal to improve the efficiency of labeling.

For studies about intracellular target engagement of small molecules click chemistry is a valuable tool^{81, 98, 125-126} and as for the kinobeads affinity enrichment, probes with a covalent mechanism can be beneficial for intracellular target engagement determination due to non-equilibrium binding. To capture the intracellular target engagement situation utilizing chemoproteomic approaches, fixation of the engagement state established in the cell prior to cell lysis or other sample processing is required. This characteristic is inherently fulfilled by covalent protein inhibitors and analogues thereof. The generation of suitable probes and the evaluation of methods to assess those tools are objectives of this work.

Since both introduced affinity enrichment-based approaches for intracellular target engagement determination require covalent compounds for fixing the intracellular situation there is also a need for more direct approaches. One of such methods recently advanced is given with cellular thermal shift assays and thermal proteome profiling.

1.2.1.3. Cellular thermal shift assay and thermal proteome profiling

A complementary chemoproteomic method to determine target engagement is given with thermal shift assays (TSAs) as described for pure proteins by *Kurganov*¹²⁷ or *Vedadi et al.*¹²⁸ The TSA is a biophysical assay which is based on the concept that proteins start to denature when they are heated to a certain temperature. This process of denaturing or protein unfolding is also called 'melting', so that the temperature at which melting is induced is termed melting temperature T_m . Techniques for analyzing unfolding of purified proteins are, for example, differential scanning fluorometry¹²⁹ and differential static light scattering.¹²⁸ The former visualizes hydrophobic regions revealed by unfolding using dyes with increased fluorescence after binding to hydrophobic sites. The latter measures an increase in light scattering due to aggregated proteins. An interesting characteristic of thermal protein stability is that modifications of the protein, including the binding of a ligand, influence the melting temperature.¹³⁰ By heating proteins to different temperatures distinct sigmoidal melting curves can be recorded. Adding a binding ligand to the protein usually results in the curves shifting to a higher temperature due to thermal stabilization of the protein.

Martinez Molina et al.^{80, 131} transferred this concept to intact cells and termed this procedure 'cellular thermal shift assay (CETSA)'. They recognized the value of the technique for the identification of target engagement without the bias of cell lysis steps or the cost- and labor-intensive establishment of suitable probes as required in ABPP approaches.¹³²⁻¹³⁶ In a CETSA experiment, whole cells are heated to induce the unfolding and precipitation of endogenous proteins. Depending on the temperature the cells are heated to and the melting temperature of the proteins a certain portion of the proteins remains folded, and thus, soluble (Figure 10A). These soluble proteins can be isolated by centrifugation or filtration and quantified, for example, by immunoblotting to derive protein melting curves. When pre-treating the cells with a protein binding ligand, shifting melting curves indicate target engagement. Another type of CETSA is given with 'isothermal dose-response (ITDR)' experiments in which not the heating temperature is varied but the ligand concentration while the heating temperature remains the same. It was shown that results achieved in ITDR experiments often correlate with affinity measurements using other techniques.¹³¹

A further advancement of this approach was the expansion of the analysis from single proteins to the cellular melting proteome, termed 'meltome', using mass spectrometry analysis as done, for example, by *Savitski et al.*¹³⁷ and others. As in common CETSA experiments, cells or lysates are treated with a small molecule or a vehicle control before heating the samples to different temperatures. For the analysis of thermal proteome stability, subsequently, up to ten different conditions are labeled with isobaric tandem mass tags and proteome-wide melting curves for the treated samples and the vehicle control are determined by mass spectrometry analysis (Figure 10B). Using this mass spectrometry-based approach, sigmoidal melting curves were derived for about 80 % of more than 7000 identified proteins.¹³⁷ The expansion to the proteome suggested terming this advancement 'thermal proteome profiling (TPP)'. As mentioned above, either living cells or cell extracts can be pre-treated with a compound under investigation prior to thermal profiling. The comparison of both allows for the discrimination of shifts in melting temperature upon ligand binding from shifts induced by downstream modifications or effects on regulated expression. However, it was shown that the average melting

temperature across the proteome is about 2.7 °C higher in lysate than in cells suggesting that the cellular environment influences thermal stability.¹³⁷

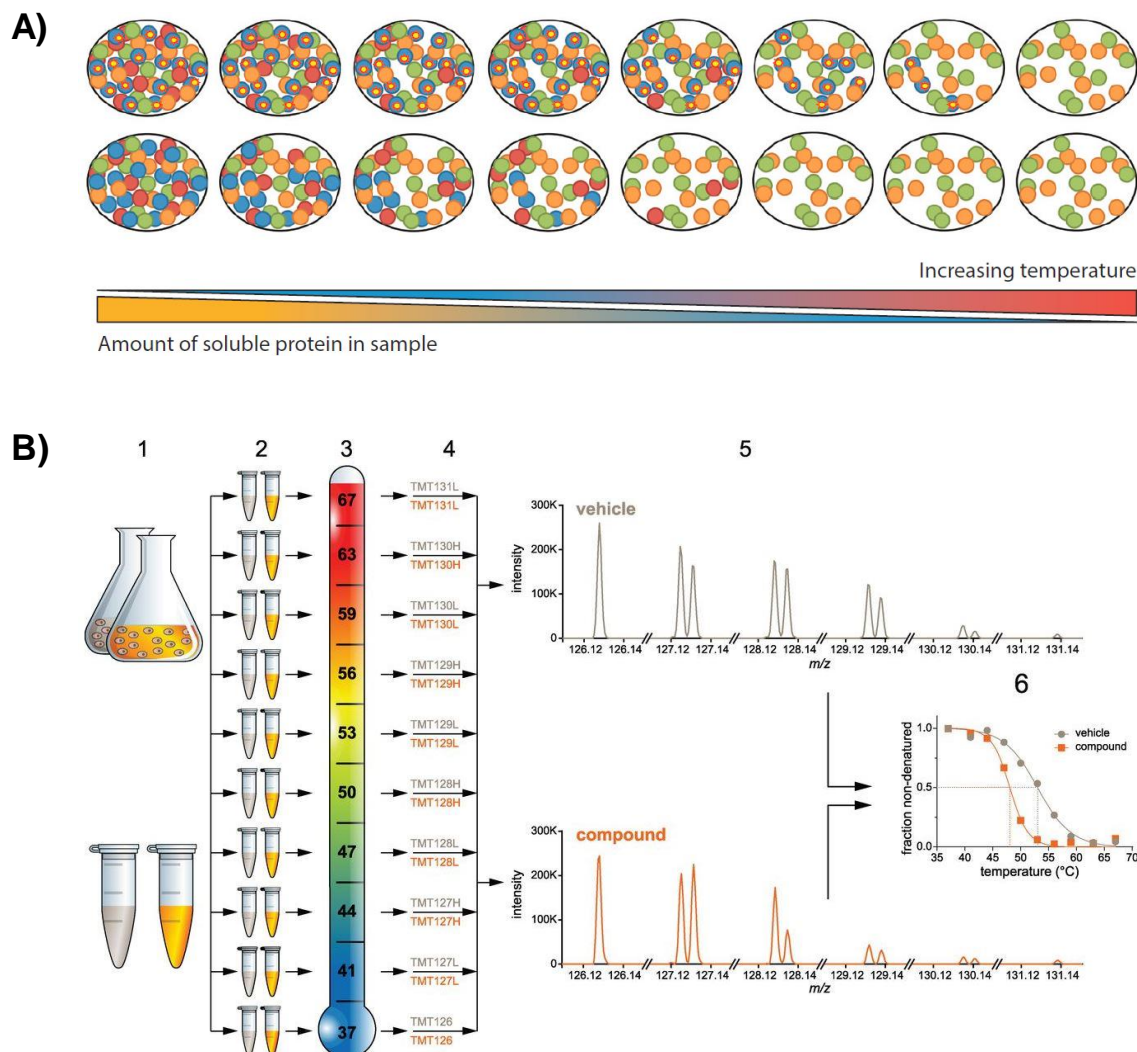


Figure 10: Cellular thermal shift assay and thermal proteome profiling. (A) With increasing temperature, the amount of soluble protein in a sample will decrease. Upon treatment with a ligand, thermal stabilization will result in a higher amount of soluble target protein (above, blue) compared to a vehicle control (below, blue). Figure adopted from *Martinez Molina, D. and P. Nordlund*.¹³¹ (B) Cells or extracted proteins are incubated with a small molecule vs a vehicle control. The samples are split into up to 10 fractions and subsequently heated to different temperatures. Aggregated proteins are removed and the soluble fraction is analyzed by mass spectrometry. Melting curves are determined for the compound treated samples and the vehicle control. Effects on the thermal stability of a protein might indicate a binding event of the small molecule to the respective protein. Figure adopted from *Savitski, M. M. et al.*¹³⁷

Using the TPP strategy, impressive findings were achieved regarding proteome-wide analysis of small molecule-induced thermal protein stability including membrane proteins,¹³⁸ and the identification of side-effect mediating off-targets of approved drugs.¹³⁹ For the latter, a two-dimensional thermal proteome profiling ('2D-TPP') strategy was applied. For this, cells or lysates are treated with four different concentrations of compound plus a vehicle control and these treated samples are split into twelve aliquots each heated to different temperatures. Ten samples comprising two consecutive temperatures are labeled by tandem mass tags and are analyzed in one TMT10 experiment. By this, typically one 2D-TPP experiment requires six parallel mass spectrometry analyses to yield information about compound- and temperature-dependent proteome melting.

Thermal proteome profiling is a valuable tool for drug discovery. It was applied to identify BRAF and ferrochelatase as off-targets of the approved drugs Vemurafenib and Alectinib, respectively,¹³⁷ thus, showing its potential for shedding light on off-target toxicity or polypharmacology. Further, its potential to analyze effects downstream of a drug's target represents a valuable tool to detect biomarkers since, in theory, any modification of a protein can affect its thermal stability.¹³⁰ Beyond, scientists speculate about thermal proteome profiling performed directly in a patient's sample representing the ideal strategy for high-throughput screening in personalized medicine.¹³¹

Besides this impressive perspective for this technique, there are also some challenges. Low abundant proteins might not be detected without enrichment, melting points of small proteins might not be covered by the chosen temperature range since they tend to be more stable, and shifts in melting temperature upon ligand binding might be too small to be significant especially for large and multidomain proteins.^{87, 140} A comparison of thermal proteome profiling and affinity enrichment of kinases using kinobeads showed that about 30 % of the kinases identified with both approaches did not show significant shifts in their melting temperatures. This might indicate that some protein kinases simply do not show thermal shifts or that the relevant active form captured by kinobeads might be masked by other forms in the thermal shift assay.¹³¹

Since today (December 21st, 2017) there is no TPP study on covalent kinase inhibitors, this dissertation includes the TPP approach for off-target identification of covalent kinase inhibitors and compares outcomes of this approach to intracellular target engagement outcomes achieved with affinity-based enrichment.

Another recent technique which could serve for the determination of intracellular target engagement is based on the use of proteolysis-targeting chimeras (PROTACs) as introduced in the next chapter.

1.2.1.4. Intracellular target engagement determination utilizing targeted degradation of proteins upon binding by proteolysis-targeting chimeras

In 2001 the concept of utilizing the cellular machinery for targeted protein degradation mediated by heterobifunctional molecules was established.¹⁴¹ The idea behind this concept is that polyubiquitination of a protein results in its degradation by the proteasome. Ubiquitination of a substrate protein is a multistep process naturally involving ubiquitin-activating enzymes (E1s), ubiquitin-conjugating enzymes (E2s), and ubiquitin ligases (E3s) (Figure 11A).¹⁴²⁻¹⁴³ Sakamoto *et al* hijacked this machinery by synthesizing a chimeric molecule which consists of two binding domains: one targeting methionine aminopeptidase-2 as the desired protein for degradation and the other targeting the ubiquitin ligase complex Skp1-Cullin-F box complex containing Hrt1. With this molecule, the ubiquitin ligase was recruited to the target protein resulting in its polyubiquitination and subsequent degradation (Figure 11B).¹⁴¹

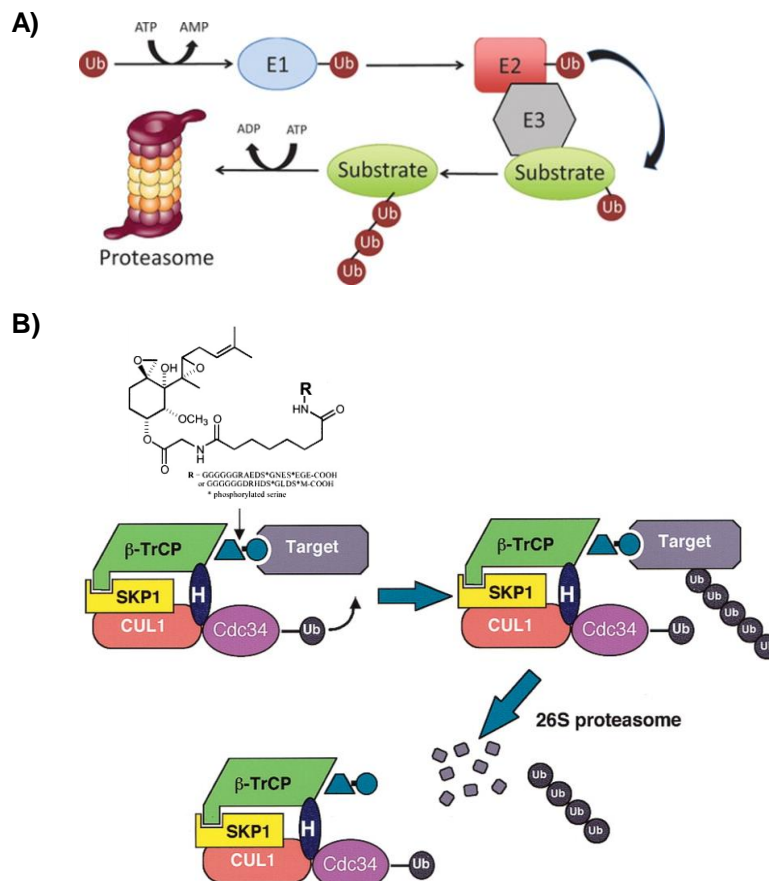


Figure 11: Concept of proteasomal degradation using proteolysis-targeting chimeras. (A) In the natural process of proteasomal degradation a multistep process involving ubiquitin-activating enzymes (E1s), ubiquitin-conjugating enzymes (E2s), and ubiquitin ligases (E3s) leads to polyubiquitination of a substrate protein. The polyubiquitination pattern serves as signal for the proteolytic degradation of the substrate in the proteasome. Figure adopted from Pagan, J. *et al.*¹⁴² (B) In the PROTAC approach as established by Sakamoto *et al* a chimeric molecule recruits the target protein to the ubiquitin ligase complex to induce target degradation by the 26S proteasome. Figure adopted from Sakamoto, K. M. *et al.*¹⁴¹

Generalizing this concept, a PROTAC molecule is comprised of three parts: a target protein binding ligand, a linker, and an E3 ubiquitin ligase recognition motif. Such molecules shall facilitate a

proximity-driven ubiquitin transfer to a suitable substrate residue (often lysine) by the E3 ligase. Tagged by polyubiquitination, protein functions are inhibited by elimination via proteasomal degradation.¹⁴³⁻¹⁴⁴ Several requirements have to be fulfilled for a successful degradation¹⁴³: first of all, the PROTAC has to reach the location of action (i.e. cellular compartment) what might be challenging for relatively large molecules. Further, affinity to both proteins must allow for assembly of the ternary complex and sterical clashes of the recruited proteins must not disrupt the complex prior to ubiquitination. These considerations suggest that the synthesis of promising PROTACs is not a trivial exercise. Several studies invested great effort in combining an E3 ligase recruiting molecule, the correct length, composition, and positioning of a linker, and a suitable protein targeting ligand. It became obvious that even for a single target protein bound by different compounds, degradation can vary with the choice of the target binder.¹⁴⁵⁻¹⁴⁶ From an optimistic point of view this may be a suitable approach to gain selectivity of the ligand. However, it increases complexity of establishing a general strategy for protein degradation. Moreover, today only a limited number of the over 600 E3 ligases encoded in the human genome was successfully hijacked for PROTAC-mediated degradation with the most success using Von Hippel Lindau (VHL) and Cereblon recognition motifs.^{145, 147-148} Also the third component of PROTAC molecules – the linker – has an important function orienting the E3 ligase towards a suitable lysine for adequate ubiquitination.¹⁴⁵⁻¹⁴⁶ These considerations suggest that a general combination of warhead, linker, and ligase recognition motif for the generic application of PROTACs for targeted protein degradation is very unlikely.¹⁴³ Beyond these technical challenges, there are some more requirements for a successful proteolysis of the target protein associated with the process of ubiquitination and degradation. Even after successful recruitment, the ubiquitination by the E3 ligase has to be faster than the deubiquitination by endogenous enzymes and degradation must be faster than the de novo synthesis of the target protein also if upregulated.

Despite of all these challenges, the strategy of proteasomal degradation induced by PROTAC-mediated ubiquitination might represent a promising therapeutic approach coming with some advantages over protein inhibition: PROTACs can bind basically every part of a protein for inducing degradation allowing to target ‘undruggable’ proteins¹⁴⁵ including proteins with scaffolding function,¹⁴⁶ degradation might avoid upregulation of an enzyme as consequence of inhibition,¹⁴⁶ and might be used at low concentrations due to their catalytic mechanism.¹⁴³

PROTAC molecules could also represent a suitable tool for intracellular target engagement studies. By the comparison of the protein pool of PROTAC-treated cells with a vehicle control, the reduced abundance of certain proteins in the PROTAC-treated samples could indicate target engagement by the molecule in the living cell. For this, TMT labeling can be applied for allowing the comparison of different treatment conditions. Further, a combination with pulsed SILAC labeling starting with the compound treatment facilitates to distinguish already existing from newly synthesized proteins. This enables the discrimination of degradation from downregulated expression. Degradation events induced by PROTAC-binding are expected to occur in the pool of mature proteins and among nascent proteins. Changes in the proteome resulting from regulated expression should only be detected in the fraction of newly synthesized proteins. The concept of combining pulsed SILAC labeling with tandem mass tags for the determination of proteome changes was just recently published as ‘multiplexed proteome dynamics profiling’.¹⁴⁹

An advantage of utilizing the PROTAC technology for target engagement studies is that it is not limited to a certain target space and that it could identify targets not captured by affinity approaches (e.g. inactive forms) or thermal shift approaches (large or thermally non-responsive proteins). Further, target engagement results in an effect directly in the living cell so that processing the sample, e.g. by cell lysis, does not bias the readout, i.e. degradation. Challenges of such an approach towards the mass spectrometry analysis might come with the dynamic range of the mass spectrometer.

In this dissertation, the PROTAC technology was applied to the covalent kinase inhibitors Ibrutinib and Afatinib for (off-)target identification. Today (December 22nd, 2017), there is no study published combining irreversibly binding protein inhibitors with the PROTAC technology. It will be interesting to see how the catalytic mechanism of proteasomal degradation will work with covalent target binders compared to intracellular target engagement measured with affinity-based enrichment approaches and 2D-TPP.

Since for all the chemoproteomic approaches for target engagement determination introduced herein mass spectrometry represents a valuable analysis technique, the next chapter will give a brief overview of the mass spectrometry applied in this work.

1.2.2. Mass spectrometry-based proteomics

Mass spectrometry is a method for identifying, characterizing, and quantifying proteins¹⁵⁰ and the continuous development of new technologies facilitates to answer more biological questions.¹⁵¹ A mass spectrometry-based proteomics experiment basically includes five steps: (1) the preparation of a protein/peptide containing sample, (2) the separation of the sample components by separating techniques (e.g. liquid chromatography), (3) the ionization of the proteins or peptides, (4) the separation of those ions according to their mass-to-charge ratio, and (5) the analysis of the generated data to derive the properties of relevance.¹⁵² Methodical and technological developments in these fields enabled proteomic approaches to identify low-abundant proteins in complex mixtures,¹⁵³ to characterize post-translational modifications,¹⁵⁴ to identify protein complexes,¹⁵⁵ as well as to analyze drug-protein interactions in cell extracts⁸² and living cells.¹⁵⁶

In principle, two major workflows for identifying proteins are used in high-throughput proteomics. For the so called ‘top-down’ proteomics approach (Figure 12A), which has some advantages regarding the identification of post-translational modifications (PTMs) and protein isoforms¹⁵¹ since intact full proteins are subjected to the mass spectrometer, it is referred, for example, to the work of *Chait*.¹⁵⁷ The alternative approach used in this work, is the so called ‘bottom-up’ or ‘shotgun’ proteomics (Figure 12B). In this approach, proteins, as for example extracted from a cell culture and optionally pre-fractionated, are cleaved into peptides prior to MS analysis. For the generation of peptides, proteins are digested with proteolytic enzymes. A typical enzyme used for this purpose is trypsin which generates defined peptides cleaving specifically after lysines and arginines. The mixture of peptides is then subjected to the LC-MS/MS analysis where peptides are separated (e.g. by reversed phase chromatography), ionized (e.g. by electrospray ionization), and analyzed in the mass spectrometer. In the mass spectrometer peptides with a defined mass-to-charge (m/z) ratio (‘precursor ions’) are selected for fragmentation to get information about the amino acid sequence of the peptide with the defined m/z . Finally, data achieved for the generated peptides including the m/z value of the precursor and the MS/MS spectra of the fragments are matched against an *in silico* generated data base to deduce for the original protein (Figure 12C).¹⁵⁷⁻¹⁵⁸

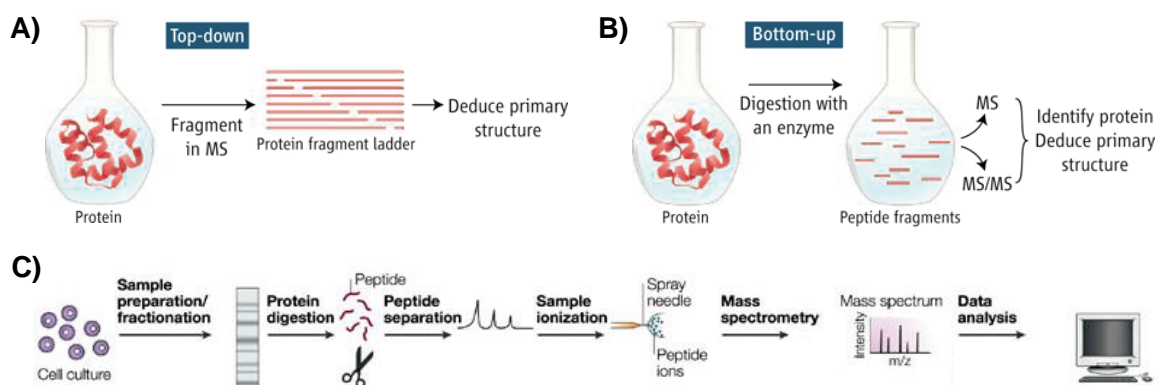


Figure 12: Workflows used for mass spectrometry-based proteomics. (A) In a ‘top-down’ approach intact proteins are subjected to the mass spectrometer where fragments of the protein are generated. (B) In contrast, in a ‘bottom-up’ approach proteins are digested with a proteolytic enzyme before subjecting the mixture to the mass spectrometer. (C) A complete bottom-up workflow. Figures adopted from *Chait, B. T. and Steen, H. and M. Mann.*¹⁵⁷⁻¹⁵⁸

1.2.2.1. Mass spectrometer and its components primarily used in this work

Many publications have focused on different types of mass spectrometers including ionization methods and mass analyzers and their use for achieving optimal results.¹⁵⁹⁻¹⁶⁰ In this dissertation predominantly a Thermo Fisher Q Exactive Hybrid Quadrupole Orbitrap¹⁶¹ (Figure 13A) was used. It is coupled to an electrospray ionization (ESI)¹⁶² which represents the preferred ionization method for complex samples, like mixtures of peptides or proteins,^{159, 163} since the continuous ionization at atmospheric pressure is compatible with upstream connected separation techniques like liquid chromatography.¹⁵⁹ Prior to ionization, a peptide mixture is injected into a chromatography system for separation. A commonly used system is reversed-phase chromatography using octadecyl carbon chain-coated silica (C18) as a stationary phase and mixtures of water and organic solvents (e.g. acetonitrile) as a mobile phase. Acidic supplements like formic or trifluoroacetic acid as proton donors aid the generation of net positively charged species in the sample.¹⁶⁴ Orthogonally coupled liquid chromatography techniques can improve robust identification of low-abundant proteins in complex samples.¹⁶⁵⁻¹⁶⁶ After separation by liquid chromatography, peptides are injected into the ESI ion source. The sample flows into a needle to which a high positive voltage is applied. By electrostatic repulsion a fine Taylor cone¹⁶⁷ is formed from which droplets with an excess of positive charges on the surface are accelerated towards the ion optics to form a fine spray. Solvent evaporation reduces the droplet size until surface tension and electrostatic repulsion of the positive charges on the droplet surface are balanced (Rayleigh limit¹⁶⁸). After exceeding this limit, droplets burst into smaller drops. This process continues until, finally, generating a stream of positively charged ions (Figure 13B).^{163, 169-171} For completion, it is noted that also negatively charged ions can be generated by applying a strong negative voltage to the spray needle. After electrospray ionization, the ions are accelerated by a radio-frequency quadrupole (RF lens) and transferred through ions guiding optics to a mass filtering quadrupole. A quadrupole consists of four hyperbolic or cylindrical rod electrodes (hexapoles of six, octapoles of eight) of which to the two opposite ones the same voltage is applied. The voltage consists of a direct current component U and an alternating current component V with the frequency ω . By modulating these parameters, repulsive and attracting electrostatic forces in x - and y -direction stabilize ions within a certain mass-to-charge (m/z) range in the quadrupole. Thus, ions accelerated in z -direction might pass the quadrupole on stable trajectories without hitting the rods (Figure 13C).¹⁷² This is used to guide only ions with a defined m/z ratio through this ion filter by setting U , V , and ω .¹⁷¹ Multipoles can be used as mass filters for the selection of pre-cursor ions (in Figure 13A referred as 'Quadrupole'), ion guiding devices (in Figure 13A referred as 'RF-lens', and 'Ion optics'), and as ion traps (in Figure 13A referred as 'C-trap', and 'HCD cell'). For trapping ions in a multipole, additional electrodes are located at the ends of the multipole. Modulation of the voltage at these trapping electrodes allows for the storage and the selective ejection of ions with a defined m/z ratio. This concept is, for example, used for the fragmentation of ions by collision induced dissociation (CID) in a MS/MS analysis. After precursor ion selection by the quadrupole, the precursor ion is transferred via the C-trap into the HCD cell. In the HCD cell, precursor ions are excited to high kinetic energy and are collided with an inert gas such as helium or nitrogen. This collisions result in the breakage of the amide bonds between two amino acids into product ions.¹⁵⁸ Depending on the position of the retaining charge these ions are called b-ions (charge retained on N-terminus) or y-ions (charge retained on C-

terminus) (Figure 13D). Ideally, b- and y-ions allow for the determination of the amino acid sequence of the fragmented peptide. The analysis of the fragments using the Q Exactive Hybrid Quadrupole Orbitrap is performed in an Orbitrap mass analyzer after transmitting the ions as a highly-condensed package over the C-trap. In an Orbitrap, ions are trapped on stable trajectories around a coaxial inner spindle-like electrode surrounded by an outer barrel-like electrode (Figure 13E). Upon transmission of the packages into the Orbitrap the ions are stabilized on their trajectories around the central electrode and oscillate in axial direction. These oscillations along the z-axis are depending on the m/z ratio of the ions and induce a current in the outer electrodes which can be converted into a mass spectrum by Fourier transformation.¹⁷³ With the information from MS¹ and MS/MS (MS²) data, the peptide / protein injected into the mass spectrometer can be identified. For this, information contained in the mass spectra (e.g. retention time of a peptide and m/z values of fragments) are compared to a database containing information about *in silico* digested and fragmented peptides. For the comparison, search algorithms like Andromeda¹⁷⁴ or Mascot¹⁷⁵ can be used returning a probability-based ranking of matching peptide sequences.

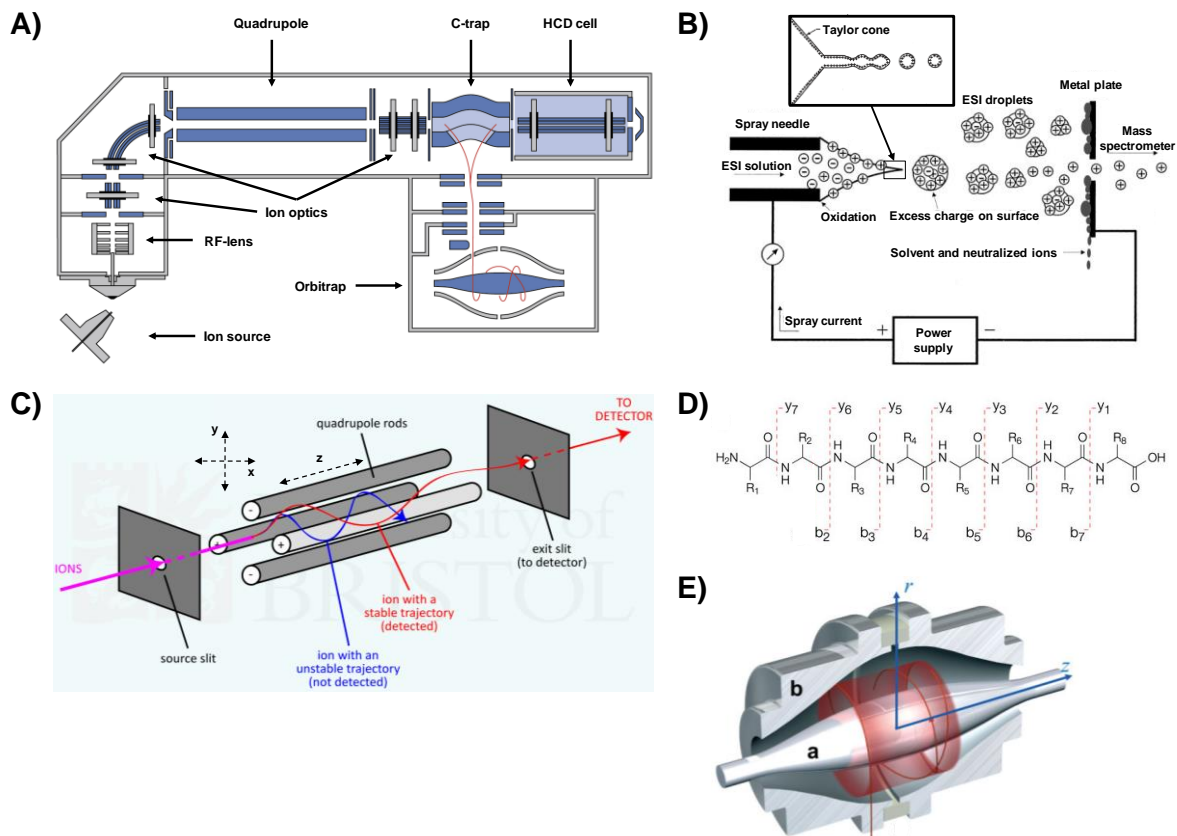


Figure 13: Basics of mass spectrometry as used in this dissertation. (A) Schematic drawing of a Q Exactive mass spectrometer. Figure adopted from Michalski, A. *et al.*¹⁶¹ (B) Generation of positively charged ions in an ESI source. Figure adopted from Cech, N. B. and C. G. Enke and Gross, J. H.^{169, 171} (C) Ions filtered by a quadrupole mass filter. Figure adopted from Gates, P.¹⁷² (D) Fragmentation of a peptide results in b- and y ions. Pattern adopted from Steen, H and M. Mann.¹⁵⁸ (E) An Orbitrap mass analyzer consisting of an inner spindle electrode (a) and an outer barrel-like electrode (b). Figure adopted from Scigelova, M. and A. Makarov.¹⁷⁶

1.2.2.2. Quantification of proteins in different samples using stable isotope labeling

The fragmentation of precursor ions as described above is an essential step for the relative quantification of proteins utilizing isobaric mass tag labeling. For comparing proteome differences in two or more samples (e.g. disease state vs control, or samples incubated with different amounts of inhibitor) abundances of relevant proteins have to be quantified. This can be done by label-free methods,¹⁷⁷ by spiking in comparable standards,¹⁷⁸ or after labeling the different states by metabolic (SILAC)¹⁷⁹ or chemical approaches (isobaric mass tag labeling).¹⁸⁰⁻¹⁸¹ In this work quantification was done by chemical labeling using isobaric mass tags and by stable isotope labeling with amino acids in cell culture (SILAC) approaches.

In SILAC approaches stable isotope-containing amino acids replace normal amino acids in the cell growth medium. Usually, arginine and lysine are exchanged by their counterparts containing ¹³C and ¹⁵N atoms. Utilizing those amino acids ensures that for a tryptic digestion each generated peptide (except the C-terminal peptide of the protein) contains at least one labeled amino acid. Peptides with a specific mass difference resulting from incorporated isotope-labeled amino acids can be compared to the unlabeled peptide allowing for the relative quantification between the samples. An advantage of metabolic labeling compared to chemical labeling is that samples can be pooled already on a cellular level reducing variability of quantification.¹⁸² Pulsed SILAC approaches were previously used for identifying newly synthesized proteins in a pool of pre-existing proteins.^{153, 183-185} For this purpose, it was also applied in this dissertation to distinguish protein degradation from downregulated expression during the PROTAC investigations.

Chemical labeling of proteins or peptides occurs after extracting proteins from suitable sources like cells or tissues. This has the advantage that also proteins derived from non-immortal cells like primary cells can be labeled. Furthermore, in contrast to SILAC, more than up to three states can be labeled. For chemical isotope-labeling, reactive reagents are used to introduce mass differences to equal peptides of different samples resolvable by mass spectrometry analysis. In approaches like isotope-coded affinity tag (ICAT) labeling¹⁸⁶ amino acid residues are labeled with reagents differently labeled for mass separation. However, ICAT has the disadvantage of increased MS¹ spectrum complexity depending on the level of multiplexing. Another concept in which differences are not resolved by MS¹ spectrum analysis but MS² spectra after fragmentation is given with isobaric mass tags. Techniques like iTRAQ ('isobaric tags for relative and absolute quantification')¹⁸⁰ and TMT ('tandem mass tags')¹⁸¹ labeling utilize reagents combining an amine reactive group, a mass normalizer, and a mass reporter (Figure 14A). Throughout the normalizer and the reporter region carbon and nitrogen atoms are reasonably substituted by heavy isotopes at different positions to give the same mass for up to ten isotopic variants ('isobaric') (Figure 14B).¹⁸⁷ Due to the isobaric character, pooled peptides of different samples labeled with these mass tags will give precursor ions with the same retention time and *m/z* value in the MS¹ scan. Upon collision-induced fragmentation of the precursors the bond between the mass reporter and the normalizer will be cleaved to release reporter ions separated by 0.997 u (Figure 14C).¹⁸⁷ These reporter ions enable a relative quantification of proteins contained in the samples.

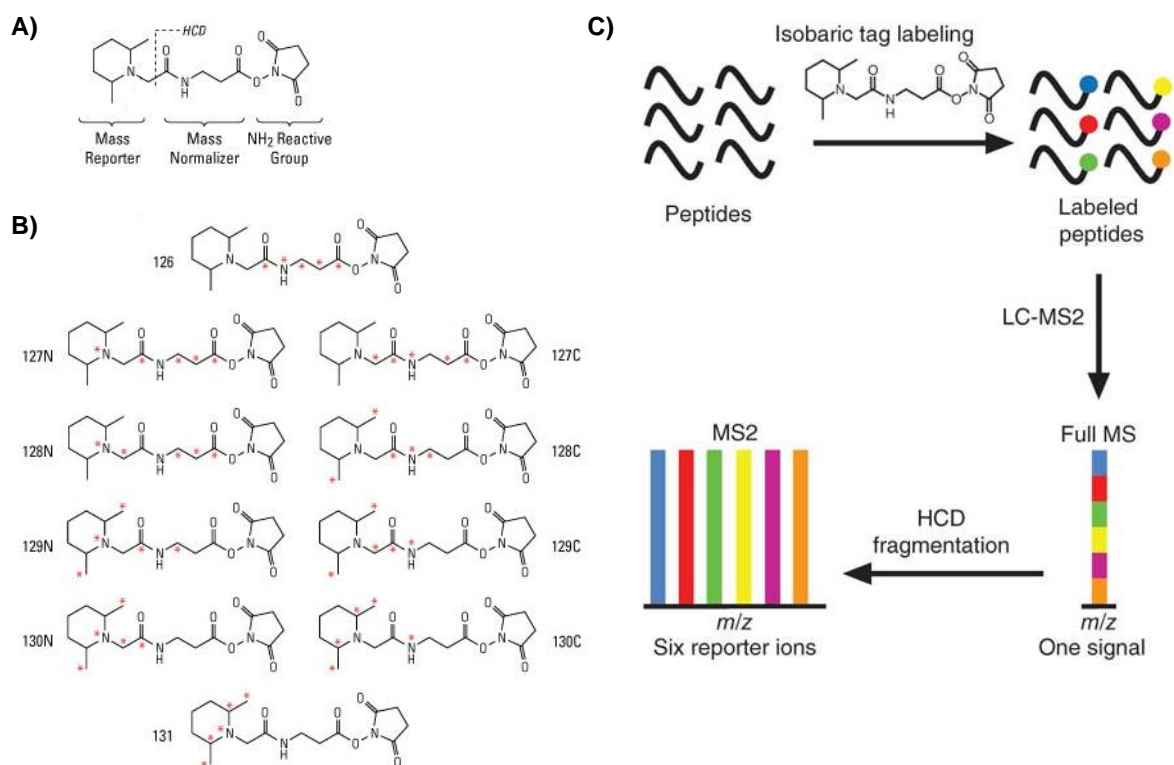


Figure 14: Relative quantification of proteome changes utilizing isobaric mass tags. (A) Generic chemical structure of an isobaric mass tag. (B) TMT10 reagents with positions at which heavy carbon or nitrogen atoms are substituted marked in red. Figures A and B adopted from the ThermoFisher Scientific website (TMT10plex™ Isobaric Label Reagent, product 90110). (C) Concept of labeling peptides from different samples with isobaric mass tags and quantification by MS² spectra. Figure adopted from *Ting, L. et al.*¹⁸⁸

Isotope labeling techniques were essential for the here presented work. It enabled comparing different compound concentrations used for the competition binding affinity enrichment experiments, different compound concentrations and temperatures in the 2D-TPP experiments, as well as for the analysis of concentration dependent degradation of mature and nascent proteins in the PROTAC experiments. In addition, it allowed for the evaluation of covalent probe binding during the establishment of new tool compounds for intracellular competition binding approaches.

1.3.Objectives

Compound attrition at late development stages of small molecule drug candidates is one of the main reasons for the increasing costs of drug discovery projects. In contrast to lysate- and recombinant protein-based assays, cellular chemoproteomics assays can assess dose-dependent engagement of endogenously expressed targets under physiologically relevant conditions. The recent clinical success of targeted covalent kinase inhibitors renewed the interest in irreversible binding mechanisms across the pharmaceutical industry and academic research.

Driven by this increasing interest in covalent inhibitors, the objective of this thesis is to investigate how well commonly applied chemoproteomic assays based on cell extracts reflect intracellular target engagement of covalent protein inhibitors. Focusing on targeted covalent inhibitors of the enzyme class of kinases, the well-established kinobeads technology, allowing the analysis of kinase engagement without the need for the labor-intensive synthesis of individually tailored probes, represents the chemoproteomic approach of choice for initially characterizing lysate-based protein binding versus target engagement in living cells. By analyzing a set of targeted covalent kinase inhibitors reacting with a homologous cysteine present in eleven different kinases with this chemoproteomic affinity enrichment approach, the differentiability of the selectivity of these molecules in lysate- and cell-based assay settings shall be elucidated. Due to the limitations of kinobeads to kinases, protein binding of targeted covalent kinase inhibitors shall also be analyzed by chemoproteomic target engagement measurement approaches not restricted to a specific target class. Comparing protein binding as determined with approaches like intracellular competition binding using bioorthogonal probes, two-dimensional thermal proteome profiling as well as multiplexed proteome dynamics profiling shall result in an evaluation of their applicability to covalent molecules. The application of targeted covalent kinase inhibitors to recently published two-dimensional thermal proteome profiling and multiplexed proteome dynamics profiling using proteolysis-targeting chimera molecules will, up to date (April 23rd, 2018), represent the first published study using these approaches for the analysis of covalent target engagement in living cells.

With this PhD study it shall be investigated if lysate- or recombinant protein-based strategies alone are sufficiently supporting the research on targeted covalent inhibitors or if cell-based analyses lead to different results regarding selectivity and potency. By this, a suitable strategy for analyzing irreversibly binding molecules shall be suggested for enabling the characterization of covalent probes which, due to their non-equilibrium binding, can represent useful tool compounds for measuring intracellular target engagement of reversible inhibitors.

2. Materials & methods

2.1. Lists of used chemicals, materials, instruments and software

Table 1: Tabular listing of used chemicals and materials

Chemical/Material	Used abbreviation	Supplier	Article no.
(+)-Sodium L-ascorbate		Sigma-Aldrich	11140-50G
(E)-cyclooct-4-en-1-yl (2,5-dioxopyrrolidin-1-yl) carbonate		Broadpharm	BP-22417
(Ethylenedinitrilo)tetraacetic acid disodium salt		Sigma-Aldrich	E7889-100ML
1 N Hydrochloric acid	HCl	Fluka	71763-1L
1-(9H-fluoren-9-yl)-3-oxo-2,7,10-trioxa-4-azatridecan-13-oic acid		ABCR	AB259679
2-(2-azidoethoxy)ethanamine		Broadpharm	BP-21611
2,2-dimethyl-4-oxo-3,8,11-trioxa-5-azatetradecan-14-oic acid		Broadpharm	BP-20627
2,5-dioxopyrrolidin-1-yl 4-azidobutanoate		Matrix Scientific	115998
2-chloroacetamide		Sigma-Aldrich	C0267
2-chloroacetyl chloride		Sigma-Aldrich	104493-5G
2-propanol		Sigma-Aldrich	59300-1L
3-(fluorosulfonyl)benzoic acid		Sigma-Aldrich	ALD00038-1G
3-mercaptopropionic acid		Sigma-Aldrich	M5801-5G
4-(fluorosulfonyl)benzoic acid		Sigma-Aldrich	224189-5G
4-12 % Bis/Tris gels		Invitrogen	diverse
5-azidopentanoic acid		PolyPeptide	AB05702
5Z-7-Oxozeaenol		Enzo Lifesciences	ALX-380-267-M005
Acalabrutinib		Cayman Chemical	19899
Acetic acid		Merck	1.00062.1000
Acetonitrile		Fisher Chemical	A/0650/PB17
Acryloyl chloride		Alfa Aesar	L10363
Afatinib		Apollo Scientific	BIFK0010
AffiniPure F(ab') ₂ Fragment Goat Anti-Human IgM		Jackson labs	109-006-129
Alkyne-Afatinib		Sigma-Aldrich	PZ0243-25MG
Ammonia solution 25%	NH ₃	Merck	1.05432.1000
Anti-BTK antibody		Santa Cruz	sc-1107
Anti-EGFR antibody		Abcam	ab2430
Anti-MAPK9 antibody		Cell signaling	4672
Anti-PARP1 antibody		Bethyl laboratories	A301-375A
Benzonase® Nuclease		Sigma-Aldrich	E1014-25KU
Blocking Buffer		LI-COR Biosciences	927-40000
Bradford reagent		Bio-Rad	5000202
Brilliant Blue G - Colloidal Concentrate		Sigma-Aldrich	B2025-1EA
Bromo-tris-pyrrolidino-phosphonium hexafluorophosphate	PyBroP	novabiochem	8.51010.0025
Bromphenol blue sodium		Sigma-Aldrich	B8026-5G
BSA standards		Bio-Rad	5000202
C18 material		Supelco	66883-U

Materials & methods

Calcium chloride dihydrate	CaCl	Merck	1.02382.1000
CellTiter-glo reagent		Promega	G7571
CGI-1640		Advanced ChemBlocks	10301
Chymotrypsin sequencing grade		Promega	V1061
CNX-774		ArkPharm	AK474037
cOmplete™, EDTA-free Protease Inhibitor Cocktail Tablets		Roche	11873580001
Copper(II) sulfate pentahydrate	CuSO ₄	Sigma-Aldrich	203165-10G
DBCO-PEG4-biotin		Sigma-Aldrich	760749
Deuterated chloroform		Sigma-Aldrich	151823-10X0.75ML
Deuterated dimethyl sulfoxide		Sigma-Aldrich	151874-25G
Deuterated methanol		Deutero	01105-25ml
Dichloromethane	DCM	Sigma-Aldrich	270997-100ML
Dimethyl formamide	DMF	Sigma-Aldrich	227056-250ML
Dimethyl sulfoxide	DMSO	Sigma-Aldrich	276855-100ML
Dithiothreitol	DTT	Biomol	4010
DMEM medium		Gibco	41965-039
Easysep™ D Magnetic Particles		Stemcell	19054
Easysep™ human B cell Enrichment Cocktail		Stemcell	19054
Endoproteinase Asp-N Sequencing Grade		Roche	11054589001
Endoproteinase Glu-C Sequencing Grade		Roche	11047817001
Endoproteinase Lys-C sequencing grade		Wako	121-05063
Ethanol	EtOH	Fisher Chemical	E/0665DF/17
Ethanolamine		Sigma-Aldrich	398136-25ML
Ethanesulfonyl fluoride		Sigma-Aldrich	746959-1G
Ethyl acetate		Fisher Chemical	E/0850/17
Fetal Bovine Serum		Gibco	10270
Fetal Bovine Serum, dialyzed		Gibco	26400-036
Fluo-4		Thermo Scientific	F14201
Formic acid		VWR Chemicals	84865.26
Glucose solution		Invitrogen	06-0033SA
Glycerol		Merck	1.04094.2500
Glycine		Arcos Organics	220910010
HEPES		Alfa Aesar	J61360
Histopaque®-1077		Sigma-Aldrich	10771
Hydroxylamine solution		Sigma-Aldrich	438227-50ML
Iodoacetamide		Sigma-Aldrich	I6125
L-Arginine		Sigma-Aldrich	A8094-25G
L-Arginine-HCl, 13C6, 15N4 for SILAC		Thermo Scientific	88434
LDS sample buffer		NuPAGE	NP0007
L-Glutamine		Gibco	25030-032
LI-COR IRDye 680 anti-goat		LI-COR Biosciences	925-68074
LI-COR IRDye 680 rabbit		LI-COR Biosciences	925-68071
LI-COR IRDye 800 anti-goat		LI-COR Biosciences	925-32214
LI-COR IRDye 800 rabbit		LI-COR Biosciences	925-32211
L-Lysine		Sigma-Aldrich	L9037-25G

L-Lysine-13C6,15N2 hydrochloride		Sigma-Aldrich	608041-1G
Magnesium chloride solution	MgCl ₂	Sigma-Aldrich	M1028-100ML
Magnetic beads 1		GE Healthcare	Sera-Mag 45152105050250
Magnetic beads 2		GE Healthcare	Sera-Mag 65152105050250
Methanol	MeOH	Honeywell	10300019
MitoCheck® Complex I Activity Assay Kit		Cayman Chemical	700930
Mitochondria Isolation Kit for Cultured Cells		Thermo Scientific	89874
MOPS SDS Running buffer (20X)		Novex	NP0001
N,N-Diisopropylethylamine	DIPEA	Sigma-Aldrich	496219-100ML
NeutrAvidin™ beads		Thermo Scientific	29202
NHS-activated Sepharose® 4 Fast Flow		GE Healthcare	17-0906-02
O-(7-Azabenzotriazol-1-yl)-N,N,N',N'-tetramethyluronium hexafluorophosphate	HATU	Bachem	Q-2780
Octylphenoxypolyethoxyethanol	IGEPAL CA-630	Sigma-Aldrich	I3021-500ML
Phenol Red Solution		Invitrogen	06-0034SA
Phosphate-Buffered Saline		Gibco	14190-094
Piperidine		Sigma-Aldrich	104094-100ML
Pluronic® F-127 powder		Thermo Scientific	F-127
Polyoxyethylene (20) sorbitan monolaurate	Tween-20	Sigma-Aldrich	P1379-500ML
Propionyl chloride		Alfa Aesar	A10940
Recombinant ACAD9		Abnova	H00028976-P01
Recombinant MAPK9		SGC	
Recombinant TEC		Sigma-Aldrich	SRP5090
Recombinant ZAK		Thermo Scientific	PR7052A
Rotenone		Sigma-Aldrich	45656-250MG
RPMI-1640 medium		Gibco	21875-034
SCX material		Supelco	66889-U
SDS PAGE protein marker 1-color		LI-COR Biosciences	928-40000
SDS PAGE protein marker unstained		Bio-Rad	161-0363
SILAC RPMI		Gibco	A24942-01
Sodium chloride	NaCl	Sigma-Aldrich	S5150-1L
Sodium dodecyl sulfate (20 % w/v)	SDS	Bio-Rad	161-0418
Sodium fluoride	NaF	Sigma-Aldrich	S7920
Sodium hydroxide	NaOH	Sigma-Aldrich	367176-500G
Sodium orthovanadate	Na ₃ VO ₄	Sigma-Aldrich	S6508-50G
Tanzisertib		ArkPharm	ArkPharm AK545582
Tert-Butanol		Sigma-Aldrich	471712-100ML
Tetrazine-Cy5		Jena Bioscience	CLK-015-05
TMT label		Thermo Scientific	90406
Triethylamine	NEt ₃	Sigma-Aldrich	T0886-100ML
Triethylammonium bicarbonate buffer	TEAB	Sigma-Aldrich	T7408-100ML
Trifluoroacetic acid	TFA	Sigma-Aldrich	302031-100ML

Tris / HCl		Sigma-Aldrich	93313-1L
Tris base		Sigma-Aldrich	T1503-1KG
Tris(2-carboxyethyl)phosphine hydrochloride	TCEP	Sigma-Aldrich	75259-10G
Tris(3-hydroxypropyltriazolylmethyl)amine	THPTA	Sigma-Aldrich	762342-100MG
Triton™ X-100		Sigma-Aldrich	T9284-100ML
Trypsin sequencing grade		Promega	V511A
Trypsin/0.05 % EDTA		Gibco	25300-054
Urea		Sigma-Aldrich	U4884-500G
Versene solution		Gibco	15040-033
Water for HPLC gradient		Fisher Chemical	W/0120/PB17

Table 2: Tabular listing of used instruments

Instrument	Manufacturer	Name
96-well MTP washer	Thermo Scientific	Matrix Wellmate
Cell analyzer	BD	FACSCalibur
Cell counter	Innovatis	Casy
Cell incubator	Hera	Cell 240
Cell ruptor	Omni Inc	Bead Ruptor 24
Centrifuge 1	Eppendorf	Centrifuge 5415D, rotor: F45-24-11
Centrifuge 2	Thermo Scientific	Multifuge3 S-R, rotor: 6445
Centrifuge 3	Thermo Scientific	Megafuge 40, rotor: 75003607
Centrifuge 4	Thermo Scientific	Multifuge X3R, rotor: TX-1000
Heating stirrer	Heidolph	MR3003
High vacuum system	CHRIST	Alpha 2-4 LDplus
Horizontal shaker 1	BioShake	XP
Horizontal shaker 2	Heidolph	Titramax 1000
Infrared Imager	LI-COR	Odyssey Infrared Imager CLx
HPLC-MS system (For compound analyses and preparative runs)	Waters	Autopurification system with detectors: 3100 Mass Detector, 2996 Photodiode Array Detector
LC-MS/MS system 1	Thermo Scientific Eksigent	Orbitrap XL 1D+ nano-LC system
LC-MS/MS system 2/3	Thermo Scientific Thermo Scientific	Q Exactive (Plus) UltiMate 3000 RSLCnano
LC-MS/MS system 4	Thermo Scientific Thermo Scientific	Orbitrap Fusion Lumos UltiMate 3000 RSLCnano
Liquid chromatography system	Biotage	Isolera Spektra Four with RP column: SNAP Cartridge KP-C18-HS 12 g
Microscope	Olympus	IX70 Fluorescence Microscope
Multiplate reader	Envision	2103 Multilabel Reader
Overhead shaker	Scientific Industries	RotoShake Genie
PCR machine	Agilent Technologies	SureCycler 8800
PCR plates	Axygen	PCR-96-HS-AC-C
pH-meter	SI Analytics	ProLab 3000
Rocking shaker	CAT	ST5

Rotary evaporator system	BUCHI	Rotavapor R-124 with waterbath B-480
Scale	KERN	ABJ
Spec Vac system	UniEquip	Univapo 150 ECH
Thermomixer	Eppendorf	Thermomixer comfort
Ultra centrifuge 1	Sorvall	Discovery 90SE, rotor: Beckman Coulter Type 50.2 Ti
Ultra centrifuge 2	Beckman Coulter	Optima Max XP, rotors: TLA100, TLA120.2
Ultrasonic bath	BANDELIN	SONOREX RK100H
Vortex mixer	Scientific Industries	Vortex Genie 2
Zeba Spin Desalting columns	Thermo Scientific	89882
Zeba Spin Desalting plates	Thermo Scientific	89807

Table 3: Tabular listing of used analysis and visualization software

Software

CambridgeSoft ChemBioOffice 2010

GraphPad Prism 7.03

Tibco Spotfire 7.0.1

Mestrelab Research MestReNova 12.0.1-20560

BIOVIA Discovery Studio Visualizer 16.1.0.15350

Venny 2.1 (*Oliveros, J.C. (2007-2015) Venny. An interactive tool for comparing lists with Venn's diagrams. <http://bioinfogp.cnb.csic.es/tools/venny/index.html>*)

GORilla - Gene Ontology enRIchment anaLysis and visualiZAtion tool (*Eden, E., Navon, R., Steinfeld, I., Lipson, D., and Z. Yakhini. "GORilla: A Tool For Discovery And Visualization of Enriched GO Terms in Ranked Gene Lists", BMC Bioinformatics 2009, 10:48. <http://cbl-gorilla.cs.technion.ac.il/>*)

2.2. Chemistry

All commercial solvents, reagents and building blocks are of reagent grade and were used as received without further purification unless otherwise specified.

Flash column chromatography was performed using a Biotage Isolera four purification system using Biotage flash silica cartridges.

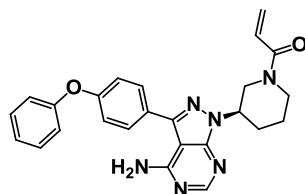
Preparative mass directed high performance liquid chromatography (preparative HPLC) was done on a XBridge BEH C18 OBD 5 μm Prep Column (19 x 150 mm) at a flow rate of 30 ml/min, eluting with acetonitrile in water (0.2 % (v/v) formic acid as modifier). Purifications were conducted on a waters autopurification system [detectors: 3100 Mass Detector and a 2996 Photodiode Array Detector].

Analytical HPLC was done on a Waters XBridge BEH C18 5 μm Column (4.6 x 150 mm) at a flow rate of 1.75 ml/min with a linear gradient over 9 min (1 to 99 % (v/v) acetonitrile in water, 0.2 % (v/v) formic acid as modifier). The instrument used for analysis was a waters autopurification system [detectors: 3100 Mass Detector and a 2996 Photodiode Array Detector].

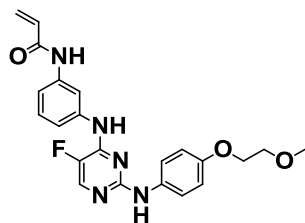
Analytical UPLC was done on a Waters Acquity BEH C18 1.7 μm Column (2.1 x 50 mm) at 40 °C and a flow rate of 0.5 ml/min with a linear gradient over 4 min (5 to 100 % acetonitrile in water, 0.2 % formic acid as modifier). The instrument used for analysis was a Waters Acquity system [detectors: Acquity SQD and Acquity PDA].

If not stated otherwise, the purity of all final compounds was 95 % or higher as determined by LC MS (UV_{256nm}) using the analytical HPLC or UPLC.

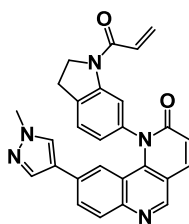
Proton (¹H) NMR spectra were recorded on a Bruker Avance 400 spectrometer (400 MHz) using the indicated deuterated solvent. Chemical shifts are given in parts per million (ppm) (δ relative to residual solvent peak for ¹H).

(R)-1-(3-(4-amino-3-(4-phenoxyphenyl)-1H-pyrazolo[3,4-d]pyrimidin-1-yl)piperidin-1-yl)prop-2-en-1-one (Ibrutinib)

Ibrutinib was synthesized by colleagues at Cellzome / GlaxoSmithKline and generously provided by the company.

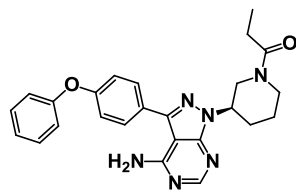
N-(3-((5-fluoro-2-((4-(2-methoxyethoxy)phenyl)amino)pyrimidin-4-yl)amino)phenyl)acrylamide (CC-292)

CC-292 was synthesized by colleagues at Cellzome / GlaxoSmithKline and generously provided by the company.

1-(1-acryloylindolin-6-yl)-9-(1-methyl-1H-pyrazol-4-yl)benzo[h][1,6]naphthyridin-2(1H)-one (QL47)

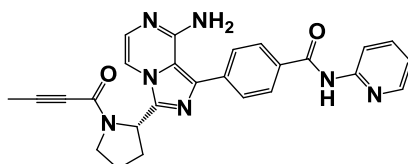
QL47 was synthesized by colleagues at Cellzome / GlaxoSmithKline and generously provided by the company.

(R)-1-(3-(4-amino-3-(4-phenoxyphenyl)-1H-pyrazolo[3,4-d]pyrimidin-1-yl)piperidin-1-yl)propan-1-one (Saturated Ibrutinib)



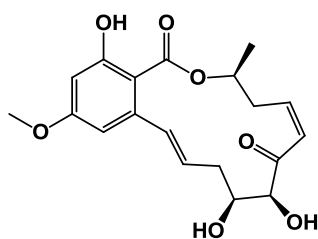
Saturated Ibrutinib was synthesized by colleagues at Cellzome / GlaxoSmithKline and generously provided by the company.

(S)-4-(8-amino-3-(1-(but-2-ynoyl)pyrrolidin-2-yl)imidazo[1,5-a]pyrazin-1-yl)-N-(pyridin-2-yl)benzamide (Acalabrutinib)



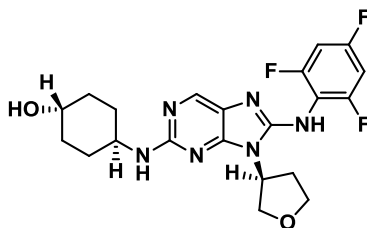
Acalabrutinib was purchased from Cayman Chemical (Product ID: 19899; Lot #: N/A)

(3S,5Z,8S,9S,11E)-8,9,16-trihydroxy-14-methoxy-3-methyl-3,4,9,10-tetrahydro-1H-benzo[c][1]oxacyclotetradecine-1,7(8H)-dione (5Z-7-Oxozeaenol)



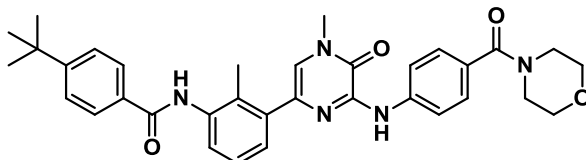
5Z-7-Oxozeaenol was purchased from Enzo Lifesciences (Product ID: ALX-380-267-M005; Lot #: 01021509)

(1S,4r)-4-((9-((S)-tetrahydrofuran-3-yl)-8-((2,4,6-trifluorophenyl)amino)-9H-purin-2-yl)amino)cyclohexanol (CC-930 / Tanzisertib)



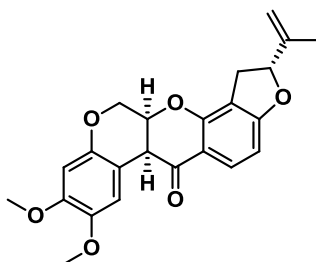
CC-930 was purchased from ArkPharm (Product ID: AK545582; Lot #: YF0629260-170807001)

4-(tert-butyl)-N-(2-methyl-3-(4-methyl-6-((4-(morpholine-4-carbonyl)phenyl)amino)-5-oxo-4,5-dihydropyrazin-2-yl)phenyl)benzamide (CGI-1746)



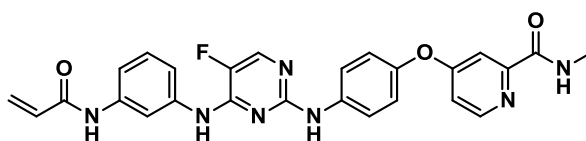
CGI-1746 was purchased from Advanced ChemBlocks (Product ID: 10301; Lot #: 10061)

(S)-4-(8-amino-3-(1-(but-2-ynoyl)pyrrolidin-2-yl)imidazo[1,5-a]pyrazin-1-yl)-N-(pyridin-2-yl)benzamide (Rotenone)

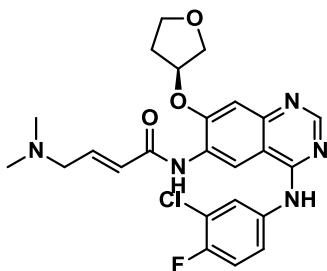


Rotenone was purchased from Sigma Aldrich (Product ID: 45656-250MG; Lot #: BCBS4281V)

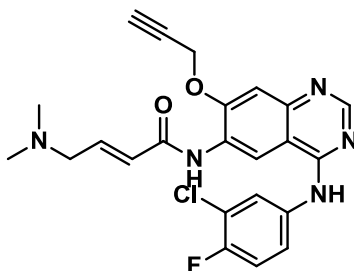
4-(4-((4-((3-acrylamidophenyl)amino)-5-fluoropyrimidin-2-yl)amino)phenoxy)-N-methylpicolinamide (CNX-774)



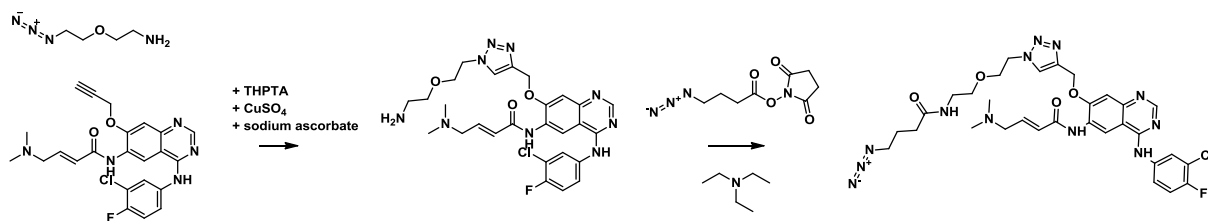
CNX-774 was purchased from ArkPharm (Product ID: AK474037; Lot #: n/a)

(S,E)-N-(4-((3-chloro-4-fluorophenyl)amino)-7-((tetrahydrofuran-3-yl)oxy)quinazolin-6-yl)-4-(dimethylamino)but-2-enamide (Afatinib)

Afatinib was purchased from Apollo Scientific (Product ID: BIFK0010; Lot #: AS455715)

(E)-N-(4-((3-chloro-4-fluorophenyl)amino)-7-(prop-2-yn-1-yloxy)quinazolin-6-yl)-4-(dimethylamino)but-2-enamide (Alkyne-Afatinib)

Alkyne-Afatinib was purchased from Sigma Aldrich (Product ID: PZ0243-25MG; Lot #: 124M4711V)

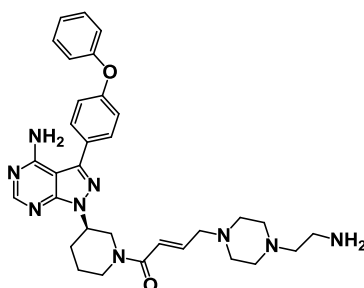
(E)-N-(7-((1-(2-(2-(4-azidobutanamido)ethoxy)ethyl)-1H-1,2,3-triazol-4-yl)methoxy)-4-((3-chloro-4-fluorophenyl)amino)quinazolin-6-yl)-4-(dimethylamino)but-2-enamide (Azide-incorporating Afatinib)

To a solution of (E)-N-(4-((3-chloro-4-fluorophenyl)amino)-7-(prop-2-yn-1-yloxy)quinazolin-6-yl)-4-(dimethylamino)but-2-enamide (10 mg, 0.022 mmol) in DMSO 2-(2-(2-(4-azidoethoxy)ethanamine) (3 μ l, 0.022 mmol), THPTA (176 μ l of a 250 mM solution in H₂O, 0.044 mmol), and CuSO₄ (220 μ l of a 100 mM solution in H₂O, 0.022 mmol), and sodium ascorbate (440 μ l of a 250 mM solution in H₂O, 0.11 mmol) were added. The reaction was stirred at room temperature for 2 h and then purified by preparative HPLC without any further work-up. For this, the whole reaction was aliquoted into 0.75 ml fractions which were individually injected onto the column. The purified product from each fraction

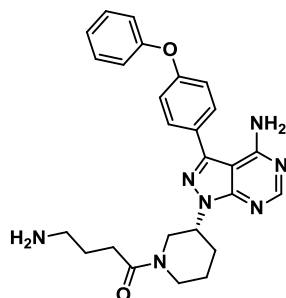
were combined and dried on high vacuum. This afforded (E)-N-(7-((1-(2-(2-aminoethoxy)ethyl)-1H-1,2,3-triazol-4-yl)methoxy)-4-((3-chloro-4-fluorophenyl)amino)quinazolin-6-yl)-4-(dimethylamino)but-2-enamide (2.5 mg, 0.004 mmol, 18 % yield). UPLC-MS (ESI, m/z): $t_R = 0.94$ min, 584.2 (M+H)⁺.

In the next step, to a solution of (E)-N-(7-((1-(2-(2-aminoethoxy)ethyl)-1H-1,2,3-triazol-4-yl)methoxy)-4-((3-chloro-4-fluorophenyl)amino)quinazolin-6-yl)-4-(dimethylamino)but-2-enamide (11.5 mg, 0.02 mmol) in 450 μ l DMSO 2,5-dioxopyrrolidin-1-yl 4-azidobutanoate (7.2 mg, 0.032 mmol), and triethylamine (8 μ l, 0.057 mmol) were added. The reaction was stirred at room temperature for 1 h and then purified by preparative HPLC without any further work-up. For this, the whole reaction was aliquoted into 0.75 ml fractions which were individually injected onto the column. The purified product from each fraction were combined and dried on high vacuum. This afforded (E)-N-(7-((1-(2-(2-(4-azidobutanamido)ethoxy)ethyl)-1H-1,2,3-triazol-4-yl)methoxy)-4-((3-chloro-4-fluorophenyl)amino)quinazolin-6-yl)-4-(dimethylamino)but-2-enamide (3.9 mg, 0.005 mmol, 27 % yield). ¹H NMR (400 MHz, DMSO-*d*₆) δ 9.82 (s, 1H), 9.63 (s, 1H), 8.90 (s, 1H), 8.53 (s, 1H), 8.28 (s, 1H), 8.13 (dd, *J* = 6.7, 2.5 Hz, 1H), 7.89 (s, 1H), 7.80 (d, *J* = 9.0 Hz, 1H), 7.54 (s, 1H), 7.42 (t, *J* = 9.0 Hz, 1H), 6.84 – 6.72 (m, 1H), 6.54 (d, *J* = 15.4 Hz, 1H), 5.44 (s, 2H), 4.55 (t, *J* = 5.2 Hz, 2H), 3.85 – 3.73 (m, 2H), 3.40 (d, *J* = 5.8 Hz, 2H), 3.27 (t, *J* = 6.8 Hz, 2H), 3.19 – 3.12 (m, 2H), 3.06 (d, *J* = 6.0 Hz, 2H), 2.54 (s, 6H), 2.12 (t, *J* = 7.4 Hz, 3H), 1.70 (p, *J* = 7.1 Hz, 2H). HPLC-MS (ESI, m/z): $t_R = 4.07$ min, 695.3 (M+H)⁺.

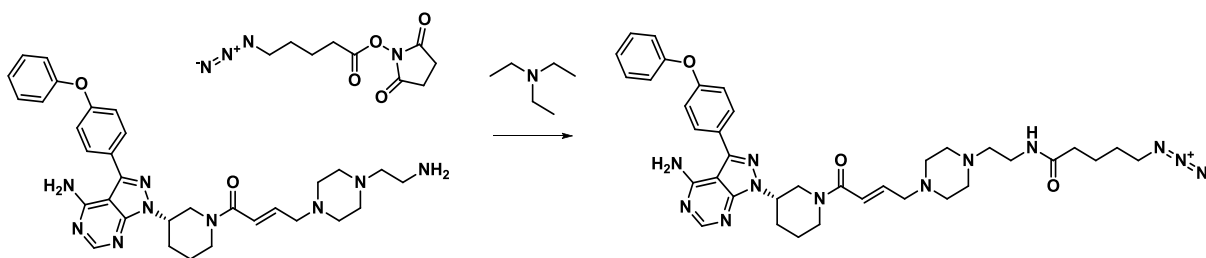
(R,E)-1-(3-(4-amino-3-(4-phenoxyphenyl)-1H-pyrazolo[3,4-d]pyrimidin-1-yl)piperidin-1-yl)-4-(4-(2-aminoethyl)piperazin-1-yl)but-2-en-1-one (Linkable Ibrutinib)



Linkable Ibrutinib was synthesized by colleagues at Cellzome / GlaxoSmithKline and generously provided by the company.

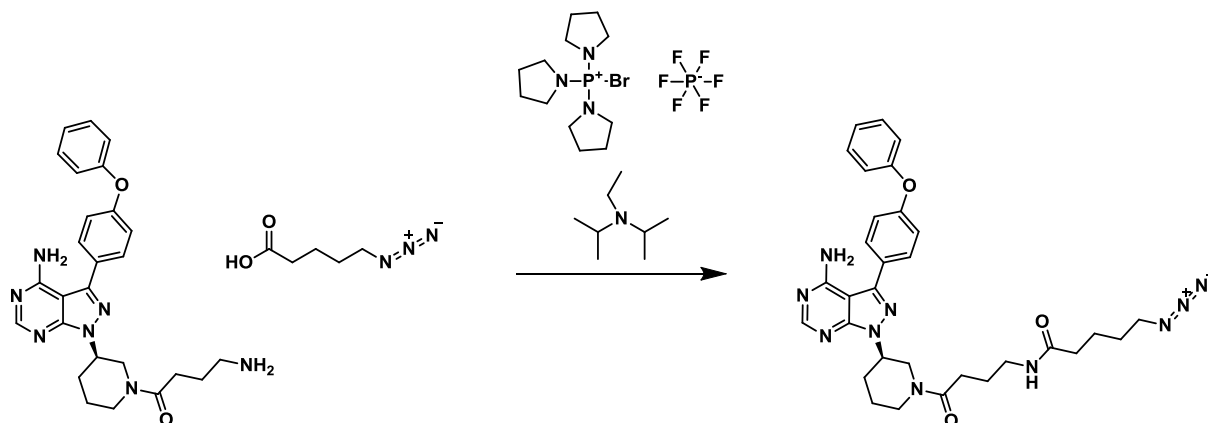
(R)-4-amino-1-(3-(4-amino-3-(4-phenoxyphenyl)-1H-pyrazolo[3,4-d]pyrimidin-1-yl)piperidin-1-yl)butan-1-one (Linkable saturated Ibrutinib)

Linkable saturated Ibrutinib was synthesized by colleagues at Cellzome / GlaxoSmithKline and generously provided by the company.

(R,E)-N-(2-(4-(4-(3-(4-amino-3-(4-phenoxyphenyl)-1H-pyrazolo[3,4-d]pyrimidin-1-yl)piperidin-1-yl)but-2-en-1-yl)piperazin-1-yl)ethyl)-5-azidopentanamide (Azide-incorporating Ibrutinib)

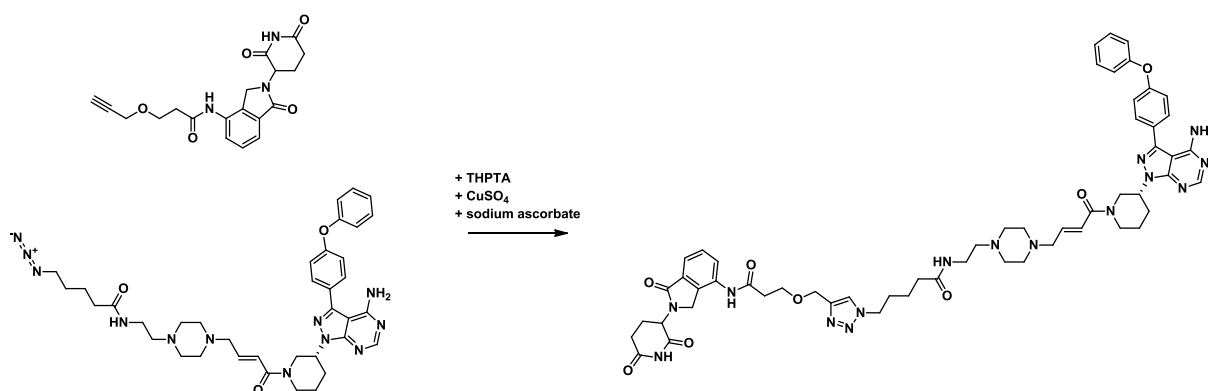
An azide-incorporating analogue of Ibrutinib was synthesized by coupling 5-azidopentanoic acid to linkable Ibrutinib. For this, a solution of (R,E)-1-(3-(4-amino-3-(4-phenoxyphenyl)-1H-pyrazolo[3,4-d]pyrimidin-1-yl)piperidin-1-yl)-4-(4-(2-aminoethyl)piperazin-1-yl)but-2-en-1-one (13.5 mg, 0.02 mmol), 2,5-dioxopyrrolidin-1-yl 5-azidopentanoate (7 mg, 0.03 mmol), and triethylamine (8.1 μ l, 0.06 mmol) in DMF (405 μ l) was stirred at RT for 1 h. The product was purified by preparative HPLC without any further work-up. For this, the whole reaction was aliquoted into 0.75 ml fractions which were individually injected onto the column. The purified product from each fraction were combined and dried on high vacuum. This afforded (R,E)-N-(2-(4-(4-(3-(4-amino-3-(4-phenoxyphenyl)-1H-pyrazolo[3,4-d]pyrimidin-1-yl)piperidin-1-yl)but-2-en-1-yl)piperazin-1-yl)ethyl)-5-azidopentanamide (5.5 mg, 0.008 mmol, 40 % yield). ^1H NMR (400 MHz, Chloroform-*d*) δ 8.35 (d, J = 9.5 Hz, 2H), 7.64 (d, J = 8.3 Hz, 2H), 7.39 (t, J = 7.7 Hz, 2H), 7.17 (dd, J = 14.3, 7.8 Hz, 3H), 7.08 (d, J = 8.0 Hz, 2H), 6.77 (d, J = 18.2 Hz, 1H), 6.44 (dd, J = 39.3, 15.3 Hz, 1H), 5.78 (s, 2H), 4.85 (s, 2H), 4.51 (d, J = 13.4 Hz, 1H), 4.07 (dd, J = 45.3, 13.6 Hz, 2H), 3.80 (t, J = 11.8 Hz, 1H), 3.52 (s, 2H), 3.38 (d, J = 12.6 Hz, 1H), 3.28 (s, 2H), 3.21 (d, J = 17.0 Hz, 2H), 2.96 (s, 1H), 2.79 (d, J = 35.8 Hz, 4H), 2.67 (s, 4H), 2.48 – 2.30 (m, 2H), 2.25 (d, J = 8.7 Hz, 3H), 2.01 (s, 1H). UPLC-MS (ESI, m/z): t_R = 1.85 min, 706.0 (M+H) $^+$.

(R)-N-(4-(3-(4-amino-3-(4-phenoxyphenyl)-1H-pyrazolo[3,4-d]pyrimidin-1-yl)piperidin-1-yl)-4-oxobutyl)-5-azidopentanamide (Azide-incorporating saturated Ibrutinib)



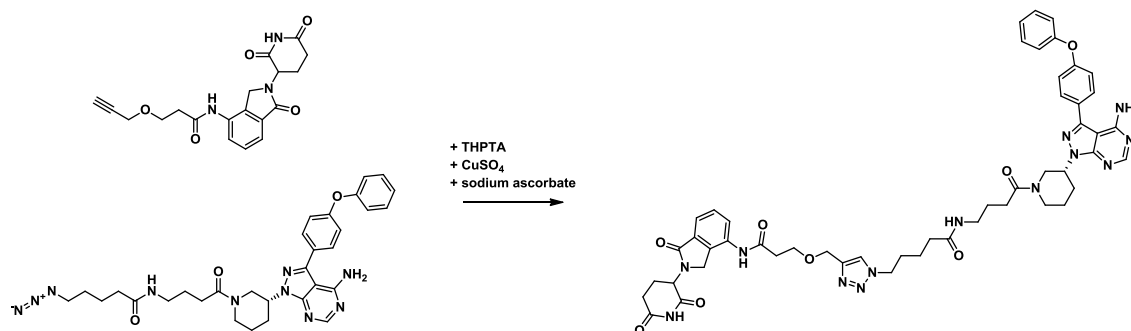
An azide-incorporating analogue of saturated Ibrutinib was synthesized by coupling 5-azidopentanoic acid to linkable saturated Ibrutinib. For this, a solution of (R,E)-1-(3-(4-amino-3-(4-phenoxyphenyl)-1H-pyrazolo[3,4-d]pyrimidin-1-yl)piperidin-1-yl)-4-(4-(2-aminoethyl)piperazin-1-yl)but-2-en-1-one (10 mg, 0.02 mmol), 5-azidopentanoic acid (7 mg, 0.05 mmol, 7 μ l), PyBrOP (37 mg, 0.08 mmol) and DIPEA (25 μ l, 0.14 mmol) in DMF (400 μ l) was stirred at room temperature, overnight. The product was purified by preparative HPLC without any further work-up. For this, the whole reaction was aliquoted into 0.75 ml fractions which were individually injected onto the column. The purified product from each fraction were combined and dried on high vacuum. This afforded (R)-N-(4-(3-(4-amino-3-(4-phenoxyphenyl)-1H-pyrazolo[3,4-d]pyrimidin-1-yl)piperidin-1-yl)-4-oxobutyl)-5-azidopentanamide (8.9 mg, 0.013 mmol, 68 % yield). ¹H NMR (400 MHz, DMSO-*d*₆) δ 8.26 (d, *J* = 8.4 Hz, 1H), 7.84 (t, *J* = 5.7 Hz, 1H), 7.76 (t, *J* = 5.6 Hz, 1H), 7.67 (dt, *J* = 8.6, 2.4 Hz, 2H), 7.48 – 7.40 (m, 2H), 7.24 – 7.10 (m, 5H), 4.82 – 4.70 (m, 1H), 4.70 – 4.60 (m, 1H), 4.59 – 4.45 (m, 1H), 4.26 (d, *J* = 12.9 Hz, 1H), 4.08 – 3.96 (m, 1H), 3.87 (d, *J* = 13.5 Hz, 1H), 3.65 – 3.52 (m, 1H), 3.27 (t, *J* = 6.3 Hz, 1H), 3.17 – 2.99 (m, 4H), 2.90 – 2.74 (m, 1H), 2.37 (q, *J* = 7.4 Hz, 2H), 2.25 (td, *J* = 14.1, 12.6, 7.7 Hz, 2H), 2.10 (t, *J* = 6.8 Hz, 2H), 2.04 (t, *J* = 6.8 Hz, 1H), 1.89 (t, *J* = 16.6 Hz, 1H), 1.65 (q, *J* = 7.2 Hz, 2H), 1.57 – 1.44 (m, 5H). UPLC-MS (ESI, *m/z*): *t*_R = 2.26 min, 596.3 (M+H)⁺.

(E)-N-(2-(4-(4-(3-(4-amino-3-(4-phenoxyphenyl)-1H-pyrazolo[3,4-d]pyrimidin-1-yl)piperidin-1-yl)-4-oxobut-2-en-1-yl)piperazin-1-yl)ethyl)-5-(4-(((3-((2-(2,6-dioxopiperidin-3-yl)-1-oxoisindolin-4-yl)amino)-3-oxopropoxy)methyl)-1H-1,2,3-triazol-1-yl)pentanamide (Ibrutinib-PROTAC)



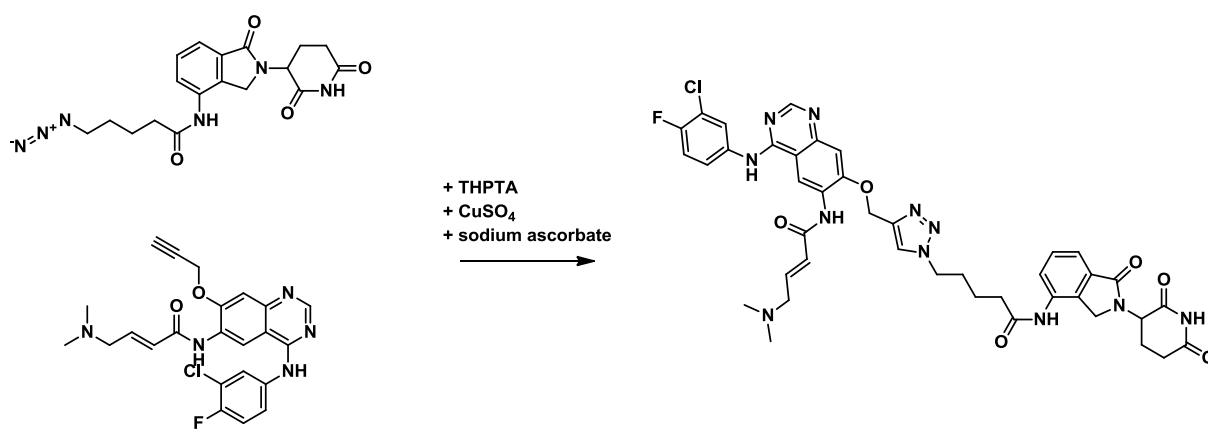
To a solution of (R,E)-N-(2-(4-(4-(3-(4-amino-3-(4-phenoxyphenyl)-1H-pyrazolo[3,4-d]pyrimidin-1-yl)piperidin-1-yl)-4-oxobut-2-en-1-yl)piperazin-1-yl)ethyl)-5-azidopentanamide (2.5 mg, 3.54 μ mol) and N-(2-(2,6-dioxopiperidin-3-yl)-1-oxoisindolin-4-yl)-3-(prop-2-yn-1-yloxy)propanamide (1.3 mg, 3.54 μ mol) in 142 μ l DMSO 71 μ l tert-Butanol, THPTA (28 μ l of a 50 mM solution in H₂O, 1.42 μ mol), and CuSO₄ (7 μ l of a 100 mM solution in H₂O, 0.71 μ mol), and sodium ascorbate (18 μ l of a 200 mM solution in H₂O, 3.54 μ mol) were added. The reaction was stirred at room temperature for 1 h and then purified by preparative HPLC without any further work-up. For this, the whole reaction was aliquoted into 0.75 ml fractions which were individually injected onto the column. The purified product from each fraction were combined and dried on high vacuum. This afforded (E)-N-(2-(4-(4-(3-(4-amino-3-(4-phenoxyphenyl)-1H-pyrazolo[3,4-d]pyrimidin-1-yl)piperidin-1-yl)-4-oxobut-2-en-1-yl)piperazin-1-yl)ethyl)-5-(4-(((3-((2-(2,6-dioxopiperidin-3-yl)-1-oxoisindolin-4-yl)amino)-3-oxopropoxy)methyl)-1H-1,2,3-triazol-1-yl)pentanamide (2.7 mg, 2.51 μ mol, 71 % yield). ¹H NMR (400 MHz, DMSO-*d*₆) δ 11.04 (s, 1H), 9.87 (s, 1H), 8.26 (s, 1H), 8.08 (s, 1H), 7.81 (d, *J* = 7.1 Hz, 1H), 7.73 (s, 1H), 7.66 (s, 2H), 7.54 – 7.47 (m, 2H), 7.44 (t, *J* = 7.9 Hz, 2H), 7.24 – 7.03 (m, 5H), 6.64 (d, *J* = 11.2 Hz, 1H), 6.46 (s, 1H), 5.15 (dd, *J* = 13.4, 5.1 Hz, 1H), 4.74 (s, 1H), 4.53 (s, 2H), 4.39 – 4.24 (m, 3H), 4.08 (s, 1H), 3.75 (t, *J* = 6.4 Hz, 2H), 3.12 (s, 3H), 2.91 (d, *J* = 12.1 Hz, 2H), 2.63 (s, 2H), 2.42 – 2.21 (m, 9H), 2.08 (t, *J* = 7.4 Hz, 4H), 1.77 (s, 2H), 1.58 (s, 2H), 1.43 (s, 2H). UPLC-MS (ESI, *m/z*): *t*_R = 1.76 min, 1076.5 (M+H)⁺.

N-(4-(3-(4-amino-3-(4-phenoxyphenyl)-1H-pyrazolo[3,4-d]pyrimidin-1-yl)piperidin-1-yl)-4-oxobutyl)-5-(4-((3-((2-(2,6-dioxopiperidin-3-yl)-1-oxoisoindolin-4-yl)amino)-3-oxopropoxy)methyl)-1H-1,2,3-triazol-1-yl)pentanamide (Saturated Ibrutinib-PROTAC)



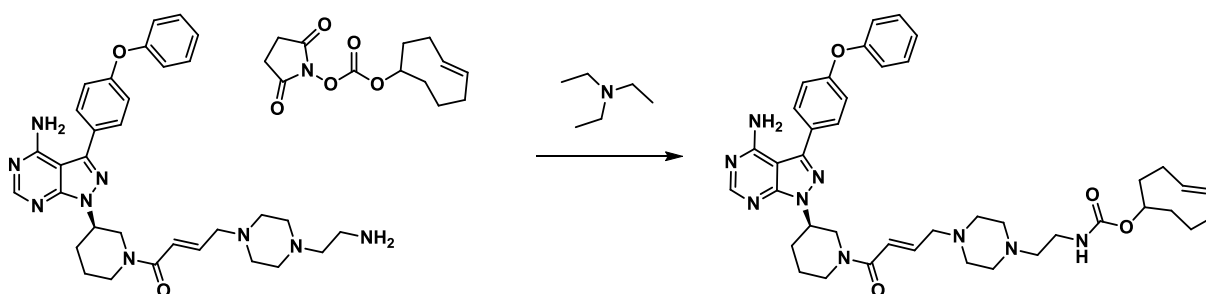
To a solution of (R)-N-(4-(3-(4-amino-3-(4-phenoxyphenyl)-1H-pyrazolo[3,4-d]pyrimidin-1-yl)piperidin-1-yl)-4-oxobutyl)-5-azidopentanamide (5.4 mg, 9.05 μmol) and N-(2-(2,6-dioxopiperidin-3-yl)-1-oxoisoindolin-4-yl)-3-(prop-2-yn-1-yloxy)propanamide (3.3 mg, 3.54 μmol) in 362 μl DMSO 181 μl tert-Butanol, THPTA (72 μl of a 50 mM solution in H₂O, 3.62 μmol), and CuSO₄ (18 μl of a 100 mM solution in H₂O, 1.81 μmol), and sodium ascorbate (45 μl of a 200 mM solution in H₂O, 9.05 μmol) were added. The reaction was stirred at room temperature for 1 h and then purified by preparative HPLC without any further work-up. For this, the whole reaction was aliquoted into 0.75 ml fractions which were individually injected onto the column. The purified product from each fraction were combined and dried on high vacuum. This afforded N-(4-(3-(4-amino-3-(4-phenoxyphenyl)-1H-pyrazolo[3,4-d]pyrimidin-1-yl)piperidin-1-yl)-4-oxobutyl)-5-(4-((3-((2-(2,6-dioxopiperidin-3-yl)-1-oxoisoindolin-4-yl)amino)-3-oxopropoxy)methyl)-1H-1,2,3-triazol-1-yl)pentanamide (4.7 mg, 4.87 μmol , 54 % yield). ¹H NMR (400 MHz, DMSO-*d*₆) δ 11.04 (s, 1H), 9.87 (s, 1H), 8.26 (d, *J* = 7.9 Hz, 1H), 8.07 (d, *J* = 12.5 Hz, 1H), 7.89 – 7.73 (m, 2H), 7.66 (dd, *J* = 8.7, 3.1 Hz, 2H), 7.55 – 7.48 (m, 2H), 7.44 (ddd, *J* = 8.5, 6.4, 2.6 Hz, 2H), 7.25 – 7.09 (m, 5H), 5.15 (dd, *J* = 13.3, 5.1 Hz, 1H), 4.74 (s, 1H), 4.61 (d, *J* = 10.9 Hz, 1H), 4.53 (d, *J* = 6.1 Hz, 2H), 4.33 (dd, *J* = 17.5, 9.4 Hz, 4H), 4.02 (d, *J* = 13.3 Hz, 1H), 3.86 (d, *J* = 13.5 Hz, 1H), 3.75 (d, *J* = 3.0 Hz, 2H), 3.15 – 2.87 (m, 5H), 2.63 (d, *J* = 6.1 Hz, 2H), 2.45 – 2.16 (m, 5H), 2.09 (t, *J* = 7.3 Hz, 2H), 2.03 (q, *J* = 7.3 Hz, 2H), 1.87 (s, 1H), 1.75 (dt, *J* = 16.5, 7.9 Hz, 2H), 1.66 – 1.54 (m, 3H), 1.42 (dt, *J* = 20.5, 7.5 Hz, 2H). UPLC-MS (ESI, *m/z*): *t_R* = 2.00 min, 966.4 (M+H)⁺.

(E)-5-(4-(((4-((3-chloro-4-fluorophenyl)amino)-6-(4-(dimethylamino)but-2-enamido)quinazolin-7-yl)oxy)methyl)-1H-1,2,3-triazol-1-yl)-N-(2-(2,6-dioxopiperidin-3-yl)-1-oxoisindolin-4-yl)pentanamide (Afatinib-PROTAC)



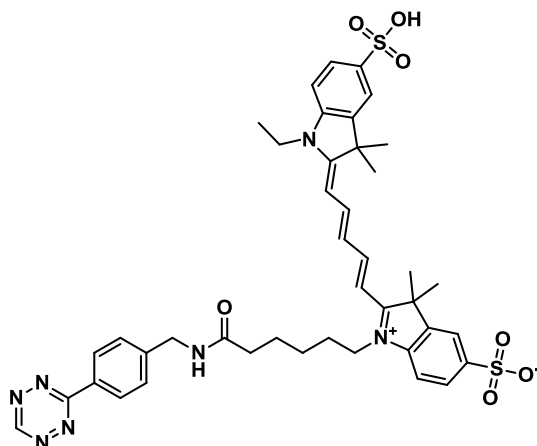
To a solution of (E)-N-(4-((3-chloro-4-fluorophenyl)amino)-7-(prop-2-yn-1-yloxy)quinazolin-6-yl)-4-(dimethylamino)but-2-enamide (10.3 mg, 0.023 mmol) and 5-azido-N-(2-(2,6-dioxopiperidin-3-yl)-1-oxoisindolin-4-yl)pentanamide (8.8 mg, 0.023 mmol) in 908 μ l DMSO 454 μ l tert-Butanol, THPTA (182 μ l of a 50 mM solution in H₂O, 9.08 μ mol), and CuSO₄ (45 μ l of a 100 mM solution in H₂O, 4.54 μ mol), and sodium ascorbate (113 μ l of a 200 mM solution in H₂O, 0.023 μ mol) were added. The reaction was stirred at room temperature for 1 h and then purified by preparative HPLC without any further work-up. For this, the whole reaction was aliquoted into 0.75 ml fractions which were individually injected onto the column. The purified product from each fraction were combined and dried on high vacuum. This afforded (E)-5-(4-(((4-((3-chloro-4-fluorophenyl)amino)-6-(4-(dimethylamino)but-2-enamido)quinazolin-7-yl)oxy)methyl)-1H-1,2,3-triazol-1-yl)-N-(2-(2,6-dioxopiperidin-3-yl)-1-oxoisindolin-4-yl)pentanamide (7.8 mg, 8.65 μ mol, 38 % yield). ¹H NMR (400 MHz, DMSO-d₆) δ 11.06 (s, 1H), 9.84 (d, *J* = 8.6 Hz, 2H), 9.63 (s, 1H), 8.91 (s, 1H), 8.55 (d, *J* = 4.2 Hz, 1H), 8.34 (s, 1H), 8.14 (dd, *J* = 6.8, 2.7 Hz, 1H), 7.81 (ddd, *J* = 8.7, 5.6, 2.7 Hz, 2H), 7.57 – 7.39 (m, 4H), 6.79 (dt, *J* = 15.3, 5.9 Hz, 1H), 6.54 (d, *J* = 15.5 Hz, 1H), 5.45 (s, 2H), 5.15 (dt, *J* = 13.7, 6.9 Hz, 1H), 4.44 (t, *J* = 7.2 Hz, 2H), 4.40 – 4.31 (m, 2H), 3.06 (d, *J* = 6.0 Hz, 2H), 2.62 (d, *J* = 17.1 Hz, 2H), 2.44 – 2.35 (m, 3H), 2.16 (s, 6H), 2.10 – 1.97 (m, 1H), 1.90 (p, *J* = 7.2 Hz, 2H), 1.61 (q, *J* = 7.7 Hz, 2H). UPLC-MS (ESI, m/z): *t*_R = 1.33 min, 838.3 (M+H)⁺.

(E)-cyclooct-4-en-1-yl (2-(4-((E)-4-((R)-3-(4-amino-3-(4-phenoxyphenyl)-1H-pyrazolo[3,4-d]pyrimidin-1-yl)piperidin-1-yl)-4-oxobut-2-en-1-yl)piperazin-1-yl)ethyl)carbamate (TCO-lbrutinib)



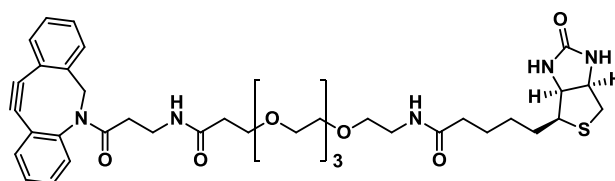
(R,E)-1-(3-(4-amino-3-(4-phenoxyphenyl)-1H-pyrazolo[3,4-d]pyrimidin-1-yl)piperidin-1-yl)-4-(4-(2-aminoethyl)piperazin-1-yl)but-2-en-1-one 2,2,2-trifluoroacetate salt (20.0 mg, 0.029 mmol) was dissolved in DMF (0.5 ml). To this solution was added (E)-cyclooct-4-en-1-yl (2,5-dioxopyrrolidin-1-yl) carbonate (8.5 mg, 0.032 mmol) followed by triethylamine (8.7 mg, 0.086 mmol). The reaction was stirred at room temperature for 2.5 h and then purified by preparative HPLC without any further work-up. For this, the whole reaction was aliquoted into 0.75 ml fractions which were individually injected onto the column. The purified product from each fraction were combined and dried on high vacuum. This afforded (E)-cyclooct-4-en-1-yl(2-(4-((E)-4-((R)-3-(4-amino-3-(4-phenoxyphenyl)-1H-pyrazolo[3,4-d]pyrimidin-1-yl)piperidin-1-yl)-4-oxobut-2-en-1-yl)piperazin-1-yl)ethyl)carbamate (yield: 12.1 mg, 0.016 mmol, 57 %). ^1H NMR (400 MHz, DMSO- d_6) δ 8.25 (s, 1H), 8.15 (s, 1H), 7.65 (d, J = 8.1 Hz, 2H), 7.49–7.38 (m, 2H), 7.24–7.09 (m, 5H), 6.86–6.73 (m, 1H), 6.71–6.57 (m, 1H), 6.51–6.41 (m, 1H), 5.69–5.35 (m, 2H), 4.26–4.14 (m, 1H), 4.15–3.96 (m, 5H), 3.14–2.87 (m, 4H), 2.45–2.06 (m, 14H), 2.03–1.77 (m, 5H), 1.69–1.42 (m, 5H). UPLC-MS (ESI, m/z): t_R = 2.13 min, 732.6 (M-H) $^-$.

1-(6-((4-(1,2,4,5-tetrazin-3-yl)benzyl)amino)-6-oxohexyl)-2-((1E,3E,5E)-5-(1-ethyl-3,3-dimethyl-5-sulfoindolin-2-ylidene)penta-1,3-dien-1-yl)-3,3-dimethyl-3H-indol-1-ium-5-sulfonate (Tz-Cy5)



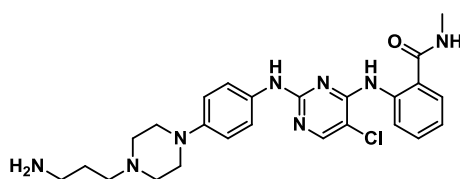
Purchased from Jena Bioscience (Product ID: CLK-015-05; Lot #: RK014-021)

Dibenzocyclooctyne-PEG4-biotin conjugate (DBCO-biotin)



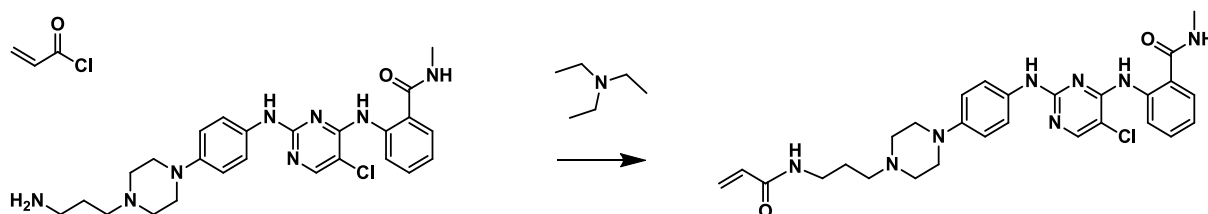
Purchased from Sigma Aldrich (Product ID: 760749; Lot #: MKCD3497)

2-((2-((4-(4-(3-aminopropyl)piperazin-1-yl)phenyl)amino)-5-chloropyrimidin-4-yl)amino)-N-methylbenzamide (Promiscuous protein kinase inhibitor PK1)



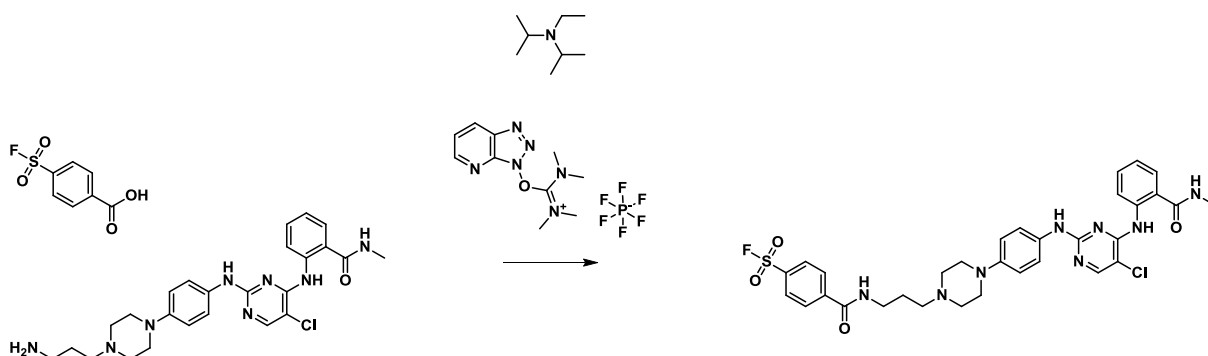
The promiscuous protein kinase inhibitor PK1 was synthesized by colleagues at Cellzome / GlaxoSmithKline and generously provided by the company.

2-((2-((4-(4-(3-acrylamidopropyl)piperazin-1-yl)phenyl)amino)-5-chloropyrimidin-4-yl)amino)-N-methylbenzamide (Probe 1A)



2-((2-((4-(4-(3-aminopropyl)piperazin-1-yl)phenyl)amino)-5-chloropyrimidin-4-yl)amino)-N-methylbenzamide (25.0 mg, 0.047 mmol) was dissolved in dichloromethane (1.5 ml). To this solution was added acryloyl chloride (4.6 μ l, 5.1 mg, 0.056 mmol) followed by triethylamine (20 μ l, 14.3 mg, 0.141 mmol). The reaction was stirred at room temperature for 1 h. To quench the acryloyl chloride 10 ml H₂O was added and the product was extracted twice in 10 ml dichloromethane. The solvent was evaporated and then the product was purified by preparative HPLC without any further work-up. For this, the whole reaction was aliquoted into 0.75 ml fractions which were individually injected onto the column. The purified product from each fraction were combined and dried on high vacuum. This afforded 2-((2-((4-(4-(3-acrylamidopropyl)piperazin-1-yl)phenyl)amino)-5-chloropyrimidin-4-yl)amino)-N-methylbenzamide (yield: 5.9 mg, 0.010 mmol, 21 %). ¹H NMR (400 MHz, Methanol-*d*₄) δ 8.71 (d, *J* = 8.5 Hz, 1H), 8.39 (s, 1H), 8.02 (s, 1H), 7.65 (dd, *J* = 7.9, 1.7 Hz, 1H), 7.46 (d, *J* = 8.5 Hz, 2H), 7.41 (t, *J* = 7.9 Hz, 1H), 7.10 (t, *J* = 7.6 Hz, 1H), 6.97 (d, *J* = 8.5 Hz, 2H), 6.25 (d, *J* = 6.0 Hz, 2H), 5.69 (t, *J* = 6.1 Hz, 1H), 3.40 – 3.34 (m, 6H), 3.12 (t, *J* = 5.2 Hz, 4H), 2.92 (s, 5H), 1.94 (p, *J* = 6.9 Hz, 2H). UPLC-MS (ESI, *m/z*): *t*_R = 1.26 min – 1.32 min, 549.2 (M+H)⁺.

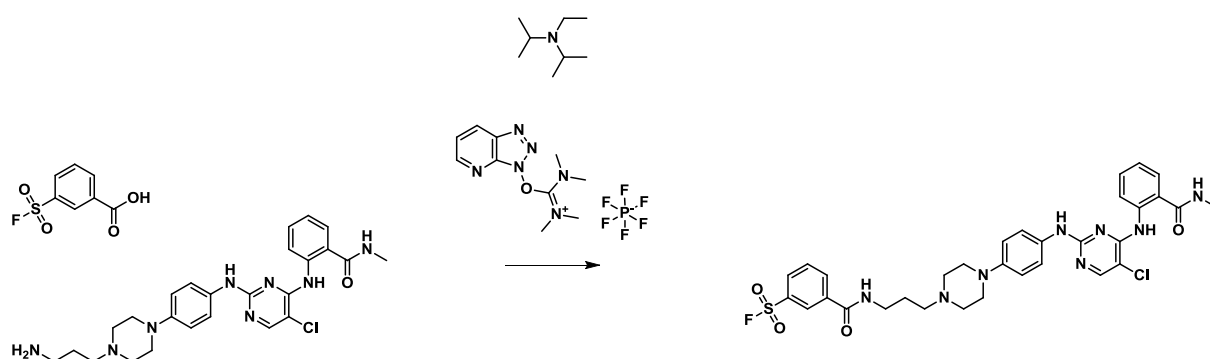
4-((3-(4-(4-((5-chloro-4-((2-(methylcarbamoyl)phenyl)amino)pyrimidin-2-yl)amino)phenyl)piperazin-1-yl)propyl)carbamoyl)benzene-1-sulfonyl fluoride (Probe 1B)



To a solution of 2-((2-((4-(4-(3-aminopropyl)piperazin-1-yl)phenyl)amino)-5-chloropyrimidin-4-yl)amino)-N-methylbenzamide (20 mg, 0.038 mmol) in 320 μ l dimethylformamide, 4-(fluorosulfonyl)benzoic acid (8.5 mg, 0.041 mmol), HATU (21.5 mg, 0.056 mmol) and DIPEA (20 μ l, 0.113 mmol) was added. The reaction was stirred at room temperature for 1 h. The product was purified by HPLC. This afforded 4-((3-(4-(4-((5-chloro-4-((2-(methylcarbamoyl)phenyl)amino)pyrimidin-

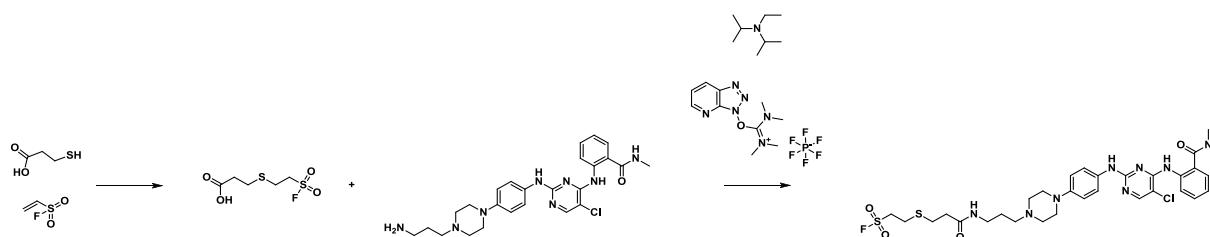
2-yl)amino)phenyl)piperazin-1-yl)propyl)carbamoyl)benzene-1-sulfonyl fluoride (11.8 mg, 0.017 mmol, 45 % yield). $^1\text{H NMR}$ (400 MHz, $\text{DMSO-}d_6$) δ 11.62 (s, 1H), 9.26 (s, 1H), 8.97 (t, $J = 5.6$ Hz, 1H), 8.76 (q, $J = 4.5$ Hz, 2H), 8.28 (d, $J = 8.4$ Hz, 2H), 8.18 (d, $J = 9.0$ Hz, 3H), 7.75 (dd, $J = 8.0, 1.6$ Hz, 1H), 7.49 (t, $J = 8.3$ Hz, 3H), 7.13 (t, $J = 7.6$ Hz, 1H), 6.92 (d, $J = 8.7$ Hz, 2H), 3.37 (d, $J = 6.2$ Hz, 3H), 3.20 (s, 4H), 3.04 – 2.70 (m, 9H), 1.93 – 1.79 (m, 2H). HPLC-MS (ESI, m/z): $t_R = 4.99$ min – 6.56 min, 681.2 ($\text{M}+\text{H}$) $^+$.

3-((3-(4-(4-((5-chloro-4-((2-(methylcarbamoyl)phenyl)amino)pyrimidin-2-yl)amino)phenyl)piperazin-1-yl)propyl)carbamoyl)benzene-1-sulfonyl fluoride (Probe 1C)



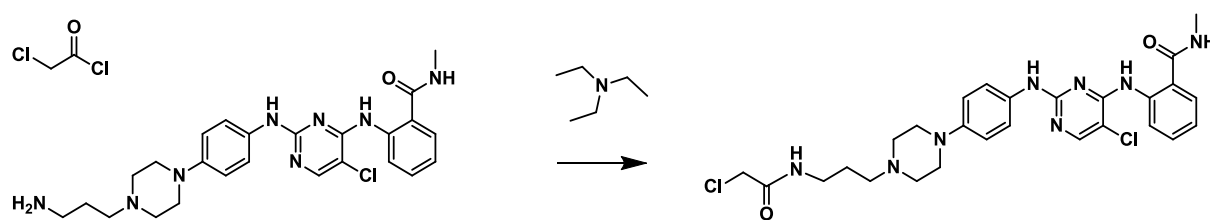
To a solution of 2-((2-((4-(4-(3-aminopropyl)piperazin-1-yl)phenyl)amino)-5-chloropyrimidin-4-yl)amino)-N-methylbenzamide (20 mg, 0.038 mmol) in 320 μl dimethylformamide, 3-(fluorosulfonyl)benzoic acid (8.5 mg, 0.041 mmol), HATU (21.5 mg, 0.056 mmol) and DIPEA (20 μl , 0.113 mmol) was added. The reaction was stirred at room temperature for 1 h. The product was purified by HPLC. This afforded 3-((3-(4-(4-((5-chloro-4-((2-(methylcarbamoyl)phenyl)amino)pyrimidin-2-yl)amino)phenyl)piperazin-1-yl)propyl)carbamoyl)benzene-1-sulfonyl fluoride (22.5 mg, 0.030 mmol, 81 % yield). $^1\text{H NMR}$ (400 MHz, $\text{DMSO-}d_6$) δ 11.64 (s, 1H), 9.29 (s, 1H), 9.07 (t, $J = 5.7$ Hz, 1H), 8.77 (q, $J = 4.7$ Hz, 2H), 8.55 (d, $J = 1.9$ Hz, 1H), 8.49 – 8.36 (m, 2H), 8.36 – 8.31 (m, 1H), 8.17 (s, 1H), 7.93 (td, $J = 7.9, 2.3$ Hz, 1H), 7.80 – 7.71 (m, 1H), 7.50 (dd, $J = 24.6, 8.2$ Hz, 3H), 7.13 (t, $J = 7.6$ Hz, 1H), 6.95 (d, $J = 8.6$ Hz, 2H), 3.40 (q, $J = 6.3$ Hz, 10H), 3.09 (s, 2H), 2.81 (d, $J = 4.4$ Hz, 3H), 1.94 (p, $J = 6.8$ Hz, 2H). HPLC-MS (ESI, m/z): $t_R = 5.06$ min – 6.62 min, 681.2 ($\text{M}+\text{H}$) $^+$.

2-((3-((3-(4-(4-((5-chloro-4-((2-(methylcarbamoyl)phenyl)amino)pyrimidin-2-yl)amino)phenyl)piperazin-1-yl)propyl)amino)-3-oxopropyl)thio)ethanesulfonyl fluoride (Probe 1D)



3-mercaptopropionic acid (3 μ l, 3.7 mg, 0.034 mmol) and ethenesulfonyl fluoride (2.9 μ l, 3.9 mg, 0.035 mmol) were pre-incubated in 120 μ l dimethylformamide for 1 h at room temperature. Subsequently, to this solution 2-((2-((4-(3-aminopropyl)piperazin-1-yl)phenyl)amino)-5-chloropyrimidin-4-yl)amino)-N-methylbenzamide (18.5 mg, 0.035 mmol) dissolved in 200 μ l dimethylformamide, HATU (19.9 mg, 0.052 mmol) and DIPEA (18 μ l, 0.104 mmol) were added. The reaction was stirred overnight at room temperature. The product was purified by HPLC. This afforded 2-((3-((3-(4-(4-((5-chloro-4-((2-(methylcarbamoyl)phenyl)amino)pyrimidin-2-yl)amino)phenyl)piperazin-1-yl)propyl)amino)-3-oxopropyl)thio)ethanesulfonyl fluoride (9.5 mg, 0.012 mmol, 36 % yield). ^1H NMR (400 MHz, DMSO- d_6) δ 11.65 (s, 1H), 9.32 (s, 2H), 8.84 – 8.68 (m, 2H), 8.21 – 8.11 (m, 2H), 7.76 (dd, J = 8.0, 1.5 Hz, 1H), 7.57 – 7.45 (m, 3H), 7.13 (t, J = 7.6 Hz, 1H), 6.97 (d, J = 8.8 Hz, 2H), 4.23 (dt, J = 11.0, 6.2 Hz, 2H), 3.76 (d, J = 12.9 Hz, 2H), 3.58 (d, J = 10.0 Hz, 2H), 3.15 (t, J = 7.0 Hz, 7H), 3.02 – 2.87 (m, 4H), 2.82 (dd, J = 10.1, 5.6 Hz, 5H), 2.41 (t, J = 6.9 Hz, 2H), 1.82 (q, J = 7.5, 6.6 Hz, 2H). UPLC-MS (ESI, m/z): t_R = 1.55 min, 693.2 (M+H) $^+$.

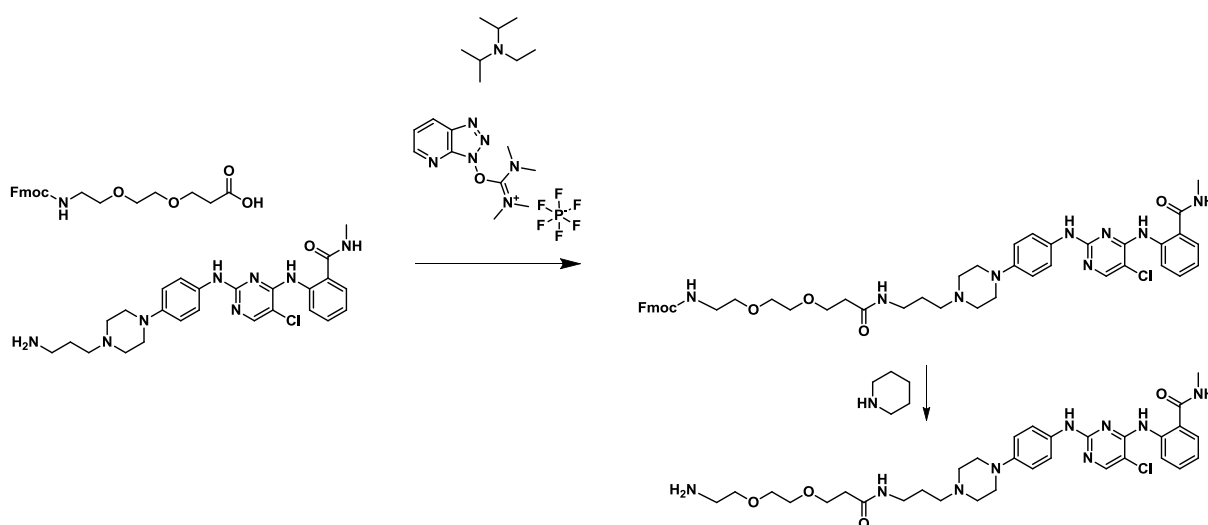
2-((5-chloro-2-((4-(4-(3-(2-chloroacetamido)propyl)piperazin-1-yl)phenyl)amino)pyrimidin-4-yl)amino)-N-methylbenzamide (Probe 1E)



2-((2-((4-(4-(3-aminopropyl)piperazin-1-yl)phenyl)amino)-5-chloropyrimidin-4-yl)amino)-N-methylbenzamide (20 mg, 0.038 mmol) was dissolved in DMSO (0.5 ml). To this solution was added 2-chloroacetyl chloride (3.3 μ l, 4.7 mg, 0.042 mmol) followed by triethylamine (16 μ l, 11.5 mg, 0.114 mmol). The reaction was stirred at room temperature for 1 h and then the product was purified by preparative HPLC without any further work-up. For this, the whole reaction was aliquoted into 0.75 ml fractions which were individually injected onto the column. The purified product from each fraction were combined and dried on high vacuum. This afforded 2-((5-chloro-2-((4-(4-(3-(2-

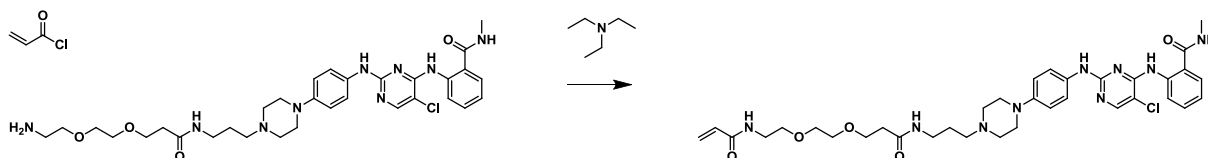
chloroacetamido)propyl)piperazin-1-yl)phenyl)amino)pyrimidin-4-yl)amino)-N-methylbenzamide (yield: 4.2 mg, 0.006 mmol, 15 %). $^1\text{H NMR}$ (400 MHz, $\text{DMSO-}d_6$) δ 11.62 (s, 1H), 9.24 (s, 1H), 8.77 (q, $J = 4.6$ Hz, 2H), 8.32 (q, $J = 5.0, 4.5$ Hz, 1H), 8.15 (d, $J = 5.2$ Hz, 1H), 7.81 – 7.68 (m, 1H), 7.48 (t, $J = 6.4$ Hz, 3H), 7.12 (t, $J = 7.6$ Hz, 1H), 6.90 (d, $J = 8.7$ Hz, 2H), 3.16 (q, $J = 6.5$ Hz, 6H), 2.80 (d, $J = 4.4$ Hz, 3H), 2.73 (d, $J = 4.9$ Hz, 4H), 2.56 (t, $J = 7.2$ Hz, 2H), 1.69 (p, $J = 7.1$ Hz, 2H). HPLC-MS (ESI, m/z): $t_R = 4.06$ min – 4.33 min, 571.0 ($\text{M}+\text{H}$) $^+$.

2-((5-chloro-2-((4-(4-(3,13-dioxo-7,10-dioxa-4,14-diazaheptadec-1-en-17-yl)piperazin-1-yl)phenyl)amino)pyrimidin-4-yl)amino)-N-methylbenzamide (Probe 2 pre-cursor)



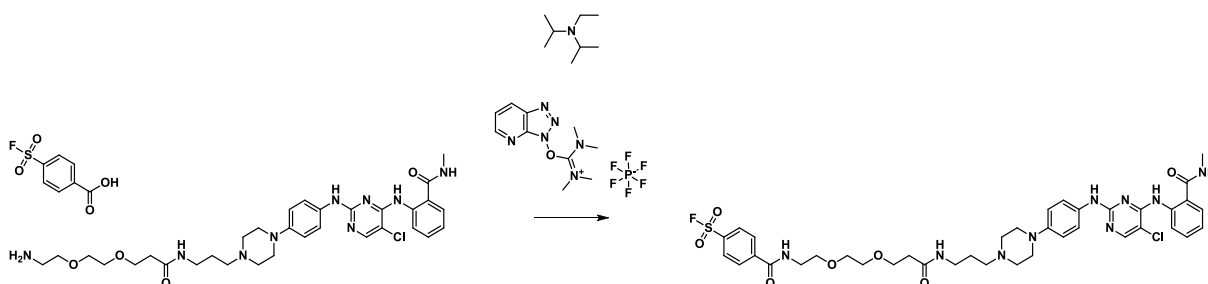
To a solution of 2-((2-((4-(4-(3-aminopropyl)piperazin-1-yl)phenyl)amino)-5-chloropyrimidin-4-yl)amino)-N-methylbenzamide (100 mg, 0.188 mmol) in 1 ml dimethylformamide, 1-(9H-fluoren-9-yl)-3-oxo-2,7,10-trioxa-4-azatridec-13-ynoic acid (85.6 mg, 0.214 mmol), HATU (130.4 mg, 0.343 mmol) and DIPEA (97 μl , 0.564 mmol) were added. The reaction was stirred at room temperature for 1 h. The product was purified by HPLC. This afforded (9H-fluoren-9-yl)methyl (2-(2-(3-((3-(4-(4-((5-chloro-4-((2-(methylcarbamoyl)phenyl)amino)pyrimidin-2-yl)amino)phenyl)piperazin-1-yl)propyl)amino)-3-oxopropoxy)ethoxy)ethyl)carbamate (115.6 mg, 0.129 mmol, 69 % yield). UPLC-MS (ESI, m/z): $t_R = 1.92$ min, 876.4 ($\text{M}+\text{H}$) $^+$. For the Fmoc deprotection, the dried intermediate product was dissolved in 1.9 ml dimethylformamide and piperidine was added (260 μl , 224 mg, 2.63 mmol). The reaction was stirred at room temperature for 1.5 h. The product was purified by HPLC. This afforded 2-((5-chloro-2-((4-(4-(3,13-dioxo-7,10-dioxa-4,14-diazaheptadec-1-en-17-yl)piperazin-1-yl)phenyl)amino)pyrimidin-4-yl)amino)-N-methylbenzamide (82.3 mg, 0.126 mmol, 100 % yield). UPLC-MS (ESI, m/z): $t_R = 1.03$ min, 654.3 ($\text{M}+\text{H}$) $^+$.

2-((5-chloro-2-((4-(4-(3,13-dioxo-7,10-dioxo-4,14-diazaheptadec-1-en-17-yl)piperazin-1-yl)phenyl)amino)pyrimidin-4-yl)amino)-N-methylbenzamide (Probe 2A)



2-((5-chloro-2-((4-(4-(3,13-dioxo-7,10-dioxo-4,14-diazaheptadec-1-en-17-yl)piperazin-1-yl)phenyl)amino)pyrimidin-4-yl)amino)-N-methylbenzamide (13.7 mg, 0.021 mmol) was dissolved in dimethylformamide (1.5 ml). To this solution was added acryloyl chloride (0.9 μ l, 0.9 mg, 0.011 mmol) followed by triethylamine (8.9 μ l, 18.6 mg, 0.063 mmol). The reaction was stirred at room temperature for 1 h and then the product was purified by preparative HPLC without any further work-up. For this, the whole reaction was aliquoted into 0.75 ml fractions which were individually injected onto the column. The purified product from each fraction were combined and dried on high vacuum. This afforded 2-((5-chloro-2-((4-(4-(3,13-dioxo-7,10-dioxo-4,14-diazaheptadec-1-en-17-yl)piperazin-1-yl)phenyl)amino)pyrimidin-4-yl)amino)-N-methylbenzamide (yield: 2.1 mg, 2.56 μ mol, 12 %). ^1H NMR (400 MHz, $\text{DMSO-}d_6$) δ 11.59 (s, 1H), 9.20 (s, 1H), 8.75 (d, J = 5.4 Hz, 2H), 8.17 (d, J = 12.2 Hz, 3H), 7.86 (t, J = 5.7 Hz, 1H), 7.74 (d, J = 7.9 Hz, 1H), 7.46 (dd, J = 8.3, 5.3 Hz, 3H), 7.12 (t, J = 7.6 Hz, 1H), 6.88 (d, J = 8.6 Hz, 2H), 6.25 (dd, J = 17.1, 10.1 Hz, 1H), 6.07 (dd, J = 17.1, 2.3 Hz, 1H), 5.57 (dd, J = 10.1, 2.3 Hz, 1H), 3.60 (t, J = 6.3 Hz, 6H), 3.44 (t, J = 5.8 Hz, 6H), 3.28 (q, J = 5.8 Hz, 3H), 3.08 (t, J = 6.3 Hz, 7H), 2.80 (d, J = 4.4 Hz, 4H), 2.31 (dt, J = 12.8, 6.8 Hz, 5H), 1.58 (p, J = 7.0 Hz, 2H). UPLC-MS (ESI, m/z): t_R = 1.30 min, 708.3 ($\text{M}+\text{H}$) $^+$.

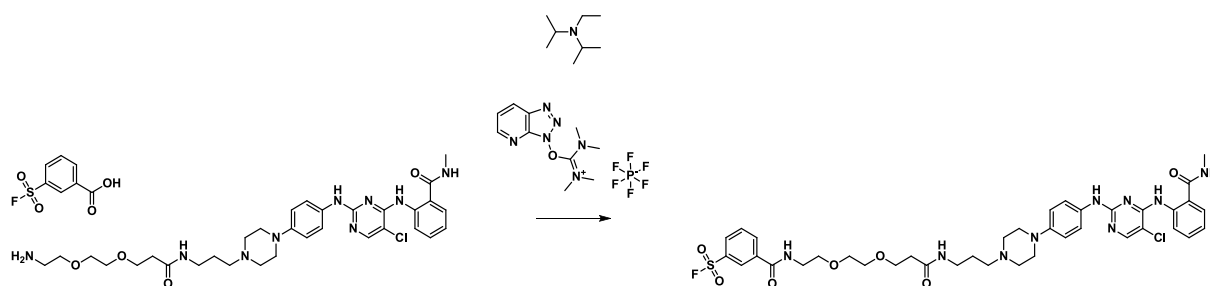
4-((2-(2-(3-((3-(4-(4-((5-chloro-4-((2-(methylcarbamoyl)phenyl)amino)pyrimidin-2-yl)amino)phenyl)piperazin-1-yl)propyl)amino)-3-oxopropoxy)ethoxy)ethyl)carbamoyl)benzene-1-sulfonyl fluoride (Probe 2B)



To a solution of 2-((5-chloro-2-((4-(4-(3,13-dioxo-7,10-dioxo-4,14-diazaheptadec-1-en-17-yl)piperazin-1-yl)phenyl)amino)pyrimidin-4-yl)amino)-N-methylbenzamide (13.7 mg, 0.021 mmol) in 600 μ l dimethylformamide, 4-(fluorosulfonyl)benzoic acid (4.5 mg, 0.022 mmol), HATU (11.3 mg, 0.030 mmol) and DIPEA (10.4 μ l, 0.060 mmol) were added. The reaction was stirred overnight at room temperature. The product was purified by HPLC. This afforded 4-((2-(2-(3-((3-(4-(4-((5-chloro-4-((2-

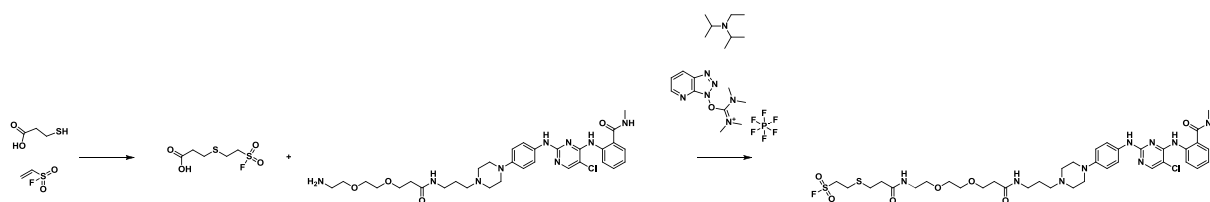
(methylcarbamoyl)phenyl)amino)pyrimidin-2-yl)amino)phenyl)piperazin-1-yl)propyl)amino)-3-oxopropoxy)ethoxy)ethyl)carbamoyl)benzene-1-sulfonyl fluoride (3.6 mg, 3.77 μ mol, 20 % yield). ^1H NMR (400 MHz, $\text{DMSO-}d_6$) δ 11.66 (s, 1H), 9.33 (s, 2H), 8.97 (t, $J = 5.5$ Hz, 1H), 8.78 (d, $J = 6.1$ Hz, 2H), 8.27 (d, $J = 8.4$ Hz, 2H), 8.22 – 8.13 (m, 3H), 8.06 (dt, $J = 19.9, 5.7$ Hz, 1H), 7.81 (d, $J = 8.0$ Hz, 1H), 7.76 (d, $J = 7.9$ Hz, 1H), 7.68 (d, $J = 8.0$ Hz, 1H), 7.61 – 7.44 (m, 3H), 7.14 (t, $J = 7.5$ Hz, 1H), 6.97 (d, $J = 8.5$ Hz, 2H), 3.77 (d, $J = 12.8$ Hz, 2H), 3.63 – 3.46 (m, 12H), 3.15 (s, 7H), 2.95 (q, $J = 14.7, 12.2$ Hz, 2H), 2.82 (d, $J = 4.4$ Hz, 3H), 2.33 (td, $J = 14.2, 13.2, 7.7$ Hz, 2H), 1.90 – 1.74 (m, 2H). UPLC-MS (ESI, m/z): $t_R = 1.73$ min, 840.3 ($\text{M}+\text{H}$) $^+$.

3-((2-(2-(3-((3-(4-(4-((5-chloro-4-((2-(methylcarbamoyl)phenyl)amino)pyrimidin-2-yl)amino)phenyl)piperazin-1-yl)propyl)amino)-3-oxopropoxy)ethoxy)ethyl)carbamoyl)benzene-1-sulfonyl fluoride (Probe 2C)



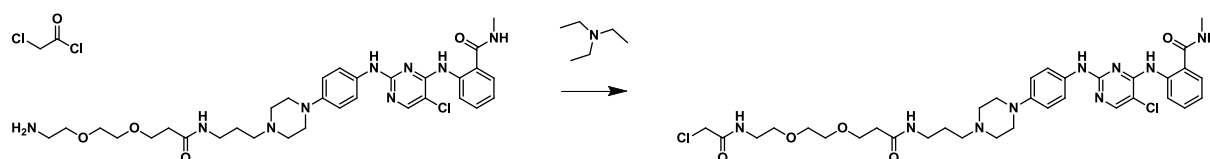
To a solution of 2-((5-chloro-2-((4-(4-(3,13-dioxo-7,10-dioxo-4,14-diazaheptadec-1-en-17-yl)piperazin-1-yl)phenyl)amino)pyrimidin-4-yl)amino)-N-methylbenzamide (13.7 mg, 0.021 mmol) in 600 μ l dimethylformamide, 3-(fluorosulfonyl)benzoic acid (4.5 mg, 0.022 mmol), HATU (11.3 mg, 0.030 mmol) and DIPEA (10.4 μ l, 0.060 mmol) were added. The reaction was stirred overnight at room temperature. The product was purified by HPLC. This afforded 3-((2-(2-(3-((3-(4-(4-((5-chloro-4-((2-(methylcarbamoyl)phenyl)amino)pyrimidin-2-yl)amino)phenyl)piperazin-1-yl)propyl)amino)-3-oxopropoxy)ethoxy)ethyl)carbamoyl)benzene-1-sulfonyl fluoride (4.2 mg, 4.8 μ mol, 24 % yield). ^1H NMR (400 MHz, $\text{DMSO-}d_6$) δ 11.65 (s, 1H), 9.31 (s, 2H), 9.03 (s, 1H), 8.77 (d, $J = 5.3$ Hz, 2H), 8.56 (s, 1H), 8.46 – 8.37 (m, 1H), 8.32 (d, $J = 8.0$ Hz, 1H), 8.19 (s, 1H), 8.08 (s, 1H), 7.92 (q, $J = 8.2, 7.8$ Hz, 1H), 7.76 (d, $J = 7.8$ Hz, 1H), 7.50 (dt, $J = 28.1, 10.2$ Hz, 3H), 7.13 (t, $J = 7.5$ Hz, 1H), 6.97 (d, $J = 8.5$ Hz, 2H), 3.77 (d, $J = 12.7$ Hz, 2H), 3.54 (ddt, $J = 30.9, 20.2, 6.0$ Hz, 14H), 3.22 – 3.07 (m, 6H), 2.97 (d, $J = 28.9$ Hz, 2H), 2.82 (d, $J = 4.5$ Hz, 3H), 2.41 – 2.25 (m, 2H), 1.82 (s, 2H). UPLC-MS (ESI, m/z): $t_R = 1.72$ min, 840.3 ($\text{M}+\text{H}$) $^+$.

20-(4-(4-((5-chloro-4-((2-(methylcarbamoyl)phenyl)amino)pyrimidin-2-yl)amino)phenyl)piperazin-1-yl)-6,16-dioxo-10,13-dioxo-3-thia-7,17-diazaicosane-1-sulfonyl fluoride (Probe 2D)



3-mercaptopropionic acid (1.7 μ l, 2.1 mg, 0.020 mmol) and ethenesulfonyl fluoride (1.6 μ l, 2.2 mg, 0.020 mmol) were pre-incubated in 100 μ l dimethylformamide for 1 h at room temperature. Subsequently, to this solution 2-((5-chloro-2-((4-(4-(3,13-dioxo-7,10-dioxo-4,14-diazaheptadec-1-en-17-yl)piperazin-1-yl)phenyl)amino)pyrimidin-4-yl)amino)-N-methylbenzamide (13.7 mg, 0.020 mmol) dissolved in 500 μ l dimethylformamide, HATU (11.3 mg, 0.030 mmol) and DIPEA (10.4 μ l, 0.060 mmol) were added. The reaction was stirred overnight at room temperature. The product was purified by HPLC. This afforded 20-(4-(4-((5-chloro-4-((2-(methylcarbamoyl)phenyl)amino)pyrimidin-2-yl)amino)phenyl)piperazin-1-yl)-6,16-dioxo-10,13-dioxo-3-thia-7,17-diazaicosane-1-sulfonyl fluoride (1.6 mg, 1.7 μ mol, 9 % yield). ^1H NMR (400 MHz, DMSO- d_6) δ 11.69 (s, 1H), 9.35 (s, 2H), 8.78 (d, J = 4.8 Hz, 2H), 8.20 (s, 1H), 8.06 (dt, J = 23.2, 5.7 Hz, 2H), 7.77 (d, J = 7.9 Hz, 1H), 7.60 – 7.43 (m, 3H), 7.14 (t, J = 7.6 Hz, 1H), 6.98 (d, J = 8.8 Hz, 2H), 4.30 – 4.17 (m, 2H), 3.78 (d, J = 12.8 Hz, 2H), 3.63 (t, J = 6.5 Hz, 4H), 3.24 – 3.12 (m, 9H), 3.00 – 2.88 (m, 4H), 2.84 – 2.77 (m, 5H), 2.37 (dt, J = 17.2, 6.6 Hz, 5H), 1.84 (s, 2H). UPLC-MS (ESI, m/z): t_R = 1.61 min, 852.3 (M+H) $^+$.

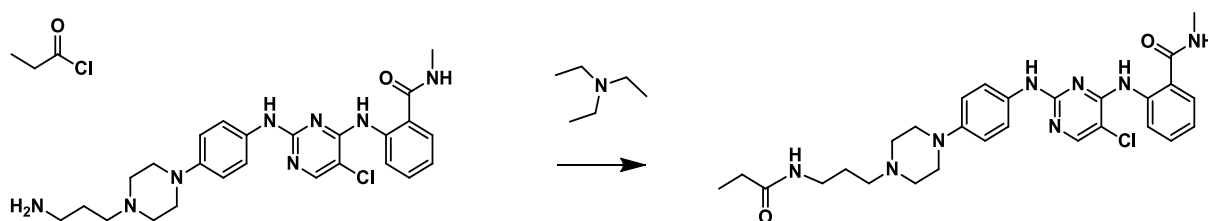
2-((5-chloro-2-((4-(4-(1-chloro-2,12-dioxo-6,9-dioxo-3,13-diazahexadecan-16-yl)piperazin-1-yl)phenyl)amino)pyrimidin-4-yl)amino)-N-methylbenzamide (Probe 2E)



2-((5-chloro-2-((4-(4-(3,13-dioxo-7,10-dioxo-4,14-diazaheptadec-1-en-17-yl)piperazin-1-yl)phenyl)amino)pyrimidin-4-yl)amino)-N-methylbenzamide (13.7 mg, 0.020 mmol) was dissolved in 500 μ l dimethylformamide. To this solution was added 2-chloroacetyl chloride (1.7 μ l, 2.5 mg, 0.022 mmol) followed by triethylamine (8.3 μ l, 6.0 mg, 0.060 mmol). The reaction was stirred overnight at room temperature and then the product was purified by preparative HPLC without any further work-up. For this, the whole reaction was aliquoted into 0.75 ml fractions which were individually injected onto the column. The purified product from each fraction were combined and dried on high vacuum. This afforded 2-((5-chloro-2-((4-(4-(1-chloro-2,12-dioxo-6,9-dioxo-3,13-diazahexadecan-16-yl)piperazin-1-yl)phenyl)amino)pyrimidin-4-yl)amino)-N-methylbenzamide (yield: 1.7 mg, 2.14 μ mol,

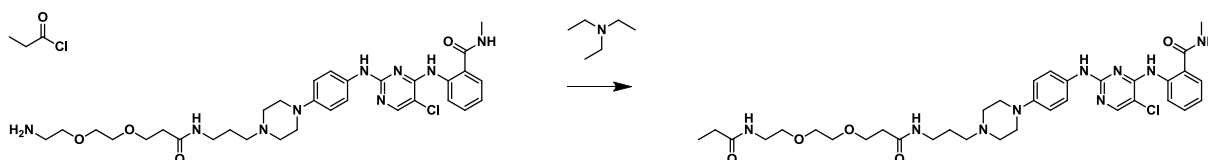
11 %). ^1H NMR (400 MHz, $\text{DMSO-}d_6$) δ 11.65 (d, $J = 23.7$ Hz, 1H), 9.28 (d, $J = 40.8$ Hz, 1H), 8.79 (s, 2H), 8.30 (s, 1H), 8.19 (d, $J = 16.5$ Hz, 1H), 7.90 (s, 1H), 7.75 (d, $J = 8.4$ Hz, 1H), 7.57 (d, $J = 8.1$ Hz, 1H), 7.48 (d, $J = 8.6$ Hz, 2H), 7.13 (s, 1H), 6.97 (s, 1H), 6.89 (d, $J = 8.5$ Hz, 1H), 4.53 (d, $J = 18.3$ Hz, 1H), 4.25 (s, 1H), 4.08 (s, 1H), 3.84 (s, 1H), 3.69 (s, 1H), 3.60 (d, $J = 6.5$ Hz, 2H), 3.45 (d, $J = 23.7$ Hz, 7H), 3.24 (s, 1H), 3.07 (d, $J = 7.4$ Hz, 4H), 2.81 (d, $J = 4.6$ Hz, 2H), 2.32 (q, $J = 6.7$ Hz, 3H), 1.88 (s, 1H), 1.59 (s, 1H). UPLC-MS (ESI, m/z): $t_R = 1.39$ min, 730.3 ($M+H$) $^+$.

2-((5-chloro-2-((4-(4-(3-propionamidopropyl)piperazin-1-yl)phenyl)amino)pyrimidin-4-yl)amino)-N-methylbenzamide (Saturated Probe 1A)



2-((2-((4-(4-(3-aminopropyl)piperazin-1-yl)phenyl)amino)-5-chloropyrimidin-4-yl)amino)-N-methylbenzamide (25 mg, 0.047 mmol) was dissolved in dimethylformamide (1 ml). To this solution was added propionyl chloride (3.1 μl , 3.3 mg, 0.035 mmol) followed by triethylamine (26 μl , 19.0 mg, 0.188 mmol). The reaction was stirred at room temperature for 1 h and then the product was purified by preparative HPLC without any further work-up. For this, the whole reaction was aliquoted into 0.75 ml fractions which were individually injected onto the column. The purified product from each fraction were combined and dried on high vacuum. This afforded 2-((5-chloro-2-((4-(4-(3-propionamidopropyl)piperazin-1-yl)phenyl)amino)pyrimidin-4-yl)amino)-N-methylbenzamide (yield: 18.4 mg, 0.030 mmol, 64 %). ^1H NMR (400 MHz, $\text{DMSO-}d_6$) δ 11.59 (s, 1H), 9.21 (s, 1H), 8.75 (q, $J = 4.5$ Hz, 2H), 8.18 (d, $J = 15.9$ Hz, 3H), 7.76 (dd, $J = 13.6, 6.8$ Hz, 2H), 7.46 (dd, $J = 8.8, 6.5$ Hz, 3H), 7.12 (t, $J = 7.6$ Hz, 1H), 6.88 (d, $J = 8.8$ Hz, 2H), 3.07 (q, $J = 7.0, 5.9$ Hz, 6H), 2.81 (s, 3H), 2.54 (t, $J = 4.7$ Hz, 4H), 2.36 (t, $J = 7.2$ Hz, 2H), 2.06 (q, $J = 7.6$ Hz, 2H), 1.59 (p, $J = 7.1$ Hz, 2H), 0.99 (t, $J = 7.6$ Hz, 3H). UPLC-MS (ESI, m/z): $t_R = 1.30$ min, 551.3 ($M+H$) $^+$.

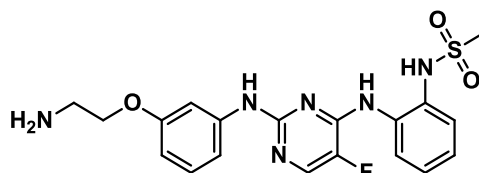
2-((5-chloro-2-((4-(4-(3,13-dioxo-7,10-dioxo-4,14-diazaheptadecan-17-yl)piperazin-1-yl)phenyl)amino)pyrimidin-4-yl)amino)-N-methylbenzamide (Saturated Probe 2A)



2-((5-chloro-2-((4-(4-(3,13-dioxo-7,10-dioxo-4,14-diazaheptadecan-17-yl)piperazin-1-yl)phenyl)amino)pyrimidin-4-yl)amino)-N-methylbenzamide (13.7 mg, 0.020 mmol) was dissolved in dimethylformamide (0.7 ml). To this solution was added propionyl chloride (0.9 μl , 1.0 mg,

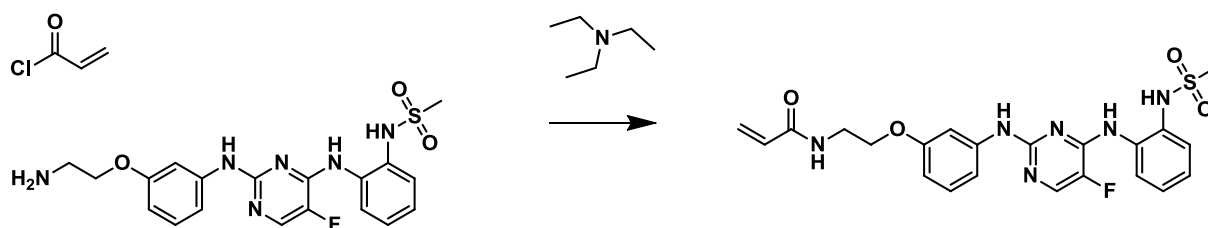
0.011 mmol) followed by triethylamine (9 μ l, 6.4 mg, 0.063 mmol). The reaction was stirred at room temperature for 1 h and then the product was purified by preparative HPLC without any further work-up. For this, the whole reaction was aliquoted into 0.75 ml fractions which were individually injected onto the column. The purified product from each fraction were combined and dried on high vacuum. This afforded 2-((5-chloro-2-((4-(3,13-dioxo-7,10-dioxo-4,14-diazaheptadecan-17-yl)piperazin-1-yl)phenoxy)amino)pyrimidin-4-yl)amino)-N-methylbenzamide (yield: 2.3 mg, 2.7 μ mol, 13 %). ^1H NMR (400 MHz, $\text{DMSO-}d_6$) δ 11.59 (s, 1H), 9.20 (s, 1H), 8.75 (d, $J = 5.4$ Hz, 2H), 8.17 (d, $J = 12.5$ Hz, 2H), 7.88 – 7.71 (m, 3H), 7.46 (d, $J = 8.1$ Hz, 3H), 7.12 (t, $J = 7.6$ Hz, 1H), 6.88 (d, $J = 8.6$ Hz, 2H), 3.59 (d, $J = 6.4$ Hz, 5H), 3.39 (t, $J = 6.0$ Hz, 8H), 3.18 (q, $J = 5.9$ Hz, 3H), 3.08 (q, $J = 6.5$ Hz, 8H), 2.80 (d, $J = 4.4$ Hz, 4H), 2.31 (dt, $J = 12.8, 6.8$ Hz, 5H), 2.10 – 2.03 (m, 3H), 1.58 (p, $J = 6.9$ Hz, 2H), 0.97 (t, $J = 7.6$ Hz, 3H). UPLC-MS (ESI, m/z): $t_R = 1.33$ min, 710.4 ($M+H$) $^+$.

N-(2-((2-((3-(2-aminoethoxy)phenyl)amino)-5-fluoropyrimidin-4-yl)amino)phenyl)methanesulfonamide (Promiscuous protein kinase inhibitor PK2)



The promiscuous protein kinase inhibitor PK2 was synthesized by colleagues at Cellzome / GlaxoSmithKline and generously provided by the company.

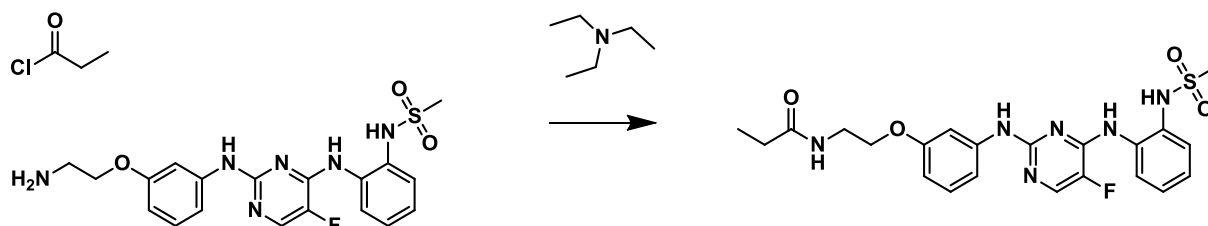
N-(2-(3-((5-fluoro-4-((2-(methylsulfonamido)phenyl)amino)pyrimidin-2-yl)amino)phenoxy)ethyl)acrylamide (Probe 3A)



N-(2-((2-((3-(2-aminoethoxy)phenyl)amino)-5-fluoropyrimidin-4-yl)amino)phenyl)methanesulfonamide (25 mg, 0.058 mmol) was dissolved in dimethylformamide (0.5 ml). To this solution was added 2-acryloyl chloride (4.7 μ l, 5.2 mg, 0.058 mmol) followed by triethylamine (24 μ l, 17.6 mg, 0.173 mmol). The reaction was stirred at room temperature for 1 h and then the product was purified by preparative HPLC without any further work-up. For this, the whole reaction was aliquoted into 0.75 ml fractions which were individually injected onto the column. The purified product from each fraction were combined and dried on high vacuum. This afforded N-(2-(3-((5-fluoro-4-((2-(methylsulfonamido)phenyl)amino)pyrimidin-2-yl)amino)phenoxy)ethyl)acrylamide (yield: 3.2 mg,

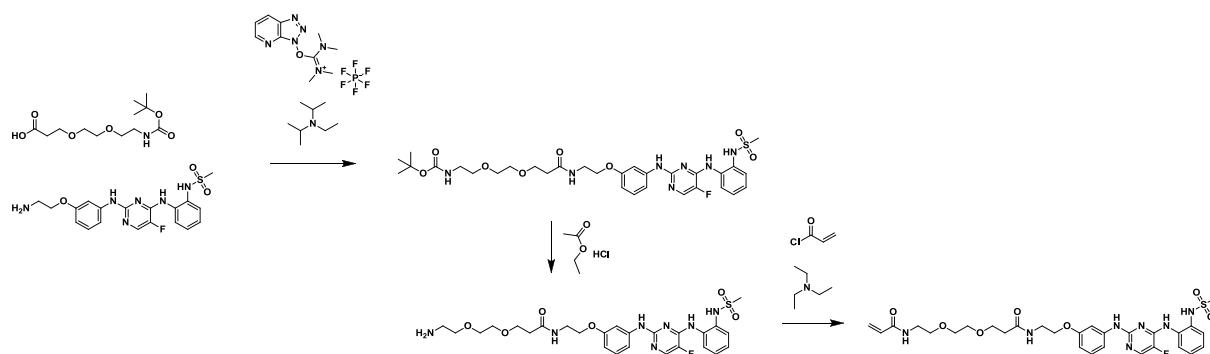
0.007 mmol, 11 %). ^1H NMR (400 MHz, $\text{DMSO-}d_6$) δ 9.10 (s, 1H), 8.69 (s, 1H), 8.29 (t, $J = 5.6$ Hz, 1H), 8.06 (d, $J = 3.4$ Hz, 1H), 7.98 – 7.78 (m, 1H), 7.32 (dd, $J = 7.2, 2.2$ Hz, 1H), 7.25 (s, 1H), 7.18 – 7.06 (m, 3H), 6.98 (t, $J = 8.1$ Hz, 1H), 6.40 (dd, $J = 8.1, 2.4$ Hz, 1H), 6.21 (dd, $J = 17.1, 10.1$ Hz, 1H), 6.04 (dd, $J = 17.1, 2.3$ Hz, 1H), 5.53 (dd, $J = 10.0, 2.3$ Hz, 1H), 3.83 (t, $J = 5.6$ Hz, 2H), 2.81 (s, 4H). HPLC-MS (ESI, m/z): $t_R = 4.58$ min, 487.2 ($\text{M}+\text{H}$) $^+$.

N-(2-(3-((5-fluoro-4-((2-(methylsulfonamido)phenyl)amino)pyrimidin-2-yl)amino)phenoxy)ethyl)propionamide (Saturated Probe 3A)



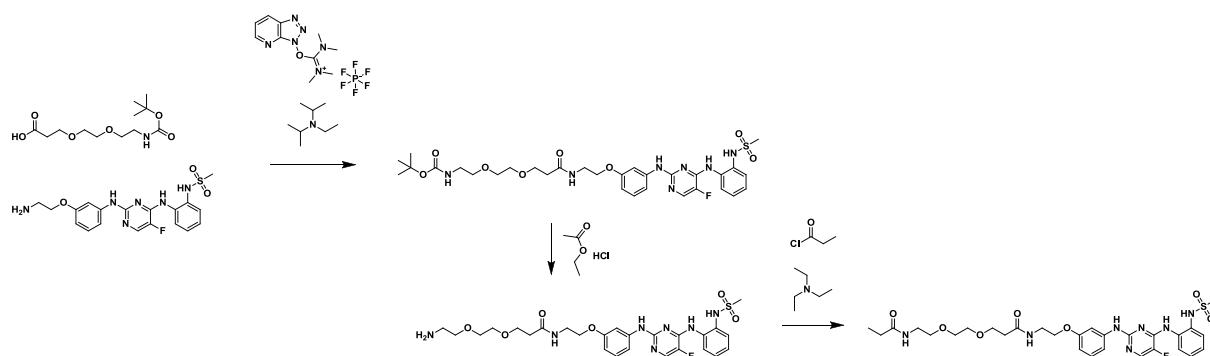
N-(2-((3-(2-aminoethoxy)phenyl)amino)-5-fluoropyrimidin-4-yl)amino)phenyl)methanesulfonamide (25 mg, 0.058 mmol) was dissolved in dimethylformamide (0.5 ml). To this solution was added propionyl chloride (5.1 μl , 5.4 mg, 0.058 mmol) followed by triethylamine (24 μl , 17.6 mg, 0.173 mmol). The reaction was stirred at room temperature for 1 h and then the product was purified by preparative HPLC without any further work-up. For this, the whole reaction was aliquoted into 0.75 ml fractions which were individually injected onto the column. The purified product from each fraction were combined and dried on high vacuum. This afforded N-(2-(3-((5-fluoro-4-((2-(methylsulfonamido)phenyl)amino)pyrimidin-2-yl)amino)phenoxy)ethyl)propionamide (yield: 5.5 mg, 0.011 mmol, 19 %). ^1H NMR (400 MHz, $\text{DMSO-}d_6$) δ 9.16 (s, 1H), 8.73 (s, 1H), 8.14 (d, $J = 3.4$ Hz, 1H), 8.00 (t, $J = 5.5$ Hz, 1H), 7.91 (d, $J = 7.8$ Hz, 1H), 7.41 (d, $J = 7.6$ Hz, 1H), 7.30 (s, 1H), 7.22 (dt, $J = 20.2, 7.6$ Hz, 3H), 7.04 (t, $J = 8.1$ Hz, 1H), 6.46 (dd, $J = 8.1, 2.4$ Hz, 1H), 3.84 (t, $J = 5.7$ Hz, 2H), 2.90 (s, 3H), 2.11 (q, $J = 7.5$ Hz, 2H), 1.00 (t, $J = 7.6$ Hz, 3H). HPLC-MS (ESI, m/z): $t_R = 4.57$ min, 489.2 ($\text{M}+\text{H}$) $^+$.

N-(2-(2-(3-((2-(3-((5-fluoro-4-((2-(methylsulfonamido)phenyl)amino)pyrimidin-2-yl)amino)phenoxy)ethyl)amino)-3-oxopropoxy)ethoxy)ethyl)acrylamide (Probe 3B)



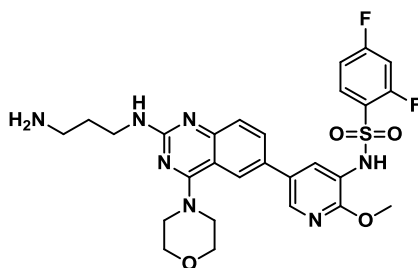
To a solution of N-(2-((2-((3-(2-aminoethoxy)phenyl)amino)-5-fluoropyrimidin-4-yl)amino)phenyl)methanesulfonamide (75 mg, 0.173 mmol) in 1 ml dimethylformamide, 2,2-dimethyl-4-oxo-3,8,11-trioxo-5-azatetradecan-14-oic acid (48.1 mg, 0.173 mmol), HATU (99 mg, 0.260 mmol) and DIPEA (90 μ l, 0.520 mmol) were added. The reaction was stirred at room temperature for 1 h. The product was purified by HPLC. This afforded tert-butyl (2-(2-(3-((2-(3-((5-fluoro-4-((2-(methylsulfonamido)phenyl)amino)pyrimidin-2-yl)amino)phenoxy)ethyl)amino)-3-oxopropoxy)ethoxy)ethyl)carbamate (77 mg, 0.104 mmol, 60 % yield). HPLC-MS (ESI, m/z): t_R = 5.34 min, 692.3 (M+H)⁺. For the boc deprotection, the dried intermediate product was dissolved in 0.5 ml ethyl acetate and 50 μ l concentrated HCl was added. The instantly forming insoluble slurry was dissolved in DMSO and the product was purified by HPLC. This afforded 3-(2-(2-aminoethoxy)ethoxy)-N-(2-(3-((5-fluoro-4-((2-(methylsulfonamido)phenyl)amino)pyrimidin-2-yl)amino)phenoxy)ethyl)propanamide (47.4 mg, 0.079 mmol, 71 % yield). HPLC-MS (ESI, m/z): t_R = 3.63 min, 592.2 (M+H)⁺. 3-(2-(2-aminoethoxy)ethoxy)-N-(2-(3-((5-fluoro-4-((2-(methylsulfonamido)phenyl)amino)pyrimidin-2-yl)amino)phenoxy)ethyl)propanamide (23.7 mg, 0.040 mmol) was dissolved in dimethylformamide (0.5 ml). To this solution was added acryloyl chloride (3.3 μ l, 3.6 mg, 0.040 mmol) followed by triethylamine (17 μ l, 12.2 mg, 0.120 mmol). The reaction was stirred at room temperature for 1 h and then the product was purified by preparative HPLC without any further work-up. For this, the whole reaction was aliquoted into 0.75 ml fractions which were individually injected onto the column. The purified product from each fraction were combined and dried on high vacuum. This afforded N-(2-(2-(3-((2-(3-((5-fluoro-4-((2-(methylsulfonamido)phenyl)amino)pyrimidin-2-yl)amino)phenoxy)ethyl)amino)-3-oxopropoxy)ethoxy)ethyl)acrylamide (yield: 5.0 mg, 7.5 μ mol, 19 %). ¹H NMR (400 MHz, DMSO-*d*₆) δ 9.17 (s, 1H), 8.70 (d, *J* = 2.2 Hz, 1H), 8.16 (dd, *J* = 10.6, 5.1 Hz, 2H), 8.10 (t, *J* = 5.5 Hz, 1H), 7.88 (dd, *J* = 8.0, 1.7 Hz, 1H), 7.43 (dd, *J* = 7.8, 1.7 Hz, 1H), 7.32 – 7.15 (m, 4H), 7.04 (t, *J* = 8.2 Hz, 1H), 6.45 (dd, *J* = 8.0, 2.4 Hz, 1H), 6.25 (dd, *J* = 17.1, 10.2 Hz, 1H), 6.07 (dd, *J* = 17.1, 2.3 Hz, 1H), 5.57 (dd, *J* = 10.1, 2.3 Hz, 1H), 3.83 (t, *J* = 5.6 Hz, 2H), 3.61 (t, *J* = 6.4 Hz, 2H), 3.41 (q, *J* = 5.5 Hz, 4H), 3.27 (q, *J* = 5.7 Hz, 4H), 2.92 (s, 3H), 2.35 (t, *J* = 6.4 Hz, 2H). HPLC-MS (ESI, m/z): t_R = 4.32 min, 646.2 (M+H)⁺.

N-(2-(3-((5-fluoro-4-((2-(methylsulfonamido)phenyl)amino)pyrimidin-2-yl)amino)phenoxy)ethyl)-3-(2-(2-propionamidoethoxy)ethoxy)propanamide (Saturated Probe 3B)



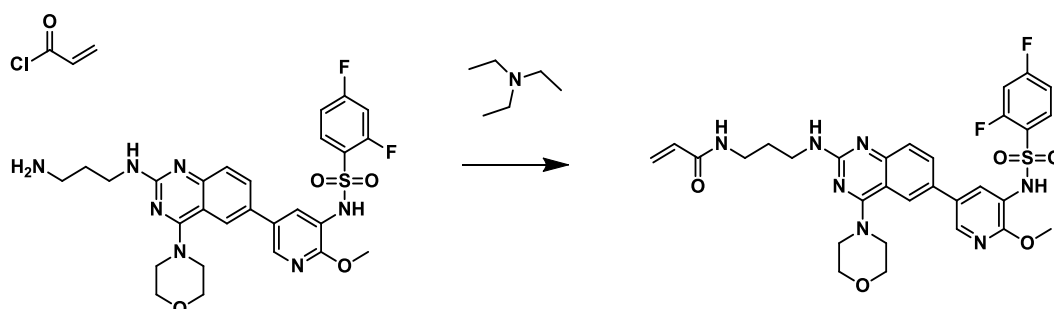
To a solution of N-(2-((2-((3-(2-aminoethoxy)phenyl)amino)-5-fluoropyrimidin-4-yl)amino)phenyl)methanesulfonamide (75 mg, 0.173 mmol) in 1 ml dimethylformamide, 2,2-dimethyl-4-oxo-3,8,11-trioxo-5-azatetradecan-14-oic acid (48.1 mg, 0.173 mmol), HATU (99 mg, 0.260 mmol) and DIPEA (90 μ l, 0.520 mmol) were added. The reaction was stirred at room temperature for 1 h. The product was purified by HPLC. This afforded tert-butyl (2-(2-(3-((3-(2-((5-fluoro-4-((2-(methylsulfonamido)phenyl)amino)pyrimidin-2-yl)amino)phenoxy)ethyl)amino)-3-oxopropoxy)ethoxy)ethyl)carbamate (77 mg, 0.104 mmol, 60 % yield). HPLC-MS (ESI, m/z): t_R = 5.34 min, 692.3 (M+H)⁺. For the boc deprotection, the dried intermediate product was dissolved in 0.5 ml ethyl acetate and 50 μ l concentrated HCl was added. The instantly forming insoluble slurry was dissolved in DMSO and the product was purified by HPLC. This afforded 3-(2-(2-aminoethoxy)ethoxy)-N-(2-(3-((5-fluoro-4-((2-(methylsulfonamido)phenyl)amino)pyrimidin-2-yl)amino)phenoxy)ethyl)propanamide (47.4 mg, 0.079 mmol, 71 % yield). HPLC-MS (ESI, m/z): t_R = 3.63 min, 592.2 (M+H)⁺. 3-(2-(2-aminoethoxy)ethoxy)-N-(2-(3-((5-fluoro-4-((2-(methylsulfonamido)phenyl)amino)pyrimidin-2-yl)amino)phenoxy)ethyl)propanamide (23.7 mg, 0.040 mmol) was dissolved in dimethylformamide (0.5 ml). To this solution was added propionyl chloride (3.5 μ l, 3.7 mg, 0.040 mmol) followed by triethylamine (17 μ l, 12.2 mg, 0.120 mmol). The reaction was stirred at room temperature for 1 h and then the product was purified by preparative HPLC without any further work-up. For this, the whole reaction was aliquoted into 0.75 ml fractions which were individually injected onto the column. The purified product from each fraction were combined and dried on high vacuum. This afforded N-(2-(3-((5-fluoro-4-((2-(methylsulfonamido)phenyl)amino)pyrimidin-2-yl)amino)phenoxy)ethyl)-3-(2-(2-propionamidoethoxy)ethoxy)propanamide (yield: 5.2 mg, 7.7 μ mol, 19 %). ¹H NMR (400 MHz, DMSO-*d*₆) δ 9.17 (s, 1H), 8.73 (s, 1H), 8.14 (s, 1H), 8.14 – 8.06 (m, 1H), 7.92 (dd, *J* = 7.9, 1.8 Hz, 1H), 7.79 (s, 1H), 7.41 (dd, *J* = 7.6, 1.9 Hz, 1H), 7.31 (t, *J* = 2.3 Hz, 1H), 7.21 (ddd, *J* = 13.0, 10.5, 6.2 Hz, 3H), 7.04 (t, *J* = 8.2 Hz, 1H), 6.45 (dd, *J* = 7.9, 2.4 Hz, 1H), 3.84 (t, *J* = 5.6 Hz, 2H), 3.61 (t, *J* = 6.4 Hz, 2H), 3.45 – 3.26 (m, 18H), 3.17 (d, *J* = 5.8 Hz, 4H), 2.90 (s, 3H), 2.35 (t, *J* = 6.5 Hz, 2H), 2.06 (q, *J* = 7.6 Hz, 2H), 0.97 (t, *J* = 7.6 Hz, 3H). HPLC-MS (ESI, m/z): t_R = 4.27 min, 648.3 (M+H)⁺.

N-(5-(2-((3-aminopropyl)amino)-4-morpholinoquinazolin-6-yl)-2-methoxypyridin-3-yl)-2,4-difluorobenzenesulfonamide (Promiscuous lipid kinase inhibitor LK)

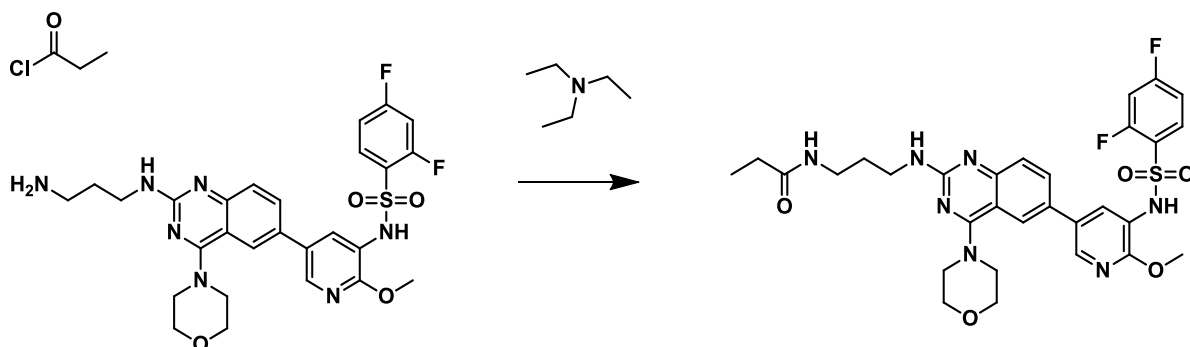


The promiscuous lipid kinase inhibitor LK was synthesized by colleagues at Cellzome / GlaxoSmithKline and generously provided by the company.

N-(3-((6-(5-(2,4-difluorophenylsulfonamido)-6-methoxypyridin-3-yl)-4-morpholinoquinazolin-2-yl)amino)propyl)acrylamide (Probe 4A)

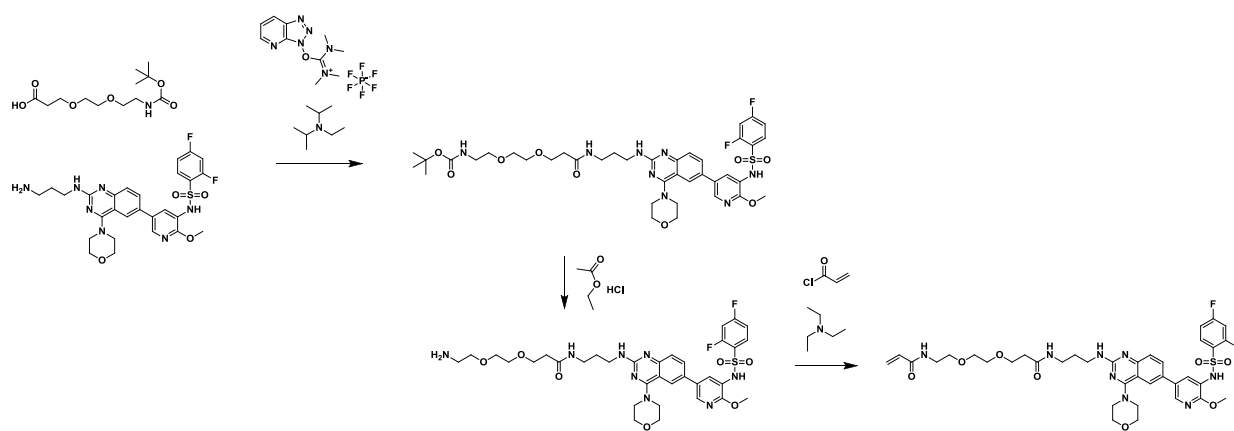


N-(5-(2-((3-aminopropyl)amino)-4-morpholinoquinazolin-6-yl)-2-methoxypyridin-3-yl)-2,4-difluorobenzenesulfonamide (25 mg, 0.043 mmol) was dissolved in DMSO (1.5 ml). To this solution was added acryloyl chloride (3.5 μ l, 3.9 mg, 0.043 mmol) followed by triethylamine (18 μ l, 13 mg, 0.128 mmol). The reaction was stirred at room temperature for 1 h and then the product was purified by preparative HPLC without any further work-up. For this, the whole reaction was aliquoted into 0.75 ml fractions which were individually injected onto the column. The purified product from each fraction were combined and dried on high vacuum. This afforded N-(3-((6-(5-(2,4-difluorophenylsulfonamido)-6-methoxypyridin-3-yl)-4-morpholinoquinazolin-2-yl)amino)propyl)acrylamide (yield: 10.1 mg, 0.014 mmol, 33 %). ^1H NMR (400 MHz, DMSO- d_6) δ 8.28 – 8.07 (m, 2H), 7.90 – 7.67 (m, 3H), 7.48 (qd, J = 14.6, 12.2, 5.4 Hz, 2H), 7.18 (td, J = 8.5, 2.5 Hz, 1H), 6.97 (s, 1H), 6.23 (dd, J = 17.1, 10.1 Hz, 1H), 6.08 (dd, J = 17.1, 2.3 Hz, 1H), 5.59 (dd, J = 10.1, 2.3 Hz, 1H), 3.84 – 3.77 (m, 5H), 3.69 (s, 9H), 3.36 (q, J = 6.6 Hz, 4H), 3.22 (q, J = 6.6 Hz, 2H), 1.73 (p, J = 7.1 Hz, 2H). HPLC-MS (ESI, m/z): t_{R} = 4.92 min, 640.2 (M+H) $^+$.

N-(3-((6-(5-(2,4-difluorophenylsulfonamido)-6-methoxypyridin-3-yl)-4-morpholinoquinazolin-2-yl)amino)propyl)propionamide (Saturated Probe 4A)

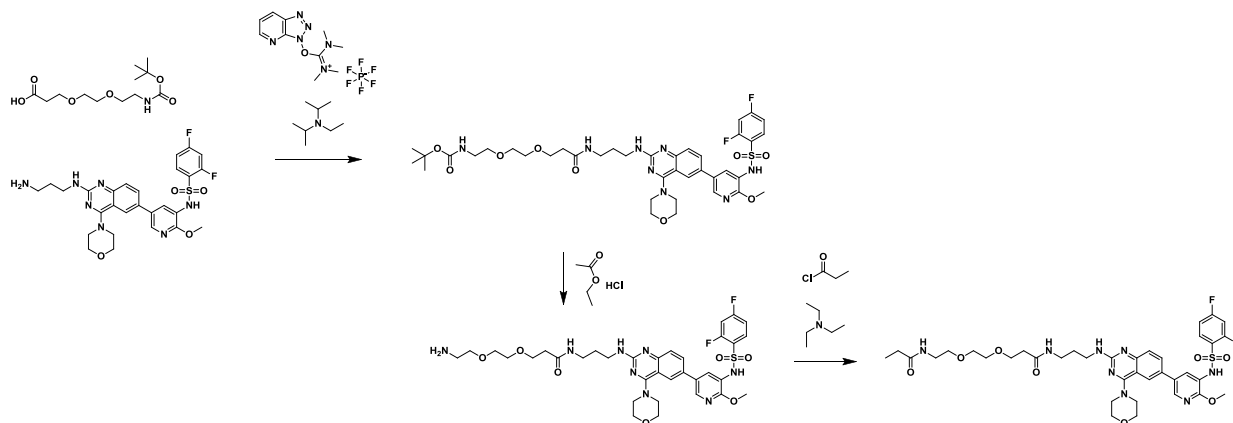
N-(5-(2-((3-aminopropyl)amino)-4-morpholinoquinazolin-6-yl)-2-methoxypyridin-3-yl)-2,4-difluorobenzenesulfonamide (25 mg, 0.043 mmol) was dissolved in dichloromethane (2 ml). To this solution was added propionyl chloride (3.7 μ l, 4.0 mg, 0.043 mmol) followed by triethylamine (18 μ l, 13 mg, 0.128 mmol). The reaction was stirred at room temperature for 1 h and then the product was purified by preparative HPLC without any further work-up. For this, the whole reaction was aliquoted into 0.75 ml fractions which were individually injected onto the column. The purified product from each fraction were combined and dried on high vacuum. This afforded N-(3-((6-(5-(2,4-difluorophenylsulfonamido)-6-methoxypyridin-3-yl)-4-morpholinoquinazolin-2-yl)amino)propyl)propionamide (yield: 17.2 mg, 0.024 mmol, 57 %). ¹H NMR (400 MHz, DMSO-*d*₆) δ 8.18 (d, *J* = 2.3 Hz, 1H), 8.12 (s, 1H), 7.82 – 7.62 (m, 5H), 7.46 (td, *J* = 9.9, 2.5 Hz, 1H), 7.37 (d, *J* = 8.8 Hz, 1H), 7.13 (td, *J* = 8.5, 2.5 Hz, 1H), 6.88 (s, 1H), 3.73 (t, *J* = 4.5 Hz, 9H), 3.28 (q, *J* = 6.6 Hz, 3H), 3.05 (q, *J* = 6.5 Hz, 3H), 2.01 (q, *J* = 7.7 Hz, 2H), 1.61 (p, *J* = 6.8 Hz, 2H), 0.93 (t, *J* = 7.6 Hz, 3H). HPLC-MS (ESI, *m/z*): *t*_R = 4.92 min, 642.2 (M+H)⁺.

N-(2-(2-(3-((3-((6-(5-(2,4-difluorophenylsulfonamido)-6-methoxy-pyridin-3-yl)-4-morpholinoquinazolin-2-yl)amino)propyl)amino)-3-oxopropoxy)ethoxy)ethyl)acrylamide (Probe 4B)

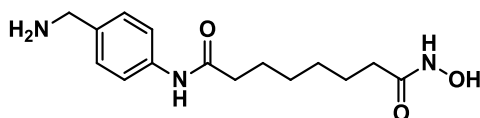


To a solution of N-(5-(2-((3-aminopropyl)amino)-4-morpholinoquinazolin-6-yl)-2-methoxypyridin-3-yl)-2,4-difluorobenzenesulfonamide (75 mg, 0.128 mmol) in 5 ml dichloromethane, 2,2-dimethyl-4-oxo-3,8,11-trioxa-5-azatetradecan-14-oic acid (35.5 mg, 0.128 mmol), HATU (73 mg, 0.192 mmol) and DIPEA (66 μ l, 0.384 mmol) were added. The reaction was stirred at room temperature for 1 h. The solvent was evaporated and the solid was dissolved in DMSO. The product was purified by HPLC. This afforded tert-butyl (2-(2-(3-((3-((6-(5-(2,4-difluorophenylsulfonamido)-6-methoxypyridin-3-yl)-4-morpholinoquinazolin-2-yl)amino)propyl)amino)-3-oxopropoxy)ethoxy)ethyl)carbamate (31.3 mg, 0.031 mmol, 24 % yield). HPLC-MS (ESI, m/z): t_R = 5.35 min, 845.3 (M+H)⁺. For the boc deprotection, the dried intermediate product was dissolved in 0.7 ml ethyl acetate and 100 μ l concentrated HCl was added. The product was purified by HPLC. This afforded 3-(2-(2-aminoethoxy)ethoxy)-N-(3-((6-(5-(2,4-difluorophenylsulfonamido)-6-methoxypyridin-3-yl)-4-morpholinoquinazolin-2-yl)amino)propyl)propanamide (20.8 mg, 0.026 mmol, 71 % yield). HPLC-MS (ESI, m/z): t_R = 4.04 min, 745.3 (M+H)⁺. 3-(2-(2-aminoethoxy)ethoxy)-N-(3-((6-(5-(2,4-difluorophenylsulfonamido)-6-methoxypyridin-3-yl)-4-morpholinoquinazolin-2-yl)amino)propyl)propanamide (11 mg, 0.015 mmol) was dissolved in dimethylformamide (0.5 ml). To this solution was added acryloyl chloride (1.2 μ l, 1.3 mg, 0.015 mmol) followed by triethylamine (6.2 μ l, 4.5 mg, 0.044 mmol). The reaction was stirred at room temperature for 1 h and then the product was purified by preparative HPLC without any further work-up. For this, the whole reaction was aliquoted into 0.75 ml fractions which were individually injected onto the column. The purified product from each fraction were combined and dried on high vacuum. This afforded N-(2-(2-(3-((3-((6-(5-(2,4-difluorophenylsulfonamido)-6-methoxypyridin-3-yl)-4-morpholinoquinazolin-2-yl)amino)propyl)amino)-3-oxopropoxy)ethoxy)ethyl)acrylamide (yield: 2.8 mg, 3.1 μ mol, 21 %). ¹H NMR (400 MHz, DMSO-*d*₆) δ 8.36 (s, 2H), 8.16 (s, 2H), 7.89 (s, 5H), 7.48 (s, 1H), 7.23 (s, 1H), 6.23 (s, 1H), 5.57 (s, 1H), 3.80 (s, 4H), 3.66 (s, 6H), 3.49 (s, 5H), 3.13 (s, 2H), 2.32 (s, 3H), 1.69 (s, 2H). HPLC-MS (ESI, m/z): t_R = 4.79 min, 799.3 (M+H)⁺.

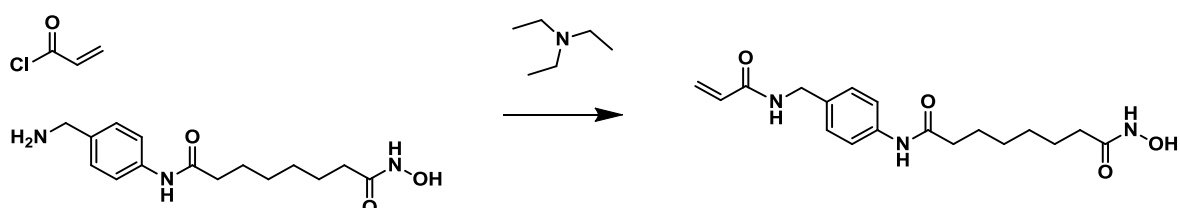
N-(3-((6-(5-(2,4-difluorophenylsulfonamido)-6-methoxypyridin-3-yl)-4-morpholinoquinazolin-2-yl)amino)propyl)-3-(2-(2-propionamidoethoxy)ethoxy)propanamide (Saturated Probe 4B)



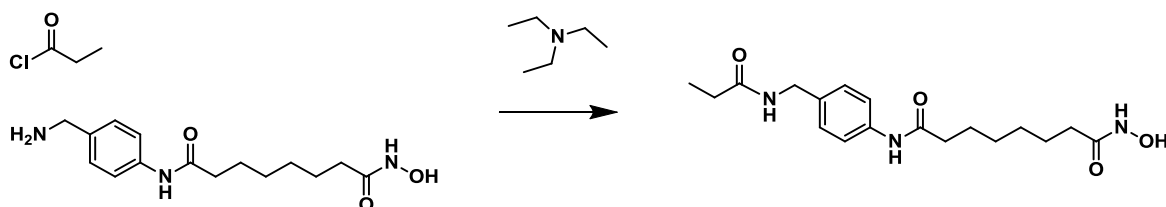
To a solution of N-(5-(2-((3-aminopropyl)amino)-4-morpholinoquinazolin-6-yl)-2-methoxypyridin-3-yl)-2,4-difluorobenzenesulfonamide (75 mg, 0.128 mmol) in 5 ml dichloromethane, 2,2-dimethyl-4-oxo-3,8,11-trioxa-5-azatetradecan-14-oic acid (35.5 mg, 0.128 mmol), HATU (73 mg, 0.192 mmol) and DIPEA (66 μ l, 0.384 mmol) were added. The reaction was stirred at room temperature for 1 h. The solvent was evaporated and the solid was dissolved in DMSO. The product was purified by HPLC. This afforded tert-butyl (2-(2-(3-((6-(5-(2,4-difluorophenylsulfonamido)-6-methoxypyridin-3-yl)-4-morpholinoquinazolin-2-yl)amino)propyl)amino)-3-oxopropoxy)ethoxy)ethyl)carbamate (31.3 mg, 0.031 mmol, 24 % yield). HPLC-MS (ESI, m/z): t_R = 5.35 min, 845.3 (M+H)⁺. For the boc deprotection, the dried intermediate product was dissolved in 0.7 ml ethyl acetate and 100 μ l concentrated HCl was added. The product was purified by HPLC. This afforded 3-(2-(2-aminoethoxy)ethoxy)-N-(3-((6-(5-(2,4-difluorophenylsulfonamido)-6-methoxypyridin-3-yl)-4-morpholinoquinazolin-2-yl)amino)propyl)propanamide (20.8 mg, 0.026 mmol, 71 % yield). HPLC-MS (ESI, m/z): t_R = 4.04 min, 745.3 (M+H)⁺. 3-(2-(2-aminoethoxy)ethoxy)-N-(3-((6-(5-(2,4-difluorophenylsulfonamido)-6-methoxypyridin-3-yl)-4-morpholinoquinazolin-2-yl)amino)propyl)propanamide (11.6 mg, 0.016 mmol) was dissolved in dimethylformamide (0.5 ml). To this solution was added propionyl chloride (1.4 μ l, 1.4 mg, 0.016 mmol) followed by triethylamine (6.5 μ l, 4.7 mg, 0.047 mmol). The reaction was stirred at room temperature for 1 h and then the product was purified by preparative HPLC without any further work-up. For this, the whole reaction was aliquoted into 0.75 ml fractions which were individually injected onto the column. The purified product from each fraction were combined and dried on high vacuum. This afforded N-(3-((6-(5-(2,4-difluorophenylsulfonamido)-6-methoxypyridin-3-yl)-4-morpholinoquinazolin-2-yl)amino)propyl)-3-(2-(2-propionamidoethoxy)ethoxy)propanamide (yield: 2.4 mg, 3.0 μ mol, 19 %). ¹H NMR (400 MHz, DMSO-*d*₆) δ 8.35 (s, 1H), 8.14 (s, 1H), 7.89 (s, 2H), 7.82 (d, *J* = 19.9 Hz, 4H), 7.58 (s, 1H), 7.46 (s, 1H), 7.22 (s, 1H), 3.80 (s, 4H), 3.66 (s, 3H), 3.61 (s, 4H), 3.48 (s, 4H), 3.16 (s, 4H), 2.32 (s, 2H), 2.06 (d, *J* = 8.6 Hz, 2H), 1.69 (s, 2H), 0.97 (t, *J* = 7.5 Hz, 3H). HPLC-MS (ESI, m/z): t_R = 4.77 min, 801.3 (M+H)⁺.

N1-(4-(aminomethyl)phenyl)-N8-hydroxyoctanediamide (Promiscuous HDAC inhibitor)

The promiscuous HDAC inhibitor was synthesized by colleagues at Cellzome / GlaxoSmithKline and generously provided by the company.

N1-(4-(acrylamidomethyl)phenyl)-N8-hydroxyoctanediamide (Probe 5A)

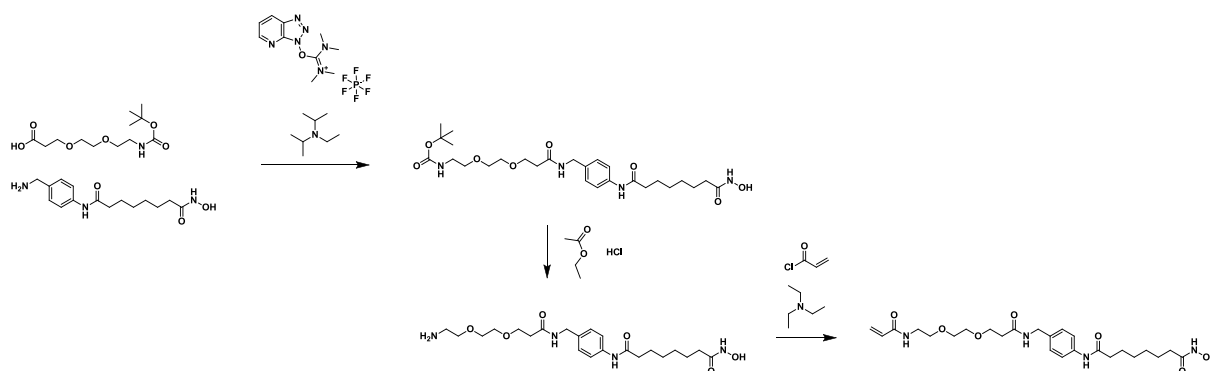
N1-(4-(aminomethyl)phenyl)-N8-hydroxyoctanediamide (20 mg, 0.061 mmol) was dissolved in dimethylformamide (1.5 ml). To this solution was added acryloyl chloride (4.9 μ l, 5.5 mg, 0.061 mmol) followed by triethylamine (25 μ l, 18.4 mg, 0.182 mmol). The reaction was stirred at room temperature for 1 h and then the product was purified by preparative HPLC without any further work-up. For this, the whole reaction was aliquoted into 0.75 ml fractions which were individually injected onto the column. The purified product from each fraction were combined and dried on high vacuum. This afforded N1-(4-(acrylamidomethyl)phenyl)-N8-hydroxyoctanediamide (yield: 12.3 mg, 0.035 mmol, 58 %). ^1H NMR (400 MHz, Methanol- d_4) δ 7.58 – 7.45 (d, 2H), 7.24 (d, J = 8.3 Hz, 2H), 6.33 – 6.20 (m, 2H), 5.67 (dd, J = 8.1, 3.9 Hz, 1H), 4.40 (s, 2H), 2.35 (t, J = 7.5 Hz, 2H), 2.09 (t, J = 7.4 Hz, 2H), 1.66 (dp, J = 21.3, 7.2 Hz, 4H), 1.44 – 1.32 (m, J = 6.2, 5.2 Hz, 4H). UPLC-MS (ESI, m/z): t_R = 1.18 min, 348.2 (M+H) $^+$.

N1-hydroxy-N8-(4-(propionamidomethyl)phenyl)octanediamide (Saturated Probe 5A)

N1-(4-(aminomethyl)phenyl)-N8-hydroxyoctanediamide (18 mg, 0.055 mmol) was dissolved in dimethylformamide (1.5 ml). To this solution was added propionyl chloride (4.8 μ l, 5.1 mg, 0.055 mmol) followed by triethylamine (23 μ l, 16.6 mg, 0.164 mmol). The reaction was stirred at room temperature for 1 h and then the product was purified by preparative HPLC without any further work-up. For this, the whole reaction was aliquoted into 0.75 ml fractions which were individually injected

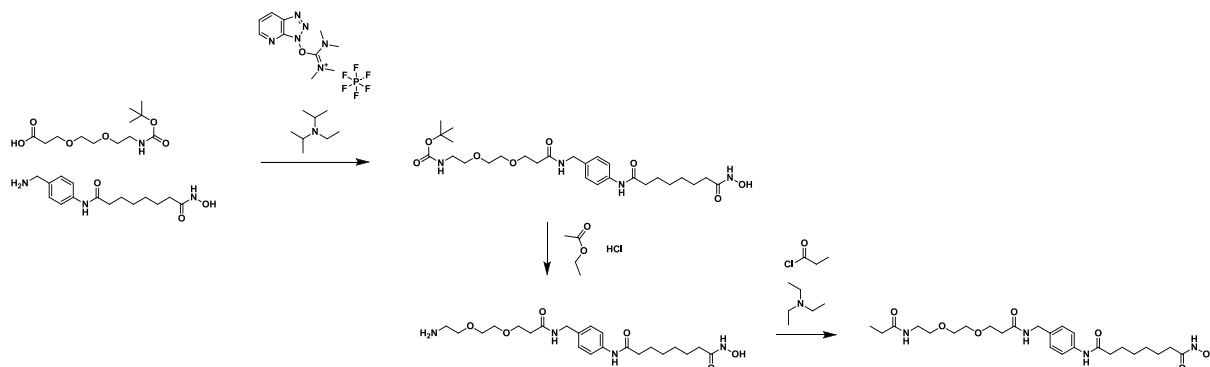
onto the column. The purified product from each fraction were combined and dried on high vacuum. This afforded N1-hydroxy-N8-(4-(propionamidomethyl)phenyl)octanediamide (yield: 10 mg, 0.028 mmol, 52 %). $^1\text{H NMR}$ (400 MHz, Methanol- d_4) δ 7.55 – 7.45 (d, 2H), 7.22 (d, $J = 8.3$ Hz, 2H), 4.31 (s, 2H), 2.36 (t, $J = 7.5$ Hz, 2H), 2.24 (q, $J = 7.6$ Hz, 2H), 2.09 (t, $J = 7.4$ Hz, 2H), 1.66 (dt, $J = 25.3, 7.0$ Hz, 4H), 1.39 (p, $J = 3.8, 3.4$ Hz, 4H), 1.14 (t, $J = 7.6$ Hz, 3H). UPLC-MS (ESI, m/z): $t_R = 1.18$ min, 350.2 (M+H) $^+$.

N1-(4-(3,13-dioxo-6,9-dioxo-2,12-diazapentadec-14-en-1-yl)phenyl)-N8-hydroxyoctanediamide (Probe 5B)



To a solution of N1-(4-(aminomethyl)phenyl)-N8-hydroxyoctanediamide (100 mg, 0.303 mmol) in 4.5 ml dimethylformamide, 2,2-dimethyl-4-oxo-3,8,11-trioxo-5-azatetradecan-14-oic acid (87 mg, 0.314 mmol), HATU (158 mg, 0.416 mmol) and DIPEA (313 μl , 1.82 mmol) were added. The reaction was stirred at room temperature for 1 h. The product was purified by HPLC. This afforded tert-butyl (2-(2-(3-((4-(8-(hydroxyamino)-8-oxooctanamido)benzyl)amino)-3-oxopropoxy)ethoxy)ethyl)carbamate (67.2 mg, 0.114 mmol, 38 % yield). HPLC-MS (ESI, m/z): $t_R = 4.70$ min, 553.3 (M+H) $^+$. For the boc deprotection, the dried intermediate product was dissolved in 3 ml ethyl acetate and 300 μl concentrated HCl was added. The product was purified by HPLC. This afforded N1-(4-((3-(2-(2-aminoethoxy)ethoxy)propanamido)methyl)phenyl)-N8-hydroxyoctanediamide (75.7 mg, 0.154 mmol, quant yield). UPLC-MS (ESI, m/z): $t_R = 0.88$ min, 453.3 (M+H) $^+$. N1-(4-((3-(2-(2-aminoethoxy)ethoxy)propanamido)methyl)phenyl)-N8-hydroxyoctanediamide (37.9 mg, 0.084 mmol) was dissolved in dimethylformamide (1 ml). To this solution was added acryloyl chloride (5 μl , 5.6 mg, 0.062 mmol) followed by triethylamine (35 μl , 25.4 mg, 0.251 mmol). The reaction was stirred at room temperature for 1 h and then the product was purified by preparative HPLC without any further work-up. For this, the whole reaction was aliquoted into 0.75 ml fractions which were individually injected onto the column. The purified product from each fraction were combined and dried on high vacuum. This afforded N1-(4-(3,13-dioxo-6,9-dioxo-2,12-diazapentadec-14-en-1-yl)phenyl)-N8-hydroxyoctanediamide (yield: 9 mg, 0.017 mmol, 20 %). $^1\text{H NMR}$ (400 MHz, Methanol- d_4) δ 7.54 – 7.48 (d, 2H), 7.24 (d, $J = 8.3$ Hz, 2H), 6.32 – 6.16 (m, 2H), 5.64 (dd, $J = 9.4, 2.6$ Hz, 1H), 4.34 (s, 2H), 3.76 (t, $J = 6.0$ Hz, 2H), 3.59 (hept, $J = 2.6$ Hz, 4H), 3.54 (t, $J = 5.5$ Hz, 2H), 3.40 (t, $J = 5.5$ Hz, 2H), 2.49 (t, $J = 6.0$ Hz, 2H), 2.36 (t, $J = 7.5$ Hz, 2H), 2.09 (t, $J = 7.4$ Hz, 2H), 1.66 (dt, $J = 25.6, 6.6$ Hz, 4H), 1.45 – 1.32 (m, 6H). UPLC-MS (ESI, m/z): $t_R = 1.20$ min, 507.3 (M+H) $^+$.

N1-(4-(3,13-dioxo-6,9-dioxa-2,12-diazapentadecyl)phenyl)-N8-hydroxyoctanediamide (Saturated Probe 5B)



To a solution of N1-(4-(aminomethyl)phenyl)-N8-hydroxyoctanediamide (100 mg, 0.303 mmol) in 4.5 ml dimethylformamide, 2,2-dimethyl-4-oxo-3,8,11-trioxa-5-azatetradecan-14-oic acid (87 mg, 0.314 mmol), HATU (158 mg, 0.416 mmol) and DIPEA (313 μ l, 1.82 mmol) were added. The reaction was stirred at room temperature for 1 h. The product was purified by HPLC. This afforded tert-butyl (2-(2-(3-((4-(8-(hydroxyamino)-8-oxooctanamido)benzyl)amino)-3-oxopropoxy)ethoxy)ethyl)carbamate (67.2 mg, 0.114 mmol, 38 % yield). HPLC-MS (ESI, m/z): t_R = 4.70 min, 553.3 (M+H)⁺. For the boc deprotection, the dried intermediate product was dissolved in 3 ml ethyl acetate and 300 μ l concentrated HCl was added. The product was purified by HPLC. This afforded N1-(4-((3-(2-(2-aminoethoxy)ethoxy)propanamido)methyl)phenyl)-N8-hydroxyoctanediamide (75.7 mg, 0.154 mmol, quant yield). UPLC-MS (ESI, m/z): t_R = 0.88 min, 453.3 (M+H)⁺. N1-(4-((3-(2-(2-aminoethoxy)ethoxy)propanamido)methyl)phenyl)-N8-hydroxyoctanediamide (37.9 mg, 0.084 mmol) was dissolved in dimethylformamide (1.5 ml). To this solution was added propionyl chloride (5.5 μ l, 5.8 mg, 0.063 mmol) followed by triethylamine (35 μ l, 25.4 mg, 0.251 mmol). The reaction was stirred at room temperature for 1 h and then the product was purified by preparative HPLC without any further work-up. For this, the whole reaction was aliquoted into 0.75 ml fractions which were individually injected onto the column. The purified product from each fraction were combined and dried on high vacuum. This afforded N1-(4-(3,13-dioxo-6,9-dioxa-2,12-diazapentadecyl)phenyl)-N8-hydroxyoctanediamide (yield: 8.1 mg, 0.015 mmol, 19 %). ¹H NMR (400 MHz, Methanol-*d*₄) δ 7.51 (d, J = 8.4 Hz, 2H), 7.24 (d, J = 8.3 Hz, 2H), 4.35 (s, 2H), 3.76 (t, J = 6.0 Hz, 2H), 3.59 (tt, J = 5.1, 2.7 Hz, 4H), 3.50 (t, J = 5.5 Hz, 2H), 2.49 (t, J = 6.0 Hz, 2H), 2.36 (t, J = 7.5 Hz, 2H), 2.19 (q, J = 7.6 Hz, 2H), 2.09 (t, J = 7.4 Hz, 2H), 1.66 (dt, J = 25.6, 6.9 Hz, 4H), 1.39 (d, J = 6.7 Hz, 5H), 1.10 (t, J = 7.6 Hz, 3H). UPLC-MS (ESI, m/z): t_R = 1.20 min, 509.3 (M+H)⁺.

2.3. Biochemistry and cell culture

Kinobeads pulldown. For a pulldown using kinobeads, the bead matrix was washed twice with 50-fold excess in volume of drug pulldown (DP) buffer (50 mM Tris/HCl pH 7.4, 5 % glycerol, 1.5 mM MgCl₂, 150 mM NaCl, 1 mM Na₃VO₄, 25 mM NaF) and equilibrated once with 50-fold excess in volume of DP/0.4 % IGEPAL CA 630. The settled beads were re-suspended in DP/0.4 % IGEPAL CA 630 to get a 5 % slurry. Beads were added to the wells of 96-well or 384-well filter plates in a 1:7 ratio protein [mg] / beads [μl]. After addition of the cell lysate to the dried beads, incubation was done at 4 °C for 1 h overhead rotating and 900 rpm horizontal shaking for 96-well plates and 384-well plates, respectively. After protein capturing, beads were washed in ~ 280 bead volumes DP/0.4 % IGEPAL CA 630 and ~ 140 bead volumes DP/0.2 % IGEPAL CA 630. Subsequently, residual washing buffer was removed by centrifugation (314 g, 2 min, RT) and bound proteins were denatured for 30 min, 50 °C using 2X LDS sample buffer (NuPAGE #NP0007) / 50 mM DTT. Elution was done by centrifugation (314 g, 4 min, RT). LDS eluates were stored at -20 °C until further processing by Western blot or mass spectrometry analysis. A *lipid kinase* and *HDAC* pulldown was performed analogously with *lipid kinobeads* and a *HDAC affinity matrix*, respectively.

Cell-based kinobeads assay with covalent kinase inhibitors. Ramos cells or B-cells isolated from human blood adjusted to a density of ~ 5.6*10⁶ cells/ml in RPMI-1640 medium (Gibco #21875-034) supplemented with 0.1 % FBS (Gibco #10270) were treated with concentrations of compound as given in the respective experiment or vehicle (final DMSO concentration: 0.5 %) for 1 h, 37 °C, 5 % CO₂, 100 rpm shaking. Cells were collected and centrifuged for 4 min, 491 g, RT. The cells were washed twice by resuspending in 25 ml fresh medium and incubation for 30 min, 37 °C, 5 % CO₂, 100 rpm shaking and subsequently twice by resuspending in 10 ml ice cold PBS (Gibco #14190-094). After every washing step, cells were centrifuged for 4 min, 491 g, at RT or 4 °C for medium incubation or PBS resuspension, respectively.

For the treatment of adherent A549 cells, 5*10⁶ cells were seeded in 25 ml DMEM medium (Gibco #41965-039) supplemented with 10 % FBS per 15 cm cell culture dish. After 72 h (→ ~ 90 % confluency), the medium was removed and replaced by 15 ml DMEM medium / 0.1 % FBS containing concentrations of compound as given in the respective experiment or vehicle (final DMSO concentration: 0.5%). Cells were incubated for 1 h, 37 °C, 10 % CO₂. After incubation, the compound containing medium was removed and the cells were incubated 1x 30 min in 15 ml medium and 1x 30 min in 15 ml pre-warmed PBS. For harvesting, 3 ml versene solution (Gibco #15040-033) was added per plate and the plates were incubated for ~ 10 min, 37 °C, 5 % CO₂, 100 rpm shaking. The cells were transferred to 15 ml tubes using 12 ml ice cold PBS. The cell suspension was centrifuged for 3 min, 491 g, 4 °C and the supernatant was removed. The cells were resuspended once more in 10 ml PBS and centrifuged for 4 min, 491 g, 4 °C.

After the last washing step, suspension and adherent cells were treated equally by removing the supernatant completely and freezing the cells in liquid nitrogen to be stored at -80 °C until cell lysis.

Kinobeads pulldown was performed for each individual lysate as described above.

Lysate-based kinobeads assay. Per data point 1000 μ l lysate (concentration: 5 mg/ml; 0.4 % IGEPAL CA 630) was incubated with concentrations of compound as given in the respective experiment or vehicle (final DMSO concentration in lysate: 0.5%). After incubation for 1 h at 4 °C, overhead rotating, kinobeads pulldown was performed as described above.

Cell culturing. All cell lines were generously provided by Cellzome / GlaxoSmithKline. Suspension cells (Jurkat, Ramos, THP-1, and YT) were cultured in RPMI-1640 medium (Gibco #21875-034) supplemented with 10 % FBS (Gibco #10270), stirring at 37 °C, 5% CO₂. Cells were seeded at a cell density of 0.5×10^6 cells/ml and split all 3-4 days.

Adherent A549 cells were cultured in DMEM medium (Gibco #41965-039) supplemented with 10 % FBS, at 37 °C, 10 % CO₂. 2.5×10^6 cells were seeded in 25 ml in a 15 cm cell culture dish and split all 3-4 days. Detachment of cells was achieved using trypsin/0.05 % EDTA (Gibco #25300-054) for routine cell culture and versene solution (Gibco #15040-033) after compound treatment.

Total lysate preparation. Cell pellets were snap frozen in liquid nitrogen and stored at -80 °C until lysis. For lysis, 2 volumes and 3 volumes of lysis buffer (50 mM Tris/HCl pH 7.4, 5 % glycerol, 1.5 mM MgCl₂, 150 mM NaCl, 1 mM Na₃VO₄, 25 mM NaF, 0.8 % IGEPAL CA 630, protease inhibitor (Roche #11873580001)) were added to pellets of adherent cells and suspension cells, respectively. The mixture was incubated rotating at medium speed, 4 °C until the whole cell pellet was thawed. Cells were mechanically lysed using a dounce homogenizer on ice. The suspension containing the dissociated cells was incubated for further 30 min rotating at medium speed, 4 °C to complete cell lysis. The homogenate was centrifuged for 10 min, 20000 g, 4 °C and the supernatant was transferred to ultracentrifugation tubes. After centrifugation for 1 h, 100000 g, 4 °C the supernatant was recovered and protein concentration was determined by Bradford assay. The lysates were snap frozen in liquid nitrogen and stored at -80 °C until usage.

For small cell pellets (< 250 μ l), 2 volumes of lysis buffer were added to the pellets. The cell pellets were re-suspended by pipetting 20x up and down. The mixture was incubated shaking at 900 rpm, 4 °C for 30 min. The suspension containing the dissociated cells was transferred to ultracentrifugation tubes centrifuged for 30 min, 100000 g, 4 °C. The supernatant was recovered and protein concentration was determined by Bradford assay. The lysates were snap frozen in liquid nitrogen and stored at -80 °C until usage.

SDS lysis and benzonase digestion. A cell pellet was re-suspended in one volume 50 mM Tris/HCl pH 7.4, 4 % SDS. Subsequently, the samples were heated for 3 min at 95 °C, 700 rpm shaking. The SDS concentration was adjusted to 1 % using 50 mM Tris/HCl pH 7.4 and DNA was digested using benzonase at 2 U/ μ l for 30 min, 37 °C, 850 rpm shaking and subsequently using benzonase at 1 U/ μ l for 45 min, 37 °C, 850 rpm shaking, Lysates were cleared by centrifugation for 20 min at 20000 g, room temperature.

Crude lysate preparation from Ramos cells. A crude Ramos cell lysate was prepared by adding 2.25 cell pellet volumes of PBS supplemented with protease inhibitor. The cells were disrupted using a Bead ruptor machine (Omni Inc) with the cycle settings 4 m/s; 10 sec; 1 cycle. 1.5 mM MgCl₂ and benzonase at 2 U/μl were added. DNA was digested for 1 h at 4 °C shaking before snap freezing the lysate.

Protein concentration determination by Bradford assay. Cell lysates were diluted 1:40 in H₂O. 2 μl of diluted protein or BSA standard (Biorad #5000202) at concentrations of 0 – 0.125 – 0.25 – 0.5 – 1 – 2 mg/ml was added per well of a black 96-well plate with clear bottom. 200 μl Bradford reagent (Biorad #5000202) was added per well. After incubation for 5 min, the plate was centrifuged for 1 min, 314 g, RT. The absorbance at 595 nm was measured using a plate reader (Envision 2103 Multilabel Reader). Protein concentration was determined in triplicates from which the average was calculated. Concentrations were calculated from the absorbance raw values using the BSA standard curve.

SDS-PAGE. Samples were denatured for 30 min at 50 °C using 2X LDS sample buffer (ThermoFisher Scientific #NP0007) / 50 mM DTT. Denatured samples were loaded to 4-12 % Bis/Tris gels (Invitrogen) and run in 1X MOPS buffer (ThermoFisher Scientific #NP0001) at constant voltage of 80 V for 15 min and 160 V to the end. For gel-based digestion of proteins for mass spectrometry analysis gel separation was done for 20 min, 80 V.

Coomassie staining. Gels containing separated proteins were fixed in fixing solution (40 % ethanol, 2 % acetic acid) for 45 min, RT, shaking. Subsequently, fixing solution was replaced by Coomassie stain (16 % colloidal Brilliant blue (Sigma #B2025-1EA), 20 % ethanol) overnight shaking at 4 °C. The stained gels were discolored using destain solution (25 % ethanol, 5 % acetic acid) until the gels were only slightly blue. Gels were incubated in 25 % ethanol until only the protein bands were stained. Finally, gels were equilibrated in H₂O. For MS analyses, gels were stored at 4 °C until further processing.

Western blot analysis. For Western blot analyses, proteins separated by SDS-PAGE were transferred to PVDF membranes using a wet transfer procedure (Constant current: 500 mA, 2 h; transfer buffer: 25 mM Tris-base, 190 mM glycine, 0.05 % SDS, 20 % ethanol). The membranes were blocked for 1 h at RT in 20 ml blocking buffer (LI-COR #927-40000) per membrane.

BTK antibody staining was done overnight at RT using BTK Santa Cruz, #sc-1107, goat, 1:2000 in blocking buffer / 0.2 % Tween 20. Incubation with secondary antibody was done for 1 h at RT using LI-COR IRDye 800/680 anti-goat (P/N 925-32214 / P/N 925-68074) 1:5000 in blocking buffer / 0.2 % Tween 20.

PARP1 antibody staining was done overnight at 4 °C using PARP1 Bethyl laboratories, #A301-375A, rabbit, 1:1000 in blocking buffer. Incubation with secondary antibody was done for 1 h at RT using LI-COR IRDye 800/680 anti-rabbit (P/N 925-32211 / P/N 925-68071) 1:5000 in blocking buffer / 0.2 % Tween 20.

EGFR antibody staining was done overnight at 4 °C using EGFR Abcam, #ab2430, rabbit, 1:1000 in blocking buffer. Incubation with secondary antibody was done for 1 h at RT using LI-COR IRDye 800/680 rabbit (P/N 925-32211 / P/N 925-68071) 1:5000 in blocking buffer.

MAPK9 antibody staining was done overnight at 4 °C using MAPK9 Cell signaling, #4672, rabbit, 1:1000 in blocking buffer. Incubation with secondary antibody was done for 1 h at RT using LI-COR IRDye 800/680 rabbit (P/N 925-32211 / P/N 925-68071) 1:5000 in blocking buffer.

Signal quantification [RLU] was done using an Odyssey fluorescence imager. For dose-response experiments, binding curves were fitted using a four-parameter non-linear regression fitting module (Graph Pad Prism 7.03 software).

On cell time course. Ramos cells at a density of $\sim 5.6 \times 10^6$ cells/ml were treated with 1 μ M Ibrutinib, 3 nM Ibrutinib, 5 μ M saturated Ibrutinib, and vehicle (final DMSO concentration: 0.5%) for 0.5- 1 - 2 - 4 - 6 - 24 h, 37 °C, 5 % CO₂, 100 rpm shaking. 2×10^7 cells were harvested and centrifuged for 4 min, 491 g, RT. The cells were washed by re-suspending twice in 12 ml ice cold PBS (Gibco #14190-094). After every washing step, cells were centrifuged for 4 min, 491 g, at 4 °C. After the last washing step, the supernatant was removed completely and cells were frozen in liquid nitrogen and stored at -80 °C until cell lysis. A kinobeads pulldown was performed for each lysate and LDS eluted proteins were separated by SDS-PAGE. A Western blot analysis was performed staining for BTK as described.

Washout procedure evaluation. Ramos cells at a density of $\sim 5.6 \times 10^6$ cells/ml were treated with 1 μ M Ibrutinib, 5 μ M saturated Ibrutinib, and vehicle (final DMSO concentration: 0.5 %) for 0.5 h, 37 °C, 5 % CO₂, 100 rpm shaking. 2×10^7 cells were harvested and centrifuged for 4 min, 491 g, RT. The cells were washed by either (a) re-suspending twice in 10 ml ice cold PBS (Gibco #14190-094) or by (b) re-suspending twice in 10 ml fresh medium (RPMI-1640 / 10 % FBS) and incubation for 30 min, 37 °C, 5 % CO₂, 100 rpm shaking and subsequently re-suspending twice in 10 ml ice cold PBS. As control a third set of samples was not washed. After every washing step, cells were centrifuged for 4 min, 491 g, at RT or 4 °C for medium incubation or PBS resuspension, respectively. After the last washing step, the supernatant was removed completely and cells were frozen in liquid nitrogen and stored at -80 °C until cell lysis. A kinobeads pulldown was performed for each lysate and LDS eluted proteins were separated by SDS-PAGE. A Western blot analysis was performed staining for BTK as described.

Isolation of B-cells from human blood. The human biological samples were sourced ethically and their research use was in accord with the terms of the informed consents under an IRB/EC approved protocol.

PBMCs were isolated from human buffy coats. For gradient separation, the blood was diluted 1:1 with RPMI-1640 without any supplements. 17 ml diluted blood was layered on 17 ml of Histopaque (Sigma #10771) in a 50 ml tube. Gradient-separation was performed by centrifugation at 872 g, 30 min, RT, slow deceleration. A ring of PBMCs was carefully collected. For B-cell isolation, the PBMCs were washed twice with B-cell isolation buffer (PBS (w/o CaCl₂, w/o MgCl₂), 1 mM EDTA (Sigma #E7889-100ML), 2 % FBS) by centrifugation at 491 g, 5 min, RT. PBMCs were re-suspended at a

concentration of 5×10^7 cells/ml in B-cell isolation buffer and 50 μ l EasysepTM human B cell Enrichment Cocktail (Stemcell #19054) was added per ml cells. After mixing, the suspension was incubated for 10 min at RT. EasysepTM D Magnetic Particles (Stemcell #19054) were vortexed for 30 sec prior to addition of 75 μ l magnetic beads per ml cell suspension. After mixing, the suspension was incubated for 5 min at RT. The B-cells were negatively isolated by removing the cells bound to magnetic particles using a magnet for 5 min. The desired B-cells were harvested by centrifugation at 491 g, for 5 min, RT.

Ca²⁺ mobilization assay. Isolated B-cells were re-suspended in 1 ml PBS (w/o CaCl₂, w/o MgCl₂) and the cell concentration was adjusted to 1.11×10^7 cells/ml. To 900 μ l cell suspension (1×10^7 cells) 100 μ l Fluo-4 (ThermoFisher Scientific #F14201) / Pluronic (ThermoFisher Scientific #F-127) mix was added and the cells were incubated for 30 min at 37 °C, 5 % CO₂, in the dark, 200 rpm shaking. Cells were washed twice with 10 ml PBS (w/o CaCl₂, w/o MgCl₂) / 10 % FBS by centrifugation (491 g, 3 min, RT). Cells were re-suspended at a concentration of 2×10^6 cells/ml in PBS (w/o CaCl₂, w/o MgCl₂) / 10 % FBS. 30 μ l of a 10X compound solution or vehicle was placed into FACS tubes before adding 240 μ l cell suspension to each tube (final DMSO concentration: 0.5%). Tubes were vortexed shortly before incubation for 45 min at RT in the dark. For a FACS readout (BD FACSCalibur), all samples were pre-warmed directly before measurement for 3 min at 37 °C. For the positive control, 6 μ l of a 50 mM calcium solution (final: 1 mM) was added to a tube, vortexed and immediately read for 200 sec at medium speed. For samples except for the negative control, 6 μ l of calcium solution plus 30 μ l of fragment goat anti-human IgM (Jackson labs, #109-006-129) solution (50 μ g/ml final) was added.

Experiments with recombinant proteins. Studies on recombinant proteins included recombinant ZAK (ThermoFisher Scientific PR7052A), recombinant ACAD9 (Abnova H00028976-P01), recombinant TEC (Sigma SRP5090), and recombinant MAPK9 (SGC). Storage buffer of the recombinant proteins was exchanged with 50 mM Tris/HCl pH 7.4, 150 mM NaCl, 10 % glycerol, 0.02 % Triton X-100 using Zeba Spin Desalting columns (ThermoFisher Scientific #89882) according to the manufacturer's protocol. Ibrutinib, 5Z-7-Oxozeaenol, probe 1A, probe 2A, probe 3A, or vehicle was added to 1 μ g protein to get a final concentration of 10 μ M / 0.5 % DMSO. The samples were incubated overnight at 22 °C, 750 rpm shaking. Proteins were digested with different enzymes including trypsin, GluC, AspN, chymotrypsin, or combinations thereof reconstituted in buffer as suggested by the supplier. Reconstituted enzymes were supplemented with chloroacetamide (for alkylation) and TCEP (for reduction) to finally yield 0.1 μ g enzyme, 5 mM chloroacetamide, and 1.25 mM TCEP. Digestion was done overnight at 22 °C, 750 rpm shaking. Digested samples were lyophilized using an Univapo SpeedVac ECH 150 lyophilizer and stored at -20 °C until used for mass spectrometry analysis. For mass spectrometry analysis, special search parameters were used searching for the respective covalent modification by the reactive compound.

Gel-based protein digestion. Protein containing bands stained by Coomassie were cut into three pieces and each piece was placed into a well of a 96-well plate with a small hole drilled into each well for enabling the removal of liquids by centrifugation. The gel pieces were destained for 2 h at 55 °C in 100 μ l 60 % 5 mM triethylammonium bicarbonate buffer pH 8.5 (TEAB), 40% Ethanol. The destained

gel pieces were dehydrated using 100 μ l 100 % ethanol twice at RT. 15 μ l LysC solution (Wako #125-05061; 0.01 μ g/ μ l in 5 mM TEAB) was added to each gel piece and the samples were incubated at 4 °C until the gel pieces were hydrated again. Then, 20 μ l 5 mM TEAB was added to each gel piece and the samples were incubated for 2 h at 37 °C. 15 μ l trypsin solution (0.01 μ g/ μ l in 5 mM TEAB) was added to each gel piece and the samples were incubated overnight at 37 °C. The digestion was stopped using 5 μ l 5 % formic acid and the proteins were extracted using 40 μ l 1 % formic acid, 20 μ l 60 % acetonitrile / 0.4 % formic acid, and 75 μ l 100 % acetonitrile. The lyophilization of samples was done after freezing at -80 °C for ~ 2 h, using an Univapo SpeedVac ECH 150 lyophilizer. For TMT labeling, lyophilized samples were dissolved in 10 μ l 90 % 200 mM TEAB / 10 % acetonitrile for 15 min at RT, 400 rpm shaking. 10 μ l TMT reagent (ThermoFisher Scientific) per sample was added followed by incubation for 1 h at RT, 400 rpm shaking. Reaction was quenched for 15 min at RT using 5 μ l hydroxylamine solution (2.5 % in 100 mM TEAB). Labeled samples were combined in 96-well plates, lyophilized and stored at -20 °C for mass spectrometry analysis.

Solid-phase sample preparation. LDS eluted proteins were captured by magnetic carboxylate modified particles (50 % GE Healthcare Sera-Mag #45152105050250 / 50 % GE Healthcare Sera-Mag #65152105050250) for 15 min, 600 rpm shaking at RT. After washing the beads 4x with 200 μ l 70 % ethanol, 40 μ l digestion solution (100 mM HEPES pH 8.5 / 1.25 mM TCEP / 5 mM chloroacetamide / 0.25 μ g trypsin / 0.25 μ g LysC) was added to the beads. Enzymatic digestion was performed overnight, 600 rpm shaking at RT. The digested peptides were collected and elution was completed by washing once with 10 μ l 2 % DMSO in H₂O. The eluates were dried in vacuo and labeled with TMT labeling reagent. For this, lyophilized peptides were re-suspended in 10 μ l ultrapure water before 10 μ l TMT reagent (Thermo; 5 mg dissolved in 580 μ l 100 % acetonitrile) was added. Labeling was done for 1 h, shaking at RT. Non-reacted TMT reagent was quenched for 15 min with 5 μ l 2.5 % NH₂OH in 100 mM HEPES pH 8.5 at RT before pooling the samples corresponding to one experiment. After lyophilization, the sample clean-up was done using the C18SCX sample clean-up as described below.

C18/SCX sample clean-up. For removing detergent and/or salts and/or TMT reagent, the lyophilized samples were re-suspended in 100 μ l 4 % trifluoroacetic acid (TFA) and loaded to three layers of C18 material (Octadecyl C18 47 mm Extraction Disks) packed on top of three layers of SCX material (Cation 47 mm Extraction Disks) into a 200 μ l pipette tip. The peptides contained in the sample were immobilized on the C18 material by centrifugation of the solution. The flow through was discarded. After washing with 100 μ l 0.5 % TFA / 2 % acetonitrile, peptides were eluted to the SCX material using 100 μ l 0.5 % TFA / 60 % acetonitrile by centrifugation. The flow through was discarded. After washing with 200 μ l 0.5 % TFA / 60 % acetonitrile, cleaned samples were eluted in 100 μ l 5 % NH₃, 80 % acetonitrile into a clean tube, dried in vacuo using an Univapo Speedvac lyophilizer and stored at -20 °C for mass spectrometry analysis.

Immobilization of amine-incorporating compound analogues to NHS-activated sepharose. Linkable analogues of Afatinib and Ibrutinib were immobilized to NHS-activated high capacity

sepharose. Sepharose beads stored in isopropanol were washed four times with ~ 20 volumes of anhydrous DMSO. The beads were re-suspended in one volume of anhydrous DMSO to get a 1:1 slurry. The linkable compound analogue dissolved in DMSO was added to the slurry to gain the desired coupling density and the reaction of the free amine of the linkable compounds with the NHS-ester on the beads was started by adding 7.5 μ l triethylamine per 1 mM coupling density of 1 ml beads. After overnight incubation rotating at room temperature, unreacted NHS-ester was blocked with aminoethanol in excess overnight rotating at room temperature. The coupling efficiency was determined by HPLC analysis comparing the compound abundance in the supernatant before adding triethylamine and after the coupling reaction. Coupled beads were washed once with ~ 20 volumes of anhydrous DMSO and three times with ~ 20 volumes of isopropanol. Beads were re-suspended in one volume of isopropanol and stored at -20 °C.

Drug centric affinity enrichment using immobilized analogues of Afatinib and Ibrutinib in cell extracts. Affinity matrices were generated by coupling a linkable analogue of Afatinib or Ibrutinib at a coupling density of 1 mM to NHS-activated high capacity sepharose as described above. Ramos lysate adjusted to a protein concentration of 5 mg/ml was pre-incubated for 1 h with 10 μ M compound or vehicle (DMSO concentration 0.5 %) at room temperature, rotating at medium speed. The bead matrices were used to capture target proteins for 2 h, room temperature according to the lysate-based kinobeads pulldown procedure. After washing of the beads, reversibly bound proteins were eluted using 2X LDS sample buffer / 50 mM DTT. 37.5 % of eluate was loaded to gels and digested following in-gel digest procedure as described above. Non-eluted proteins were digested directly on the beads. For this, the beads were re-suspended in 1 ml WB1 (50 mM TEAB / 2 % SDS) and transferred to 15 ml tubes. The beads were washed 1x with 5 ml WB1, 3x with 10 ml WB2 (8 M urea in 50 mM TEAB), and 1x with 5 ml WB3 (2 M urea in 50 mM TEAB) by re-suspension, centrifugation (3 min, 1200 rpm, RT) and removal of the supernatant. The beads were incubated with 30 μ l 45 mM DTT and 30 μ l 100 mM iodoacetamide for 45 min, RT and 30 min, RT, in the dark, respectively. After incubation, the beads were centrifuged and the supernatant was removed. After washing the beads 1x with 10 ml WB3, the beads were transferred to filter columns, the supernatant was removed by centrifugation and 40 μ l 2 M urea in 50 mM TEAB was added onto the beads. In addition, 20 μ l of 0.02 μ g/ μ l trypsin was added, followed by overnight incubation, 25 °C, 700 rpm shaking. Again, 20 μ l of 0.02 μ g/ μ l trypsin was added, followed by further incubation for 4 h, 25 °C, 700 rpm shaking. The digests were collected by centrifugation for 3 min, 1200 rpm. To get comparable amounts of protein in the LDS eluted fraction and the bead digest fraction, 37.5 % of the bead digest (~ 30 μ l) was separated, frozen in liquid N₂ and lyophilized using an Univapo SpeedVac lyophilizer. The lyophilized sample was labeled together with the fraction achieved by LDS elution (see 'gel-based protein digestion') and analyzed by mass spectrometry analysis as described below.

Mass spectrometry analyses. For deep proteome analyses for selectivity profiling, the samples were fractionated by using reversed-phase chromatography at pH 12 [1 mm Xbridge column (Waters, Milford, MA)], as previously described.⁸⁴ The following procedure accounts for fractionated as well as for unfractionated samples. Samples were dried in vacuo and resuspended in 0.05 % trifluoroacetic

acid in water. 50 % of the sample was injected into an Ultimate3000 nanoRLSC (Dionex, Sunnyvale, CA) coupled to a Q Exactive or Q Exactive Plus (Thermo Fisher Scientific). Peptides were separated on custom-made 50 cm x 100 μ m (ID) C18 reversed-phase columns (Reprosil) at 40 °C. Gradient elution was performed from 2 % acetonitrile to 40 % acetonitrile in 0.1 % formic acid over 2 h. Samples were online injected into Q-Exactive mass spectrometers operating with a data-dependent top 10 method. MS spectra were acquired by using 70,000 resolution and an ion target of 3E6 for MS1 scans. Higher energy collisional dissociation (HCD) scans were performed with 35 % NCE at 35,000 resolution (at m/z 200) and the ion target settings was set to 2E5 so as to avoid coalescence.¹⁸⁷ The instruments were operated with Tune 2.2 or 2.3 and Xcalibur 2.7 or 3.0.63. Peptide and protein identification and quantification was done as previously described.^{149, 189-190} For searching for covalent modifications by compounds, the following modifications were allowed: for the identification of ZAK covalently modified by Ibrutinib or 5Z-7-Oxozeaenol, variable modifications of cysteines by a mass shift of +440.20 u and +362.14 u for Ibrutinib and 5Z-7-Oxozeaenol, respectively, were allowed. For identifying the site of reaction of covalent probes 1A, 2A, and 3A on recombinant MAPK9 and TEC, variable modifications of cysteines by a mass shift of +548.24 u, +707.33 u and +486.15 u for probes 1A, 2A, and 3A, respectively, were allowed.

Viability assay. The cell viability was determined using Promega's CellTiter-Glo® Luminescent Cell Viability Assay according to the manufacturer's protocol (Revision 3/15; TB288). In short: 10 μ l 10-fold concentrated compound or vehicle (5 % DMSO in medium) was added to 5000 cells in 90 μ l medium. After incubation of the cells with compound or vehicle, 100 μ l CellTiter-Glo reagent was added and the plates were incubated for 30 min at room temperature. Luminescence was measured using a plate reader (Envision) and cell viability relative to the vehicle control was determined.

Apoptosis evaluation by analysis of caspase 3-mediated PARP1 cleavage. To assess caspase 3-mediated apoptosis Western blot analysis was used. After treating Ramos cells with Ibrutinib, Afatinib or a vehicle control (DMSO) at 20 μ M, 1 μ M, and 0.05 μ M (final DMSO concentration: 0.5 %) for 24 – 48 – 72 h, cells were lysed using SDS lysis and benzonase digestion as described above. Protein concentrations were determined by Bradford assay and adjusted to 3 mg/ml using 50 mM Tris/HCl pH 7.4. 20 μ l diluted lysate was mixed with 20 μ l 2X LDS sample buffer / 50 mM DTT and 15 μ l per sample were loaded to SDS-PAGE gels. After gel run and blotting to PVDF membranes, the membranes were blocked and stained with anti-PARP1 as described above. Gel bands were analyzed for caspase 3 substrate PARP1 (~ 116 kDa) and cleaved PARP1 (~ 24 kDa).

Intracellular competition binding experiment with clickable analogues of Afatinib and Ibrutinib. Ramos cells adjusted to a density of $\sim 5.6 \times 10^6$ cells/ml in RPMI-1640 medium (Gibco #21875-034) supplemented with 0.1 % FBS (Gibco #10270) were pre-incubated with 10 – 2 – 0.4 – 0.08 – 0.016 – 0.0032 μ M Afatinib/Ibrutinib or vehicle (final DMSO concentration: 0.25 %) for 1 h, 37 °C, 5 % CO₂, 100 rpm shaking. After pre-incubation, to one vehicle control DMSO was added and to the other samples including a second vehicle control azido-Afatinib/azido-Ibrutinib was added to get a final concentration of 5 μ M azido-probe at 0.5 % DMSO. The cells were incubated for 1 h, 37 °C, 5 % CO₂,

100 rpm shaking. The cells were collected by centrifugation for 4 min, 491 g, RT. The supernatant was completely removed and the cells were frozen in liquid nitrogen to be stored at -80 °C until cell lysis. The cells were lysed as described above using 50 mM HEPES pH 7.4 instead of 50 mM Tris/HCl pH 7.4 to get a total lysate and protein concentrations were determined as described above. The cell lysates were adjusted to 2 mg/ml protein concentration using HEPES buffer (50 mM HEPES pH 7.4 / 5 % glycerol / 1.5 mM MgCl₂ / 150 mM NaCl / 1 mM Na₃VO₄) to perform a SPAAC click reaction of the azide-incorporating probes with DBCO-PEG4-biotin (Sigma #760749). For this, DBCO-PEG4-biotin was added to the samples to saturate all theoretically available azide-moieties at a final DMSO concentration of 0.5 %. The SPAAC reaction was performed for 2 h, 4 °C, overhead rotating before removing non-reacted DBCO-PEG4-biotin using size-exclusion chromatography with the Zeba Spin Desalting plates (Thermo Scientific #89807) equilibrated with HEPES buffer according to the manufacturer's protocol. The cleaned lysates were incubated with 7.5 µl neutravidin beads (Thermo Scientific #29202) for 2 h, 4 °C, overhead rotating in a 96-well 0.45 µm filter plate. After incubation, the beads were washed 10x with 200 µl 1X DP buffer / 0.4 % IGEPAL CA 630 and subsequently 5x with 200 µl 1X DP buffer / 0.2 % IGEPAL CA 630 as described for a kinobeads pulldown. The reversibly captured targets were eluted with 50 µl 2X LDS sample buffer / 50 mM DTT after incubating for 45 min at RT. For a subsequent digestion of captured proteins directly on the beads, again, beads were washed 10x with 200 µl 20 mM Tris / 400 mM NaCl / 0.4 % SDS, 10x with 200 µl 20 mM Tris / 400 mM NaCl, 10x with 200 µl 50 mM TEAB / 2 M urea, and 3x with 200 µl 50 mM HEPES pH 8.5. After removing residual washing buffer by centrifugation (1200 rpm, 2 min, RT), 50 µl digestion solution (25 mM HEPES pH 8.5, 2.5 mM TCEP, 7.5 mM chloroacetamide, 0.001 µg/µl trypsin, 0.001 µg/µl LysC) was added to all samples. After overnight digestion at room temperature, the digestion solution including the peptides of bead-bound proteins was collected and dried in vacuo using an Univapo Speedvac lyophilizer. The lyophilized samples were labeled with TMT labeling reagent and cleaned as described above for the solid-phase sample preparation and the C18/SCX sample clean-up, respectively. The samples were lyophilized and stored at -20 °C for mass spectrometry analysis.

Intracellular competition of BTK binding to TCO-Ibrutinib by targeted covalent inhibitors.

Ramos cells adjusted to a density of $\sim 5.6 \cdot 10^6$ cells/ml in RPMI-1640 medium (Gibco #21875-034) supplemented with 0.1 % FBS (Gibco #10270) were pre-incubated with Ibrutinib at concentrations of 25 – 5 – 1 – 0.2 – 0.04 nM, CC-292 at concentrations of 250 – 50 – 10 – 2 – 0.4 nM, QL47 at concentrations of 2500 – 500 – 100 – 20 – 4 nM or vehicle (final DMSO concentration: 0.25 %) for 1 h, 37 °C, 5 % CO₂, 100 rpm shaking. After pre-incubation, TCO-Ibrutinib was added to get a final concentration of 0.1 µM TCO-probe at 0.5 % DMSO. The cells were incubated for 1 h, 37 °C, 5 % CO₂, 100 rpm shaking. After incubation, the cells were transferred to 15 ml tubes containing 10 ml ice cold PBS and were centrifuged for 4 min, 491 g, 4 °C. The supernatant was completely removed, the cells were re-suspended in 10 ml ice cold PBS and were centrifuged for 4 min, 491 g, 4 °C. This was repeated once. After washing, the supernatant was removed completely and the cells were frozen in liquid nitrogen to be stored at -80 °C until cell lysis. The cells were lysed as described above to get a total lysate and protein concentrations were determined as described above. The cell lysates were adjusted to 2 mg/ml protein concentration using DP buffer (50 mM Tris/HCl pH 7.4 / 5 % glycerol /

1.5 mM MgCl₂ / 150 mM NaCl / 1 mM Na₃VO₄) to perform a IEDDA click reaction of the TCO-incorporating probe with Tz-Cy5 dye (Jena Bioscience #CLK-015-05). For this, Tz-Cy5 was added to the samples to get a final concentration of 10 μM (0.1 % DMSO). The IEDDA reaction was performed for 30 min, 4 °C, 500 rpm, in the dark. After incubation, 2X LDS sample buffer / 50 mM DTT was added and the samples were incubated for 8 min, 70 °C. The samples were loaded to a SDS-PAGE gel (4-12 % Bis-Tris) and separated as described above. After scanning the gel for fluorescence using an Odyssey fluorescence imager the gel was Coomassie stained as described above.

Intracellular competition of BTK binding to TCO-Ibrutinib by reversible inhibitors. The experiment was performed as described for the 'Intracellular competition of BTK binding to TCO-Ibrutinib by targeted covalent inhibitors'. Saturated Ibrutinib and CGI-1746 were used at concentrations of 2500 – 500 – 100 – 20 – 4 nM, TCO-Ibrutinib was used at a final concentration of 0.01 μM and incubation with the covalent probe was done for 30 min.

Kinobeads-based intracellular competition of MAPK9 binding to covalent probe 1A by reversible inhibitor Tanzisertib. The cell treatment was performed as described for the 'Intracellular competition of BTK binding to TCO-Ibrutinib by reversible inhibitors'. Tanzisertib was used at concentrations of 1000 – 200 – 40 – 8 – 1.6 nM, Probe 1A was used at final concentrations of 0.1 μM and 0.01 μM. For assuring removal of reversibly bound compound, intensive cell washing was done by incubating the cells twice in 10 ml fresh medium for 30 min followed by re-suspension of cells in 10 ml ice cold PBS. The cell pellets were frozen in liquid N₂ and stored at -80 °C until lysis. A total lysate was prepared from the cell pellets and a kinobeads pulldown was performed as described above. The analysis for enriched MAPK9 was done using immunostaining as described above.

Mitochondria isolation from compound treated Ramos cells and MitoCheck Complex I Activity assay. 2*10⁷ Ramos cells adjusted to a density of ~ 1*10⁶ cells/ml in RPMI-1640 medium (Gibco #21875-034) supplemented with 0.1 % FBS (Gibco #10270) were incubated with 10 μM Afatinib, 10 μM Ibrutinib, 10 μM Rotenone or vehicle (final DMSO concentration: 0.5 %) for 24 h, 37 °C, 5 % CO₂, 100 rpm shaking. After compound treatment, mitochondria from each sample were isolated using a 'Mitochondria Isolation Kit for Cultured Cells' (Thermo Scientific #89874) according to the manufacturer's protocol. Such isolated mitochondria were either analyzed by mass spectrometry for expressed proteins or subjected to the 'MitoCheck Complex I Activity assay' (Cayman Chemical #700930) according to the manufacturer's protocol. Decreasing absorbance at 340 nm corresponding with the oxidation of NADH to NAD⁺ was measured for 15 min every 30 sec using an Envision plate reader.

Lysate-based 2D-TPP with Ibrutinib and Afatinib. A crude Ramos cell lysate was prepared as described above and diluted to have a protein concentration of 2 mg/ml. For generating a reference meltome in this lysate, 2x 1.5 ml lysate were incubated with DMSO at a final concentration of 0.5 % for 15 min at RT, shaking. Subsequently, the lysates were aliquoted into 2x 10 wells of a PCR plate each 100 μl and heated for 3 min to 37.0 – 40.4 – 44.0 – 46.9 – 49.8 – 52.9 – 55.5 – 58.6 – 62.0 – 66.3 °C.

For the 2D-TPP analyses of Ibrutinib and Afatinib, the compounds were used at final concentrations of 20 – 4 – 0.57 – 0.082 μM or vehicle (final DMSO concentration: 0.5 %) for 15 min at RT, shaking. 100 μl of each lysate was added to two PCR plates to allow for heating individually to twelve individual temperatures. The sealed PCR plates were heated to 42.0 – 44.1 – 46.2 – 48.1 – 50.4 – 51.9 – 54.0 – 56.1 – 58.2 – 60.1 – 62.4 – 63.9 $^{\circ}\text{C}$ for 3 min. The heated samples were put to room temperature for 3 min and then on ice. 4 μl 20% IGEPAL CA630 detergent solution and 5 μl benzonase solution was added to each sample to yield finally 100 U enzyme. After mixing, the plates were incubated for 1 h shaking at 700 rpm, 4 $^{\circ}\text{C}$. The lysates were then centrifuged at 100000 g for 20 min at 4 $^{\circ}\text{C}$ to remove aggregated proteins. The supernatants were mixed 1:1 with sample buffer (200 mM Tris/HCl, 250 mM Tris Base, 20 % glycerol, 4 % SDS, 0.01 % Bromophenol Blue) and cleaned up as described above for the C18/SCX sample clean-up but only using C18 material. Data analysis was done using a Cellzome-internal pipeline as described previously.^{139, 191}

Cell-based 2D-TPP with Ibrutinib and Afatinib. Ramos cells adjusted to a density of $\sim 5.6 \times 10^6$ cells/ml in RPMI-1640 medium (Gibco #21875-034) supplemented with 0.1 % FBS (Gibco #10270) were incubated with Ibrutinib or Afatinib at concentrations of 10 – 2 – 0.29 – 0.041 μM or vehicle (final DMSO concentration: 0.5 %) for 1 h, 37 $^{\circ}\text{C}$, 5 % CO_2 , 100 rpm shaking. After incubation, the cells were centrifuged for 4 min, RT, 1500 rpm, the supernatant was removed and the cells were re-suspended in 10 ml PBS containing the respective compound concentration to not remove reversibly bound inhibitor. This PBS washing step was repeated once before re-suspending the cell pellets in 1.3 ml PBS containing the respective compound concentration. 100 μl of each cell suspension was added to PCR plates to allow for heating cell pellets incubated with compound or vehicle individually to twelve individual temperatures. The PCR plates were centrifuged for 3 min, 1200 rpm at 4 $^{\circ}\text{C}$ and 80 μl supernatant were removed. After sealing the plates with PCR foils, twelve sets of cell pellets consisting of the four different compound concentrations and a vehicle control were heated to 42.0 – 44.1 – 46.2 – 48.1 – 50.4 – 51.9 – 54.0 – 56.1 – 58.2 – 60.1 – 62.4 – 63.9 $^{\circ}\text{C}$ for 3 min. The heated cell pellets were put to room temperature for 3 min before adding 50 μl lysis buffer (PBS / 1.12 % IGEPAL CA 630 / 2.1 mM MgCl_2 / protease inhibitor) and re-suspending cell pellets 20 times. Subsequently, 3 μl benzonase (3.75 U benzonase in PBS / 0.8 % IGEPAL CA 630 / 1.5 mM MgCl_2 / protease inhibitor) was added to each sample and the plates were incubated for 1 h shaking at 750 rpm, 4 $^{\circ}\text{C}$. After lysis, the plates were centrifuged for 3 min, 1500 rpm, 4 $^{\circ}\text{C}$ and the supernatants were transferred to 0.45 μm filter plates equilibrated with PBS / 0.8 % IGEPAL CA 630 / 1.5 mM MgCl_2 / protease inhibitor. The filtered solution was collected into a fresh plate by centrifugation for 3 min, 1500 rpm, 4 $^{\circ}\text{C}$. 35 μl of the collected samples was mixed with 35 μl 2X LDS sample buffer / 50 mM DTT and incubated for 45 min at room temperature. The protein concentration of the samples heated to 42.0 $^{\circ}\text{C}$, 44.1 $^{\circ}\text{C}$, and 63.9 $^{\circ}\text{C}$ was determined and by averaging across all ten samples from the first two temperatures the dilution factor was determined needed for sample dilution to get a protein concentration of 1.25 mg/ml. All samples were adjusted with 2X LDS sample buffer / 50 mM DTT using this dilution factor. 31.25 μg protein per sample was processed using the solid-phase sample preparation and C18/SCX sample clean-up as described above. Samples heated to two adjacent

temperatures were considered as two replicates and labeled together to yield one set of TMT10 labeled samples. The following table shows an example for the both lowest temperatures:

TMT label	126	127L	127H	128L	128H	129L	129H	130L	130H	131
Temperature	42 °C					44.1 °C				
Compound concentration	10 µM	2 µM	0.29 µM	0.041 µM	DMSO	10 µM	2 µM	0.29 µM	0.041 µM	DMSO

Using this scheme, six 2D-LC-MS analyses as described above covered the whole temperature gradient for the 5-point compound dose-response. Data analysis was done using a Cellzome-internal pipeline as described previously.^{139, 191}

Expression profiling comparing A549 cell proteomes after treatment with Afatinib-lenalidomide or Afatinib. A549 cells were grown in DMEM medium (Gibco #41965-062) / 10 % FBS (Gibco #41965-062) to get 2x6 15 cm plates with a cell confluency of ~ 90 % for generating 6 conditions in 2 replicates. The medium was removed and the cells were washed once with 20 ml pre-warmed PBS (+MgCl₂ / +CaCl₂) (Gibco #14040-091). The PBS was removed and 20 ml DMEM medium / 0.1 % FBS containing a final concentration of 10 µM Afatinib, 10 – 2 – 0.4 – 0.08 µM Afatinib-lenalidomide or vehicle (final DMSO concentration: 0.5 %) was added. The plates were incubated for 24 h, 37 °C, 10 % CO₂. After incubation, cells were harvested with a cell scraper and cells were lysed with SDS and benzonase digestion as described above. For mass spectrometry analysis, 100 µg protein of each condition was applied to the solid-phase sample preparation as described above. Each replicate was TMT6 labelled and cleaned up as described above. 30 % of the sample was measured over a 120 min-gradient. For the data analysis, fold changes were calculated relating the abundance at a certain Afatinib-lenalidomide concentration to the 10 µM Afatinib control to identify Afatinib-lenalidomide specific effects not observed with Afatinib only.

Proteome dynamics analysis of Ramos cells treated with lenalidomide analogues of Ibrutinib saturated Ibrutinib, and Afatinib. For labeling Ramos cell proteomes with heavy and light amino acids, SILAC medium was prepared. For this, 500 ml SILAC compatible RPMI-1640 (Gibco #A24942-01) was supplemented with 250 µl phenol red (Invitrogen #06-0034SA), 50 ml dialyzed FCS (Gibco #26400-036), 5 ml glucose solution (Sigma #06-0033SA), and 5 ml glutamine solution (Gibco #25030-032). This medium was split into 2x 275 ml. For preparing light SILAC medium, to one fraction 60 mg light arginine (Sigma #A8094-25G) were weighed in and dissolved in 600 µl RPMI-1640 medium. 60 mg light lysine (Sigma #L9037-25G) were weighed in and dissolved in 600 µl RPMI-1640 medium. 550 µl of each solution was added to 275 ml prepared medium to get 100 µg/ml SILAC amino acids. The same was done with the second fraction using heavy arginine (Thermo #88434) and heavy lysine (Sigma #608041-1G) to get heavy SILAC medium. Both media were sterile filtered through a 0.22 µm filter. Proteome conversion was done by incubating Ramos cells in the respective medium as described above for standard cell culturing. Routinely performed cell viability measurements were compared to a normal growth medium control. After two weeks culturing, cells were considered as fully converted and used for the proteome dynamics experiment.

For switching medium from heavy to light and vice versa, 2×10^8 Ramos cells grown in heavy medium and light medium were centrifuged (4 min, 491 g, RT), medium was removed, and cells were re-suspended in 30 ml light and heavy medium, respectively. 1.5 ml heavy cell suspension ($\rightarrow 5 \times 10^6$ cells) were transferred to 5 wells of 3x 12-well cell culture plates. To another five wells, light cell suspension was added. 500 μ l of a 4X compound dilution prepared by diluting a DMSO stock 1:250 in the corresponding SILAC medium was added to the wells to finally yield 2 ml sample volume at a DMSO concentration of 0.1 % DMSO as given in the following overview:

	1	2	3	4
A	DMSO (H \rightarrow L)	0.1 μ M PROTAC (H \rightarrow L)	1 μ M PROTAC (H \rightarrow L)	10 μ M PROTAC (H \rightarrow L)
B	1 μ M parent compound (H \rightarrow L)		DMSO (L \rightarrow H)	0.1 μ M PROTAC (L \rightarrow H)
C	1 μ M PROTAC (L \rightarrow H)	10 μ M PROTAC (L \rightarrow H)	1 μ M parent compound (L \rightarrow H)	

The plates were incubated for 24 h, 37 °C, 5 % CO₂, 100 rpm shaking. After incubation, the cell suspensions were transferred to 15 ml tubes containing 10 ml ice cold PBS. After centrifugation for 4 min, 491 g, 4 °C, the supernatant was removed, the cells were frozen in liquid N₂ and stored at -80 °C until cell lysis. The cell pellets were lysed with SDS and benzonase digestion as described above. 37.5 μ g protein of each sample was prepared according to the solid-phase sample preparation. The five samples per compound type pulse labeled by switching from heavy to light and from light to heavy were considered as replicate 1 and replicate 2, respectively, and were labeled by TMT10. After C18/SCX clean-up of the pooled samples as described above, a 2D-LC-MS analysis was done as described above. Data analysis was done using a Cellzome-internal pipeline as described previously.¹⁴⁹

3. Results

3.1. Chemoproteomic identification of cellular (off-)target engagement of covalent kinase inhibitors

3.1.1. BTK engagement measured in cells correlates with a functional effect but differs from lysate-based values

The first intention when starting to work with covalent BTK TCIs was to investigate if covalent inhibitors show the same potency in lysate-based and cellular assays considering equal incubation times. Therefore, a lysate-based kinobeads competition binding assay was performed incubating cell extract derived from primary human blood B-cells with Ibrutinib, CC-292, and QL47 over a range of concentrations. BTK not engaged after pre-incubation with the TCIs was enriched by kinobeads, eluted and analyzed by immunostaining. From calculated binding curves, the concentration was derived for which binding to the kinobeads was reduced by 50 % for the applied conditions compared to the vehicle control and the negative log₁₀ value (pIC₅₀) was plotted for each compound (Figure 15). In the lysate-based assay similar values were determined for all three tested compounds: pIC_{50,Ibrutinib} = 6.7±0.1, pIC_{50,CC-292} = 6.9±0.1, and pIC_{50,QL47} = 6.5±0.1. When the compounds were applied on live cells from which individual lysates were produced prior to a kinobeads enrichment, however, significant differences in BTK engagement for the inhibitors were determined with pIC₅₀s spanning nearly two orders of magnitude between binding by Ibrutinib (pIC₅₀ = 8.8±0.0) and binding by QL47 (pIC₅₀ = 7.0±0.2). For analyzing if the rank order of target engagement measured for the three different BTK TCIs in the cell-based kinobeads assay correlates with the functional effect of BCR inhibition, an assay was performed measuring calcium-dependent fluorescence in living cells upon stimulation of the B-cell receptor. As a response of BCR signaling, calcium mobilization was visualized by fluorescent probes as a measure for concentration-dependent inhibition of this BTK-mediated pathway. By calculating dose-response curves, the concentration for which fluorescence is 50 % of the non-inhibited signal was determined and plotted as pIC₅₀ value for each of the BTK TCIs. This showed that also for the functional effect of BTK inhibition a rank order in agreement with the cellular kinobeads assay can be observed. This comparison suggests that measuring target engagement upon the treatment of living cells is more predictive for a functional effect than determining target engagement of BTK TCIs in a lysate-based setup. Differences between the lysate-based measurement and the cellular assays for the same compound might be explained by different affinity of the compound towards BTK due to different concentrations of the target kinase and competing substrates as well as the structural integrity of proteins and protein complexes differing in lysate from the native intracellular environment. In addition, the reactivity of the compounds in both assay settings might differ due to differences regarding temperature, the native redox environment⁵¹ and local pH^{49, 192} and lysis-caused chemical lability⁵¹ or oxidation of sulfhydryl groups.¹⁹³ The different potency measured across the compounds with the cell-based assays could result from more or less precise positioning of the reactive acrylamide moiety by affinity-driven BTK engagement. Different cell permeability of the compounds could also represent a reason for the rank order in target engagement

and the functional effect of BTK inhibition measured by the cell-based kinobeads assay and the Ca^{2+} -mobilization assay, respectively.

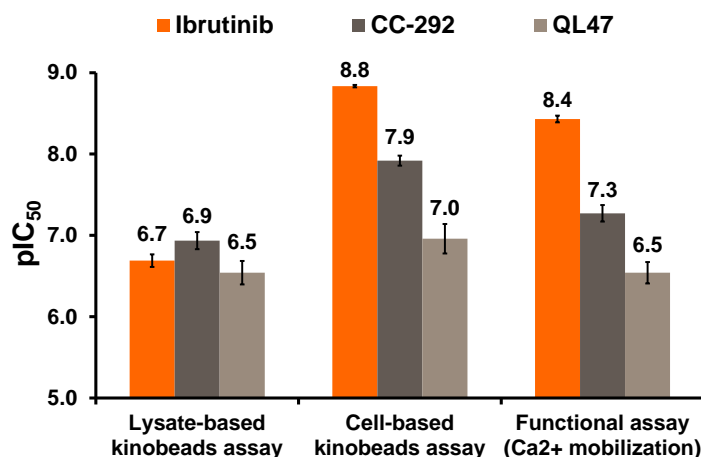


Figure 15: BTK engagement of Ibrutinib, CC-292, and QL47 as determined in a lysate- and a cell-based kinobeads assay compared to a functional effect. A cell-based kinobeads assay allows for a more reliable prediction of a covalent inhibitor's functional effect than a lysate-based approach. pIC₅₀ averages were calculated from ≥ 2 replicates and the error bars represent the standard error of the mean.

3.1.2. Differences in lysate- and cell based target engagement enable the identification of covalent and reversible kinase targets

The differences observed for BTK covalently engaged by Ibrutinib, CC-292, and QL47 triggered the idea to exploit these differences in target engagement measured in lysate and in cells for the discrimination of covalent targets and reversibly engaged binders. For this purpose, an adequate competition binding-based assay should a) allow for the determination of pIC₅₀ values which can be compared in a cell-based and a lysate-based kinobeads assay and b) should assure that non-covalent targets show lower potency in a cell-based assay than in a lysate-based assay while irreversibly bound kinases show somewhat similar or even higher target engagement in cells compared to lysates. This concept was termed 'differential kinobeads selectivity profiling' (Figure 16).¹⁹⁴ It is based on the hypotheses that for reversibly bound targets lower potencies will be observed due to re-equilibration of drug target interactions after cell lysis and, in contrast, covalent drug-target interactions would not be affected by cell lysis and dilution of the protein extracts. Hence, irreversible binding would appear at least equipotent if not more potent in cell-based experiments due to more efficient target engagement in cells.

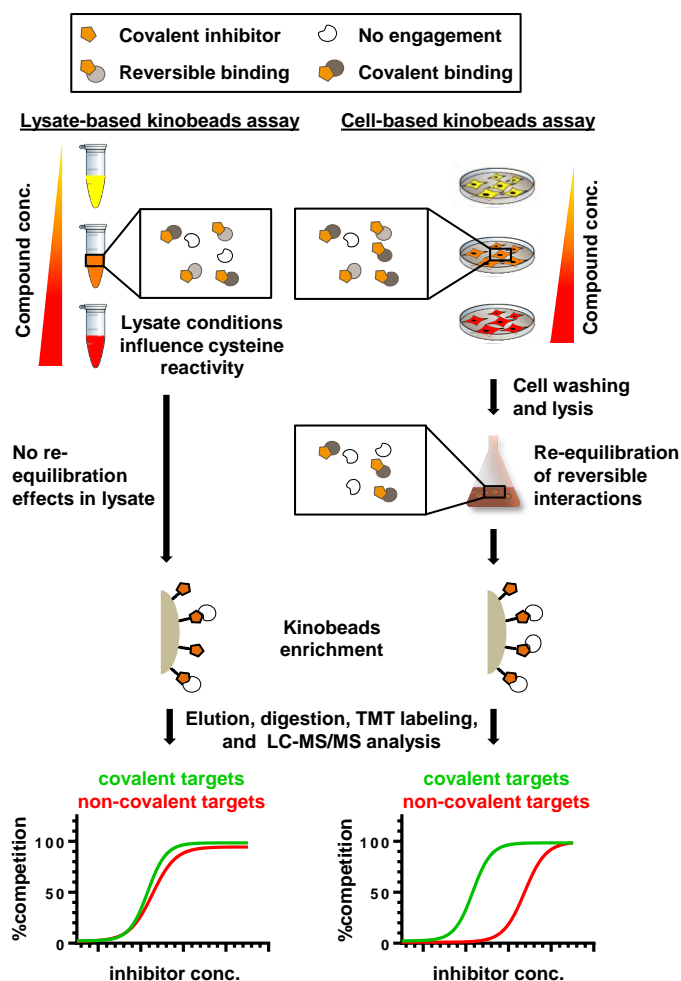


Figure 16: Concept of differential kinobeads selectivity profiling using an optimized cellular kinobeads assay. Covalent and reversible targets of reactive kinase inhibitors can be distinguished by different target engagement measured in living cells and cell extracts.

To establish the aforementioned characteristics for an adequate kinobeads assay two parameters were identified for optimization: since pIC_{50} values are depending on the incubation time with covalent inhibitors (\rightarrow non-equilibrium binding) the duration of cell treatment had to be specified for which a broad range of compound concentrations enables the generation of binding curves from which pIC_{50} values can be derived. Further, cell washing conditions had to be established which allow for a sufficient dissociation of non-covalently bound compound from a respective target. Ibrutinib represented an excellent tool for setting up such conditions since the difference between the cellular and lysate-based pIC_{50} value was especially prominent for this compound. In a first experiment, the B-cell derivative cell line Ramos was treated with a fixed concentration of Ibrutinib and a non-reactive saturated analogue with otherwise identical structure (Figure 17A) as a control for up to six hours. After treatment, the cells were lysed and non-engaged BTK was enriched using kinobeads. BTK occupancy normalized to the vehicle control was determined. While for 1 μ M Ibrutinib full target occupancy was already determined at the first time point, i.e. 0.5 h, a time-dependent increase in BTK engagement was observed for Ibrutinib at low nanomolar concentration (Figure 17B). For 3 nM Ibrutinib, which is close to the previously reported IC_{50} concentration for active site occupancy,³⁰ 50 % BTK engagement was determined after 1 h of cell incubation in the cell-based kinobeads assay. For

the non-reactive control compound, an increase in target engagement over time was not observed. After 6 h, a stagnation in occupancy increase for the covalent compound and even a drop in BTK engagement for the saturated analogue could be related to a combined result from cell growth and re-synthesis of BTK. In agreement with the published data and since being in the dynamic range of BTK engagement allowing for pIC_{50} determination at low nanomolar concentrations the optimized incubation time in the cellular kinobeads assay was fixed to be 1 h.

For finding suitable compound washout conditions which allow for a sufficient dissociation of the compound from non-covalent targets, Ramos cells were washed weakly by just re-suspending the cells in PBS after compound treatment or more intensively by incubating the cells twice in fresh medium for 30 min prior to re-suspending them in PBS. As a control, non-washed cells were also lysed and subjected to a kinobeads pulldown experiment. Enriching and visualizing non-engaged BTK shows differences between the applied washing procedures (Figure 17C). Irreversibly bound Ibrutinib cannot be washed out from BTK so that it is not possible to enrich this kinase by a kinobeads pulldown. In contrast, for the saturated analogue a washout dependent enrichment of BTK is possible. While BTK binding to kinobeads is fully competed by 5 μ M saturated Ibrutinib when not washing the cells, about the half of the maximal BTK signal achieved for the DMSO control can be enriched when washing the cells weakly. When washing the cells intensively, about 100 % of BTK can be enriched which means that two-times incubation of the cells in fresh medium followed by PBS re-suspension enables full dissociation of non-covalently bound compound from its target. Therefore, this kind of compound washout was used in differential kinobeads selectivity profiling for the discrimination of irreversible and reversible targets of covalent kinase inhibitors.

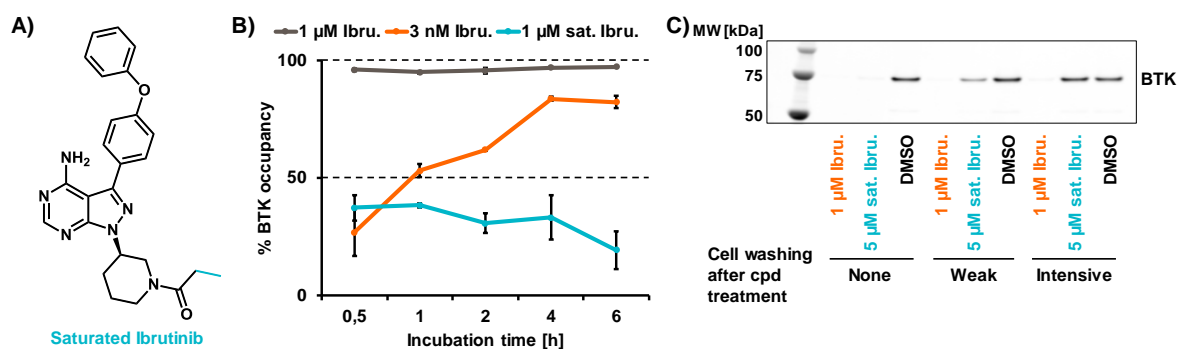
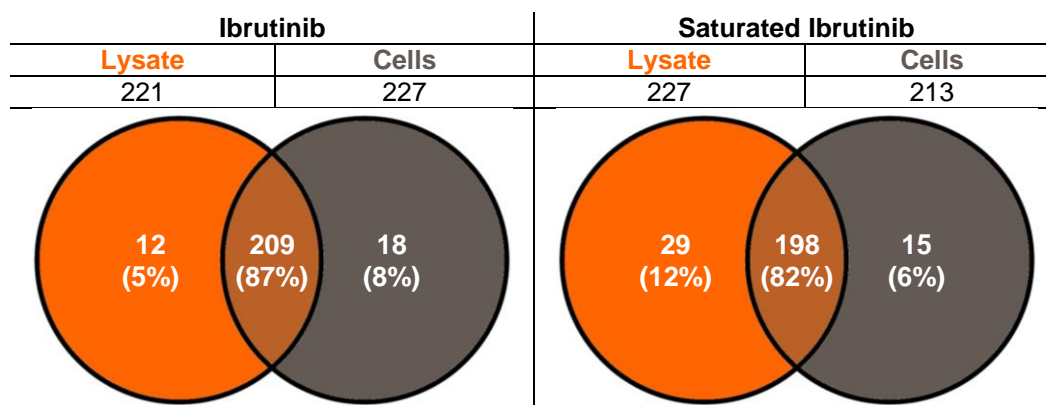


Figure 17: Optimizing conditions of cell-based kinobeads assay utilizing saturated Ibrutinib. (A) Chemical structure of a saturated Ibrutinib analogue. (B) Determination of target engagement in the dynamic range of reaction kinetics. Increasing occupancy of BTK can be observed for the reactive compound. For low nanomolar concentrations of Ibrutinib, 50 % occupancy is achieved after 1 h of cell treatment. No increase in BTK occupancy can be observed for the non-reactive analogue. The average of the BTK signals and standard error of the mean was calculated from three replicates. (C) Full dissociation of the compound reversibly bound to proteins is assured by intensive cell washing (2x incubation in fresh medium for 30 min). Weak washing by re-suspension of cells in PBS removes about 50 % of 5 μ M saturated Ibrutinib from BTK compared with no washing. The representative Western blot shows the BTK signals after enrichment of kinases using kinobeads and elution of the captured proteins.

3.1.3. Differential kinobeads selectivity profiling for the discrimination of covalent and reversible targets of covalent kinase inhibitors

With the optimized incubation and washout conditions for the cell-based kinobeads assay, kinobeads selectivity profiles were generated for Ibrutinib and the saturated analogue in Ramos cells and lysate. For this, kinobeads-enriched kinases were analyzed by quantitative mass spectrometry. For both compounds a large number of proteins was robustly identified in lysate and cells (Table 4).

Table 4: Kinases robustly identified in differential kinobeads selectivity profiling of Ibrutinib and a saturated analogue



For the comparison of kinase engagement of Ibrutinib and the saturated analogue in the lysate- and cell-based kinobeads assay, pIC_{50} values were determined and plotted against each other (Figure 18). Among the kinases most potently engaged by Ibrutinib the TEC family kinases BTK and TEC as well as BLK were identified. The TEC family kinases as well as the SRC kinase BLK contain a cysteine residue at the hinge 6 position with which Ibrutinib is designed to react.³⁰ Another kinase which was identified with a higher pIC_{50} value in cells than in lysate suggesting covalent binding by Ibrutinib is ZAK. Although not containing a cysteine but a serine at hinge 6 position ZAK has been suggested as an additional covalent target of Ibrutinib in a recent report.⁹⁸ All other kinase for which a submicromolar pIC_{50} value was determined including RIPK2 and 3, FGR and SRC family kinases show a lower pIC_{50} value in cells than in lysate. This decrease in potency indicates re-equilibration effects of non-covalently bound kinase targets. For the saturated, non-reactive analogue of Ibrutinib, all kinase targets show higher potency in lysate than in cells. For all non-covalent targets, it is possible to predict the fold decrease of target engagement roughly by considering the dilution factor during cell lysis. The comparison of Ibrutinib and the non-reactive control validates the concept of differential kinobeads selectivity profiling for the discrimination of irreversible and reversible targets of covalent kinase inhibitors.

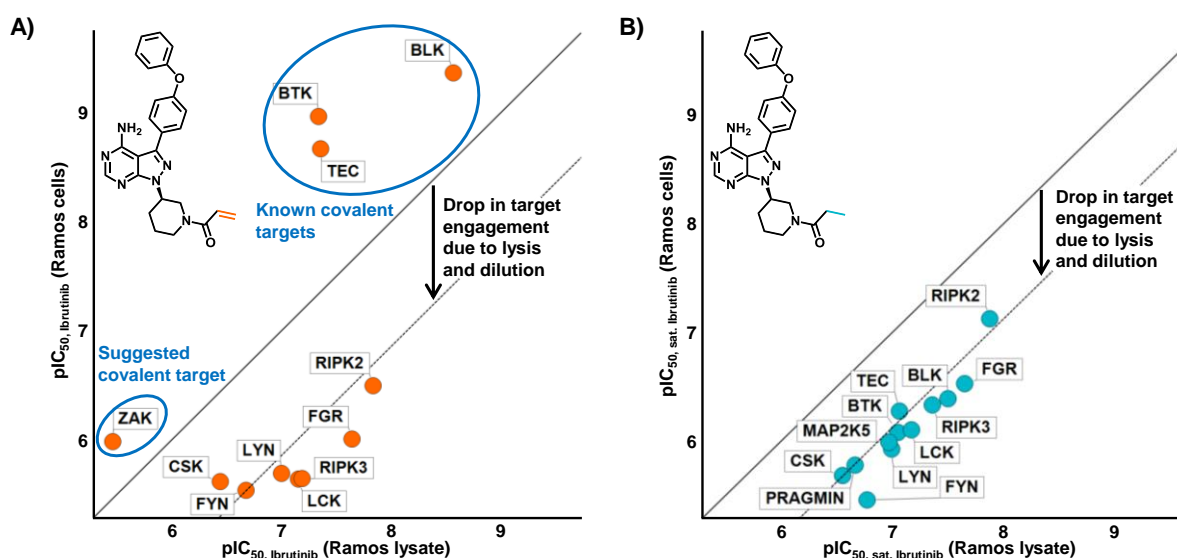
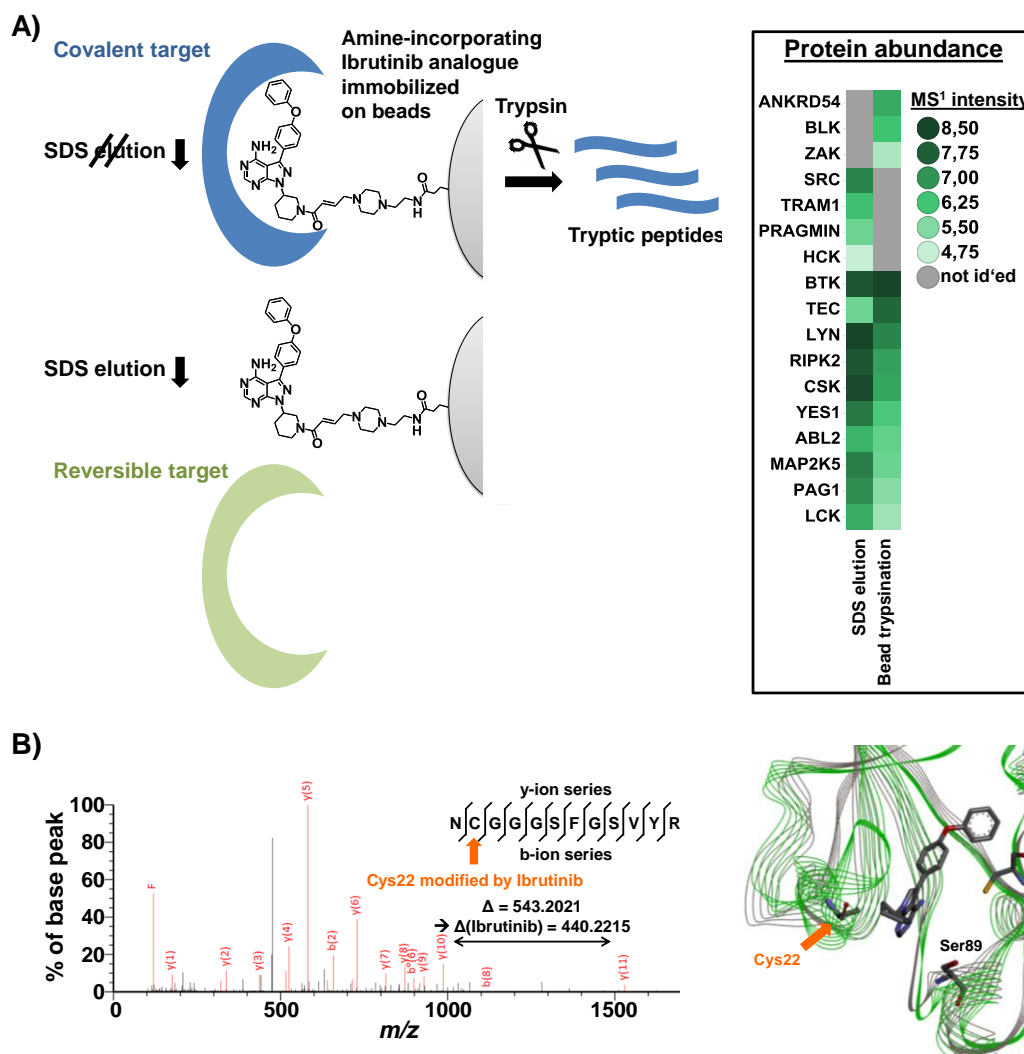


Figure 18: Differential kinobeads selectivity profiling for the identification of covalent and reversible kinase (off-) targets – proof-of-concept. (A) Kinases robustly identified to be inhibited with $pIC_{50} \geq 6$ by Ibrutinib and (B) saturated Ibrutinib as determined by differential kinobeads profiling. The dashed lines represent the calculated dilution factors due to lysis. All values are average values from 2 replicates.

While BTK, TEC, and BLK were rationalized as covalent targets by the hinge 6 cysteine, differential kinobeads selectivity profiling had to be validated regarding the identification of ZAK as a covalent binder of Ibrutinib with additional approaches. In a first experiment, an amine-incorporating analogue of Ibrutinib was immobilized on sepharose beads to enrich for the targets of the linkable analogue. Reversibly bound proteins were removed from the beads by SDS elution and covalently enriched proteins were accessed by direct proteolysis on the beads (Figure 19A). Competing the binding to the affinity matrix by 10 μ M underivatized Ibrutinib enabled the discrimination of specific targets and non-specific background captured by the beads. The abundance of proteins represented by MS¹ intensity was determined in the SDS eluate and the fraction directly digested on the beads. Of the proteins for which binding to the bead matrix was specifically competed only three proteins were solely present in the bead digest. One of those proteins is ZAK confirming it as real covalent target of Ibrutinib. While BLK is also a reasonable covalent target of Ibrutinib, ANKRD54 which was also exclusively identified in the bead digests is known as a BTK associated protein but not as a covalent binder of Ibrutinib.¹⁹⁵ For validating that ZAK was not just co-enriched as a complex partner of a covalent target, recombinant ZAK was incubated with Ibrutinib, enzymatically digested, and submitted to mass spectrometry analysis. In this analysis, a potential mass modification of nucleophilic amino acids by the molecular weight of Ibrutinib was allowed for peptide identification. A unique peptide containing a cysteine covalently modified by Ibrutinib was identified (Figure 19B). The peptide was identified with $m/z = 822.36$ u which corresponds to the doubly-charged state of the neutral monoisotopic mass 1642.72 u. With the neutral monoisotopic mass of the unmodified peptide being 1202.51 u the mass difference of 440.21 u corresponds to a modification by Ibrutinib (MW = 440.2 g/mol). To analyze the reasonability of Cys22 being modified by Ibrutinib the crystal structures of BTK complexed with an Ibrutinib pre-cursor (brown; PDB ID: 3GEN¹⁹⁶) and ZAK (green; PDB ID: 5HES¹⁹⁷) were overlaid. By this, it was possible to explain covalent binding of Ibrutinib to ZAK by the close proximity of the position at which Ibrutinib incorporates the reactive acryl amide to Cys22 adjacent to the hinge 6 Ser89. By the

identification of the covalent binding site of Ibrutinib in ZAK, the differential kinobeads selectivity profiling approach suggesting ZAK as a covalent binder of Ibrutinib was validated.



For the x-y graphs shown above (Figure 18), only kinases were plotted for which pIC₅₀ values 0.5 log units above the maximal compound concentration used in the respective assay were determined. However, for some kinases a prominent pIC₅₀ value was determined exclusively in the lysate assay while no pIC₅₀ value could be determined due to concentration limits in the cell based assay (Table 5). These kinases should not be ignored since they might represent important non-covalent off-targets of the compounds. Especially, the binding of ABL1 (pIC_{50, Ibru.} = 6.3±0.1 vs pIC_{50, sat. Ibru.} = 6.3±0.0), ABL2 (pIC_{50, Ibru.} = 6.5±0.1 vs pIC_{50, sat. Ibru.} = 6.3±0.0), LATS1 (pIC_{50, Ibru.} = 6.3±0.1 vs pIC_{50, sat. Ibru.} = 6.2±0.0), MAP3K2 (pIC_{50, Ibru.} = 6.3±0.2 vs pIC_{50, sat. Ibru.} = 6.4±0.1), PIK3CB (pIC_{50, Ibru.} = 6.2±0.1 vs pIC_{50, sat. Ibru.} = 6.2±0.0), STK35 (pIC_{50, Ibru.} = 5.5±0.1 vs pIC_{50, sat. Ibru.} = 5.8±0.1), and TNK2 (pIC_{50, Ibru.} = 5.3±0.1 vs

$pIC_{50, \text{ sat. lbru.}} = 5.3 \pm 0.1$) to kinobeads is competed very similarly by the reactive TCI and the non-reactive analogue suggesting them as true non-covalent targets of Ibrutinib.

Table 5: Kinases for which a pIC_{50} value significantly above the used maximal compound concentration was determined only in lysate-based selectivity profiling of Ibrutinib and saturated Ibrutinib.

Kinase	lysate-based assay		cell-based assay	
	average (pIC_{50})	s.e.m. (pIC_{50})	average (pIC_{50})	s.e.m. (pIC_{50})
ABL1	6.3	0.1	5.0	0.0
ABL2	6.5	0.1	5.3	0.3
FRK	6.2	0.1	5.0	0.0
JAK3	5.6	0.0	5.0	0.0
LATS1	6.3	0.1	5.0	0.0
MAP2K5	6.7	0.0	5.5	0.5
MAP3K1	5.0	0.2	5.0	0.0
MAP3K2	6.3	0.2	5.0	0.0
PIK3CB	6.2	0.1	5.0	0.0
PRAGMIN	6.6	0.0	5.2	0.2
STK35	5.5	0.1	5.0	0.0
TNK2	5.3	0.1	5.0	0.0

Kinase	lysate-based assay		cell-based assay	
	average (pIC_{50})	s.e.m. (pIC_{50})	average (pIC_{50})	s.e.m. (pIC_{50})
ABL1	6.3	0.0	5.0	0.0
ABL2	6.3	0.0	5.2	0.1
LATS1	6.2	0.0	5.2	0.1
LIMK1	4.9	0.1	5.0	0.0
MAP3K2	6.4	0.1	5.0	0.0
PIK3CB	6.2	0.0	5.0	0.0
STK35	5.8	0.1	5.0	0.0
TNK2	5.3	0.1	5.0	0.0

In the B-cell derivative cell line Ramos expressed covalent kinase targets of Ibrutinib were clearly distinguishable from non-covalent binders. As there are also kinases containing a cysteine at hinge 6 position which are predominantly or exclusively expressed in adherent cells, namely EGFR, ErbB2, and ErbB4,¹⁹⁸⁻¹⁹⁹ differential kinobeads selectivity profiling was also applied to the adherent cell line A549 expressing EGFR at reasonable levels. Ibrutinib profiling in epithelial A549 cells suggested EGF-receptor as an additional covalent target albeit with lower potency (Figure 20). Covalent binding can be rationalized by reaction to Cys847 that corresponds to Cys481 of BTK. Further, in A549 cells, TEC and ZAK were validated as covalent targets as identified in Ramos cells.

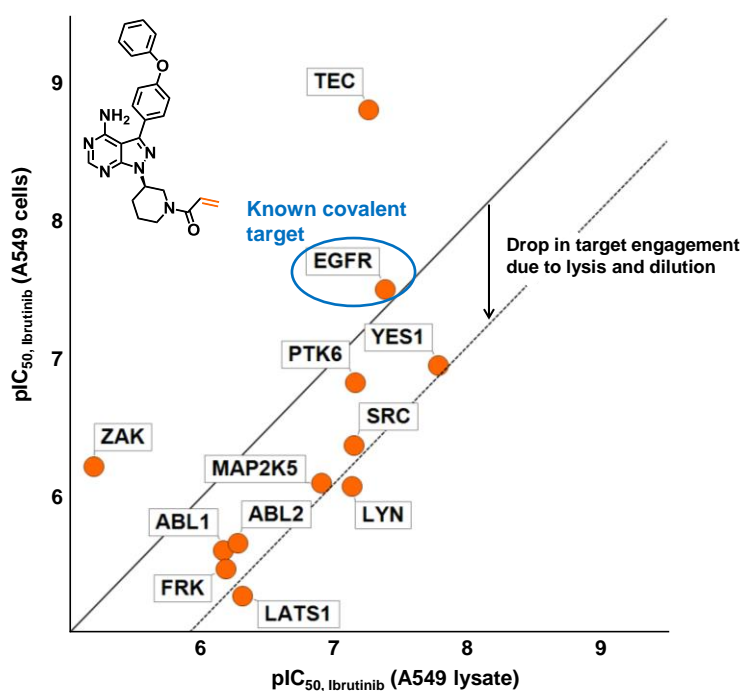


Figure 20: Differential kinobeads selectivity profiling of Ibrutinib in A549 cells and lysate. Kinases robustly identified to be inhibited with $pIC_{50} \geq 6$ by Ibrutinib in the cellular or lysate-based kinobeads assay are shown. The dashed line represents the calculated dilution factors due to lysis. All values are average values from 2 replicates.

Combining the data from Ramos and A549 cells, for Ibrutinib 247 kinases were identified in total of which 5 were engaged irreversibly, and 17 were indicated as non-covalent binders.

Table 6: Kinases robustly identified as targets of Ibrutinib in A549 and Ramos cells.

Kinases robustly identified in total		Covalent kinase targets	Reversible kinase targets	
<p>Kinases in A549 Kinases in Ramos</p> <p>38 (16%) 144 (58%) 65 (26%)</p>		BLK	ABL1	MAP2K5
		BTK	ABL2	MAP3K2
		EGFR	CSK	PRAGMIN
		TEC	FGR	PTK6
		ZAK	FRK	RIPK2
			FYN	RIPK3
			LATS1	SRC
			LCK	YES1
			LYN	

3.1.3.1. Application of differential kinobeads selectivity profiling to clinically relevant TCIs

The differential kinobeads profiling strategy was applied to characterize target kinases for a small panel of covalent kinase inhibitors in Ramos and A549 cells. The set of inhibitors comprised the covalent BTK inhibitors CC-292, the structural very similar CNX-774 as well as Acalabrutinib (Figure 21), the covalent EGFR inhibitor Afatinib (Figure 22), and 5Z-7-Oxozeaenol (Figure 23), a natural product of fungal origin.²⁰⁰⁻²⁰¹ For comparing only pIC₅₀ values calculated from reasonable binding curves, a pIC₅₀ was only defined if it was 0.5 log units above the maximal concentration used in the respective assay:

- Lysate-based: max. concentration = 50 µM → pIC₅₀ = 4.3; pIC₅₀ only valid if ≥ 4.8
- Cell-based: max. concentration = 10 µM → pIC₅₀ = 5; pIC₅₀ only valid if ≥ 5.5

For the following radar plots the cutoff was set to be pIC₅₀ ≥ 5.5 so that lysate-based pIC₅₀s below this value are not represented in the figures but only mentioned in the text.

By profiling of CC-292 for its selectivity against 253 kinases in a cell-based assay using A549 and Ramos cells valid cellular pIC₅₀s were determined for five kinases. Comparing those to 231 kinases identified in lysate suggests all five targets as covalent targets of CC-292. These include the previously described covalent targets TEC and BTK⁴⁵ as well as BLK. Whilst TEC and BTK were more potently inhibited in cells, BLK binding was equipotent in lysate as in cells. Further, FGFR1 and MAP3K4 both containing a reactive cysteine at glycine loop 5 and hinge 2 position, respectively, were identified as covalent binders. Lysate-based binding was determined to be lower as for the other covalent binders: pIC_{50, FGFR1} = 4.7±0.1 and pIC_{50, MAP3K4} = 4.8±0.2. This might indicate untargeted reactivity of the compound which does not occur in lysate due to unfavorable reaction conditions. For ten kinases, low binding in lysate and no potency in cells was determined suggesting them as reversible targets of CC-292.

CNX-774, structurally only discriminated from CC-292 by incorporating a N-methylpicolinamide instead a methoxyethane, showed a very similar selectivity profile as CC-292. Cellular pIC₅₀s for the hinge 6 incorporating kinases BTK, TEC, and BLK are almost identical. Same is true for FGFR1. Noteworthy, although having some cellular potency, pIC₅₀ values determined in lysate were generally lower than for CC-292. This might indicate that affinity driven-binding is decreased by the bulkier N-methylpicolinamide. Reactivity with cysteines others than at the hinge 6 position, however, might result in similar cellular potency. This would correlate with the fact that kinase targets containing a reactive cysteine at positions different from hinge 6 can be covalently bound by the compound backbone.

An improved kinase selectivity of Acalabrutinib over Ibrutinib as stated by recent reports⁶² was confirmed by differential kinobeads profiling. Among 236 kinases compared in lysate and cells the only cellular targets determined to be covalently inhibited with pIC₅₀ values of 8.1 and 7.8 are BTK and TEC, respectively. LIMK1, RIPK2 and RIPK3 as well as BLK showed reasonable target engagement in lysate but not in the cell-based kinobeads assay suggesting those as reversible binders of Acalabrutinib. A higher BTK potency of Acalabrutinib compared with Ibrutinib as stated previously⁶³ could not be confirmed using kinobeads selectivity profiling neither in lysate (pIC_{50, BTK, Acalabrutinib} = 7.1±0.0 vs pIC_{50, BTK, Ibrutinib} = 7.4±0.1) nor in cells (pIC_{50, BTK, Acalabrutinib} = 8.1±0.2 vs pIC_{50, BTK, Ibrutinib} = 9.0±0.1).

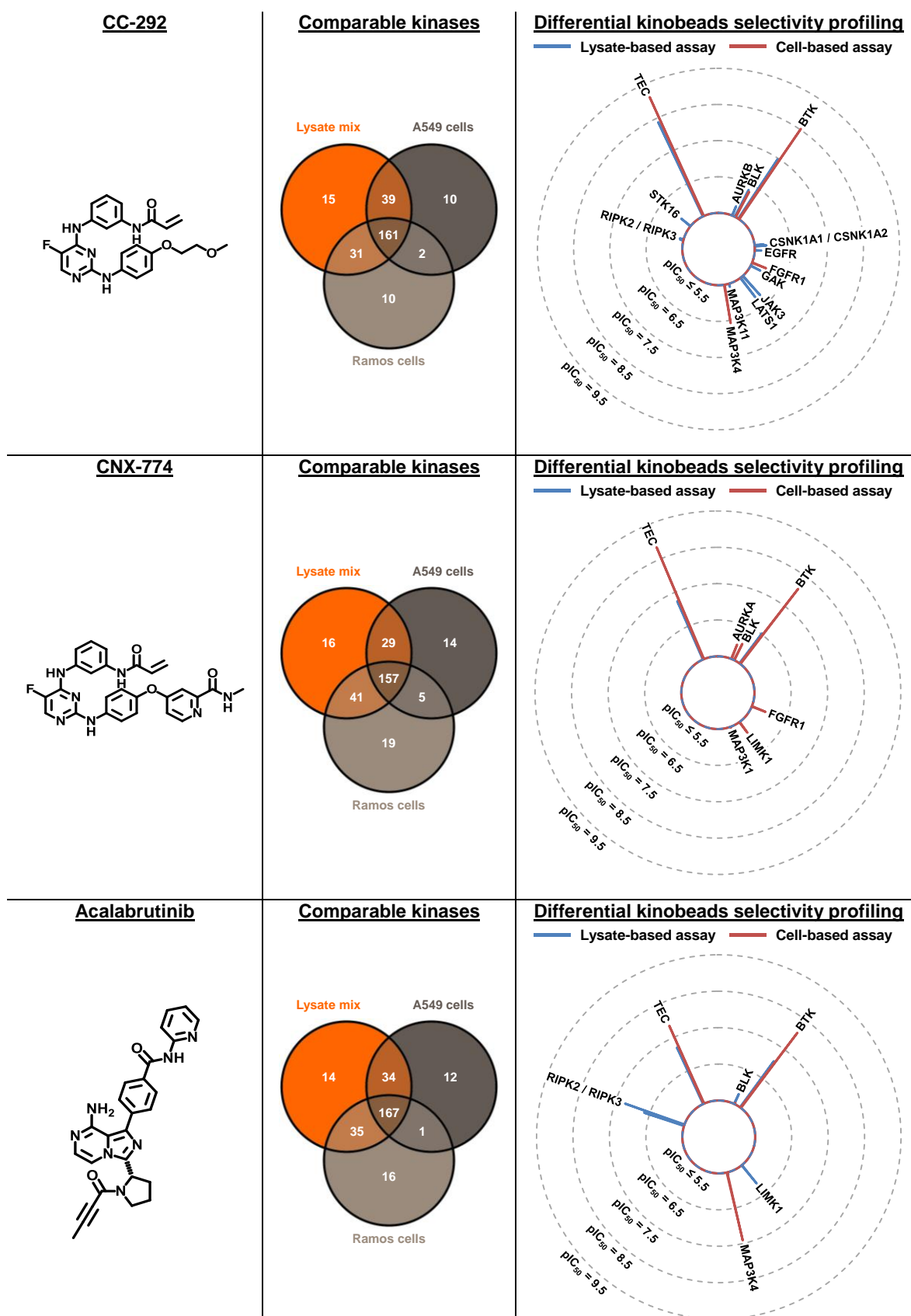


Figure 21: Differential kinobeads selectivity profiling of the BTK TCIs CC-292, CNX-774, and Acalabrutinib. The Venn diagrams give an overview of the kinases which can be compared due to common abundance in the lysate-mix and one of the used cell lines. The radar plots show average pIC_{50} values as determined across 2 replicates in lysate (blue) or cells (red). The pIC_{50} cutoff was set to be ≥ 5.5 in this representation. Reasonable lysate-based values ≥ 4.8 and < 5.5 are not shown in these plots.

In a next step, the investigation on targeted covalent inhibitors was expanded beyond BTK inhibitors to the targeted covalent EGFR inhibitor Afatinib (Figure 22). Afatinib was designed to react with a hinge 6 cysteine in EGFR (Cys797) so that it was analyzed if a similar selectivity profile is achieved with this compound. For Afatinib, differential kinobeads selectivity profiling against 227 comparable kinases yielded pIC_{50} values for only four kinases. Of those, EGFR is the only target with low nanomolar potency (cellular $pIC_{50} = 8.7 \pm 0.0$). For GAK and BLK cellular potency was determined above or somewhat equal as in the lysate-based kinobeads assay suggesting them as covalent off-targets while RIPK2 is predominantly bound in a reversible manner. A notable finding is that BLK was the only kinase target identified in Ramos cells while all other targets were expressed in A549 cells. This high selectivity against the Ramos cell kinome contrasts with cell toxicity observed for this cell line upon Afatinib treatment. This finding will be picked up again below.

When comparing the selectivity profiles of the different targeted covalent kinase inhibitors, the data achieved for Ibrutinib, CC-292, CNX-774, Acalabrutinib, and Afatinib shows only a limited number of common covalent (off-)targets indicated by equal or even slightly stronger target engagement in cells than in lysate. Comparing the different covalent BTK inhibitors and Afatinib a noticeable difference is the covalent engagement of BLK. BLK is the only kinase target bound by all TCIs with Acalabrutinib being the only inhibitor for which no covalent binding was suggested. A recent report demonstrated the benefit of co-inhibition of BTK and BLK by Ibrutinib in the treatment of pre-BCR⁺ B-cell acute lymphoblastic leukemia.²⁰² It will be interesting to see how Acalabrutinib will perform in the treatment of B-cell lymphoma indications.

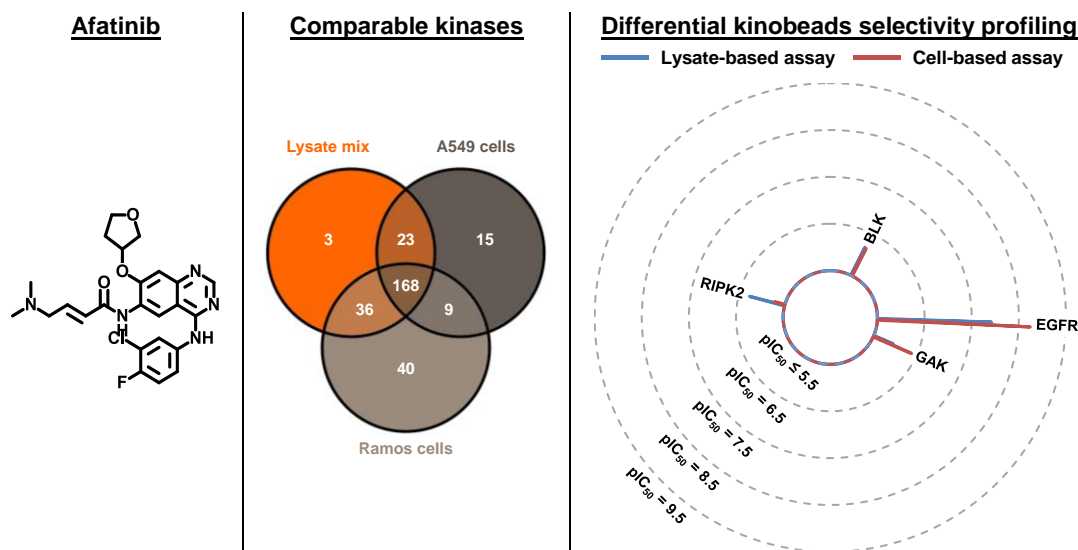


Figure 22: Differential kinobeads selectivity profiling of the EGFR TCI Afatinib. The Venn diagram gives an overview of the kinases which can be compared due to common abundance in the lysate-mix and one of the used cell lines. The radar plot shows average pIC_{50} values as determined across 2 replicates in lysate (blue) or cells (red). The pIC_{50} cutoff was set to be ≥ 5.5 in this representation. Reasonable lysate-based values ≥ 4.8 and < 5.5 are not shown in this plot.

For comparing how selectivity of designed covalent inhibitors differentiates against a natural product acting as covalent inhibitor via a Michael system, differential kinobeads selectivity profiling was performed using the resorcylic acid lactone 5Z-7-Oxozeaenol (Figure 23). For 5Z-7-Oxozeaenol, 26 kinases were identified as targets. Amongst these, eight kinases were clearly indicated as covalently

bound by the compound including the previously identified covalent targets BMP2K, GAK, MAP3K7²⁰⁰⁻²⁰¹ as well as the novel covalent targets MKNK1, ZAK, GSK3B, MAPK1, and MAPK3. Beyond these clearly suggested covalent targets, six putative covalent targets were identified: AAK1, CDKL5, MAP2K1, MAP2K2, MAP2K5, and MAP2K6. Putative means that although not showing higher potency in cells than in lysate, binding of all these kinases to kinobeads was still competed strongly after washing and processing the cells indicating a certain portion of irreversible target engagement. All kinases identified to be (putative) covalent binders contain a cysteine directly preceding the DFG motif (DFG-1 position) that was previously identified as covalent binding site of 5Z-7-Oxozeaenol underscoring the plausibility of the generated data. In addition, twelve kinases were bound in a predominantly non-covalent manner. These included a number of kinases containing a conserved cysteine residue at the DFG-1 position which apparently displayed little or no reactivity towards the compound.

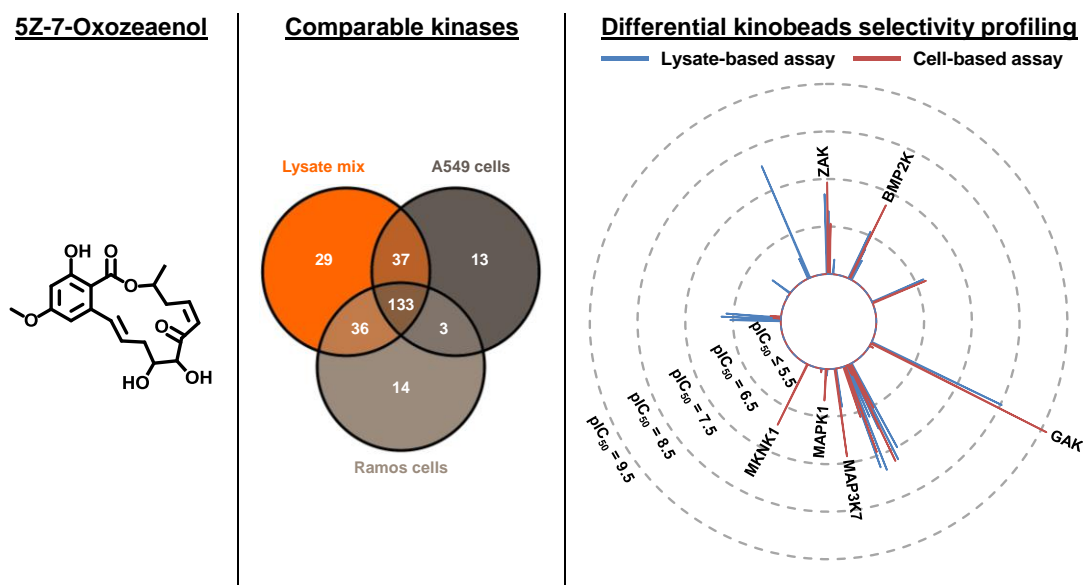


Figure 23: Differential kinobeads selectivity profiling of the covalent kinase inhibitor of fungal origin 5Z-7-Oxozeaenol. The Venn diagram gives an overview of the kinases which can be compared due to common abundance in the lysate-mix and one of the used cell lines. The radar plot shows average pIC_{50} values as determined across 2 replicates in lysate (blue) or cells (red). The pIC_{50} cutoff was set to be ≥ 5.5 in this representation. Reasonable lysate-based values ≥ 4.8 and < 5.5 are not shown in this plot. Due to the complexity of the unselective resorcylic acid lactone 5Z-7-Oxozeaenol only a selection of peaks is labeled. BMP2K, GAK, MAPK1, MAP3K7, and MKNK1 represent known covalent targets of the compound which were also suggested as covalent binders by differential kinobeads profiling. In addition, ZAK is highlighted representing a common strong covalent binder of 5Z-7-Oxozeaenol and Ibrutinib.

The differential kinobeads selectivity profiling of 5Z-7-Oxozeaenol identified ZAK as a not yet described covalent target of the compound. For Ibrutinib, the covalent binding site was identified to be Cys22 (Figure 19). ZAK was used to validate novel covalent targets of 5Z-7-Oxozeaenol and to further investigate if structurally very different covalent kinase inhibitors would necessarily react with the same cysteine residue in covalent targets. For this, recombinant ZAK was incubated with 5Z-7-Oxozeaenol. After enzymatic digestion, mass spectrometry was applied to identify peptides with a mass shift corresponding to the covalent modification of the nucleophilic amino acids cysteine, serine, or tyrosine with the compound. Cysteine residues of two peptides were identified showing mass differences corresponding to a 5Z-7-Oxozeaenol modification (Figure 24). A covalent modification of cysteine

Cys150 was identified which is part of the CDFG sequence (DFG-1 position), and thus, is located inside the ATP-binding site of ZAK. Reactivity of 5Z-7-Oxozeanol with this cysteine residue is in agreement with a previous report demonstrating covalent modification of CDFG sequence motifs in other kinases.²⁰⁰ Competition effects observed in the differential kinobeads profiling can be assigned to Cys150 binding. In addition, modification of the cysteine residue Cys231 was observed upon incubation with a 30-fold molar excess of 5Z-7-Oxozeanol for 24 h. Covalent binding to Cys231 being located far apart of the 5Z-7-Oxozeanol binding site in ZAK might be explained by unspecific reactivity of the compound with partially unfolded protein. The validation of ZAK as novel covalent target of 5Z-7-Oxozeanol confirmed the plausibility of the differential kinobeads selectivity profiling approach for the identification of irreversible binders of covalent kinase inhibitors.

Peptide	I <u>C</u> DFGASR
neutral mass of peptide (monoisotopic)	867.39 u
detected m/z	615.77
detected charge state	2+
neutral mass detected (monoisotopic)	1229.54 u
delta (detected-unmodified)	362.15 u
corresponding modification	5Z-7-Oxozeanol (+362.14 u)
modification site	Cys150

Peptide	RLTIPSS <u>C</u> PR
neutral mass of peptide (monoisotopic)	1128.61 u
detected m/z	497.92
detected charge state	3+
neutral mass detected (monoisotopic)	1490.76 u
delta (detected-unmodified)	362.15 u
corresponding modification	5Z-7-Oxozeanol (+362.14 u)
modification site	Cys231

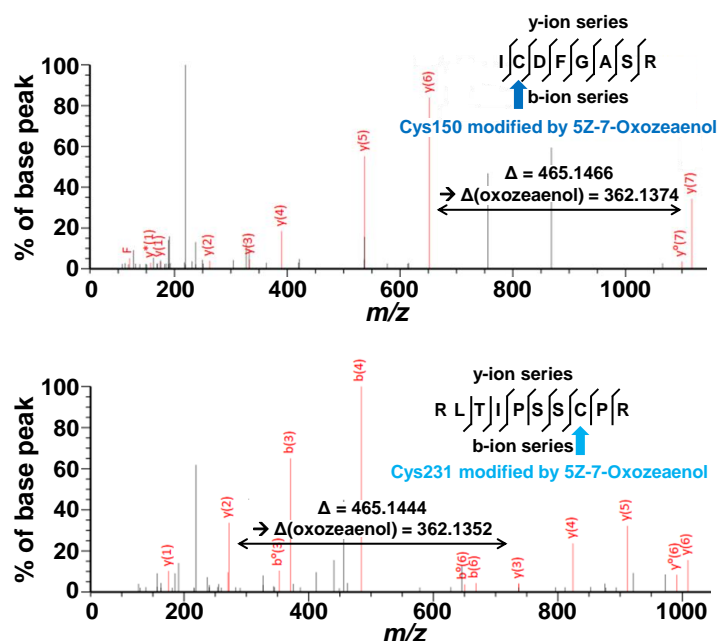


Figure 24: MS/MS spectra indicating a covalent reaction of 5Z-7-Oxozeanol with two distinct cysteines in ZAK.

Setting up conditions for a cell-based kinobeads assay enabled the investigation of target engagement of covalent kinase inhibitors in living cells. It was shown that cellular target engagement differs from lysate-based outcomes and that cellular measures predict the functional effect of kinase inhibition exemplified by BTK inhibition with Ibrutinib in a more suitable way. In addition, with differential kinobeads selectivity a technique was established to discriminate covalent and reversible targets of covalent kinase inhibitors without the need for labor-intensive probe synthesis. In this work, it will be referred to the application of differential kinobeads selectivity profiling for the analysis of covalent probes again in a later chapter.

While the strategy to use broad-spectrum inhibitors of one target class on a solid surface as affinity matrix has some advantages over target-specifically tailored probes regarding the labor-intensive design and synthesis, it also has limitations. This became especially obvious during the cellular experiments shown above when observing Afatinib toxicity in Ramos cells. Limited to the target space of kinases, investigations with kinobeads might not reveal off-target binding responsible for a non-favored phenotype. Therefore, several different, target class independent chemoproteomic

approaches were investigated for their applicability to covalent inhibition with two goals: first, these approaches should enable the identification of the toxicity causing off-target of Afatinib in Ramos cells. Beyond that, the general comparison of the data generated with different chemoproteomic approaches should allow for evaluating these techniques for their suitability for intracellular target engagement measurements of covalent inhibitors.

3.1.4. Application of chemoproteomic strategies for off-target identification causing an unexpected phenotype in Ramos cells

Comparing the kinase selectivity profiles generated for Afatinib and Ibrutinib in Ramos cells and lysate revealed that for BLK and RIPK2, which are most strongly engaged by Afatinib in cells as well as in lysate, pIC₅₀ values at least 1.5 log units higher were determined for Ibrutinib (Table 7).

Table 7: Kinases identified as targets of Afatinib in comparison with Ibrutinib.

Kinase	Afatinib				Ibrutinib			
	avg pIC ₅₀ (lysate)	s.e.m. pIC ₅₀ (lysate)	avg pIC ₅₀ (cells)	s.e.m. pIC ₅₀ (cells)	avg pIC ₅₀ (lysate)	s.e.m. pIC ₅₀ (lysate)	avg pIC ₅₀ (cells)	s.e.m. pIC ₅₀ (cells)
BLK	6.2	0.4	6.2	0.0	8.6	0.0	9.3	0.1
RIPK2	6.3	0.6	≤ 5.0	-	7.8	0.0	6.5	0.3
CHEK2	5.0	0.2	≤ 5.0	-	≤ 4.3	-	≤ 5.0	-
GAK	6.0	0.2	5.3	0.3	≤ 4.3	-	≤ 5.0	-
MAPK14	4.9	0.1	≤ 5.0	-	≤ 4.3	-	≤ 5.0	-
MAPKAPK2	5.3	0.2	≤ 5.0	-	≤ 4.3	-	≤ 5.0	-
MKNK1	5.3	0.1	≤ 5.0	-	≤ 4.3	-	≤ 5.0	-
PHKG2	4.9	0.1	≤ 5.0	-	≤ 4.3	-	≤ 5.0	-

To characterize if engagement of BLK or RIPK2 might result in cell toxicity, cell viability was compared after treating Ramos cells with Ibrutinib and Afatinib. Cell viability was analyzed by ATP-dependent luminescence and dose-response curves for both compounds were determined to allow for the calculation of compound concentrations reducing cell viability by 50 % (EC₅₀) (Figure 25). For Afatinib, stronger cell toxicity was observed than for Ibrutinib with the most prominent effect after 24 h (EC₅₀_{Afatinib} ~ 4 μM vs EC₅₀_{Ibrutinib} ~ 25 μM). This result suggests that BLK and RIPK2 binding cannot be the kinase targets responsible for inducing cell death since Ibrutinib would be expected to be more cell toxic than Afatinib when engaging those kinases stronger. In a next step, it was analyzed if cell toxicity is a non-specific effect caused by necrosis upon treatment of the cells with high compound concentrations. By analyzing caspase-3 mediated apoptosis resulting in PARP1 cleavage it was possible to define cell death to be apoptosis-driven.

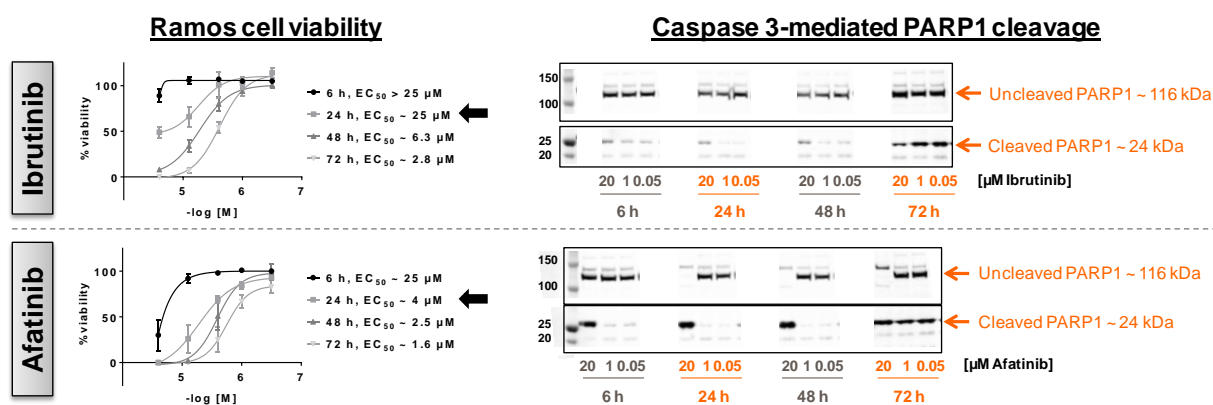


Figure 25: Ramos cell viability after treatment with Ibrutinib and Afatinib. Ramos cell viability was measured with the ATP-dependent CellTiter-Glo® assay (Promega) and dose-response curves were generated from 3 replicates using GraphPad Prism 7.03 software with a built-in four parameters curve fitting module. The error bars represent the standard error of the mean. The Western blot show signals detected after immunostaining for PARP1. Cleavage of PARP1 as indicator for Caspase 3-mediated apoptosis can more prominently being observed after treating Ramos cells with Afatinib than after incubation with Ibrutinib.

To further characterize if the apoptosis-inducing off-target is exclusively expressed in Ramos cells, it was analyzed if cell toxicity is specific for Ramos cells or if this effect can be generally observed for other cell lines. With this rationale, cell viability was also determined for the peripheral blood cell lines Jurkat (T cell leukemia), THP-1 (acute monocytic leukemia), and YT (T/NK cell leukemia). For Afatinib, EC_{50} values in the low μM range were obtained (EC_{50} s ~ 1.6 - $7 \mu\text{M}$) while Ibrutinib did only slightly affect Jurkat cell viability after 24 h ($EC_{50} \sim 20 \mu\text{M}$) (Table 8). This data suggests that Afatinib induces apoptosis rather via a generally expressed target than through a Ramos cell specific kinase like BLK.

Table 8: Cell viability of different peripheral blood cell lines upon treatment with Afatinib and Ibrutinib as determined with the CellTiter-glo assay (Promega).

Compound	Cell line	Cell viability EC_{50}			
		6 h	24 h	48 h	72 h
Afatinib	Ramos	$\sim 25 \mu\text{M}$	$4 \mu\text{M}$	$2.5 \mu\text{M}$	$1.6 \mu\text{M}$
	THP-1	$\sim 25 \mu\text{M}$	$5 \mu\text{M}$	$1.6 \mu\text{M}$	$\sim 1 \mu\text{M}$
	YT	$\sim 25 \mu\text{M}$	$7 \mu\text{M}$	$3.5 \mu\text{M}$	$1.8 \mu\text{M}$
	Jurkat	$5 \mu\text{M}$	$1.6 \mu\text{M}$	$1 \mu\text{M}$	$0.9 \mu\text{M}$
Ibrutinib	Ramos	$> 25 \mu\text{M}$	$\sim 25 \mu\text{M}$	$6.3 \mu\text{M}$	$2.8 \mu\text{M}$
	THP-1	$> 25 \mu\text{M}$	$> 25 \mu\text{M}$	$\sim 25 \mu\text{M}$	$13 \mu\text{M}$
	YT	$> 25 \mu\text{M}$	$> 25 \mu\text{M}$	$\sim 25 \mu\text{M}$	$16 \mu\text{M}$
	Jurkat	$> 25 \mu\text{M}$	$20 \mu\text{M}$	$9 \mu\text{M}$	$5 \mu\text{M}$

Based on the at this point available data sets it was not possible to clearly indicate a kinase as apoptosis-inducing off-target of Afatinib in Ramos cells. Thus, additional chemoproteomic approaches were applied to either confirm a kinase as off-target or, by expanding the target space beyond kinases, identify binding to a non-kinase potentially responsible for Afatinib's cell toxic effect.

3.1.4.1. Further chemoproteomic approaches to study target engagement of covalent inhibitors in cells

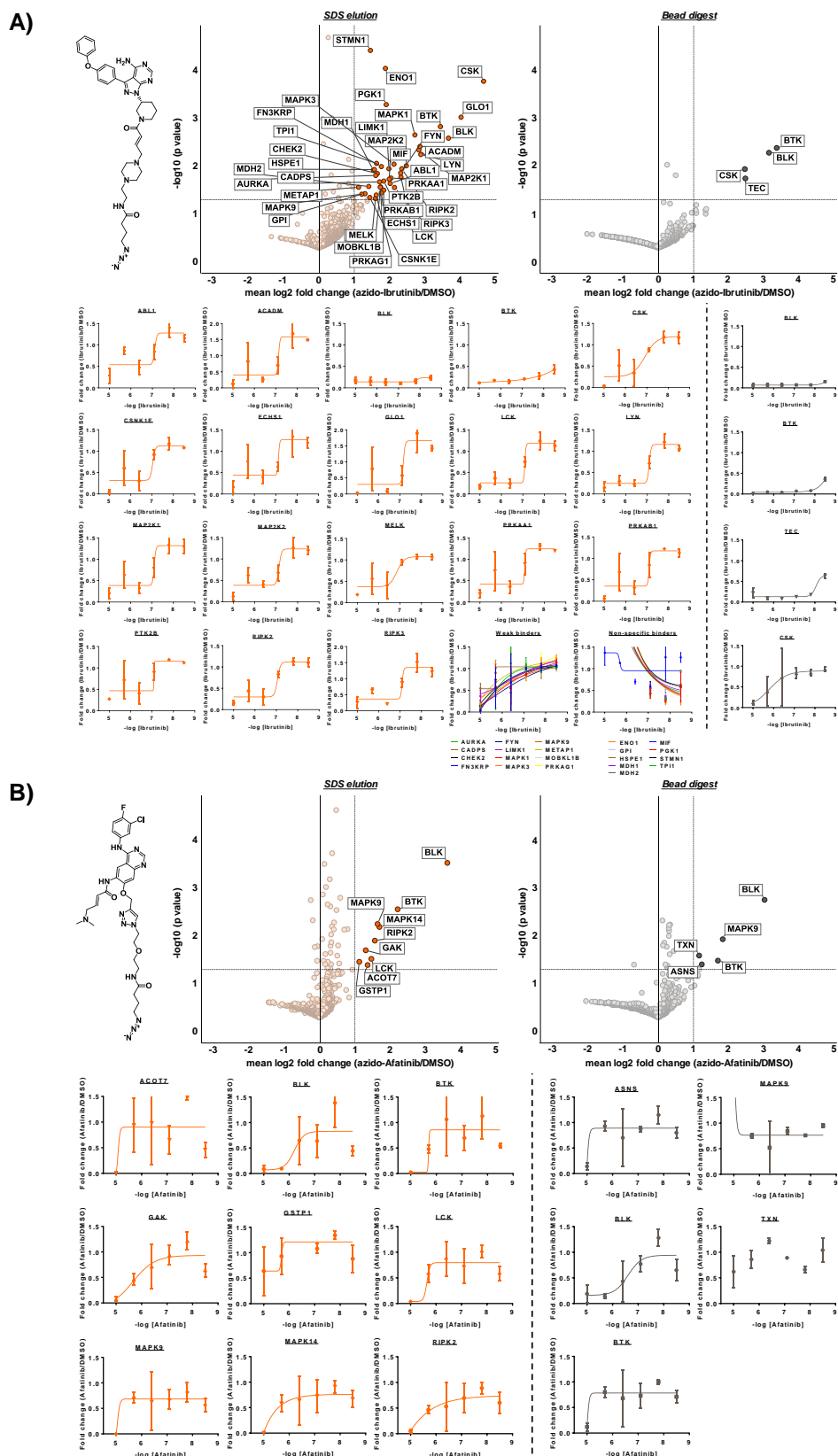
3.1.4.1.1. Orthogonal affinity enrichment approach using clickable inhibitor analogues

The immobilization of linkable analogues of compounds to enrich their targets and the accession of covalent binders by direct bead-proteolysis after eluting the reversible binders under denaturing conditions enables a proteome-wide characterization of covalent compound targets. Such a lysate-based orthogonal affinity enrichment approach was used above for the identification of ZAK as covalent target of Ibrutinib (Figure 19A). Using click chemistry, this kind of studies can be transferred from target engagement studies in cell extracts to experiments directly done in living cells. It was shown above that especially for covalent inhibitors this represents a more suitable evaluation of target engagement as performing lysate-based experiments. For intracellular competition binding experiments with covalent inhibitors, cells are additionally treated with a clickable analogue of the inhibitor under investigation prior to lysis and enrichment of proteins via the bioorthogonal handle. As above, reversibly immobilized proteins can be eluted by denaturing reagents and covalent binders can be accessed by proteolysis. Competing the binding to the clickable analogue in dose-response allows for the discrimination of specific binders and non-specifically captured proteins.²⁰³

With such an intracellular competition binding approach, for Ibrutinib, 39 proteins were identified as reversibly enriched 2-fold and more with a p value < 0.05 after performing a one-sided t test (Figure 26A, left panel). Of those, 24 proteins were kinases including targets of Ibrutinib as identified in the kinobeads pulldown experiments: ABL1, AURKA, BLK, BTK, CSK, FYN, LCK, LIMK1, LYN, RIPK2, RIPK3, and TEC. With exception of AURKA, FYN and LIMK1, for those, dose-dependent competition was observed. For AURKA, FYN and LIMK1, incomplete binding curves were derived, i.e. weak competition was measured at the highest compound concentrations. This is in correlation with the weak reversible binding determined in a lysate-based kinobeads pulldown. Beyond the targets also identified in the kinobeads experiments, for ten more proteins including seven kinases reasonable binding curves were generated: ACADM, CSNK1E, ECHS1, GLO1, MAP2K1, MAP2K2, MELK, PRKAA1, PRKAB1, and PTK2B. ACADM, ECHS1, and GLO1 as non-kinases were not captured by kinobeads, and thus, might represent true targets only revealed by this orthogonal approach. The kinases, with exception of PRKAB1, were robustly identified but not competed in the kinobeads experiments. Since the binding curves result in reliable pIC_{50} values of around 7 for the six kinase targets, the lysate-based kinobeads experiment should have captured those as targets as well. As this was not the case, it might suggest that these kinases were only accessibly as binders of Ibrutinib in the cellular environment highlighting the value of cellular target engagement measurements. A similar argumentation could explain why the kinases CHEK2, MAPK1, MAPK3, and MAPK9 were identified as weak binders of Ibrutinib using the clickable probe in cells but no engagement was determined in the kinobeads assay despite of robust identification. For nine significantly enriched proteins, no competition by Ibrutinib was observed. This suggests all of them as non-specifically enriched proteins being no targets of Ibrutinib. The known covalent targets BLK and BTK are also found in the SDS eluates with BTK being about 4-fold stronger abundant (MS^1 intensity) in the bead digests as in the SDS eluate and BLK being equally abundant. This indicates that reversible binding to the beads probably cannot be abrogated at the used conditions.

In the bead digest fraction, the covalent targets BLK, BTK, and TEC as well as the non-covalent binder CSK were identified as significantly enriched (Figure 26A, right panel). The occurrence of CSK among the significantly enriched proteins in the bead digest cannot be fully rationalized. CSK contains a serine at hinge 6 position which is also a nucleophilic amino acid which is, however, not known to be bound by low reactive acrylamides as used in Ibrutinib. Another cysteine in close proximity is not available. Further, no complex formation with one of the identified covalent targets of Ibrutinib is known. It has to be noted that CSK was also identified in the bead digest fraction using an orthogonal approach in lysate (Figure 19). This false positive identification of CSK as partial covalently bound target might indicate a shortcoming of these orthogonal approaches for the discrimination of covalent and reversible targets of covalent inhibitors. The identification of the others as covalent binders is in correlation with previous experiments and binding of those targets was competed by free Ibrutinib. Dose-response curves showed strong competition for BLK, BTK, and TEC so that pIC_{50} values are estimated to be < 1 nM, ~ 1 nM, and ~ 10 nM, respectively. This rank order and the magnitude (low nanomolar range) are in accordance with previous cell-based experiments and demonstrate the plausibility of the generated data.

For an equivalent experiment using Afatinib and a clickable analogue, less proteins were identified upon SDS elution. The proteins enriched 2-fold and more with a p value < 0.05 are the seven kinases BLK, BTK, GAK, LCK, MAPK9, MAPK14, and RIPK2, as well as the two non-kinases ACOT7 and GSTP1. Among those, binding curves suggest BLK, BTK, GAK, LCK, and RIPK2 as well as the MAP kinases being weak binders of Afatinib. With $10 \mu\text{M}$ Afatinib, probe binding of ACOT7 and GSTP1 was also competed. BTK, BLK, and MAPK9 were also identified in the bead digest fraction which indicates partial covalent binding of those three kinases by the azide analogue of Afatinib. Suitable cysteines are Cys481, Cys319, and Cys116 in BTK, BLK, and MAPK9, respectively. For BLK, a dose-response curve suggests specific binding with a pIC_{50} correlating with previous experiments. For BTK and ASNS, a non-kinase identified as covalently bound by the compound, competition was observed at the highest concentration. For TXN and MAPK9, no competition was determined in the bead digests. For the latter, however, weak binding was determined in the SDS fraction, MAPK9 might represent a weak reversible target of Afatinib probably being identified as non-specific binder in the bead digests. BLK, RIPK2, and GAK were also identified as Afatinib targets with kinobeads while the MAP kinases, LCK, and BTK were not bound by Afatinib in a lysate-based kinobeads assay. This, again, might demonstrate the differences of target engagement in lysate and in a cellular environment.



A comparison across the two different types of affinity enrichment, kinobeads vs intracellular competition binding using clickable probes, shows that for Ibrutinib ABL1, AURKA, BLK, BTK, CSK, FYN, LCK, LIMK1, LYN, RIPK2, RIPK3 and TEC and for Afatinib BLK, GAK, MAPK14, and RIPK2 were identified as targets in both approaches (Figure 27). This means, that for Ibrutinib, all targets identified by kinobeads and robustly identified with the intracellular approach were also indicated as targets in the latter. Kinases suggested as target in only one assay although being robustly identified in both are CHEK2, CSNK1E, MAP2K1, MAP2K2, MAPK1, MAPK3, MAPK9, MELK, PRKAA1, and PTK2B, and BTK, LCK, MAPK9, and CHEK2 for Ibrutinib and Afatinib, respectively. In the kinobeads assay some kinases were identified as targets which were not robustly found in the data set using the clickable analogue. The six non-kinase proteins identified with the clickable analogue approach (ACADM, CADPS, ECHS1, GLO1, METAP1, and MOBKL1B) are conceptually not covered by kinobeads. The fact that some kinase targets were exclusively identified using the clickable analogue directly in living cells suggest that the structural integrity of proteins, and thus, the potential to capture those might differ between the cellular environment and lysate conditions. The kinases identified in the kinobeads approach include proteins expressed at low levels in the used cell line. Thus, they might be true binders of Ibrutinib but not the azide-analogue and only detectable by mass spectrometry after enriching for those kinases with kinobeads. Targets identified in only one approach would require additional validation.

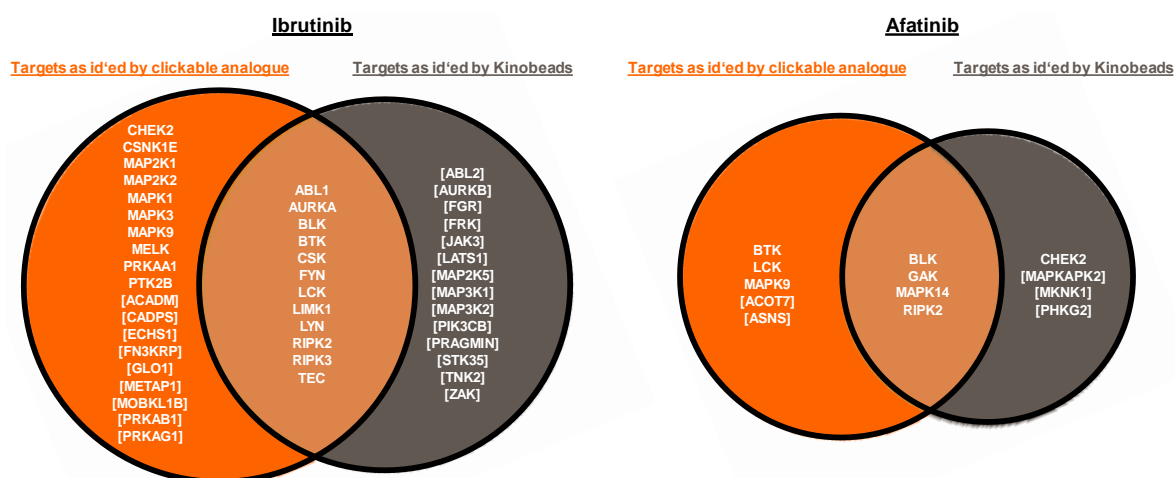


Figure 27: Comparison of targets of Ibrutinib and Afatinib identified with chemoproteomic affinity enrichment approaches. Target proteins in squared brackets were exclusively identified in the respective assay.

3.1.4.1.2. Multiplexed proteome dynamics profiling upon treatment with proteolysis targeting chimeric molecules (PROTACs)

An advancing technique for investigations on the function of proteins and inhibition of them is PROTAC-induced proteolytic targeting.²⁰⁴ By analyzing degradation of proteins upon treatment of cells with PROTAC analogues of covalent inhibitors this concept could also be applied to identify (off-)targets in a proteome-wide manner. Compared to the chemoproteomic affinity enrichment approaches, PROTACs exert their effects directly in living cells, and thus, avoid biases introduced by lysis of the cells like re-equilibration of non-covalent binding. Triggered by the observation of Afatinib causing Ramos cell toxicity, this cell line was used for proteome dynamics studies upon treatment with PROTAC analogues of Afatinib, Ibrutinib, and saturated Ibrutinib. A pulsed SILAC approach switching the amino acid pool from light to heavy and vice versa when starting to incubate the cells with the PROTACs and the respective parent compound enabled to discriminate effects on mature and nascent proteins. Since the PROTAC induced degradation is a very complex process as introduced above, for the design of PROTAC analogues of Afatinib, Ibrutinib, and saturated Ibrutinib, it was relied on the findings of *Huang et al* and *Lai et al* identifying Cereblon as best working E3 ligase for kinases.¹⁴⁵⁻¹⁴⁶ Hence, lenalidomide conjugates were synthesized on the basis of amine-incorporating analogues of the compounds.

Although 80 % of all proteins indicated as target of Afatinib in another assay were robustly identified in the proteome dynamics experiment, for Afatinib it was not possible to identify significant degradation (change in abundance ≥ 33 % and p value < 0.05) of any mature or nascent protein among both replicates (Figure 28A). For completeness, it should be noted that also BLK was identified but with only one quantified unique peptide, therefore, not considered as being identified robustly. Thus, it was excluded from the analysis as shown below. However, for BLK, normalized degradation (Afatinib-PROTAC vs Afatinib control) was observed for 1 μ M and 10 μ M Afatinib-lenalidomide with fold changes (log₂ of the mean of both replicates) of -0.38 and -0.35, respectively, suggesting it as tagged by the PROTAC analogue of Afatinib.

For the Ibrutinib-PROTAC, several proteins indicated as targets in other assays were identified including the kinases BTK, CSK, LCK, and LYN. Among those, significant and dose-dependent degradation triggered by the Ibrutinib-lenalidomide conjugate was observed for the known non-covalent kinase targets CSK, LCK, and LYN (Figure 28B). For the covalent Ibrutinib target BTK no effect was determined with the covalent PROTAC molecule but with the saturated analogue (Figure 28C). Since no further covalent target of Ibrutinib (BLK, TEC, or ZAK) was identified in this experiment, at this point it is up to speculation if the covalent mechanism might influence degradation of irreversibly bound targets. When treating the Ramos cells with the Ibrutinib-PROTAC, PITPNC1 was indicated as upregulated beyond the significance threshold among the nascent proteins. PITPNC1 is a lipid transporter protein and might be involved in a response to reduced hydrolysis of phosphatidylinositol 4,5-bisphosphate by phospholipase C upon BTK signaling inhibition. However, since this upregulation is close to miss the significance criteria additional investigations would be required for validation. For the PROTAC analogue of saturated Ibrutinib, several proteins are indicated as significantly regulated. Besides BTK, together with CSK, showing the most prominent degradation, protein degradation can also be observed for LYN, LAT2, CD19, and INPP5D. For LYN, affinity was already determined in the

previous pulldown experiments. LAT2 is described to potentially being involved in BCR signaling,²⁰⁵ and thus, could be influenced by BTK degradation. Lower abundancies of CD19 observed for increasing PROTAC concentrations only in the nascent protein fraction indicates a downregulation effect of this protein upon treatment with the PROTAC. Since CD19 is involved in BCR signaling²⁰⁶⁻²⁰⁷ this downregulation might be a consequence of impaired BTK signaling due to proteolysis of therein involved proteins. INPP5D, again, is involved in phosphoinositol signaling²⁰⁸ and associated with LYN.²⁰⁹ The indication of significant regulation of PFDN6 seems to be a borderline effect. A clear dose-dependent effect cannot be observed indicating rather assay variance as a true effect.

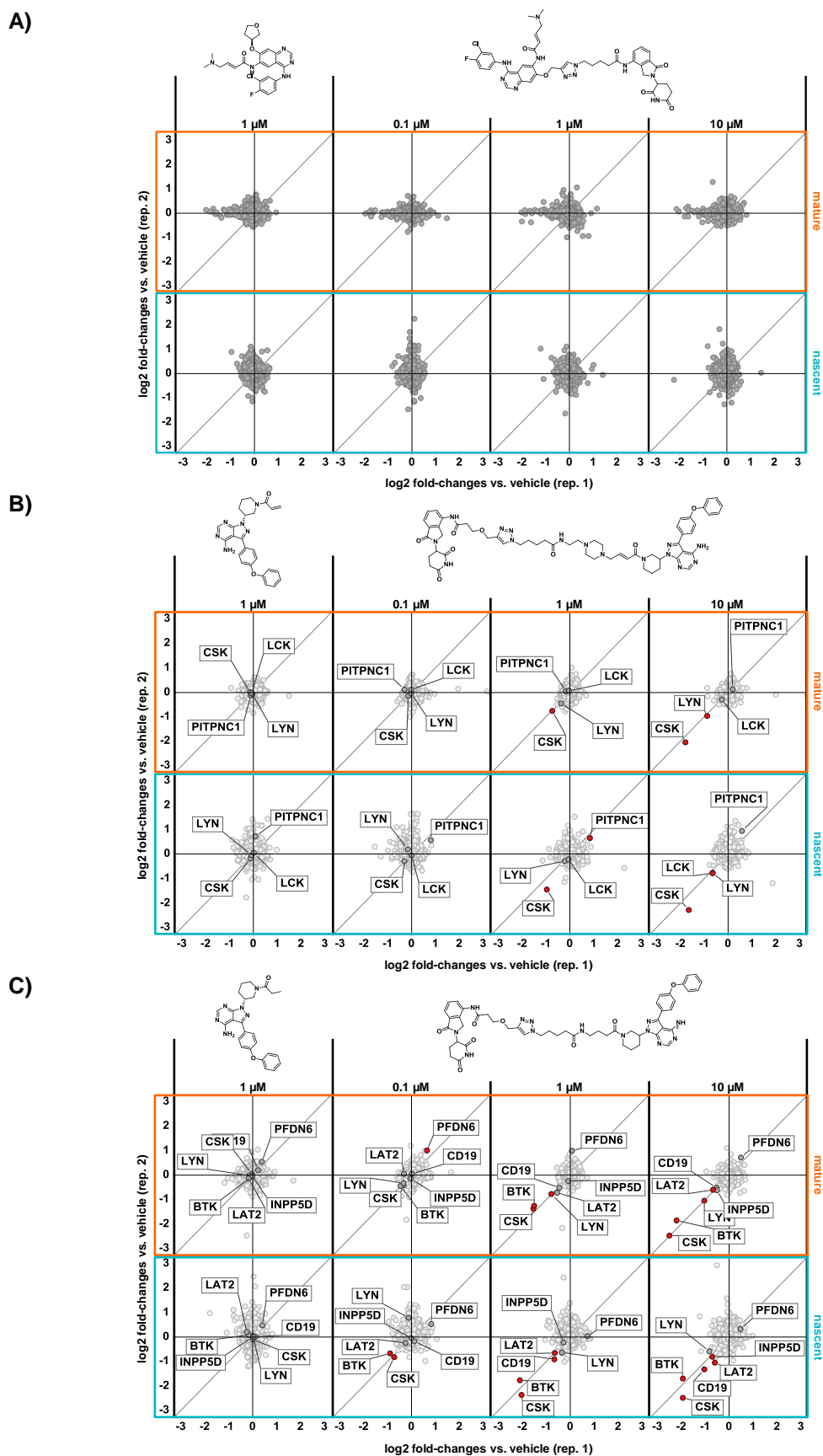


Figure 28: Multiplexed proteome dynamics profiling of Ramos cells upon PROTAC treatment. Ramos cells were incubated with (A) Afatinib, (B) Ibrutinib or (C) saturated Ibrutinib and different concentrations of lenalidomide-conjugates thereof for 24 h. Discrimination of mature and nascent proteins was enabled by a pulse SILAC approach. The graphs show fold change values (log₂ scale) of abundance compared to the vehicle control of replicate 2 over replicate 1 for each condition. In the upper panels framed in orange and in the lower panels framed in blue effects on mature proteins and nascent proteins, respectively, are shown. Marked in red are the proteins significantly regulated in at least one condition (fold change $\geq 33\%$ and p value ≤ 0.05).

Since no regulation effects on any protein were observed for the Afatinib-PROTAC it was tested whether the Afatinib-lenalidomide conjugate induces degradation of the covalent Afatinib target EGFR. A549 cells were treated for 24 h with this analogue at different concentrations and protein abundance in these samples was analyzed. For EGFR, no PROTAC-specific degradation was observed (Figure 29). Taken together with the observations made for BTK using the Ibrutinib-PROTAC in Ramos cells, this finding might indicate that the covalent reaction of kinase inhibitors avoids degradation of irreversibly bound targets. Among the 1348 proteins robustly identified in both replicates, no significant regulation (p value < 0.05) more than 33 % ($\text{meanlog}_2 \pm 0.59$) was observed for the PROTAC in a concentration-dependent manner. The only downregulation indicated as significant was seen for TMSL3 upon treatment with 0.4 μM Afatinib-PROTAC. Since this effect is only determined in this sample and not for the other PROTAC concentrations it might rather represent a false positive than a true PROTAC-mediated effect. After treating the cells with 10 μM Afatinib, the abundancies of a multitude of proteins differed as compared with the vehicle control. A GO term analysis of the more abundant proteins associates many with small molecule / drug metabolic processes (GO:0044281, p value = $7.05 \cdot 10^{-5}$ / GO:0017144, p value = $1.79 \cdot 10^{-6}$). This indicates a general response to drug treatment which could also be expected for the treatment of cells with the PROTAC. For the proteins significantly less abundant as in the vehicle control, no GO term was enriched with a p value threshold of 0.001.

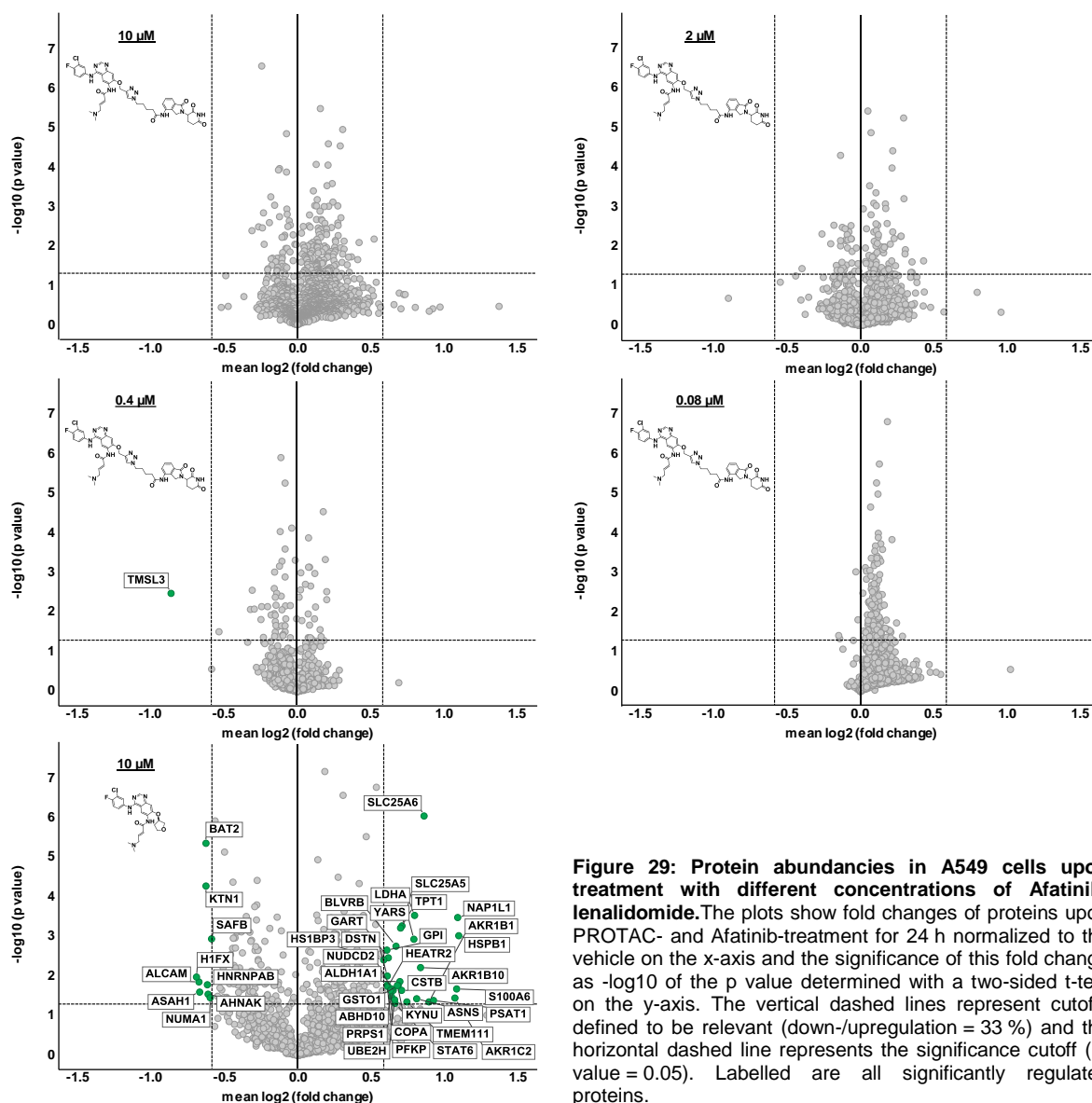


Figure 29: Protein abundancies in A549 cells upon treatment with different concentrations of Afatinib-lenalidomide. The plots show fold changes of proteins upon PROTAC- and Afatinib-treatment for 24 h normalized to the vehicle on the x-axis and the significance of this fold change as $-\log_{10}$ of the p value determined with a two-sided t-test on the y-axis. The vertical dashed lines represent cutoffs defined to be relevant (down-/upregulation = 33 %) and the horizontal dashed line represents the significance cutoff (p-value = 0.05). Labeled are all significantly regulated proteins.

Due to the failed degradation of EGFR and the lack of a responsive regulation of other proteins upon treatment with the lenalidomide analogue of Afatinib, protein binding and cell permeability was evaluated for the molecule. For this, a lysate-based selectivity profiling and a cellular engagement assay in EGFR-expressing A549 cells were performed with the PROTAC. Selectivity profiling data in an A549/Ramos lysate mix suggests that coupling the lenalidomide does not influence the binding affinity to EGFR and other targets identified in previous kinobeads experiments (Figure 30A). A cellular EGFR engagement assay was done by treating A549 cells with Afatinib, the PROTAC molecule at three different concentrations and a vehicle control. Subsequently, cells were washed, harvested and lysed for performing a kinobeads pulldown. The Western blot demonstrates that binding of EGFR to kinobeads was efficiently competed by Afatinib and the PROTAC analogues at 10 μM and 1 μM while 0.1 μM of the PROTAC did only partially reduce kinobeads enrichment (Figure 30B).

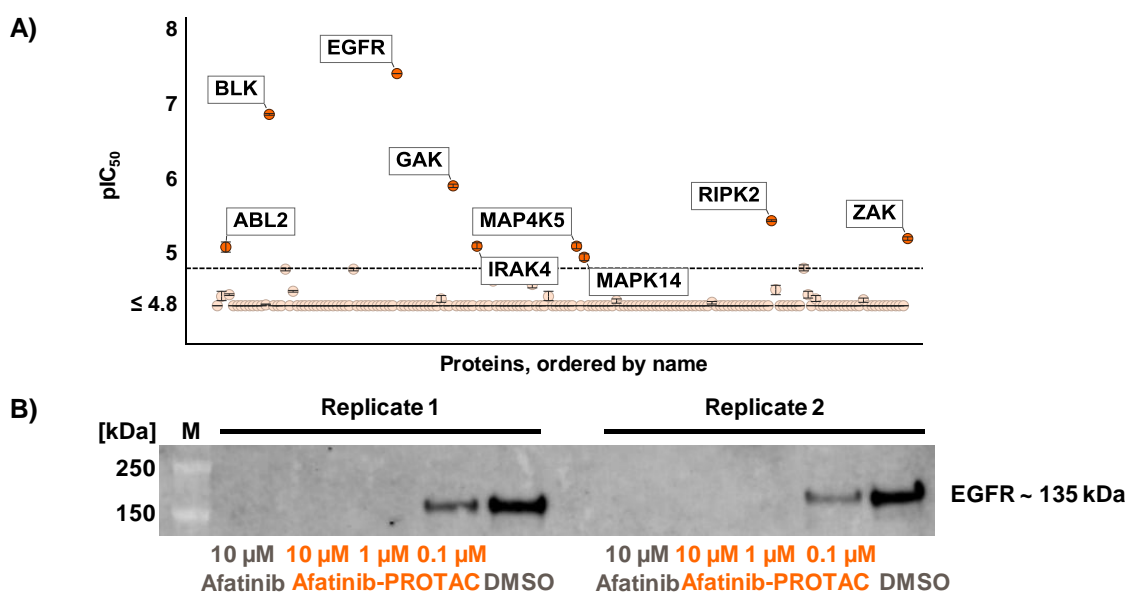


Figure 30: Target binding assessment of the Afatinib-lenalidomide conjugate in lysate and cells. (A) In a lysate-based kinobeads experiment using a A549/Ramos lysate mix, target binding very similar to the results achieved with the parent compound was determined. Averages of 2 replicates and standard errors of the mean are shown. (B) After treating A549 cells with Afatinib and the Afatinib-PROTAC, a cell based kinobeads assay with compound washout followed by immunostaining of EGFR confirms cell permeability and protein binding of the compound.

The lysate-based selectivity profiling and the cellular target engagement assay allows for the conclusion that impaired engagement of EGFR is not causative for the lack of EGFR degradation. Thus, the complexity of PROTAC-induced degradation of target proteins including especially the irreversible binders of covalent inhibitors requires more investigation which is beyond the scope of this dissertation.

3.1.4.1.3. Two-dimensional thermal proteome profiling

For both approaches, the orthogonal affinity enrichment as well as the PROTAC strategy, a linkable analogue of Ibrutinib and Afatinib was used for which the binding mode was optimized for accessing kinases. Therefore, a less probe biased approach given with 2D-TPP analyses as established by *Savitski et al*¹³⁷ was used. For a cellular thermal proteome profiling experiment, Ramos cells were treated with Afatinib or Ibrutinib at different concentrations for 1 h before heating up the cell pellets to temperatures from 42 °C to 64 °C for inducing aggregation. After lysis, the aggregated proteins were removed and soluble proteins were analyzed by mass spectrometry to identify compound concentration-dependent thermal de-/stabilization.

4788 proteins were robustly identified (qupm > 1) in the 2D-TPP analysis of Ibrutinib-treated Ramos cells. Among those, effects on thermal stabilization were detected for 20 proteins in at least two adjacent temperatures, with a rather dose-dependent destabilizing effect on six proteins and a stabilizing effect on 14 proteins (Figure 31A). The stabilized proteins include LYN and CSK, both kinases identified as targets of Ibrutinib in previous assays. For analyzing the kinase space specifically, the filtering for effects at two adjacent temperatures was not applied and thermal effects also observed at only one temperature were determined (dashed box). In total, the robustly identified proteins included 152 kinases among which BTK and BLK were found as well. A prominent effect on thermal stability was not observed for those two known covalent targets of Ibrutinib. For RIPK2, RIPK3, and LCK representing non-covalent targets, as identified in kinobeads pulldowns, thermal

stabilization was observed. For FYN, another reversible target identified in the pulldown experiments, no prominent effect was observed. FGR was not identified in the 2D-TPP analysis. The kinases identified to be destabilized most strongly are CAMK2D, TTK, and RIOK1 of which none has been identified as kinase target of Ibrutinib in the pulldown experiments.

Among 5396 robustly identified proteins, for Afatinib, thermal stabilization and destabilization were determined for 20 proteins and two proteins, respectively (Figure 31B). Comparing those results to the cell-based competition binding experiment, eleven of the thermally affected proteins were robustly identified with only ASNS matching the filtering criteria of being enriched ≥ 2 -fold with a p value < 0.05 . ASNS is involved in the biosynthesis of L-asparagine and contains a ATP binding site. Potential binding of Afatinib to this site might result in impaired asparagine synthesis. One ATP binding site contains a cysteine (Cys255) which could represent an amino acid potentially reacting with Afatinib.

Analyzing the 197 robustly identified kinases specifically without the filter as mentioned above (dashed box), for MAPK14, GAK, and BLK dose-dependent stabilization can be observed at one temperature. Those were identified in the kinobeads and orthogonal pulldown experiments. Three further identified targets, LCK, MAPK9, and RIPK2, cannot be confirmed by a relevant thermal effect at the used conditions. This correlates, however, with the weak binding of Afatinib to these targets as determined in the pulldown experiments. Thermal destabilization can be observed with the most prominent effects on GSK3A, CHEK1, WNK1, LYN, and BMP2K. For none of those, affinity was determined using the other chemoproteomic compound profiling approaches.

A notable finding in the 2D-TPP experiments was that Afatinib stabilized ACAD9, ECSIT, and NDUFAF1 which are all associated with the assembly of mitochondrial complex I, one of the complexes involved in the respiratory chain of cells. Since Afatinib-induced apoptosis was identified to be a general effect among different cell lines it was suggested that influences on this fundamental process might be the driver of apoptosis induction in cells not expressing EGFR. In addition, for Ibrutinib an effect on thermal stability of any of the proteins affected by Afatinib was not determined correlating with the lack of toxicity of Ibrutinib on Ramos cells. Experiments for the validation of these observations were performed. Identifying an adduct resulting from covalent modification of recombinant ACAD9 by Afatinib failed. A commercially available assay analyzing the integrity of mitochondrial complex I (Cayman MitoCheck Complex I Activity Assay) showed reduced activity of complex I in mitochondria isolated from Afatinib treated Ramos cells. However, it was not possible to distinguish a specific effect on complex I assembly from reduced activity due to an increased number of apoptotic cells even not by analyzing expression levels of proteins in such isolated mitochondria.

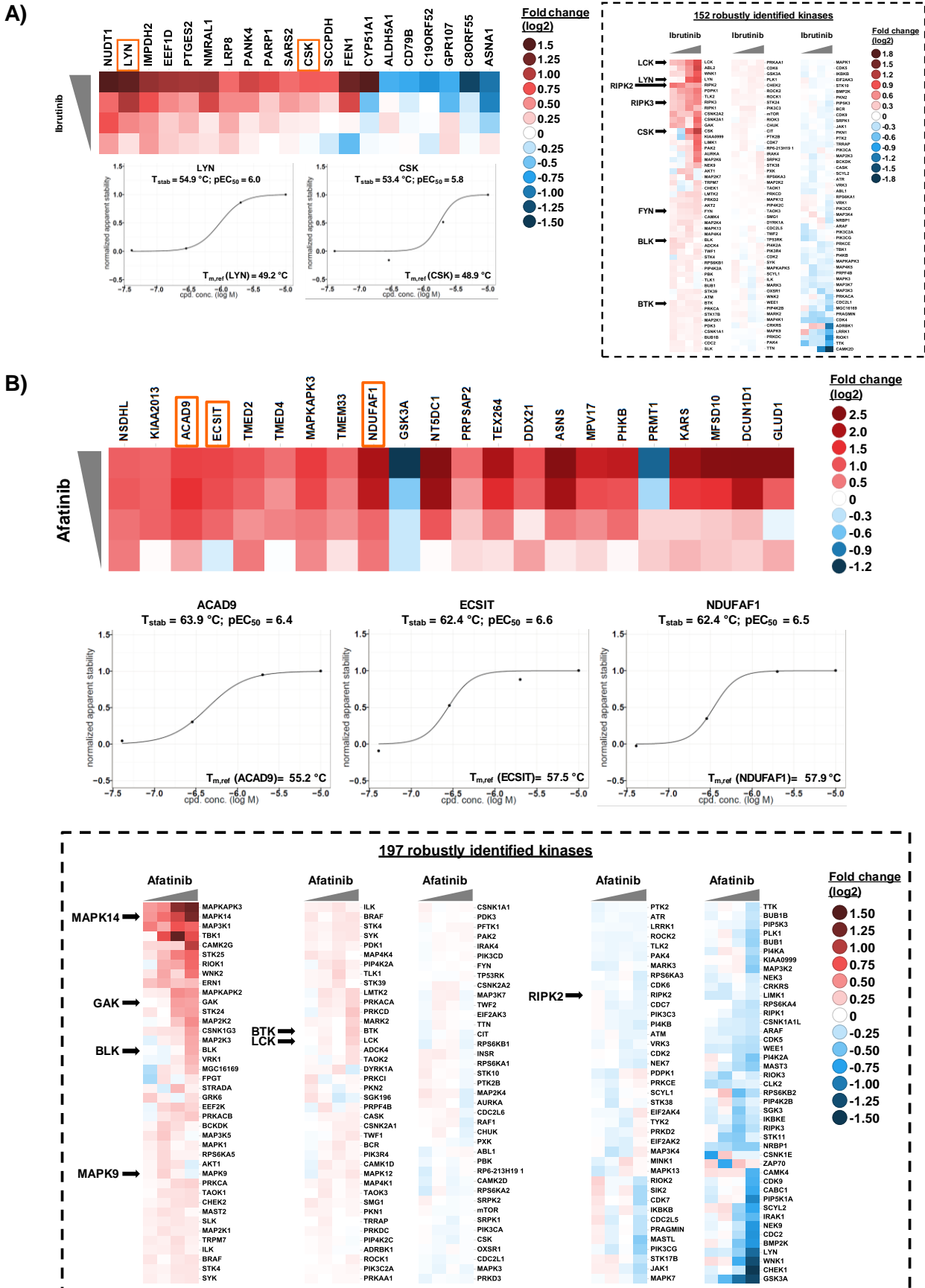


Figure 31: 2D-TPP analysis of Ibrutinib and Afatinib in Ramos cells. For all proteins, robust targets are shown for which a thermal effect was observed in at least two adjacent temperatures. Increasing and decreasing fold change values indicate stabilization and destabilization of a protein, respectively. Grey triangles indicate increasing concentrations of the compounds. For the kinases, a manual QC was done identifying the dose-response curves most reasonable over all temperatures; this includes effects only seen for one instead of two adjacent temperatures.

For discriminating effects truly resulting from protein binding and apparent stabilization rather representing regulation effects, a lysate-based 2D-TPP analysis was performed. The achieved data was analyzed specifically for all proteins for which in the cell-based assay a thermal effect was observed in at least two adjacent temperatures and for the most strongly affected kinases. With exception of the Afatinib target MAP3K1 and STK25 as well as MAP2K5, both suggested as engaged by Ibrutinib, all proteins indicated as targets in the cell-based 2D-TPP analysis (Figure 31) were identified robustly in the lysate-based assay. For eleven proteins and 14 proteins thermal effects were determined after lysate incubation with Ibrutinib and Afatinib, respectively. After incubation with Ibrutinib, predominantly kinases were identified as being also affected in lysate (Figure 32A). Binding to RIPK2, ABL2, CSK, LYN, LCK, RIPK3, and LIMK1 as indicated by the 2D-TPP analyses was confirmed in the course of this work also by other target engagement approaches. The thermal effects on the non-kinases NUDT1 and CYP51A1 as well as the kinases ADRBK1 and CAMK2D were only observed in the thermal proteome profiling experiments. The determination of affected thermal stability in cells as well as in lysate indicates true binding by the compound.

Upon Afatinib treatment, the thermal stability of the non-kinases NDUFAF1, ECSIT, ACAD9, MFSD10, TEX264, NT5DC1, MPV17, DCUN1D1, and ASNS as well as the kinases GAK, MAPK14, CABK1, PHKB, and MAPKAPK3 was determined to be affected in the cell-based 2D-TPP analysis. For those, thermal (de-)stabilization as determined in the lysate-based thermal profiling experiment confirmed true binding by Afatinib rather than regulatory effects (Figure 32B). Especially, the true binding of NDUFAF1, ECSIT, and ACAD9 substantiate the hypothesis that Afatinib might impair the assembly of mitochondrial complex I.

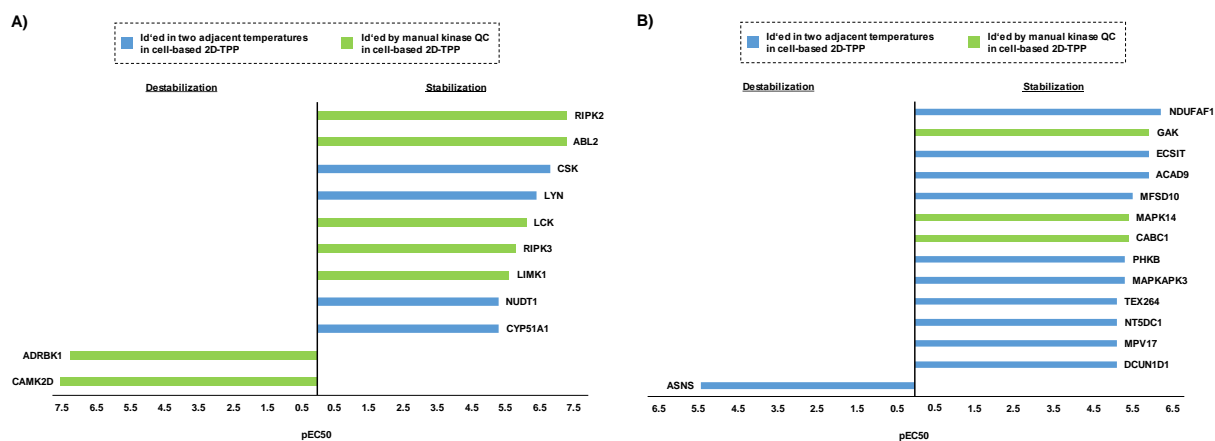


Figure 32: Crude Ramos lysate-based 2D-TPP analysis upon incubation with Ibrutinib and Afatinib. For Ibrutinib, eleven robustly identified proteins were thermally affected (A) including four proteins for which a thermal effect was seen in two adjacent temperatures (blue) and seven kinases for which a significant effect was only seen in one temperature (green) in the cell-based thermal proteome profiling experiment. For Afatinib, 14 robustly identified proteins were thermally affected (B) including eleven proteins for which a thermal effect was seen in two adjacent temperatures (blue) and three kinases for which a significant effect was only seen in one temperature (green) in the cell-based thermal proteome profiling experiment.

After applying the covalent kinase inhibitors Afatinib and Ibrutinib to the kinobeads pulldown experiment, the orthogonal affinity enrichment approach with the clickable analogues of the TCIs, as well as to a PROTAC profiling and a cell-based 2D-TPP approach, the proteins suggested as targets of the compounds in Ramos cells were compared across the chemoproteomic assay platforms (Figure 33). Among the investigated kinases, CSK and LYN were indicated as targets of Ibrutinib in all assays.

The most prominent intersection of two approaches is given for Ibrutinib comparing the affinity enrichment approaches. Generally, a reasonable intersection was also observed for the affinity enrichment approaches and the thermal shift assay with eight and three common targets for Ibrutinib and Afatinib, respectively. Notable: the covalent targets BTK, BLK, TEC, and ZAK were exclusively identified as targets in the pulldown experiments. This suggests that the covalent mechanism and accompanying high target potency might be underrepresented by the PROTAC and the thermal protein stability approaches. Further, the 2D-TPP approach suggests a relatively large number of proteins, kinases as well as non-kinases, as (off-)targets of the compounds.

For comparing non-kinase targets, the kinobeads experiment was not considered. Across the other three approaches, ASNS was the only non-kinase identified as off-target of Afatinib in the intracellular competition binding assay and the 2D-TPP analysis. Thus, cross-validation by a complementary approach is not possible for the majority of the identified non-kinase off-targets. This complicates the interpretation of the suggested binders for their reasonability and especially for their potential to induce phenotypic perturbations.

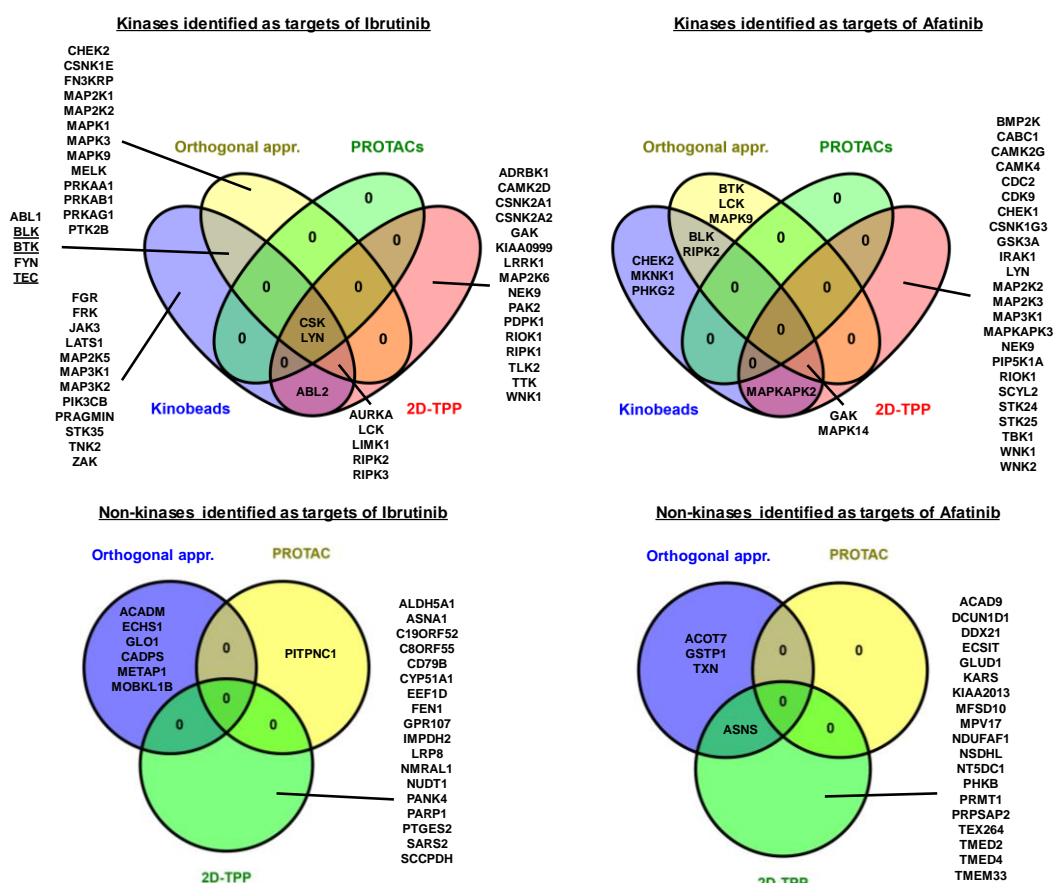


Figure 33: Comparison of targets identified for Ibrutinib and Afatinib with different chemoproteomic approaches. A robustly identified protein in a specific assay was defined as target as follows: Kinobeads approach \rightarrow $pI_{C_{50}} \geq 0.5$ over top concentration; cell-based orthogonal approach \rightarrow reasonable binding curve determined for proteins enriched ≥ 2 -fold with a p value ≤ 0.05 ; PROTACs \rightarrow significantly regulated (33 % difference in abundance with a p value ≤ 0.05); 2D-TPP \rightarrow for non-kinases: thermal effect observed in at least two adjacent temperatures, for kinases: fold change < 0.7 or > 1.3 in any condition and a reasonable binding curve. The underlined labels represent the known covalent targets of the compound.

Summing up, 72 proteins and 57 proteins were identified as bound by Ibrutinib and Afatinib, respectively, in any assay. The common targets of Ibrutinib and Afatinib which can be excluded as being responsible for exclusive apoptosis induction by Afatinib are the kinases BLK, BTK, CHEK2,

GAK, LYN, MAP2K2, MAP3K1, NEK9, RIOK1, RIPK2, and WNK1. Although the applied chemoproteomic approaches did not reveal the apoptosis inducing off-target of Afatinib in Ramos cells which triggered the comparison of the different techniques, this chapter demonstrated a possible route for off-target identification after identifying unwanted side-effects in cell-based assays. The comparison of the selectivity of the compounds determined with the different assays in Ramos cells shows that, as of today, there is no universal chemoproteomic approach for (off-)target identification.

The need for cell-based target engagement assays was highlighted by the observation of Afatinib's toxic effect on peripheral blood cell lines which would not have been detected in lysate-based assays. Therefore, the establishment of a new intracellular competition binding assay combining covalent probes and the kinobeads technology will be topic of the next chapter.

3.2. Application of differential kinobeads selectivity profiling: characterization of covalent tool compounds enabling the analysis of intracellular target engagement of reversible inhibitors

3.2.1. Proof of concept of intracellular competition binding with reversible inhibitors

3.2.1.1. BTK TCIs in dose-response competing for the binding of TCO-Ibrutinib to BTK

The previous chapter demonstrated that non-cellular target engagement measurements can significantly differ from cell-based outcomes. An early application of cellular target engagement assays, therefore, is essential for the identification of non-promising molecules. Due to the equilibrium binding mode-of-action of non-covalent inhibitors, however, tool compounds have to be introduced fixing the intracellular target engagement situation prior to lysing the cells for analyses. Covalently binding probes represent valuable tools for this purpose. Such probes could be used in competition binding experiments directly performed in living cells where binding of a protein (class) to a covalent probe is competed by a (non-)covalent inhibitor under investigation. To analyze how well intracellular competition-binding correlates with other cellular assays regarding the measured compound potency, in a first step, a linkable analogue of Ibrutinib was functionalized with a bioorthogonal clickable TCO-moiety. This compound was used to bind endogenous BTK not engaged after pre-incubation of intact Ramos cells with different concentrations of the covalent BTK inhibitors Ibrutinib, CC-292, and QL47. After cell lysis, a click reaction was performed coupling a fluorescent tetrazine conjugate to the TCO-moiety provided by the Ibrutinib analogue. Proteins were separated by gel electrophoresis which, in parallel, removed excess of the fluorescent dye. Scanning the gel for fluorescence allowed for the identification of dose-dependently competed binding of the TCO-Ibrutinib to BTK. From this fluorescence staining it was possible to derive pIC_{50} values correlating with the values achieved for the different BTK TCIs in other cellular assays performed at similar conditions (Figure 34).

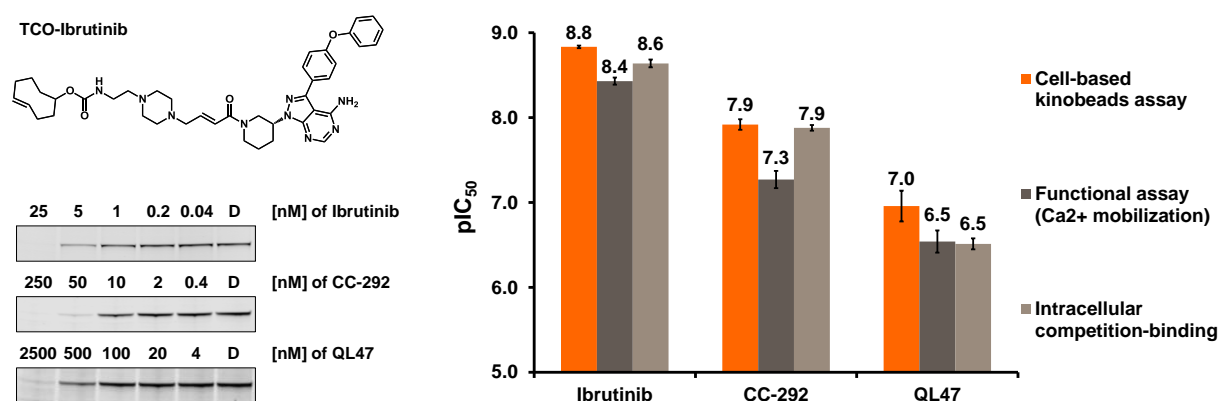


Figure 34: Intracellular competition binding assay using TCO-Ibrutinib as enrichment probe compared to alternative cell-based assays reporting BTK engagement. The intracellular competition-binding assay achieves very similar pIC_{50} values as a cell-based kinobeads and a functional assay. TCO-Ibrutinib was used at 0.1 μ M. The bands from a representative fluorescence scan show dose-response dependent intensities at a molecular weight of \sim 75 kDa which corresponds to the size of BTK. The column chart shows averages and standard errors of the mean of ≥ 2 replicates.

3.2.1.2. Reversible BTK inhibitors competing for the binding of TCO-Ibrutinib to BTK

In a next step, the concept of intracellular competition binding was transferred to non-covalent compounds competing for BTK binding to the TCO-Ibrutinib probe. For this, CGI-1746, a published non-covalent inhibitor of BTK,⁶⁶ and the saturated analogue of Ibrutinib were used at different concentrations for a Ramos cell treatment. After incubating the cells with the non-covalent inhibitors, the covalently binding TCO-Ibrutinib probe was added to the cells for 30 min to bind BTK not engaged by the non-covalent inhibitors. After washing the cells, cell extracts were generated in which the click chemistry reaction between the TCO-Ibrutinib probe and a tetrazine-Cy5 conjugate was done. Proteins were separated by gel electrophoresis and the gels were scanned for fluorescence. A band with a molecular weight of BTK (~ 76 kDa) was identified showing dose-dependent fluorescence intensity from which dose-response curves were generated (Figure 35). The pIC_{50} value achieved for the saturated Ibrutinib analogue ($pIC_{50} \sim 6.9$) correlates very well with the value determined in a lysate-based kinobeads pulldown experiment ($pIC_{50} \sim 7.1$). This indicates that treatment conditions with the covalent TCO-Ibrutinib probe have been chosen reasonably. For CGI-1746 a slightly higher pIC_{50} was determined as for saturated Ibrutinib. This higher binding affinity is reasonable for an inhibitor specifically designed for binding BTK potentially compared to a saturated analogue of Ibrutinib not optimized for high affinity binding. At this point, it should be noted that these pIC_{50} values are depending on the incubation time with the TCO-Ibrutinib probe and the concentration used. By shifting the binding equilibrium, the covalently binding probe would alter the determined pIC_{50} values when modulating these parameters. Nevertheless, this assay allows for a ranking of non-covalent inhibitors' intracellular binding affinity and additionally provides information if, in a living cell, the desired target is engaged at all by a non-covalent inhibitor under investigation.

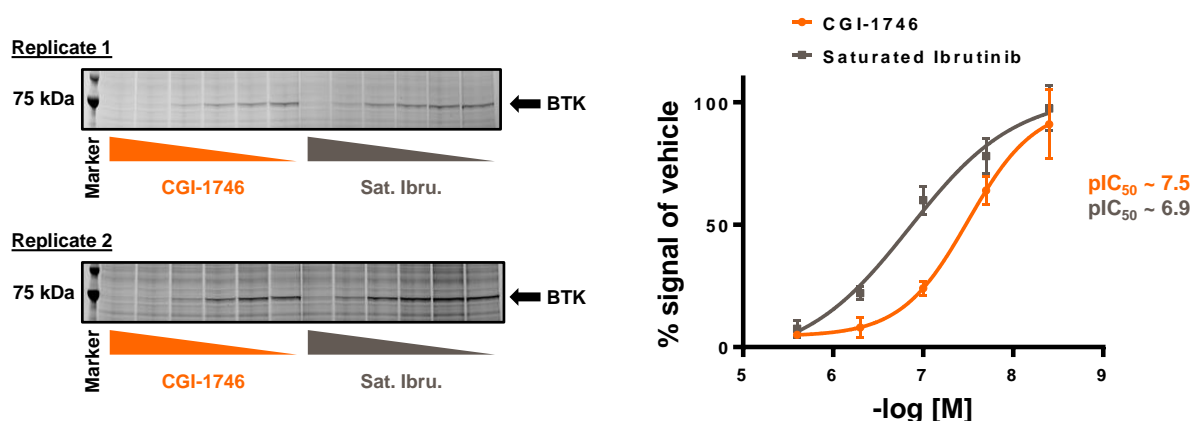


Figure 35: Intracellular competition binding using non-covalent BTK inhibitors CGI-1746 and saturated Ibrutinib competing the binding of TCO-Ibrutinib to BTK. The bands show dose-dependent fluorescence signals achieved after clicking a tetrazine-Cy5 conjugate to TCO-Ibrutinib. TCO-Ibrutinib was used at 0.01 μ M. The binding curves were derived from averages of two replicates using GraphPad Prism 7.03 software with a built-in 4 parameters curve fitting algorithm. The error bars represent the standard errors of the mean.

3.2.2. Evaluation of a generic strategy for synthesizing covalent probes from non-selective, reversible inhibitors

As this kind of intracellular competition binding approach requires covalent protein binders, a generic strategy to generate such probes based on non-selective inhibitors was assessed. In contrast to a target-based approach in which small molecules are stepwise modified to finally react selectively with a specific amino acid contained in a protein sequence, in this work a more generic approach was applied. Therefore, promiscuous inhibitors with a large spectrum of targets were equipped with amino acid reactive functionalities. By this approach amino acids located outside the binding pocket of the small molecule might be accessible via different linker lengths (Figure 36). This target-independent strategy may indicate potentially approachable targets and could result in either the starting point for rationally designed targeted covalent inhibitors for a specific protein or yield compounds specifically binding a wide range of targets covalently and, by this, representing suitable tools to investigate inhibitors for these targets.

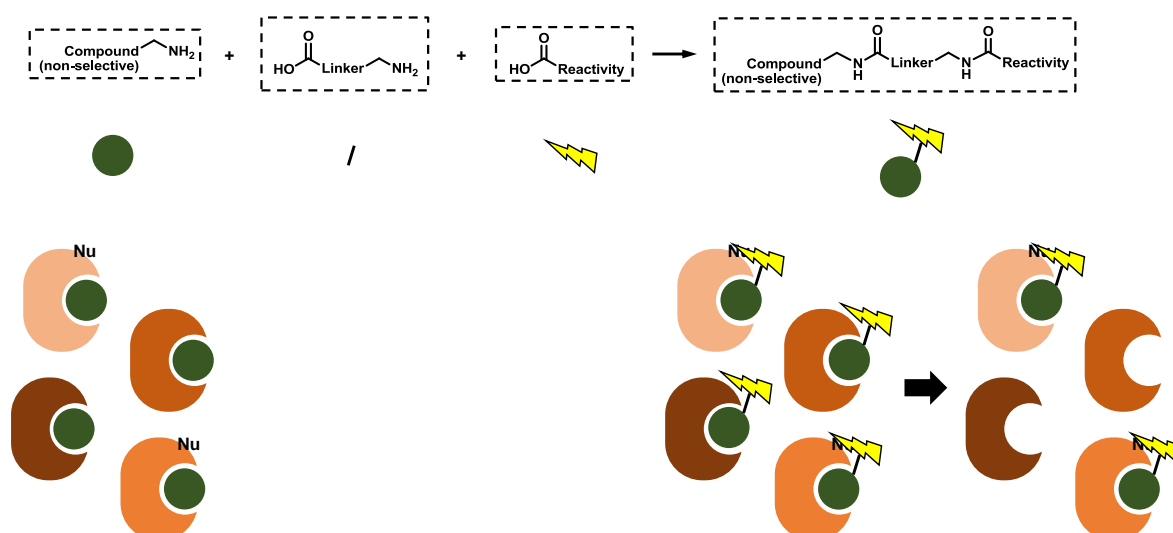


Figure 36: General approach to get covalent probes from promiscuous protein inhibitors. A promiscuous inhibitor (green) binding to different proteins (shades of brown) is coupled with a reactive moiety (yellow flash) via a linker (black line). Nucleophilic amino acid side chains (Nu) outside the binding pocket of the inhibitor might be covalently bound by the reactive moiety.

3.2.2.1. Synthesis of different reactive probes and evaluation of covalent binding using differential kinobeads selectivity profiling

Since differential kinobeads selectivity profiling represents a valuable technique to identify covalent binders, this strategy was initially used for evaluating covalent probes synthesized from promiscuous, reversible kinase inhibitors. The inhibitor chosen to be modified with reactive moieties is part of the kinobeads affinity matrix as used in this work and binds to a large spectrum of kinases, i.e. kinase selectivity profiling identified 184 kinases bound with $pIC_{50} > 5.0$ (Figure 37).

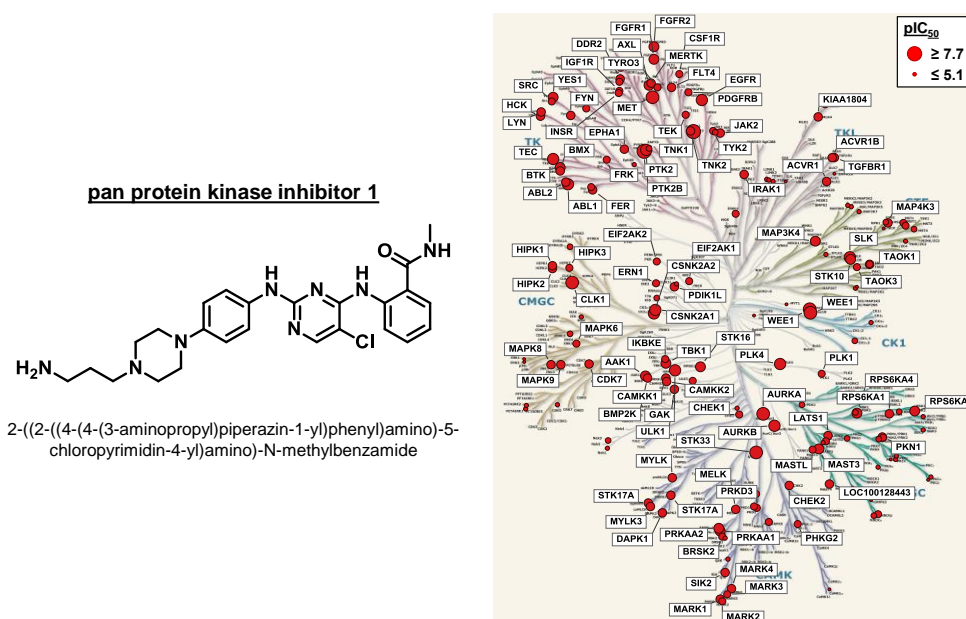


Figure 37: Amine-incorporating promiscuous protein kinase inhibitor 1. The red dots in the kinase tree indicate all kinases which were identified as targets of the compound in kinobeads selectivity profiling experiments done at Cellzome / GlaxoSmithKline. The different sizes of the dots correlate with the potency of the compound determined for the respective kinase.

From this amine-incorporating compound, analogues were synthesized following two synthesis routes (Figure 38). Either the reactive moiety was directly coupled to the compound [1] or the reactive moiety was attached via a PEG2 linker (3-[2-(2-Aminoethoxy)ethoxy]propanoic acid) [2]. Analogues incorporating five different reactive moieties were synthesized to compare potential covalent binding to a subset of kinases bound by the broad-spectrum protein kinase inhibitor: an acrylamide (A), two sulfonyl fluorides attached to aromatic rings in meta (B), and para (C) position, a linear sulfonyl fluoride, and a chloride (E). Additional compounds incorporating iodine, bromine, and vinyl sulfone functionalities were synthesized but turned out to be not stable so that an assessment of those for their potential to bind proteins covalently was not possible. To get a linear sulfonyl fluoride as a reactive functionality 3-mercaptopropanoic acid was pre-coupled with ethenesulfonyl fluoride in a Michael addition [3]. With the intention to compare sterical influences of the aromatic ring versus a linear sulfonyl fluoride this was necessary due to commercial unavailability of such a linear building block.

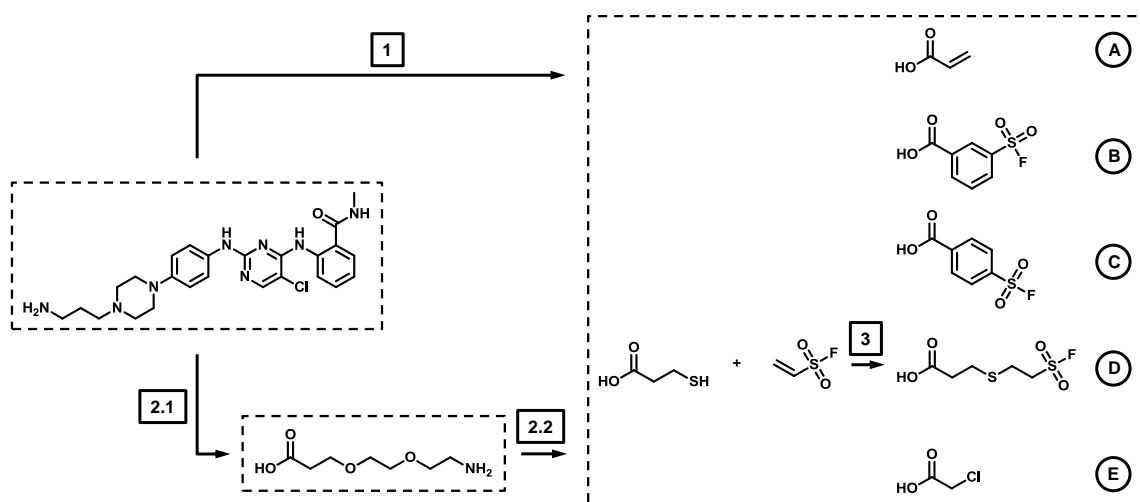


Figure 38: Reaction scheme for the synthesis of covalent probes from promiscuous protein inhibitors.

The coupling of the respective individual building blocks was done by forming an amide bond between a free amine and a carboxylic acid. For this reaction, an active ester was formed from the carboxylic acid using the coupling reagent 1-[Bis(dimethylamino)methylene]-1H-1,2,3-triazolo[4,5-b]pyridinium 3-oxide hexafluorophosphate (HATU). Using N-Ethyl-N-(propan-2-yl)propan-2-amine (DIPEA) as a base enabled the acetylation of the amine-incorporating compound by the activated ester to form the respective product. This reaction afforded ten reactive compound analogues of which yields and purities were sufficiently good for assessing the compounds in differential kinobeads selectivity profiling (Figure 39).

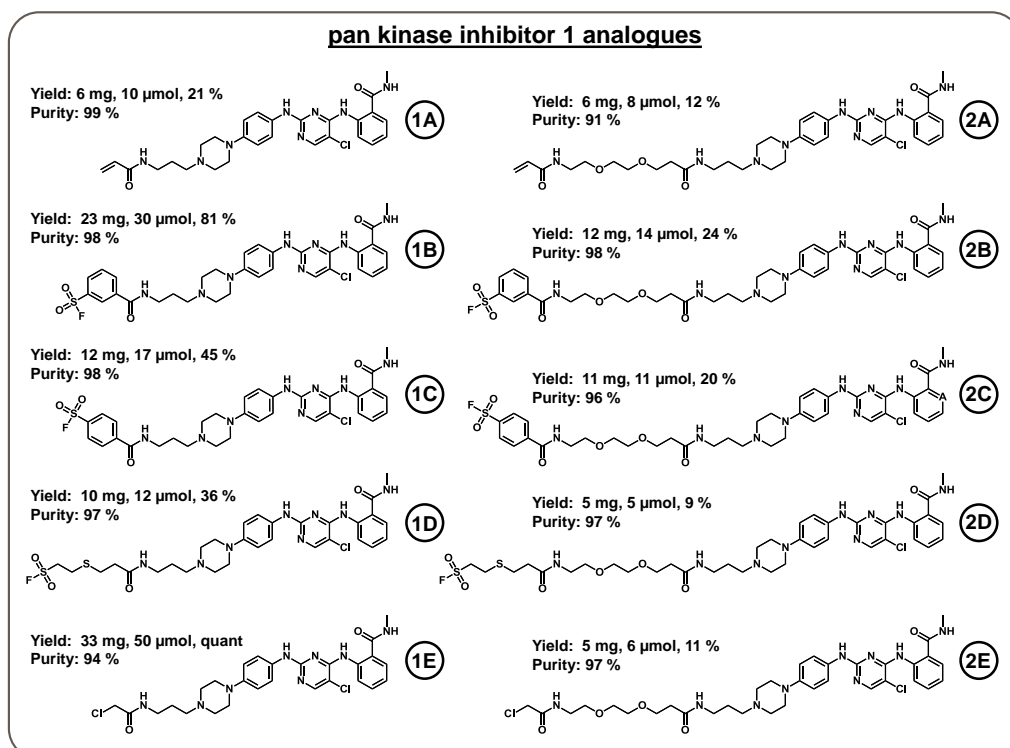


Figure 39: Covalent probes synthesized from linkable analogues of pan protein kinase inhibitor 1.

With the usually applied 8-points dose-response, ten compounds would rapidly exhaust capacity for assessing their potential for covalent target binding:

10 compounds * (7 compound concentrations + vehicle control) * 2 replicates mean 160 cell samples and 20 TMT8 mass spectrometry analyses each 120 min resulting in 40 h instrument time. For the comparison to lysate-based assays this number is doubled so that it becomes clear that a reduction of samples was desirable. Therefore, the number of compound concentrations used for generating binding curves was reduced to three compound concentrations. Thereby, the sample number was reduced from 320 samples to 136 samples for all probes in duplicate resulting in a third of the mass spectrometry instrument time (Figure 40).

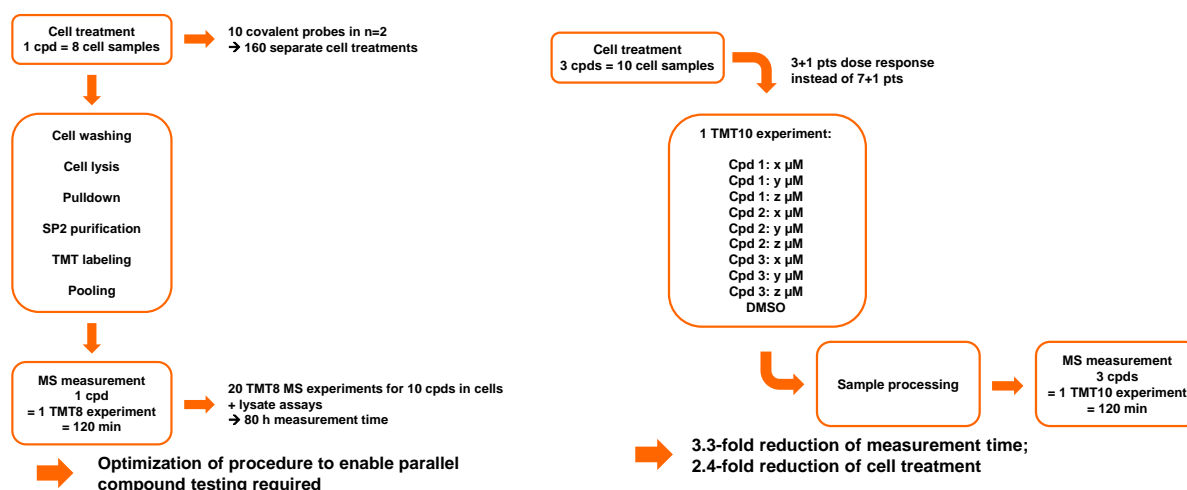


Figure 40: Reduction in sample number for the assessment of covalent kinase probes by mass spectrometry. The left scheme represents the usually applied experiment for generating 8-points dose-response curves for evaluating covalent binding by differential kinobeads selectivity profiling. The right scheme demonstrates how the sample number was decreased to allow for the evaluation of the ten covalent probes synthesized above.

Fold-change values were achieved for three concentrations for each probe. To generate binding curves, it was assumed that for 1 fM compound competition would basically be 0% and 1 M compound would compete for binding to the kinobeads essentially by 100%. With these assumptions, five points were used for the calculation of binding curves using GraphPad Prism software with a built-in four-parameter nonlinear regression curve fitting module. From these binding curves pIC_{50} values were estimated. Since the reduction of data points results in less accurate binding curves and derived pIC_{50} values might differ from full 8-point dose-response curve values, for probes 1A and 2A a direct comparison of the pIC_{50} values was done in a cell-based and in a lysate-based kinobeads assay (Figure 41). The better correlation of the data was achieved for the cell-based pIC_{50} values with R^2 values of 0.94 and 0.92 for probe 1A and 2A, respectively. For the lysate-derived values correlation yielded $R^2_{1A} = 0.83$ and $R^2_{2A} = 0.84$. This indicates differences when estimating pIC_{50} values using the 3-points model or when deriving pIC_{50} values from full dose-response curves. In consequence, a potential covalent binder identified by estimated pIC_{50} values should be confirmed by full dose-response experiments. Nonetheless, for a first estimation of covalent binding and for excluding unpromising probes from further investigations, the experiments with reduced sample number might be preferred over labor-intensive and time-consuming full dose-response curves. Moreover, differences in potency measured in cells and in lysate were expected to be in the range of 0.8 to 1 log units so that imprecision around 0.2 – 0.3 log units is acceptable.

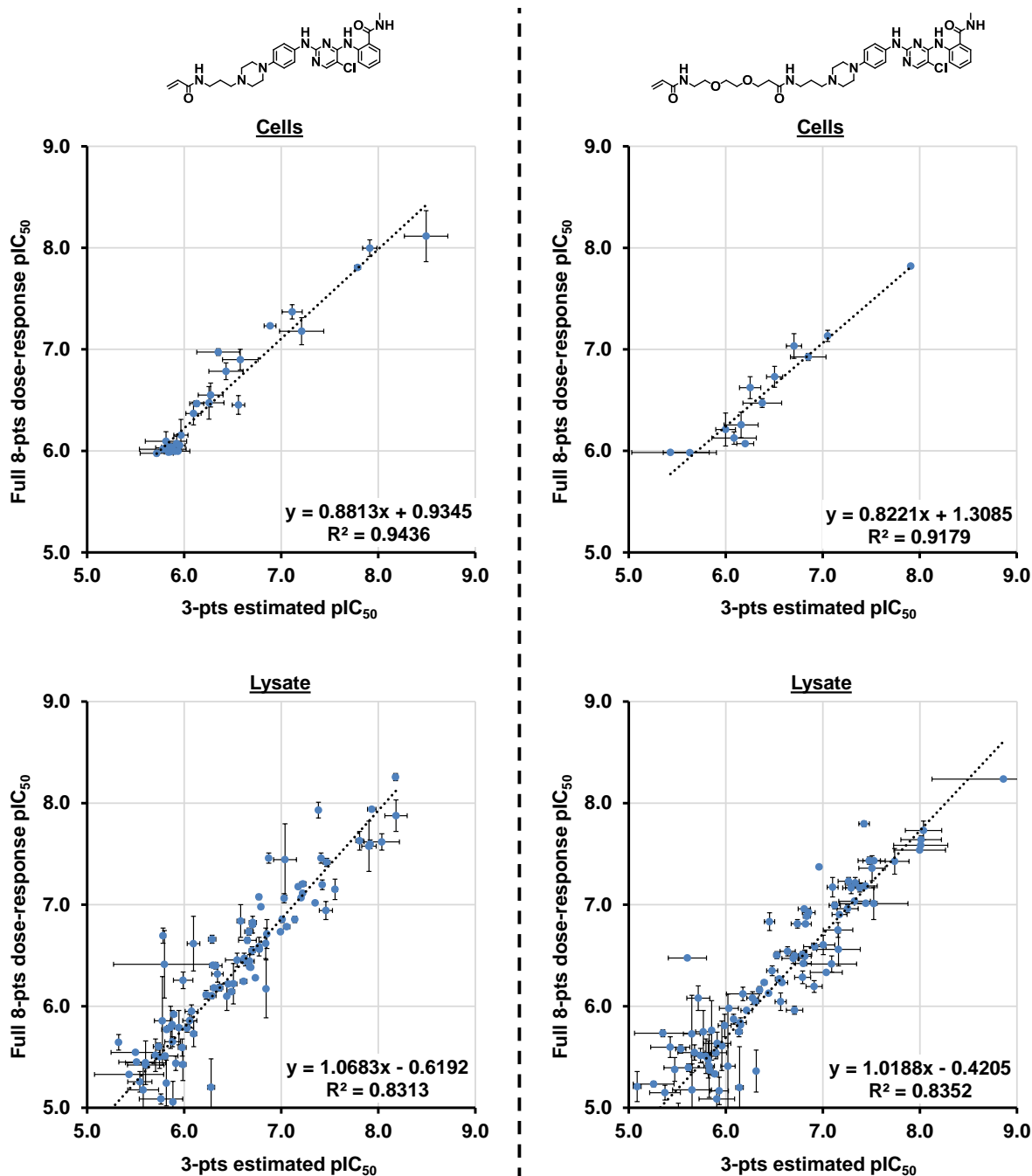


Figure 41: Comparison of pIC_{50} values determined for probe 1A and probe 2A by estimating from 3 points dose-response approximation vs full 8 points dose-response curves.

For all covalent probes, estimated pIC_{50} values were determined in cells and in lysate and compared to each other for identifying potential covalent binders by differential kinobeads selectivity profiling. For the majority of identified kinases covalent binding was not indicated by a significantly higher pIC_{50} value in cells than in lysate compared with the totality of identified kinases. For the probes 1A and 2A some kinases separated from the majority of kinases in the differential kinobeads selectivity profiling assay. With probe 1A, binding of IRAK1, MAPK8, MAPK9, PTK2, and TEC to the beads was competed with high cellular pIC_{50} values with the strongest competition determined for MAPK9 in the low nanomolar range (Figure 42A). For probe 2A, only TEC was identified with higher cellular potency in the cell-based than the lysate-based kinobeads assay ($pIC_{50,cell} = 7.9 \pm 0.0$ vs $pIC_{50,lys} = 7.7 \pm 0.1$) (Figure 43A).

For the probes 1B and 1C incorporating aromatic rings with sulfonyl fluorides substituted in meta and para position, MAP3K4 and TBK1 were identified with cellular potency separating them from the cloud of totally identified kinases (Figure 42B and Figure 42C). The separation from the majority of kinases is more obvious for the compound incorporating the sulfonyl fluoride in para position. This might indicate that the reactive moiety of this analogue is better positioned towards a suitable amino acid side chain. To rationalize MAP3K4 and TBK1 as covalent binders, crystal structure analyses were performed. Since sulfonyl fluorides are described to preferentially react with lysines,²¹⁰ the analysis was limited to this amino acid. The 3D model of TBK1 (PDB ID: 4IW0) suggested two lysines potentially approachable by the reactive moiety of the probes: Lys38 and Lys137. Since a crystal structure of MAP3K4 is not available, a sequence alignment was performed trying to match lysines in the sequence of MAP3K4 to lysines around the ATP-binding site of TBK1. For Lys137 a homologous lysine was identified in the MAP3K4 sequence (Lys1465). Further potential reactive lysines in MAP3K4 were identified by using a MAP2K7 crystal structure (PDB ID: 3WZU) and aligning suitable lysines to the sequence of MAP3K4. By this, Lys1372, Lys1382, and Lys1385 were identified in MAP3K4 to be aligned in close sequence proximity to Lys152 representing a potential reaction site for the compound in MAP2K7. Analogously, it was possible to match Lys261 in MAP2K7 to Lys1478 in MAP3K4. It has to be noted, that this kind of rationalization of MAP3K4 and TBK1 as covalent binders is highly speculative and would need further validation by suitable approaches. For the PEG2-linked analogues 2B and 2C incorporating the same reactive moieties the targets were not identified with cellular potency (Figure 43B and Figure 43C). This position-dependent effect might indicate true covalent binding by probes 1B and 1C.

For the compound with the thiol-linked sulfonyl fluoride (probe 1D), differential kinobeads selectivity profiling identified kinases as preferentially reversible binders of the compounds (Figure 42D) and a very similar observation was made for the PEG2-linked compound 2D (Figure 43D). This triggered to analyze the stability of the compounds in an aqueous environment. A HPLC quality control comparing the individual compounds in DMSO and PBS at room temperature and 37 °C confirmed that in aqueous solution the compounds hydrolyze to yield the non-reactive sulfonyl hydroxide analogues of the compound. This hydrolyzation was not observed for the sulfonyl fluorides substituting an aromatic ring. This instability finding for the linear sulfonyl suggests the inapplicability of such probes for covalent protein binding.

For the chloride probes 1E and 2E it is hard to identify potential covalent binders separating from the majority of kinases. Common kinase targets identified to be potential covalent binders of probe 1E (without linker) and probe 2E (PEG2 linker) were TEC, PTK2, WEE1, and SIK2 (Figure 42E and Figure 43E). IRAK1 is suggested as covalent binder of only probe 1E and CDK7 as well as BLK as irreversibly bound by only probe 2E. CDK7, BLK, TEC, PTK2, and WEE1 are known to contain reactive cysteines.^{10, 17} For IRAK1, and SIK2 no information about reactive cysteines is available. However, the high reactivity of the chlorine might allow for reacting with less nucleophilic moieties than cysteines so that covalent binding could occur without the availability of suitable cysteines. Since for the chlorine-incorporating compounds, as for probe 1B incorporating the sulfonyl fluoride in meta position on the aromatic ring, a equipotency or even higher cellular potency as in lysate was determined for many kinases, these compounds might represent very reactive broad-spectrum

covalent kinase inhibitors binding at many nucleophilic attack points in cells as well as in lysate in a non-specific way. Their suitability for performing intracellular competition binding experiments with reversible kinase inhibitors of different targets has, yet, to be proven and would have exceeded the scope of this work.

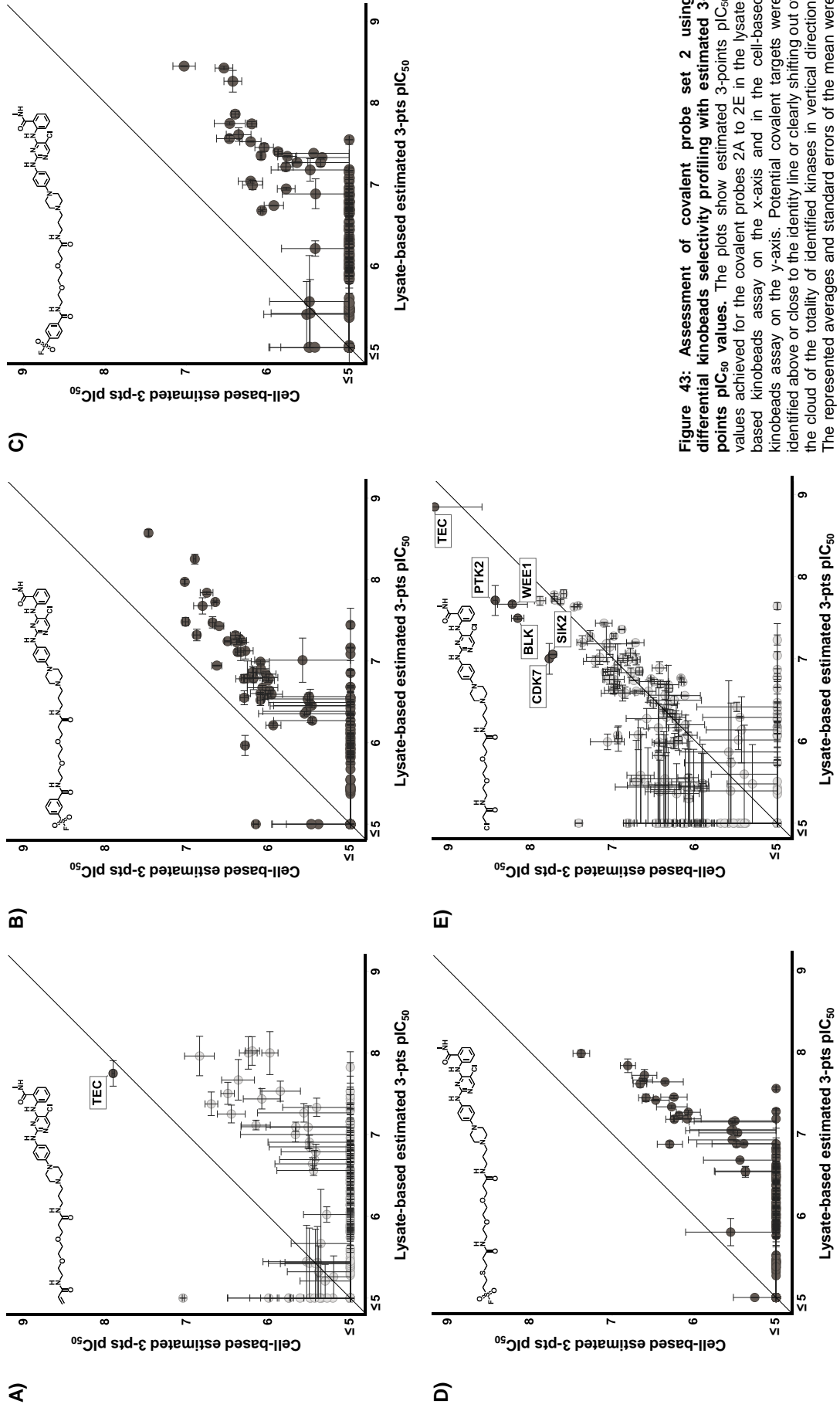


Figure 43: Assessment of covalent probe set 2 using differential kinobeads selectivity profiling with estimated 3-points pIC_{50} values. The plots show estimated 3-points pIC_{50} values achieved for the covalent probes 2A to 2E in the lysate-based kinobeads assay on the x-axis and in the cell-based kinobeads assay on the y-axis. Potential covalent targets were identified above or close to the identity line or clearly shifting out of the cloud of the totality of identified kinases in vertical direction. The represented averages and standard errors of the mean were calculated from two replicates.

3.2.2.2. Validation of covalent targets as identified by differential kinobeads selectivity profiling

For validating the potential covalent targets of probes 1A and 2A, a non-reactive analogue of these probes was synthesized incorporating a propionamide instead of an acrylamide which then was also subjected to a full dose-response cell-based kinobeads assay (Figure 44). Comparing kinase binding of the reactive compound with the non-reactive control shows that for kinases suggested as covalent binders, in fact, pIC_{50} values significantly above the compound concentration limit were only determined for the covalent probe while the non-reactive control dissociates completely from those targets.

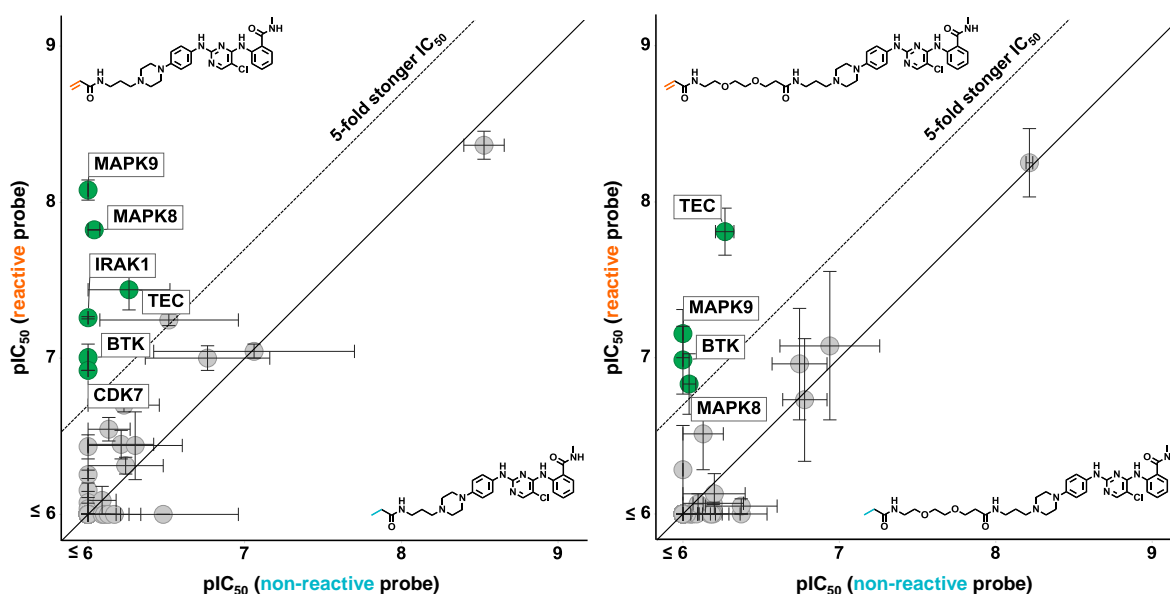


Figure 44: Comparison of the reactive probes 1A and 2A to non-reactive analogues of both in a cell-based kinobeads assay. Significantly higher cellular target engagement was determined for some kinases using the reactive compound compared to the non-reactive control. Complete dissociation of the non-reactive compounds but not of the reactive probes confirms MAPK9 and TEC as covalent targets of probes 1A and 2A.

With this experiment, MAPK9 and TEC were confirmed as covalent binders as indicated by differential kinobeads selectivity profiling. At this point, it should be noted that comparing a reactive compound and a non-reactive control might give clearer results than comparing a reactive compound in cells and in lysate to identify covalent binders. However, for the former approach two compounds have to be synthesized and for each a set of cells has to be treated. In contrast, differential kinobeads selectivity profiling offers the advantages of analyzing a single compound and performing one cell experiment for the comparison to a less labor-intensive lysate-based experiment.

To finally validate both kinases as covalent targets of the probes and to identify the site of reaction, recombinant MAPK9 and recombinant TEC was incubated with probe 1A and probe 2A, respectively. Subsequently, the proteins were digested with suitable enzymes and mass spectrometry searching for amino acids modified by the molecular weight of the compounds was applied. For MAPK9, a unique peptide with a mass modification corresponding to a reaction of cysteine with probe 1A was identified (Figure 45). The modification of Cys116 is in agreement with previously published data¹⁶ and confirms the plausibility of the data presented in this work. For TEC, no modification was detected. Several protocols including different digestion enzymes to optimize the sequence coverage were applied.

Despite of the good coverage of about 70 % including the most reasonable binding site **MERGCL**, no modification was identified. Same is true for incubating recombinant TEC with another probe suggested as covalent binder below. This suggests that either TEC is no covalent binder of the probes and falsely indicated as such by the pulldown approaches or that the formation of a covalent bond did not occur with the recombinant protein at the used conditions. Bad 'flyability' of the covalently modified peptide could also be contemplable.

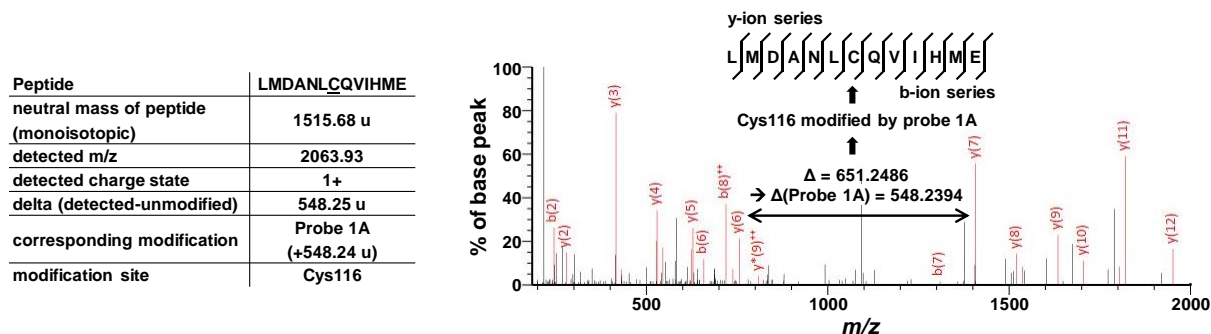


Figure 45: MS/MS spectrum indicating a covalent reaction of probe 1A with Cys116 in MAPK9.

The covalent analogue of the amine-incorporating kinase inhibitor showed also increased selectivity and potency when comparing both molecules directly in a lysate-based kinobeads assay. Incubating lysate with both molecules for 5 h at 4 °C resulted in improved potency for MAPK8 and MAPK9 identified as covalent targets previously. For BUB1 also a higher potency was determined. For a number of kinases, (weak) binding was determined for the parent compound but no binding was determined for the covalent probe. This might suggest an increase in selectivity for those targets. Apart of those, it seems that the determined pIC_{50} values for the majority of kinases are slightly higher for the parent compound than for the covalent probe. This suggests that coupling the acrylamide to the parent compound might slightly decrease binding to these kinases. Thus, coupling the acrylamide seems to serve the purpose of increasing potency and selectivity for a distinct number of kinases.

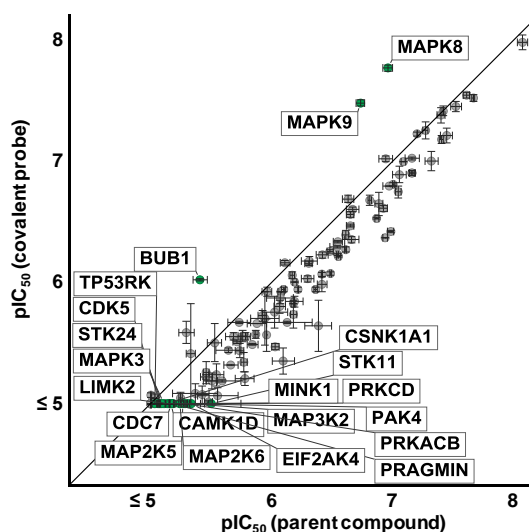


Figure 46: Direct comparison of selectivity and potency of the covalent probe 1A and its parent compound in a lysate-based kinobeads assay. Higher potency of the reactive probe can be observed for MAPK8, MAPK9, and BUB1 of which the former two are validated as covalent targets by other approaches. For a number of robustly identified kinases, potency was only determined for the parent compound which indicates an increase

in selectivity upon coupling the acrylamide to the compound. The dots in the plot represent average values from two replicates. Error bars represent the standard errors of the mean. To potentially achieve a covalent probe for further protein kinases and to assess if the strategy for yielding covalent protein probes from non-selective inhibitors can also be transferred to other protein classes, analogues from another protein kinase inhibitor, a promiscuous lipid kinase inhibitor, and a non-selective HDAC inhibitor were synthesized by coupling linkers and reactive moieties to the amine-incorporating compounds. Since acrylamide probes performed best for the first probe set other reactive moieties were not considered in the following (Figure 47).

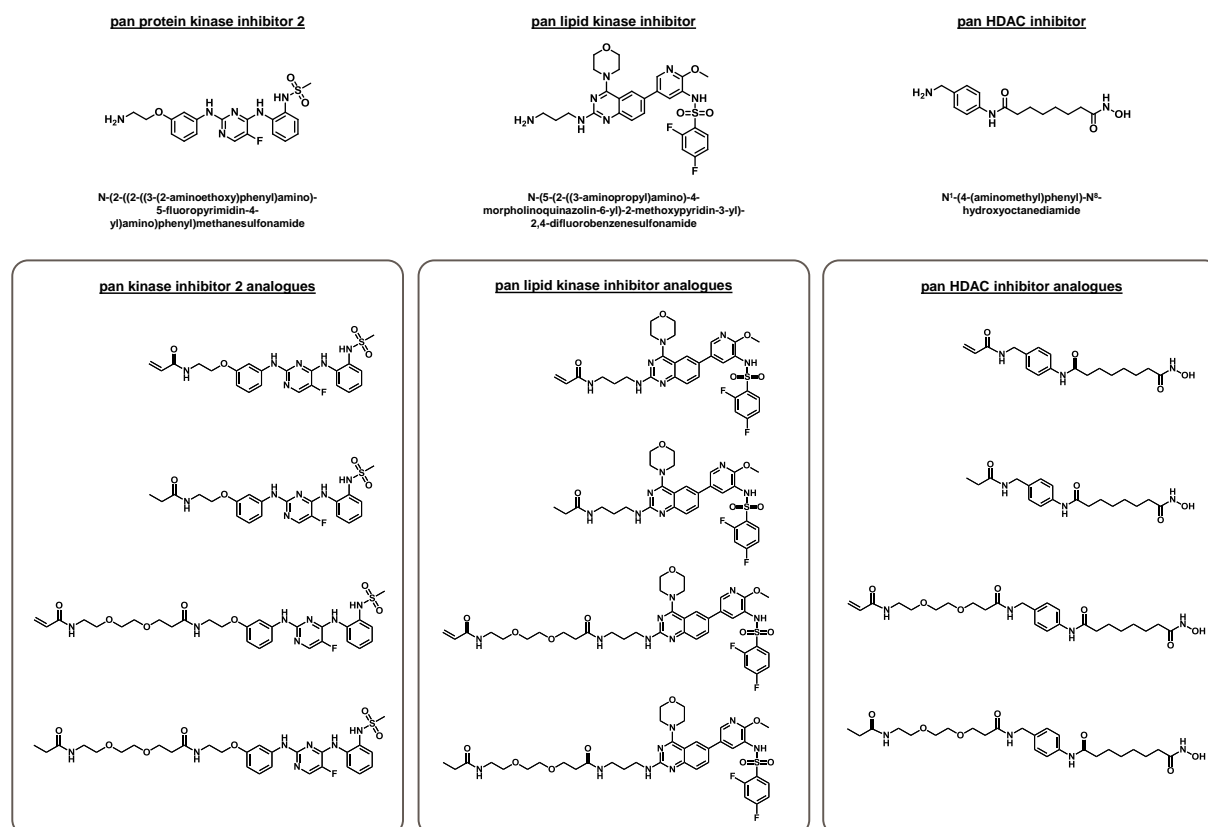


Figure 47: Covalent probes synthesized from amine-incorporating inhibitors of protein kinases, lipid kinases, and the non-selective HDAC inhibitor Vorinostat.

For the protein kinase inhibitor, TEC, BTK, and BLK were indicated as covalent binders of the reactive probe not incorporating a linker (Figure 48). This suggests that this probe binds the hinge 6 cysteine conserved across those kinases as done by the targeted covalent inhibitors described above. Remarkably, the probe achieved by the generic strategy of attaching reactive moieties to promiscuous kinase inhibitors shows similar selectivity regarding the covalent targets as the designed TCIs of BTK. Exclusive target binding in lysate was determined to be in a submicromolar range for 16 kinase targets. A confirmation of TEC as covalent target using recombinant protein was not successful as described above for the covalent probe 1A.

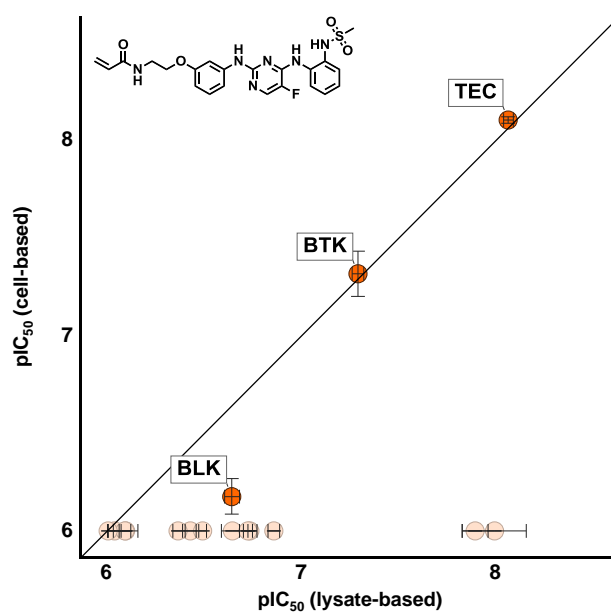


Figure 48: Differential kinobeads selectivity profiling of the covalent probe 3A. Across the Ramos cell kinome covered by kinobeads, compound 3A shows high selectivity in cells only binding to TEC, BTK, and BLK. While BLK potency drops almost to the base line in cells, BTK and TEC are equipotently engaged in cells and in Ramos cell extract. In lysate, 16 kinases are bound with pIC₅₀ values ≥ 6 . The dots represent averages of two replicates. The error bars represent the standard error of the mean.

Differential beads profiling using a lipid kinase- and a HDAC-enriching affinity matrix for the lipid kinase probes and the HDAC probes, respectively, as well as the comparison of the reactive compounds to a non-reactive control in cellular experiments did not indicate a covalent binder so that this approach was not further pursued.

3.2.3. Application of probe 1A for measuring intracellular target engagement of the reversible MAPK9 inhibitor Tanzisertib with a kinobeads-based approach

With the results achieved for the fluorescence-based intracellular target engagement assay for reversible inhibitors as shown above (Figure 35), in a last step, the concept of intracellular competition of covalent binding by a reversible inhibitor was transferred to a kinobeads-based readout. The rationale of this experiment was to bind kinases not engaged by a non-covalent molecule by a covalent probe of the same targets, followed by dissociation of reversibly bound compound and kinobeads enrichment of the released proteins (Figure 49). After treating the cells in dose-response with the non-covalent compound and processing of the samples, the strongest target kinase enrichment should occur for the highest concentration. The vehicle control should allow for covalent binding of the majority of target kinases of the covalent probe. Thus, after enrichment with kinobeads, subsequent elution and Western blot analysis, the strongest signal should be achieved for the highest concentration of reversible inhibitor used while the weakest signal should be determined for the vehicle control.

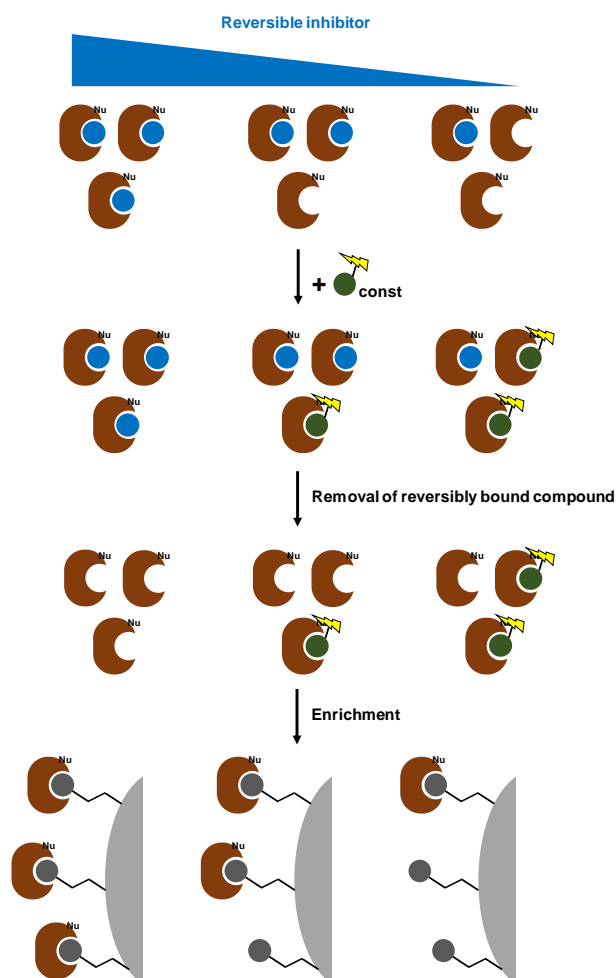


Figure 49: Concept of intracellular competition binding of non-covalent inhibitors based on kinobeads affinity enrichment. Proteins providing a suitable nucleophilic amino acid side chain (brown) for a covalent probe (green with yellow flash) are pre-incubated with a reversible inhibitor of the same target (blue) at different concentrations. After pre-incubation, a constant concentration of the covalent probe binding to the same target irreversibly is added to the cells to bind target proteins not engaged by the reversible inhibitor. After removal of non-covalently bound inhibitor, the disengaged proteins are enriched by kinobeads (grey) and subsequently analyzed after elution.

For proofing the concept of this kinobeads-based intracellular engagement assay for reversible inhibitors, the covalent MAPK9 probe 1A established from the promiscuous inhibitor above was applied to measure target engagement of the non-covalent MAPK9 inhibitor CC-930 / Tanzisertib (Figure 50).

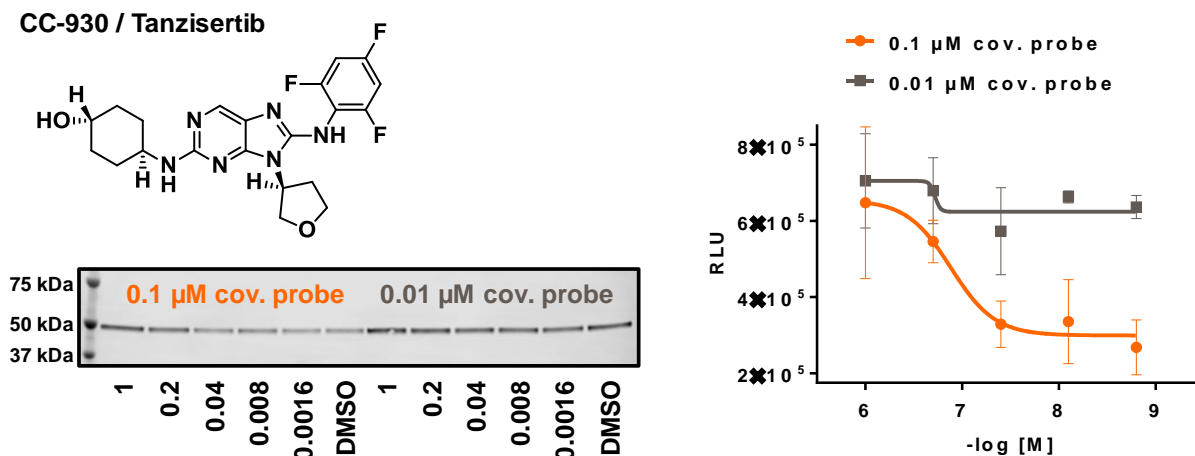


Figure 50: Kinobeads-based intracellular target engagement measurement of CC-930 / Tanzisertib using the covalent MAPK9 probe 1A established in this work. The representative Western blot stained for MAPK9 shows dose-dependent band signal intensities for a covalent probe concentration of 0.1 μM. For the lower probe concentration, very similar signals are determined across the concentration range of Tanzisertib. Quantifying the signal intensities allows for the determination of dose-response curves of the reversible MAPK9 inhibitor based on averages from two replicates. Error bars represent the standard error of the mean.

For the higher probe concentration, a dose dependent signal was determined from which a binding curve was derived. This indicates the potential of the concept to measure dose-response curves of reversibly binding inhibitors with the use of a covalent probe. For the lower probe concentration, no dose-response curve was generated. This is reasonable, suggesting that the binding of CC-930 (published $IC_{50} \sim 7$ nM) was strong enough for not being outcompeted by the covalent probe with the applied conditions. Increasing the incubation time of the cells with the covalent probe at the lower concentration could also result in competition of the reversible compound due to non-equilibrium binding by the covalent MAPK9 probe. In general, there is a potential for optimization when setting up a kinobeads-based intracellular competition binding assay for reversible inhibitors using covalent probes. However, proofing the concept was successful and it must be kept in mind that using covalent probes in an assay always results in condition-dependent measurement of the reversible inhibitor's potency. Thus, this assay rather allows for a ranking of intracellular target engagement by reversible inhibitors than for the determination of fixed potency values.

4. Discussion

4.1. Formulated goal

The goal of this PhD thesis was the chemoproteomic characterization of covalent protein inhibitors in living cells. Providing a test system for target engagement measurements more suitably addressing physiological conditions than cell extracts or recombinant proteins, in a first step, a lysate-based chemoproteomic affinity enrichment assay was to be compared to a cell-based variant for identifying potential differences in target engagement as determined in cells and lysate.

Building up on the expertise at Cellzome, which was the hosting company for this PhD work, these initial investigations were planned to be done using the kinobeads technology for analyzing kinase binding of targeted covalent kinase inhibitors such as Ibrutinib and Afatinib.

For overcoming limitations regarding the target space of kinases and, by this, for identifying off-targets across the proteome, the FDA approved targeted covalent kinase inhibitors Ibrutinib and Afatinib ought to be subjected to very recent chemoproteomic techniques. Since covalent inhibitors were not yet applied to cellular thermal proteome profiling and multiplexed proteome dynamics profiling using PROTACs their applicability for such molecules should be evaluated and compared to an affinity enrichment approach based on bioorthogonal probes capturing their (off-)targets directly in living cells.

The most suitable target engagement assay for identifying covalent binders of reactive small molecules should then be applied for evaluating different covalent probes based on a generic synthesis strategy for their potential to bind nucleophilic amino acids outside the binding pocket of a reversible pan protein inhibitor. This was thought to provide a strategy for getting new covalent probes or to gain selectivity for a certain subset of the promiscuous inhibitors due to the covalent mechanism.

This dissertation shall elucidate the applicability of chemoproteomic approaches for measuring covalent target engagement in living cells and for identifying covalent and reversible (off-)targets of a reactive compound.

4.2. Achievements

4.2.1. Covalent binding in cells differs significantly from lysate-based measurements

During the first kinobeads experiments analyzing the selectivity of the targeted covalent inhibitors of BTK Ibrutinib, CC-292, and QL47, significant differences in binding to BTK were observed for a lysate-based and a cell-based kinobeads pulldown experiment. The most prominent effect was observed for Ibrutinib engaging BTK more than 100-fold stronger in a cell-based kinobeads assay than in a lysate-based version. The methodological difference between those two types of kinobeads pulldown is that in the former case living cells are incubated with the inhibitor prior to lysing them while in the latter lysates are generated from cells before incubating this with the inhibitor.

The dissection of the mechanism of covalent target engagement into its two parts reveals that both, reversible affinity binding and the subsequent irreversible reaction of the compound with its target, might contribute to the observed differences. Non-covalent affinity-driven equilibrium binding depends on concentrations of ligand and protein as well as competing substrates. Those usually differ between

living cells and lysates which might fundamentally contribute to differences in target engagement measured in cells and lysate. Along the process of lysing the cells changes concentrations of endogenous molecules influencing the binding affinity of the compound. A recent publication analyzed further reasons for differing potency comparing cellular outcomes to lysate or recombinant protein investigations. Decisive factors explaining differences include the cellular localization of the compounds' target, endogenous interactions between biomolecules, metabolism in living cells and post-translational modifications usually not considered when using recombinant proteins.²¹¹ Further, lysate-based assays might also not maintain structural integrity of proteins and protein complexes influencing the binding characteristics of the inhibitor to the target protein.

For covalent inhibitors, the reactive component might even more increase different outcomes in living cells and cell extracts. The reactivity of covalent inhibitors depends as every chemical reaction, for example, on the temperature as described by Arrhenius and van 't Hoff. Assays with protein containing solutions are usually carried out at low temperature for avoiding protein degradation. Using reactive compounds in such assays easily decreases the reaction temperature about 30 K and more compared to living cells incubated at 37 °C. Additional parameters influencing the reaction rate are the concentrations of the reaction partners. Here, the same considerations apply as for the affinity binding described above. In addition, cysteine reactivity was shown to depend on the native redox environment⁵¹ and local pH.^{49, 192} For targeted covalent inhibitors reacting with cysteines this has to be considered. Finally, lysis can cause chemical lability of cysteine PTMs (oxidation, nitrosation, palmitoylation, prenylation, and Michael additions to oxidized lipids)⁵¹ and promotes rapid oxidation of sulfhydryl groups¹⁹³ so that the reaction of covalent inhibitors with cysteines might be impaired.

These considerations can be used to explain the differences observed for the different BTK TCIs in the lysate-based and cell-based kinobeads assay. The lysate-based kinobeads assay achieved very similar pIC₅₀ values for the three BTK TCIs while spanning about two log units in the cell-based kinobeads assay. This might indicate that similar affinity of the compounds is reflected by the lysate-based assay while a very different reactivity is observed when using the cell-based kinobeads assay. Differences in the aforementioned parameters result in a faster reaction rate in cells than in lysate.

The differences in cellular potency as determined for Ibrutinib, CC-292, and QL47 could be related to a higher reaction rate for Ibrutinib than for the other both compounds. This could result from a better positioning of Ibrutinib's acrylamide moiety towards the hinge 6 cysteine as achieved with the other TCIs. Issues with cell permeability might also result in lower apparent potency of a compound in a cellular kinobeads assay. For completely cell impermeable compounds, in the cell-based assays IC₅₀ values $\geq 10 \mu\text{M}$ which is the top concentration of compound used in the assays would be expected. The highest cellular IC₅₀ determined for BTK binding and BCR signaling inhibition, however, was still at 100 nM for QL47 so that cell permeability is expected also for this compound. Thus, full cell impermeability should not be causative for the decreased cellular potency of the compound compared to Ibrutinib. However, a slower cell permeation or even active import/export of one or the other compound can hardly be elucidated by cellular kinobeads assays. Additional assays determining the efficiency and speed of cell permeation, like compound localization assays based on biorthogonal probes and fluorescence microscopy,¹²⁵ would be required.

The comparison of the pIC_{50} values achieved in the cell-based kinobeads assay to the functional effect of BCR signaling inhibition suggests that the cell-based target engagement assay achieves results more predictive for the true functional effect than lysate-based assays. Only with the cellular systems a clear ranking of the different BTK TCIs regarding their potential to inhibit BCR signaling can be done. In drug discovery programs, this would enable the selection of the best candidate for further studies what would be difficult only relying on data achieved with lysates or recombinant proteins. The most precise characterization of irreversible inhibition of course is given with the determination of k_{inact}/K_i . Approaches enabling the measurement of both parameters, however, can be laborious and time-consuming and are often performed using enzyme assays not representing physiological conditions.²⁷ The interpretation of the data is an additional challenge so that previous studies focused on simplifying the determination of k_{inact} and K_i .²¹²⁻²¹³ A cell-based kinobeads assay, therefore, represents a suitable tool for rapidly discriminating more promising drug candidates from less promising ones.

The good correlation between the cell-based kinobeads target engagement assay and the effect on BCR signaling inhibition suggests that a cell-based affinity enrichment assay could represent a suitable way to predict functional effects of inhibitors on proteins lacking a functional readout. Requirements for methods equivalent to the cell-based kinobeads assay are the availability of a suitable affinity matrix and tool compounds fixing the intracellular target engagement situation. The concept of generating affinity matrices from small molecule analogues is well-established and routinely done in chemoproteomic research.^{82, 214-216} Preserving the intracellular target engagement situation can be facilitated by irreversibly binding probes as assessed in this work.

The comparison of the cell-based and the lysate-based kinobeads assay indicated a faster reaction rate of covalent kinase inhibitors in cells than in lysate. This, combined with the re-equilibration of non-covalent compound/target binding upon cell lysis, resulted in the idea to discriminate covalent targets from reversibly bound proteins by comparing cellular and lysate-based potency in a kinome-wide manner.

4.2.2. Differential kinobeads selectivity profiling enables the discrimination of covalent and reversible targets of covalent kinase inhibitors

Suitable conditions regarding cell incubation time, compound concentration and cell washing were established for the cell-based kinobeads assay. This enabled the discrimination of covalent and reversible compound targets across a large number of kinases. A small set of covalent kinase inhibitor including several clinically relevant molecules targeting a homologous cysteine was analyzed with the approach published as 'differential kinobeads selectivity profiling'.¹⁹⁴

The clinically relevant covalent kinase inhibitors were designed to bind a hinge 6 cysteine present in eleven kinases: BLK, BMX, BTK, ITK, TEC, TXK, EGFR, ERBB2/HER2, ERBB4, JAK3, and MAP2K7. Since in the cell material used in this study only BLK, BTK, TEC, EGFR, ERBB2/HER2, JAK3, and MAP2K7 are expressed (Cellzome-internal expression proteomics data set), the following conclusions about hinge 6 reactivity can only be done for these kinases.

The proof-of-concept study was performed using Ibrutinib and a saturated analogue. For Ibrutinib, all targets identified to be covalent binders can be rationalized by the presence of a suitable cysteine. BTK, TEC, BLK, and EGFR all share the homologous cysteine at hinge 6 position. While BTK, TEC,

and BLK show similar cellular potency EGFR was found with about 10-fold lower potency. This indicates a better positioning of the reactive acrylamide of Ibrutinib towards the hinge 6 position of the former three kinases. This is in agreement with the finding that Afatinib only covalently binds to EGFR with low nanomolar potency and BLK at the micromolar range. This clearly supports the concept of targeted covalent inhibition for which irreversible binding is specifically achieved by reasonable design of the compound structure and not by unspecific reactivity of the low reactive acrylamide. This might be an indicator that idiosyncratic toxicity due to unwanted side-reactivity or haptene formation hardly occurs with targeted covalent inhibitors if even affinity-targeted kinases do not necessarily react although providing a suitable cysteine.

Another kinase which was identified to be a covalent target of Ibrutinib is ZAK. ZAK does contain a serine instead of a cysteine at hinge 6 position. Serine is also a nucleophile and is described to react with electrophilic moieties.^{53, 217} However, a reactivity with acrylamides in a cellular context is not described. It was possible to rule out Ser89 binding and to detect Cys22 to covalently react with Ibrutinib by mass spectrometry. Co-crystallization analyses rationalized this site of reaction and the observed competition of ZAK binding to kinobeads. This finding supports the reasonability of the differential kinobeads selectivity profiling approach for the identification of covalent targets. Moreover, an advantage of empirical data over computational prediction of covalent off-targets was shown by the example of ZAK. Without available co-crystallization data, it might be difficult to identify covalent reactions of compounds with amino acids coming close to the reactive compound moiety in the native, three-dimensional structure of the protein. Especially kinome-wide investigations as applied in this work allow for the identification of covalent targets among several hundreds of kinases without requiring co-crystals of each protein.

The comparison of several BTK TCIs identified two kinases as covalent binders of all four compounds: BTK and TEC. Selectivity in covalent binding regarding those apparently is hard to achieve. Even Acalabrutinib reported not to bind TEC⁶²⁻⁶³ did show significant covalent engagement of this kinase. Besides BTK and TEC covalent selectivity seems to be achievable by rational design of the compound. BLK is a prominent covalent off-target of Ibrutinib even stronger engaged than BTK. In contrast, Acalabrutinib does not irreversibly bind to BLK. A recent report demonstrated the benefit of co-inhibition of BTK and BLK by Ibrutinib in the treatment of pre-BCR⁺ B-cell acute lymphoblastic leukemia.²⁰² It is yet to be seen if the superior selectivity of second generation covalent BTK inhibitors such as Acalabrutinib leads to a better therapeutic index in the treatment of B-cell lymphoma indications. BLK might represent a disease relevant target and its function could be elucidated by either optimizing binding of Ibrutinib to increase selectivity for BLK or by reasonable discrimination of effects resulting from Ibrutinib and Acalabrutinib treatment in phenotypic assays.

Besides BTK, TEC, and BLK further kinases were identified to be irreversibly engaged by the BTK TCIs. For MAP3K4 and FGFR1 reactive cysteines are described at positions DFG+1/hinge 2 and glycine loop 5, respectively.¹⁰ The structural proximity of these positions to hinge 6 could explain side-reactivity of some of the compounds. Structural analyses of the proteins, for which today no crystallization data is available, could reveal more detailed information about the mode of reaction. For AURKA and LIMK1 no reactive cysteines are described, yet. Since potency was determined below $pIC_{50} = 6$, and thus, close to the compound concentration maximum used in the experiment (i.e.

10 μ M), this borderline observation could represent false positive outcomes of this approach. Especially the findings on FGFR1, AURKA, and LIMK1 representing disease relevant targets, a validation of the covalent reaction would be required. This could potentially represent a starting point to design irreversible inhibitors for these kinases.

Beyond the differences in potency for covalent targets, differential kinobeads selectivity profiling also reveals a different kinase selectivity of the TCIs in lysate and cells. Some kinases are exclusively identified as compound targets in cells (e.g. FGFR1 and MAP3K4) while others exclusively show potency in lysate. For drug discovery programs these differences can have significant relevance. If the window between target and off-target binding determined in lysate is small, as for example $pIC_{50, \text{Ibrutinib}} (\text{BTK}) \approx pIC_{50, \text{Ibrutinib}} (\text{RIPK3})$, promising compounds might be terminated due to selectivity issues. However, cellular assessment revealed a > 3000-fold window due to the covalent mechanism of the compound. This suggests that selectivity might be achieved for low compound concentrations while still inducing a clinical relevant phenotype. Vice versa, if a compound shows potency in lysate and is carried on it still might not bind a target in the cell due to problems with cell permeability or competition by endogenous substrates. This again indicates the importance of cellular assessment of, especially covalent, inhibitors.

For Afatinib, only a few kinase targets were identified in lysate and in cells. Besides the intended covalent target EGFR, Afatinib additionally engages BLK, GAK, and RIPK2. While the latter was identified as a non-covalent target, irreversible binding was suggested for BLK and GAK. Although Afatinib as well as all investigated BTK TCIs are designed to target homologous hinge 6 cysteines, a different kinase selectivity profile for Afatinib was determined. This supports the concept of targeted covalent inhibition.

The investigations on 5Z-7-Oxozeaenol confirmed several, yet, published covalent targets.²⁰⁰⁻²⁰¹ Additionally, in the same experiment novel covalent targets were identified without the need for target specific investigations. In this case, the identified covalent targets all contained a cysteine preceding the DFG motif which on the one hand validates the plausibility of differential kinobeads selectivity profiling. On the other hand, speculation about those kinases as covalent targets due to the DFG-1 cysteine might already have been made on base of the amino acid sequences without experimental efforts. However, the results for 5Z-7-Oxozeaenol show that differential kinobeads selectivity profiling could also reveal yet unknown, because unpredictable, covalent targets.

Summarizing the application of differential kinobeads selectivity profiling it represents a suitable tool for the identification of irreversible kinase targets of covalently binding molecules, i.e. clinically relevant inhibitors as well as tool compounds. It offers several advantages over alternative approaches for identifying covalent targets:

- a) The approach is not biased by introduced enrichment handles, and thus, can be used for analyzing the original molecule without further synthesis efforts.
- b) Using kinobeads allows for the parallel analysis of a large number of kinases enriched by the affinity matrix.
- c) Compared to washout experiments, for the identification of covalent targets cell-treatment work can be reduced by replacing it with less labor-intensive lysate-based pulldown assays.

- d) Alternative approaches like jump dilution experiments²²⁷ are exclusively lysate-based, while differential kinobeads selectivity profiling considers cellular target engagement.

A critical view on this approach for identifying covalent compound targets reveals two limitations: first, the identification of covalent and reversible targets is based on the competition of kinase binding to the bead matrix. If the covalent inhibitor reacts at a position on the kinase without blocking the ATP binding site competition would not occur. Thus, differential kinobeads selectivity profiling would be blind for such effects. Related to this, using a bead matrix for a certain target class limits this approach to this subset of proteins, in this work kinases. For the identification of irreversibly bound targets beyond the kinase space additional techniques must be applied.

During this PhD work, this limitation became significant when trying to characterize the observed toxicity of Afatinib in Ramos cells. The effect on toxicity could not be clearly explained by kinase binding as determined by differential kinobeads selectivity profiling. This triggered the expansion of intracellular target engagement investigations to other chemoproteomic approaches including an bioorthogonal affinity enrichment approach, two-dimensional thermal proteome profiling as well as the evaluation of PROTAC-induced target degradation for target engagement determination.

4.2.3. Expansion of cellular target engagement investigations with further chemoproteomic approaches: affinity enrichment using bioorthogonal probes, 2D-TPP and PROTAC-induced target degradation

Among the kinases identified by kinobeads to be targets of Afatinib it was not possible to clearly identify the mediator of apoptosis observed for Afatinib-treated Ramos cells. This resulted in the hypothesis that apoptosis might be kinase-independent. For identifying a potential non-kinase off-target characterizing the apoptotic effect, alternative chemoproteomic approaches were applied for the intracellular off-target identification of the covalent kinase inhibitor.

One approach was a competition binding strategy directly performed in living cells using bioorthogonal probes of Ibrutinib and Afatinib. Such an approach provides the advantage of enriching also proteins beyond the kinome. Moreover, compared to lysate, the clickable probe binds to proteins in their native environment conserving the structural integrity of the proteins compared to lysate. It was demonstrated that especially covalent target engagement can significantly differ in cells and extracts thereof. Further, general differences in protein binding also for reversible binding was described.²¹¹

The bioorthogonal probes enriched some non-kinases which were suggested as true targets by competition. Going beyond the target space covered by kinobeads, the determination of binding to these proteins represents an advantage over the kinobeads approach. Since, with exception of ASNS, none of the captured non-kinases was indicated as target by another approach further validation of these protein binders is necessary.

As an advantage of kinobeads it has to be noted that kinobeads enrich also low abundant kinases, and thus, might reveal targets of the original kinase inhibitor not efficiently captured by the clickable probe.

For the kinase targets, overall, good correlation was achieved comparing kinobeads and the intracellular competition binding approach. For the covalent targets of Ibrutinib, pIC₅₀ values

determined with the latter are in accordance with previous cell-based experiments demonstrating the plausibility of the generated data.

Some kinases were exclusively identified as targets in the experiment using bioorthogonal probes although also robustly enriched with kinobeads. This suggests that some kinases are only accessible as binders of the compounds in the cellular environment highlighting the value of cellular target engagement measurements.

Conceptually, both affinity enrichment approaches suffer from the bias of lysing cells at a certain step of sample processing. For reversible targets of the compound as of the clickable probe, re-equilibration will occur resulting in biased information about non-covalent target engagement. A possibility to approach this challenge would be to use probes derived from the inhibitor which additionally incorporate an inducible reactive moiety non-specifically reacting with the captured protein. This concept, for example, is fulfilled by photoaffinity labeling probes.²¹⁸⁻²¹⁹ With such probes based on covalent inhibitors, two fractions could be produced: one prior to photo induction containing the covalent targets of the compound and one after inducing irreversible binding of the non-covalent targets via the photosensitive reactivity. By this, the compound would not dissociate anymore from actual reversible targets of the compound.

The PROTAC technology was applied with the intention to degrade, yet unknown, off-targets of the compounds and by this determining target engagement without the bias of lysing the cells. A proteome dynamics approach was used for distinguishing pre-existing and nascent proteins. By this, a masking of a degradation effects due to rapid re-synthesis should be excluded.

Using the Afatinib-lenalidomide PROTAC in this approach did not result in a significant degradation of any identified protein in Ramos cells. This correlates with the observation that cell toxicity was not induced by the PROTAC molecule in viability measurements. A lack of degradation could have several reasons. The coupling of the relatively large lenalidomide analogue to the linkable Afatinib might result in reduced binding affinity for targets only bound with low potency by the underivatized Afatinib as expected for the apoptosis-inducing off-target considering the high EC₅₀ concentrations in the viability assay. To investigate on that, a lysate-based kinobeads selectivity profiling was performed using the Afatinib-PROTAC. For the kinase targets, no differences in engagement compared to the original Afatinib were observed. This indicates that the incorporation of the E3 ligase binder does not impair the engagement of the kinase targets of Afatinib. Since it is speculated about a non-kinase off-target effect inducing apoptosis of Ramos cells upon treatment with Afatinib, it remains unclear if this off-target is not degraded with the PROTAC approach due to binding issues using kinobeads.

Potentially reduced binding affinity towards a weakly engaged non-kinase could be overcome by using the PROTAC at concentrations $\geq 10 \mu\text{M}$. However, at such high concentrations unspecific perturbations could result in misleading observations regarding protein degradation or upregulation. Since binding is only one of multiple requirements for a successful induction of degradation by PROTAC molecules the lack of proteasomal degradation upon treatment with the Afatinib-PROTAC might not be a problem of binding but, for example, the improper positioning of the E3 ligase towards an amino acid susceptible for ubiquitination.

In addition to an Afatinib-PROTAC, also PROTACs on basis of Ibrutinib and its saturated analogue were analyzed for their potential to induce degradation of their targets during this study. For both compounds, it was possible to identify proteins being degraded in a concentration-dependent manner. This indicates that it was possible to synthesize working PROTAC molecules using a modular system of clickable protein inhibitors and E3 ligase binders. This modularity allows for the establishment of a generic library of clickable protein binders and E3 ligase attracting molecules for the systematic analysis of suitable combinations. This approach might have a significant impact in the field of PROTAC research since the complexity of PROTAC-induced protein degradation seems to require the evaluation of many combinations of binder, linker, and degrader to achieve PROTACs for a certain target protein.^{143, 148, 220}

It was observed that, in contrast to its saturated analogue, the treatment of Ramos cells with the Ibrutinib-PROTAC did not result in degradation of its known covalent target BTK. However, the molecule did induce significant degradation of CSK, LCK, and LYN all identified as non-covalent targets of Ibrutinib by differential kinobeads selectivity profiling. In addition, weak degradation of FYN also representing a non-covalent target of Ibrutinib was observed when using the PROTAC at 10 μ M. Together with the observation that the saturated Ibrutinib-PROTAC reversibly binding to BTK did induce degradation of this kinase, this could indicate a general problem of the catalytical process of PROTAC-mediated proteolysis with irreversible binding of proteins. The covalent attachment of the compound-lenalidomide conjugate to the target protein might negatively influence proteasomal degradation. It is also conceivable that the BTK-Ibrutinib-lenalidomide-Cereblon complex is less flexible as for non-covalently bound targets due to the covalent reaction so that the E3 ligase is not able to access a suitable substrate residue for ubiquitination. A multiple sequence alignment of BTK, CSK, LCK, and LYN matches several lysines to be present at homologous positions in the latter three but not in BTK, for example, Lys196_{CSK} \equiv Lys246_{LCK} \equiv Lys248_{LYN} or Lys218_{CSK} \equiv Lys268_{LCK} \equiv Lys270_{LYN}. These lysines might be accessible by the E3 ligase considering the ATP pocket binding mode of Ibrutinib to BTK but only if a certain mobility is allowed by non-covalent binding. For investigating the general applicability of covalent inhibitors for PROTAC molecules in a more detailed way, different combinations of Ibrutinib, linker, and E3 ligase targeting compounds would be required. If irreversible protein binding would generally impair proteasomal degradation induced by PROTACs this approach would not be suitable for studying covalent target engagement.

Beyond, it shall be noted that the Ibrutinib-lenalidomide conjugate as used in this dissertation represents a very selective CSK and LYN degrader molecule. This could enable new studies on the function of these disease-relevant kinases.

The PROTAC approach applied for intracellular target engagement studies as done in this work indicated only a very small fraction of compound targets as identified by other approaches. This suggests that PROTACs are not a suitable tool for this purpose. The complexity of the proteasomal degradation of proteins mediated by PROTACs might require immense optimization of every PROTAC analogue of a small molecule. Or, as stated by *Ian Churcher* in a recent perspective: "The concept of an "all-purpose" combination of a binder to a specific E3 ligase and linker which can be appended to any ligand to ensure optimal degradation is unlikely to become reality".¹⁴³ Further, the synthesis of

PROTACs comes with the same efforts regarding design and synthesis as affinity-based probes and result in a similar bias towards certain binding modes due to the incorporation of the linker and E3 ligase binder. From that perspective, small molecule probes based on the chemical structure of the inhibitor under investigation combined with a suitable readout should be preferred over PROTACs. However, for accessing off-targets which, for example, are bound via a shallow binding site, and thus, not sufficiently tagged by affinity-based probes PROTACs still might represent a suitable tool for off-target determination.

The bioorthogonal probe-based approach and the PROTAC approach applied herein for investigating intracellular target engagement have the limitation to require tool compounds synthesized from the original molecules. Besides the synthesis effort, these modifications might represent a bias towards certain binding modes, and thus, could fail to identify targets of the original compound. With the intention to reduce this bias, two-dimensional thermal proteome profiling was applied after incubating Ramos cells with Ibrutinib and Afatinib.

For the analysis of the generated data sets, two approaches were applied: for the proteome-wide target identification, thermal effects on proteins were filtered to those observed in at least two adjacent temperatures. For identifying effects on protein kinases in a less stringent way, thermal de-/stabilization was manually evaluated for all robustly identified kinases. For Ibrutinib, CSK and LYN were the only protein kinases among the proteins affected in at least two adjacent temperatures. Analyzing the kinase space specifically also revealed thermal effects on LCK, RIPK2, and RIPK3. All are reversible targets of Ibrutinib as identified in this study. For the covalent targets BLK and BTK, no thermal effect was determined across the applied concentration range. This finding indicates that stronger engagement due to covalent binding not necessarily effects thermal stability of a protein. Since the covalent reaction usually occurs only at one position this will not stabilize the three-dimensional structure of the protein. In general, the lack of a thermal effect on proteins could have several reasons: for big proteins, binding of a small molecule might not influence the proteins' overall stability. The major part of the protein initiating precipitation by unfolding might not be affected by compound binding. Similarly, for multidomain proteins, binding to one domain could result in stabilization of this part of the protein but the unfolding of others could still result in precipitation. It might also be conceivable that protein complexes precipitate together although one of the complex partners is in fact stabilized by the small molecule under investigation. All these considerations could result in masked stabilization effects.

Beyond the protein kinases, 18 proteins were identified being thermally affected in at least two adjacent temperatures by Ibrutinib. Of those, NUDT1 and CYP51A1 were also thermally stabilized by the TCI in a lysate-based 2D-TPP analysis. However, none of the 18 proteins was identified as target with another approach than thermal proteome profiling so that a validation of these proteins as true binders of the compound would be required. A GO term analysis mapped nine of the non-kinase targets, including NUDT1 and CYP51A1, to a small molecule metabolic process (GO:0044281). This indicates that seven proteins were rather involved in a response to the treatment of the cells with the small molecule than representing true targets of Ibrutinib. Also the other proteins not confirmed by the lysate-based 2D-TPP analysis might not be truly engaged by the inhibitor. This demonstrates another challenge when interpreting cell-based thermal proteome profiling data: an apparent stabilization effect

of a protein could result from increased abundance in a certain fraction due to upregulation of this protein in this sample. Such an effect, however, should be observed temperature independently in all samples of the same compound concentration, and could be discriminated from a true thermal effect by combining compound treatment with pulsed SILAC labeling of the cellular proteome. Thermal effects resulting from cellular target engagement as determined in cell-based thermal proteome profiling experiments could also be confirmed by the comparison to cell extract-based thermal proteome experiments as done in this study. However, differences in lysate-based target engagement compared to cellular binding as demonstrated above for affinity enrichment potentially do also occur in thermal shift assays. The validation of true compound targets, in any case, requires additional experimental and analytical effort.

For Afatinib, several protein kinases were determined to be thermally affected. Among those, MAPK14, MAPKAPK2, GAK, and BLK were also identified as targets of Afatinib with other approaches. Together with the non-kinase targets, a GO term analysis suggested two major mechanisms in which the identified proteins are involved: oxidation/reduction processes (GO:0055114), specifically the assembly of mitochondrial complex I (GO:0032981), and the regulation of the p38MAPK cascade (GO:1900744). Both might be involved in the apoptotic response of Ramos cells to Afatinib treatment. Especially, the involvement of the respiratory chain might explain apoptosis generally observed among different cell lines. The identification of ACAD9, ECSIT, and NDUFAF1 as being thermally stabilized by Afatinib also in a lysate-based assay supports this theory by indicating those as true compound binders. The observed stabilization of MAPK14, also known as p38, and MAPKAPK3 as well as the significant destabilization of PRMT1 and GSK3A suggest dysregulation of Wnt signaling upon Afatinib treatment. MAPK14 was identified as weak reversible target of Afatinib with the affinity enrichment approaches, and together with MAPKAPK3, also identified as thermally stabilized in the lysate-based experiment. PRMT1 and GSK3A have not been identified as being bound by the compound using another approach. This could indicate regulation of PRMT1 and GSK3A in consequence of binding to another protein rather than a direct destabilization effect resulting from compound engagement. MAPKAPK2/3 and MAPK14 are involved in Wnt signaling and the latter is known to phosphorylate GSK3A. Decreased GSK3A activity upon phosphorylation of Thr390 is associated with an increase of β -catenin and subsequent activation of Wnt signaling genes.²²¹ Also PRMT1 is described to influence Wnt signaling by stabilizing Axin, a partner of the β -catenin complex.²²² Less stabilization of Axin due to a lack of PRMT1 would also result in an accumulation of β -catenin. Today, there is no published study about Afatinib influencing Wnt signaling so that such an effect remains to be validated.

As a final thought about 2D-TPP it shall be noted that a limitation of this approach compared to affinity enrichment assays is given in the sensitivity of the mass spectrometers used for data acquisition. While affinity enrichment allows for the identification of low abundant targets, in a 2D-TPP analysis those targets might not be identified among the usually more than 6000 identified proteins. Combining heat treatment with subsequent enrichment of a subset of soluble proteins could solve the problem of dynamic range.

Summing up the results of this part of the dissertation: the investigations on off-target engagement of Afatinib did not provide enough evidence to conclude for the apoptosis-mediating mechanism. To date

(April 4th, 2018), in this study targeted covalent kinase inhibitors were applied to 2D-TPP analyses and multiplexed proteome dynamics profiling using PROTAC analogues for the first time for evaluating intracellular target identification with these approaches. The suitability of these approaches for determining covalent (off-)target binding in living cells has still to be validated. It shall be noted that the discrimination of covalent and reversible targets can conceptually only be done by compound washout strategies using those techniques. The affinity enrichment approaches given with differential kinobeads selectivity profiling and bioorthogonal probes might, therefore, represent the preferable, since less labor-intensive, alternative.

The comparison of the different approaches to study target engagement revealed that there, yet, is no general technique to identify target engagement of small molecules comprehensively. The affinity probe- and PROTAC-based approaches come with the bias of introducing reporter moieties into the small molecule. Moreover, the former also suffers from re-equilibration effects for non-covalently bound proteins and the suitability of the latter due to its complexity still has to be investigated. The cell-based 2D-TPP showed limitations regarding thermal stability of some known kinase targets of the inhibitors. Further, when performing cellular 2D-TPP analyses it has to be considered that apparent effects on thermal protein stability upon compound treatment might also result from indirect proteome changes (e.g. altered affinity for endogenous substrates, different PTM patterns, or expression effects due to altered regulation) rather than indicating direct target engagement of the affected protein by the compound under investigation. For discriminating indirect effects from direct target engagement, a lysate-based 2D-TPP should be contemplated. Advantages and limitations for each approach suggest that a combination of several chemoproteomic approaches, preferentially affinity enrichment and thermal proteome profiling, is required to comprehensively characterize (off-)target engagement of covalent inhibitors.

4.2.4. Assessment of a generic strategy for synthesizing covalent probes from non-selective, reversible inhibitors

Using differential beads selectivity profiling as being the most suitable method for identifying covalent and reversible binders of kinase inhibitors, a generic synthesis strategy for the generation of covalent probes from reversible pan kinase inhibitors was assessed. For this, reactive moieties were coupled to unselective protein inhibitors of different target classes. For the unselective HDAC inhibitor and the lipid kinase inhibitor used in this work, the coupling of an acrylamide moiety did not result in the covalent binding of any targeted protein as indicated by differential HDAC bead selectivity profiling and differential lipid-kinobeads selectivity profiling. This indicates that the cysteine-reactive acrylamide moiety did not come close to a suitable amino acid. Some potentially approachable cysteines are rarely distributed across the HDACs and attacking those covalently would represent a valid strategy for gaining selectivity of the promiscuous inhibitor. However, the generic procedure of attaching acrylamides to the amine incorporating SAHA analogue is not precise enough to approach those cysteines. Beyond cysteines, different HDACs provide some serines and tyrosines outside the SAHA binding site which apparently do not react with the covalent compounds used in this work. For some lipid kinases, a crystal structure analysis identified some lysines which might represent suitable attack points for a covalent reaction. Since sulfonyl fluorides are described to react with serines, tyrosines,

and lysines,^{53, 210} it could be interesting to see how these reactive moieties coupled to the promiscuous lipid kinase inhibitor and the promiscuous HDAC inhibitor would perform in a differential lipid kinobeads assay and a differential HDAC beads assay, respectively.

Specific covalent binding was observed for the acrylamide functionalized analogues of the promiscuous protein kinase inhibitors. MAPK9 was most clearly indicated as covalent binder of probe 1A and the comparison of cellular potency of the reactive probe to a non-reactive analogue confirmed this finding among others. The site of reaction was identified to be Cys116 and correlates with previously published data.¹⁶ This supports the concept of generating covalent compounds from promiscuous inhibitors on the one hand and the value of differential kinobeads profiling for the identification of irreversible targets of covalent probes on the other. For the PEG2-linked probe 2A it was also possible to identify a covalent target which is TEC and comparison to a non-reactive control compound did suggest MAPK9 as covalent target, too. While cellular potency seems to be slightly increased for TEC, using the PEG2 linker instead of direct coupling resulted in slightly lower cellular potency for MAPK9. This could be related to a better and worse positioning of the acrylamide moiety towards TEC and MAPK9, respectively. Further, with the generic approach used for these investigations a covalent TEC inhibitor (probe 3A) was synthesized with a high selectivity for TEC compared to BTK without any optimization efforts. This might represent an interesting starting point for additional optimization of the compound to enable new studies on TEC signaling being involved in a plethora of hematopoietic cell functions. However, for TEC the site of reaction was not identified for probes 2A and 3A despite of reasonable sequence coverage when analyzing recombinant TEC incubated with the covalent probes. This might either indicate that the compounds did not react with recombinant TEC at the applied conditions or that they are generally not binding irreversibly. The validation of TEC as covalent target of the reactive probes by identifying the covalently bound amino acid has yet to be done.

With the attachment of a reactive moiety, a gain in selectivity was achieved as demonstrated for probe 1A. The covalent mechanism allows using the compound at low concentrations due to non-equilibrium binding. With prolonged incubation time, engagement of the covalent targets would increase while the reversible binding would stay at low levels or even decrease due to the depletion of the compound from the binding equilibrium by the reaction of the compound with its covalent targets.

The generic approach of synthesizing covalent probes from unselective inhibitors can serve two purposes: it can be used to gain selectivity for a certain subset of targets by covalent binding as shown for probe 1A or it can generate still promiscuous but irreversible binding tool compounds which would allow for broad-spectrum intracellular competition binding experiments. For the latter, another reactivity than the acrylamide would probably be required for binding more amino acids than just the small number of suitable cysteines covalently. Therefore, reactive moieties other than acrylamides were assessed for covalent binding to kinases. The identification of another suitable reactivity might enable the transfer of the generic synthesis concept of covalent probes to other enzyme classes.

4.2.5. Evaluation of different reactive moieties for binding amino acids around the ATP-binding pocket of kinases irreversibly

For extending the set of reactive moieties, sulfonyl fluorides described to covalently bind context-specifically to serine, threonine, lysine, tyrosine, cysteine and histidine,⁵³ and chlorine functionalities were coupled to the promiscuous kinase inhibitors. Additional reactive moieties coupled to the inhibitors were bromine, and iodine as well as a vinyl sulfone which turned out to yield unstable analogues, i.e. instantly decomposing during their synthesis, and thus, being not applicable as covalent probes.

Among the used sulfonyl fluorides two aromatic versions were used incorporating the sulfonyl fluoride in meta and para position as well as a linear sulfonyl fluoride coupled via a thiol to the linkable compound. The latter compound was synthesized to compare potential differences between the more rigid aromatic molecules and the more sterically flexible linear version. However, linear sulfonyl fluorides are hardly available as building blocks, probably related to their instability as experienced during this work for 2,2-difluoro-2-(fluorosulfonyl)acetic acid, so that the thiol generating workaround had to be applied. It was not possible to identify higher cellular potency for any target of the thiol-linked linear sulfonyl fluorides. After observing this, a stability analysis showed that the linear sulfonyl fluoride analogues hydrolyze in aqueous solution. This suggests that a major portion of the reactive moiety is not available anymore quickly after adding it to the cells. Together with the observation that linear sulfonyl building blocks instantly decomposed during synthesis this additionally suggests that linear sulfonyl fluorides are not suitable as reactive moieties for covalent protein probes.

For the 3-methylbenzene-1-sulfonyl fluoride analogue incorporating the reactive moiety at meta position, the majority of identified compound targets showed higher potency in cells than in lysate. An explanation for this observation could be that the compound fulfills the requirements of an unspecific ATP-competitive covalent kinase probe by, for example, reacting with the catalytic lysine very conserved across the kinome. Especially the comparison to the para analogue of the compound (4-methylbenzene-1-sulfonyl fluoride) which showed higher potency in cells only for a TBK1 and MAP3K4 might indicate that the findings in fact might result from proper positioning of the reactive moiety. That the positioning of a sulfonyl fluoride in para or meta position at the aromatic ring influences covalent kinase binding was shown previously.²¹⁰

When comparing the data achieved for the directly coupled covalent probes to the PEG2-linked variants, it has to be noted that for the aromatic sulfonyl fluorides with the longer linker no kinase was indicated as potential covalent binder. The different profiles of the PEG0 and the PEG2 analogues in the cell-based assay might deliver additional evidence that the versions with the shorter linker in fact bind the indicated kinases irreversibly. Further validation would be necessary to analyze the potential of the 3-methylbenzene-1-sulfonyl fluoride analogue to serve as an unselective covalent kinase probe to enable broad-spectrum intracellular competition binding experiments according to the kinobeads approach demonstrated for the reversible MAPK9 inhibitor Tanzisertib in this work.

For the chlorine compounds, both the short and the long linker analogues, the majority of identified kinase targets can be found with similar potency in lysate and cells. This could mean that the relatively reactive chlorine quickly reacts in both environments. This is reasonable since chlorinated compounds (chloroacetamide) are efficiently used as alkylating agents in proteomic approaches under lysate-

based conditions. However, alkylation predominantly occurs at cysteines. Thus, covalently tagged kinases identified in the kinobeads approach would require offering a cysteine close to their ATP binding site. This, yet, remains to be validated.

Among the tested reactivities, the acrylamide turned out to be the most suitable for selective binding due to low reactivity and reasonable stability. For the aromatic sulfonyl fluoride and the chlorine analogues additional investigations need to clarify if really a non-specific covalent labeling of a large number of kinases is observed. If so, those might represent a suitable starting point to get promiscuous covalent probes comparable to those recently published.²¹⁰ If covalent binding was established by binding to amino acids different from cysteine, sulfonyl fluorides or chlorine could potentially be used to bind proteins of other target classes irreversibly.

Finally, it shall be noted that beyond generating tool compounds for intracellular target engagement, the generic approach assessed in this work also could serve the purpose of mapping which members of a certain target class might be covalently bound at all. This means, the targets identified as covalently approachable by the generically synthesized probes might offer suitable amino acids as attack point for a more target-specific design of irreversible inhibitors.

With the generic synthesis approach, a covalent MAPK9 probe was achieved. This was used to set up an intracellular competition binding assay based on kinobeads for quantifying target engagement of the non-covalent MAPK9 inhibitor Tanzisertib. This kinobeads-based approach using covalent probes for fixing the in-cell established target binding represents an alternative to intracellular target engagement assays for reversible inhibitors requiring clickable analogues of covalent probes as discussed in the next chapter.

4.2.6. Proofing the concept of a intracellular competition binding assays for reversible inhibitors utilizing covalent tool compounds

The concept of covalently binding the portion of targets not engaged by a reversible inhibitor was demonstrated using saturated Ibrutinib and CGI-1746, a commercially available reversible BTK inhibitor, in combination with a clickable analogue of Ibrutinib (TCO-Ibrutinib). Dose-dependent fluorescence was observed after clicking a tetrazine-Cy5 conjugate to a constant concentration of TCO-Ibrutinib when competing BTK binding by a reversible inhibitor. This indicates that increasing amounts of reversible inhibitors avoid covalent binding of TCO-Ibrutinib to BTK at the used conditions. Reasonable pIC_{50} values were derived from the fluorescence measured. The pIC_{50} value for saturated Ibrutinib correlates very well with the potency determined in a lysate-based kinobeads assay. The comparison of saturated Ibrutinib to CGI-1746 shows that for the latter a higher pIC_{50} value was determined. This is reasonable for a compound specifically optimized for high potent BTK binding compared with an analogue of Ibrutinib depending on the covalent mechanism to achieve high potency. However, for this interpretation it must be noted that this approach represents only a snapshot of the intracellular situation at the moment of compound washout. This means by longer incubation with the covalent probe the potency determined for the reversible inhibitors would decrease over time. Thus, this approach rather enables a ranking of different compounds for the same target

and equal incubation conditions than giving concrete potency values. It should be noted that this applies for all investigations on covalently binding compounds.

The advantage of binding kinases not engaged by reversible inhibitors with covalent probes is the fixation of the intracellular target engagement situation. In such a setting, re-equilibration of reversible binding will not influence the interpretation of target engagement by the non-covalent inhibitor. This concept was exploited when using kinobeads enrichment instead of a fluorescence measurement for analyzing intracellular, reversible target engagement. For this, reversible target engagement established by the MAPK9 inhibitor Tanzisertib in living cells was fixed using the covalent MAPK9 probe 1A synthesized in this work. Subsequently, intensive cell washing was applied for removing Tanzisertib from reversibly bound MAPK9. After cell lysis, this MAPK9 fraction was enriched by kinobeads and identified in a concentration dependent manner by Western blotting. Although the outcome of this approach can be optimized regarding probe concentrations and incubation time, it was shown in this proof-of-concept experiment that the strategy of intracellular competition binding with reversible inhibitors works when fixing this intracellular target engagement situation by covalent helper compounds. This kinobeads approach enables the investigations on reversible inhibitors for the kinases for which covalent binding can be achieved. Probes binding a wide range of kinases irreversibly as demonstrated in the work of *Zhao et al*²¹⁰ are preferable for such a purpose.

With this intracellular competition binding approach for non-covalent inhibitors, a strategy was set up elucidating if a compound under investigation reaches and binds to its target. Further, this competition binding approach performed in living cells enables the ranking of non-covalent compounds for their intracellular target affinity. Key for expanding this approach to protein classes others than kinases will be to get generic covalent probes for different target classes. Promiscuity of the irreversibly binding compounds might here represent an advantage allowing for the analysis of many proteins using the same probe.

4.3. Outlook

Covalently inhibiting drugs can have excellent pharmacokinetic properties and can achieve high selectivity across the proteome. The development of new covalent drugs is desirable. With the concept of differential kinobeads selectivity profiling, a strategy was set up to identify covalent and reversible targets of irreversible kinase inhibitors. With this method there is no need for synthesizing linkable or bioorthogonal analogues of the covalent compound under investigation. For a large set of covalent kinase inhibitors this represents a substantial advantage over ABPP approaches. This strategy, in general, is applicable to other target spaces for which covalent inhibitors might be developed. This requires the generation of suitable affinity matrices comprising promiscuous probes which enrich for a broad range of proteins of the target class under investigation. The development of such matrices should be expedited.

With the expansion of differential kinobeads selectivity profiling to other target classes, a suitable strategy for assessing new covalent compounds would be available. Developing such covalent probes enables to study intracellular target engagement and could potentially result in selectivity for binding certain protein domains or isoforms. During this study, it was planned to synthesize a covalent probe for BRD proteins. This probe should covalently bind to two tyrosines very conserved across BRD proteins. Probe backbones for synthesizing such probes were (S)-2-(4-(4-chlorophenyl)-2,3,9-trimethyl-6H-thieno[3,2-f][1,2,4]triazolo[4,3-a][1,4]diazepin-6-yl)acetic acid, which is a commercially available carboxylic acid analogue of JQ1, or the two scaffolds, 6-(5-bromo-2-methoxyphenyl)-7H-purine and 6-(5-bromo-2,3-dihydrobenzofuran-7-yl)-7H-purine, as described by *Picaud et al.*²²⁶ Commercially available building blocks allow for a straight forward synthesis of analogues incorporating a reactive moiety pointing towards one of the tyrosines mentioned above. A reasonably positioned sulfonyl fluoride might enable the covalent binding of the BRD proteins. Although the synthesis and evaluation of these probes was not realized in this work, it might yield a suitable covalent probe for enhancing investigations on BRD proteins binding molecules, in future.

For evaluating target engagement of a large set of covalently acting drugs using a differential bead selectivity profiling strategy, it would be advantageous to optimize the cell-based and the lysate-based affinity enrichment assays regarding required material. This will enable to perform these assays in a multiplexed plate format and will simplify the handling of many samples in parallel.

Ideally, a cell-based assay could be designed such that the sample preparation enables an analysis using different chemoproteomic approaches. The analysis of homogeneous samples with target class- and drug-centric affinity enrichment approaches in parallel with thermal proteome profiling would yield a comprehensive assessment of intracellular target engagement. This study demonstrated that information about target engagement can strongly differ across various chemoproteomic assays with advantages and limitations of each.

While thermal proteome profiling and affinity enrichment strategies are well established and efficiently identify intracellular targets of protein inhibitors, the PROTAC technology was, yet, not applicable as a routinely used assay for evaluating intracellular target engagement. This is largely caused by the

complex mechanism of PROTAC-induced proteasomal degradation requiring an optimal combination of the target binding compound, the E3 ligase recruiting molecule, and the linker connecting both.¹⁴³ A possible strategy overcoming this challenge might be to apply bioorthogonal chemistry. After treating cells with a TCO-incorporating protein inhibitor, the addition of tetrazine analogues of different E3 ligase targeting molecules, potentially attached to different linkers, to the cells could increase the chance for degradation of the targeted proteins. The universal “cocktail” of E3 ligase binders could be applied in combination with a large set of TCO-probes without requiring the individual synthesis and purification of many whole PROTAC molecules.

Using covalent probes synthesized from promiscuous kinase inhibitors as tool compounds enabled to set up a kinobeads-based intracellular target engagement assay for reversible inhibitors. A prerequisite for this was the availability of a covalent probe of the target under investigation, in this case, MAPK9. To achieve covalent probes also for other targets more compound cores as well as more reactivities and linkers connecting both have to be assessed. This, on the one hand, requires a lot of synthesis effort which could be potentially simplified using a modular click chemistry strategy with suitable building block analogues. On the other hand, the evaluation of the compounds in cell-based assays necessitates optimization of this assay as described above. A general challenge of intracellular target engagement assays for reversible inhibitors using covalent probes as demonstrated in this work is the progressive competition of non-covalent target engagement by the irreversible probe. This requires fine-tuned assay conditions allowing for sufficient labeling of the target protein by the covalent probe without competing out the reversible compound completely. A strategy to circumvent this problem could be to incorporate photo-reactive moieties instead of electrophiles into the molecules. This would not require having certain nucleophilic amino acids in proximity to the reactive moiety and would reduce the bias of time-dependency for intracellular competition binding experiments with covalent probes. The equilibrium of reversible inhibitor engagement and photo-reactive probe binding could establish before photo-inducing the reaction for “snap freezing” the intracellular target engagement situation. Synthesizing photo-inducible probes based on promiscuous inhibitors of a certain target class would yield suitable tools for competition binding experiments in living cells for a broad spectrum of targets analogous to kinobeads used in cell extracts.

5. Conclusion

In this study, it was shown that measuring target engagement of covalent inhibitors in cells can significantly differ from cell extract-based outcomes. A kinobeads-based cellular assay was set up and BTK engagement of three different TCIs measured with this assay did very well correlate with the functional effect on BCR signaling upon BTK inhibition. Lysate-based measurements did not allow for concluding on the quality of BTK binding by the different compounds. Thus, a cell-based chemoproteomic enrichment assay as demonstrated in this work provides a suitable alternative for correlating functional effects to target engagement as determined in the cellular context. This indicates the need for intracellular target engagement measurements to achieve more predictive data as gained with cell extract- or recombinant protein-based methods.

The differences in lysate- and cell-based target binding were exploited to establish a strategy for discriminating kinases covalently and reversibly bound by targeted covalent inhibitors. The value of this kinobeads-based approach is that it does not require the labor-intensive design and synthesis of suitable probes potentially impairing certain binding modes. Rather, the original molecule under investigation can be analyzed. Applying this strategy to a set of clinically relevant molecules demonstrated different selectivity of these compounds although targeting a homologous cysteine. Thus, the validity of the concept of targeted covalent inhibition was confirmed. Beyond, with ZAK a covalent target of Ibrutinib was identified not containing a Hinge 6 cysteine but a serine at this position. Without crystal structures of ZAK it would be difficult to predict this side-reactivity which was identified by differential kinobeads selectivity profiling by computational analyses.

During the investigation on the targeted covalent kinase inhibitors used in this work an Afatinib-induced toxicity was observed in Ramos cells, which was not seen for treating the cells with Ibrutinib. The Afatinib-specific effect would not have been identified using lysate or recombinant proteins. This, again, demonstrates the value of cell-based assays allowing for a phenotypic readout and providing the whole proteome as target space in contrast to only a limited panel of selected proteins. For identifying the apoptosis-mediating target in peripheral blood cells not expressing Afatinib's main target EGFR, several chemoproteomic approaches for intracellular target engagement determination were applied. This was done for expanding the target space of investigation beyond kinases enriched by kinobeads. The intracellular competition binding experiment using clickable probes of Afatinib and Ibrutinib correlated well with the kinobeads achieved data. Some differences were seen for non-kinases conceptually not covered by kinobeads. Among the kinome, some kinase targets were exclusively identified in the kinobeads assay. This indicates the value of differential kinobeads selectivity profiling of the original molecule and might indicate impaired kinase binding to these kinases by the clickable probes. Vice versa, some kinase targets were also identified exclusively using the clickable probe although being robustly enriched by kinobeads. This suggests that there might be a difference regarding structural integrity in the living cell and in lysates produced from the cells prior to affinity enrichment.

The thermal proteome profiling of the cells upon compound treatment did suggest several compound targets also identified with the affinity enrichment approaches. Among the most significantly stabilized proteins after treatment with Ibrutinib the kinases CSK and LYN were identified. For the kinases most strongly engaged due to the covalent mechanism, BTK and BLK, no thermal effect was observed. This suggests that irreversible target engagement might only be identified using competition binding assays.

After Ramos cell treatment with Afatinib, several proteins were determined to be thermally affected including members of the assembly complex of mitochondrial complex I and proteins involved in Wnt signaling. Both represent universal cell mechanisms which could cause cell toxicity if impaired. The only non-kinase suggested as target of Afatinib with the affinity enrichment approach and in the 2D-TPP analysis is asparagine synthetase ASNS. Being involved in the asparagine biosynthesis, inactivation of this enzyme by Afatinib could also result in cell toxicity. However, a validation of any of these mechanisms has still to be done.

The PROTAC technology was successfully applied to degrade non-covalent targets of Ibrutinib. The covalent targets BTK, BLK, MAP2K7, and TEC were not degraded as indicated by proteome dynamics analyses. Instead, a very selective degrader of CSK, LCK, and LYN was achieved coupling an amine-incorporating Ibrutinib analogue to a Cereblon binder. Using a saturated PROTAC analogue of Ibrutinib not able to bind BTK irreversibly did degrade the kinase in a concentration dependent manner. Since EGFR as covalent target of Afatinib was also not degraded using the Afatinib-PROTAC in EGFR-expressing A549 cells, it could be concluded that PROTAC-induced proteasomal degradation is not compatible with irreversible drug target binding. For confirmation, more investigations on that are required. Yet, it seems that the PROTAC technology is understood too little to apply it as general target engagement assay. The modular assembly of PROTAC molecules used in this work to achieve lenalidomide analogues of the covalent kinase inhibitors, allows for a simple combination of different E3 ligase binders to optimize degradation. This could potentially be done directly in cells using suitable bioorthogonal analogues of protein inhibitors and E3 ligase binding molecules.

From this comparison of intracellular target engagement assays, it can be concluded that, yet, there is no universal strategy to get a comprehensive picture of compound (off-)target binding. A combination of different methods is desirable. Differential bead selectivity profiling expanded the toolbox for that purpose for covalent inhibitors.

A generic strategy to synthesize covalent probes was introduced. This concept aimed on the coupling of electrophilic moieties to a promiscuous kinase inhibitor to potentially react with suitable amino acids outside of the inhibitors binding pocket. For two different promiscuous kinase inhibitors, both coupled on the herein used version of kinobeads, a small number of kinases were indicated as covalent binders of an acrylamide-incorporating analogue. The most prominent effect observed for MAPK9 was validated using mass spectrometry for identifying the site of reaction. Exploiting the covalent mechanism allows to use the probe at low concentrations minimizing reversible target binding with still gaining reasonable MAPK9 engagement over time. Thus, for the inhibitor an apparent selectivity for MAPK9 was achieved. For other reactive moieties including sulfonyl fluorides, no significant gain in

selectivity was observed. Differential kinobeads selectivity profiling rather suggested covalent binding of many kinases using a sulfonyl fluoride or a chlorine. Those might represent promiscuous covalent probes usable for investigations on many different kinases bound irreversibly by the probe. This, however, has yet to be validated. Increasing the linker length to potentially react with nucleophilic amino acids more distant from the binding pocket did not result in any covalent binding suggesting that this is not a suitable strategy to increase the target space of covalent binding.

For the protein kinase space, it was shown that the generic strategy for achieving covalent probes works. The transfer of this concept to other target classes including HDACs and lipid kinases was not successful using an acrylamide as reactive moiety. A suitable cysteine apparently is not approachable by the used compounds. Expanding the investigations to further reactive moieties might result in an effective application of the generic synthesis approach for other target classes.

Using one of the synthesized covalent probes, a kinobeads-based strategy for measuring intracellular target engagement also of reversible inhibitors was introduced. After treating cells with reversible inhibitor, non-engaged targets are covalently bound by the probe. This fixes the target engagement situation of the reversible inhibitor which can be washed out from the system in a next step. Kinobeads can be applied for enriching disengaged kinase targets of the reversible inhibitor. The concept of this strategy was proven using Tanzisertib, a MAPK9 inhibitor, competing for the binding to the covalent MAPK9 probe. However, it has to be noted that this strategy is highly depending on the concentration of the covalent probe used and the incubation time of the cells with it. A potential path forward to optimize this kind of intracellular target engagement assay would be to use photo-inducible promiscuous kinase inhibitors instead of electrophilic probes. This could increase the target space covered by the probes, including proteins beyond kinases, since suitable reactive moieties, like diazirines, would not require a nucleophilic amino acid to react with. Furthermore, the dependency on incubation time and probe concentration could be overcome avoiding non-equilibrium binding with photo-inducible reactive probes.

Irreversible inhibitors and probes will remain an interesting topic for research due to their relevance as drugs with preferable pharmacokinetic characteristics and as tool compounds for investigations on intracellular target engagement. This study enhanced the knowledge about the applicability of chemoproteomic approaches for determining target engagement of this kind of molecules in living cells.

Literature

1. Landry, Y.; Gies, J.-P., Drugs and their molecular targets: an updated overview. *Fundamental & Clinical Pharmacology* **2008**, *22* (1), 1-18.
2. Bull, S. C.; Doig, A. J., Properties of protein drug target classes. *PLoS One* **2015**, *10* (3), e0117955.
3. Xu, H.; Xu, H.; Lin, M.; Wang, W.; Li, Z.; Huang, J.; Chen, Y.; Chen, X., Learning the drug target-likeness of a protein. *PROTEOMICS* **2007**, *7* (23), 4255-4263.
4. Hopkins, A. L.; Groom, C. R., The druggable genome. *Nat Rev Drug Discov* **2002**, *1* (9), 727-730.
5. Alberts B, J. A., Lewis J, et al., *Molecular Biology of the Cell*. 4 ed.; Garland Science: New York, 2002.
6. O'Connor, C. M. A., J. U., *Essentials of Cell Biology*. NPG Education: Cambridge, MA, **2010**.
7. Bailey, R. The Function and Structure of Proteins. <https://www.thoughtco.com/protein-function-373550> (accessed December 1st, 2017).
8. Lundblad, R. L., *Chemical Reagents for Protein Modification*. Forth edition ed.; CRC Press: **2014**.
9. Garuti, L.; Roberti, M.; Bottegoni, G., Irreversible protein kinase inhibitors. *Curr Med Chem* **18** (20), 2981-94.
10. Liu, Q.; Sabnis, Y.; Zhao, Z.; Zhang, T.; Buhlage, S. J.; Jones, L. H.; Gray, N. S., Developing irreversible inhibitors of the protein kinase cysteinome. *Chem Biol* **2013**, *20* (2), 146-59.
11. Shannon, D. A.; Weerapana, E., Covalent protein modification: the current landscape of residue-specific electrophiles. *Curr Opin Chem Biol* **2015**, *24*, 18-26.
12. Ihle, N. T.; Williams, R.; Chow, S.; Chew, W.; Berggren, M. I.; Paine-Murrieta, G.; Minion, D. J.; Halter, R. J.; Wipf, P.; Abraham, R.; Kirkpatrick, L.; Powis, G., Molecular pharmacology and antitumor activity of PX-866, a novel inhibitor of phosphoinositide-3-kinase signaling. *Molecular Cancer Therapeutics* **2004**, *3* (7), 763-772.
13. Dagher, J.-P.; Zambaldo, C.; Abegg, D.; Barluenga, S.; Tallant, C.; Müller, S.; Adibekian, A.; Winssinger, N., Identification of Covalent Bromodomain Binders through DNA Display of Small Molecules. *Angewandte Chemie International Edition* **2015**, *54* (20), 6057-6061.
14. Lawrence, C. P.; Kadioglu, A.; Yang, A. L.; Coward, W. R.; Chow, S. C., The cathepsin B inhibitor, z-FA-FMK, inhibits human T cell proliferation in vitro and modulates host response to pneumococcal infection in vivo. *J Immunol* **2006**, *177* (6), 3827-36.
15. Leproult, E.; Barluenga, S.; Moras, D.; Wurtz, J. M.; Winssinger, N., Cysteine mapping in conformationally distinct kinase nucleotide binding sites: application to the design of selective covalent inhibitors. *J Med Chem* **2011**, *54* (5), 1347-55.
16. Zhang, T.; Inesta-Vaquera, F.; Niepel, M.; Zhang, J.; Ficarro, S. B.; Machleidt, T.; Xie, T.; Marto, J. A.; Kim, N.; Sim, T.; Laughlin, J. D.; Park, H.; LoGrasso, P. V.; Patricelli, M.; Nomanbhoy, T. K.; Sorger, P. K.; Alessi, D. R.; Gray, N. S., Discovery of potent and selective covalent inhibitors of JNK. *Chem Biol* **2012**, *19* (1), 140-54.
17. Kwiatkowski, N.; Zhang, T.; Rahl, P. B.; Abraham, B. J.; Reddy, J.; Ficarro, S. B.; Dastur, A.; Amzallag, A.; Ramaswamy, S.; Tesar, B.; Jenkins, C. E.; Hannett, N. M.; McMillin, D.; Sanda, T.; Sim, T.; Kim, N. D.; Look, T.; Mitsiades, C. S.; Weng, A. P.; Brown, J. R.; Benes, C. H.; Marto, J. A.; Young, R. A.; Gray, N. S., Targeting transcription regulation in cancer with a covalent CDK7 inhibitor. *Nature* **2014**, *511* (7511), 616-20.
18. Chen, Y. C.; Backus, K. M.; Merkulova, M.; Yang, C.; Brown, D.; Cravatt, B. F.; Zhang, C., Covalent Modulators of the Vacuolar ATPase. *J Am Chem Soc* **2017**, *139* (2), 639-642.
19. Pettinger, J.; Le Bihan, Y. V.; Widya, M.; van Montfort, R. L.; Jones, K.; Cheeseman, M. D., An Irreversible Inhibitor of HSP72 that Unexpectedly Targets Lysine-56. *Angew Chem Int Ed Engl* **2017**, *56* (13), 3536-3540.
20. Ostrem, J. M.; Peters, U.; Sos, M. L.; Wells, J. A.; Shokat, K. M., K-Ras(G12C) inhibitors allosterically control GTP affinity and effector interactions. *Nature* **2013**, *503* (7477), 548-551.

21. Lim, S. M.; Westover, K. D.; Ficarro, S. B.; Harrison, R. A.; Choi, H. G.; Pacold, M. E.; Carrasco, M.; Hunter, J.; Kim, N. D.; Xie, T.; Sim, T.; Janne, P. A.; Meyerson, M.; Marto, J. A.; Engen, J. R.; Gray, N. S., Therapeutic targeting of oncogenic K-Ras by a covalent catalytic site inhibitor. *Angew Chem Int Ed Engl* **2014**, *53* (1), 199-204.
22. Ruddraraju, K. V.; Zhang, Z. Y., Covalent inhibition of protein tyrosine phosphatases. *Mol Biosyst* **2017**, *13* (7), 1257-1279.
23. Akcay, G.; Belmonte, M. A.; Aquila, B.; Chuaqui, C.; Hird, A. W.; Lamb, M. L.; Rawlins, P. B.; Su, N.; Tentarelli, S.; Grimster, N. P.; Su, Q., Inhibition of Mcl-1 through covalent modification of a noncatalytic lysine side chain. *Nat Chem Biol* **2016**, *12* (11), 931-936.
24. Johnson, D. S.; Weerapana, E.; Cravatt, B. F., Strategies for discovering and derisking covalent, irreversible enzyme inhibitors. *Future Med Chem* **2010**, *2* (6), 949-64.
25. Mah, R.; Thomas, J. R.; Shafer, C. M., Drug discovery considerations in the development of covalent inhibitors. *Bioorg Med Chem Lett* **2014**, *24* (1), 33-9.
26. Singh, J.; Petter, R. C.; Baillie, T. A.; Whitty, A., The resurgence of covalent drugs. *Nat Rev Drug Discov* **2011**, *10* (4), 307-17.
27. Strelow, J. M., A Perspective on the Kinetics of Covalent and Irreversible Inhibition. *SLAS DISCOVERY: Advancing Life Sciences R&D* **2017**, *22* (1), 3-20.
28. Robertson, J. G., Mechanistic Basis of Enzyme-Targeted Drugs. *Biochemistry* **2005**, *44* (15), 5561-5571.
29. Yocum, R. R.; Waxman, D. J.; Rasmussen, J. R.; Strominger, J. L., Mechanism of penicillin action: penicillin and substrate bind covalently to the same active site serine in two bacterial D-alanine carboxypeptidases. *Proc Natl Acad Sci U S A* **1979**, *76* (6), 2730-4.
30. Honigberg, L. A.; Smith, A. M.; Sirisawad, M.; Verner, E.; Loury, D.; Chang, B.; Li, S.; Pan, Z.; Thamm, D. H.; Miller, R. A.; Buggy, J. J., The Bruton tyrosine kinase inhibitor PCI-32765 blocks B-cell activation and is efficacious in models of autoimmune disease and B-cell malignancy. *Proc Natl Acad Sci U S A* *107* (29), 13075-80.
31. Li, D.; Ambrogio, L.; Shimamura, T.; Kubo, S.; Takahashi, M.; Chirieac, L. R.; Padera, R. F.; Shapiro, G. I.; Baum, A.; Himmelsbach, F.; Rettig, W. J.; Meyerson, M.; Solca, F.; Greulich, H.; Wong, K. K., BIBW2992, an irreversible EGFR/HER2 inhibitor highly effective in preclinical lung cancer models. *Oncogene* **2008**, *27* (34), 4702-11.
32. Rabindran, S. K.; Discafani, C. M.; Rosfjord, E. C.; Baxter, M.; Floyd, M. B.; Golas, J.; Hallett, W. A.; Johnson, B. D.; Nilakantan, R.; Overbeek, E.; Reich, M. F.; Shen, R.; Shi, X.; Tsou, H. R.; Wang, Y. F.; Wissner, A., Antitumor activity of HKI-272, an orally active, irreversible inhibitor of the HER-2 tyrosine kinase. *Cancer Res* **2004**, *64* (11), 3958-65.
33. Walter, A. O.; Sjin, R. T.; Haringsma, H. J.; Ohashi, K.; Sun, J.; Lee, K.; Dubrovskiy, A.; Labenski, M.; Zhu, Z.; Wang, Z.; Sheets, M.; St Martin, T.; Karp, R.; van Kalken, D.; Chaturvedi, P.; Niu, D.; Nacht, M.; Petter, R. C.; Westlin, W.; Lin, K.; Jaw-Tsai, S.; Raponi, M.; Van Dyke, T.; Etter, J.; Weaver, Z.; Pao, W.; Singh, J.; Simmons, A. D.; Harding, T. C.; Allen, A., Discovery of a mutant-selective covalent inhibitor of EGFR that overcomes T790M-mediated resistance in NSCLC. *Cancer Discov* **2013**, *3* (12), 1404-15.
34. Lodish H, B. A., Zipursky SL, et al., *Molecular Cell Biology*. 4th edition ed.; W. H. Freeman: New York, **2000**.
35. Manning, G.; Whyte, D. B.; Martinez, R.; Hunter, T.; Sudarsanam, S., The protein kinase complement of the human genome. *Science* **2002**, *298* (5600), 1912-34.
36. Duong-Ly, K. C.; Peterson, J. R., The Human Kinome and Kinase Inhibition. In *Current Protocols in Pharmacology*, John Wiley & Sons, Inc.: **2001**.
37. Besant, P. G.; Tan, E.; Attwood, P. V., Mammalian protein histidine kinases. *The International Journal of Biochemistry & Cell Biology* **2003**, *35* (3), 297-309.
38. Ciesla, J.; Fraczyk, T.; Rode, W., Phosphorylation of basic amino acid residues in proteins: important but easily missed. *Acta Biochim Pol* **2011**, *58* (2), 137-48.
39. Ubersax, J. A.; Ferrell Jr, J. E., Mechanisms of specificity in protein phosphorylation. *Nat Rev Mol Cell Biol* **2007**, *8* (7), 530-541.
40. Patterson, H.; Nibbs, R.; McInnes, I.; Siebert, S., Protein kinase inhibitors in the treatment of inflammatory and autoimmune diseases. *Clin Exp Immunol* **2014**, *176* (1), 1-10.

41. Wu, P.; Nielsen, T. E.; Clausen, M. H., FDA-approved small-molecule kinase inhibitors. *Trends Pharmacol Sci* **2015**, *36* (7), 422-39.
42. Fedorov, O.; Muller, S.; Knapp, S., The (un)targeted cancer kinome. *Nat Chem Biol* **2010**, *6* (3), 166-169.
43. Tigno-Aranjuez, J. T.; Benderitter, P.; Rombouts, F.; Deroose, F.; Bai, X.; Mattioli, B.; Cominelli, F.; Pizarro, T. T.; Hoflack, J.; Abbott, D. W., In vivo inhibition of RIPK2 kinase alleviates inflammatory disease. *J Biol Chem* **2014**, *289* (43), 29651-64.
44. Genne, P.; Berthet, C.; Raguin, O.; Chalon, S.; Tizon, X.; Serriere, S.; Provent, P.; Boisferon, M. H. d.; Vercoullie, J.; Mothes, C.; Gourand, F.; BARRE, L.; Guilloteau, D.; Blom, P.; Hoflack, J., Abstract 1875A: Preclinical proof of concept for the first Nanocyclix TKI-PET radiotracer targeting activated EGFR positive lung tumors. *Cancer Research* **2017**, *77* (13 Supplement), 1875A-1875A.
45. Evans, E. K.; Tester, R.; Aslanian, S.; Karp, R.; Sheets, M.; Labenski, M. T.; Witowski, S. R.; Lounsbury, H.; Chaturvedi, P.; Mazdiyasi, H.; Zhu, Z.; Nacht, M.; Freed, M. I.; Petter, R. C.; Dubrovskiy, A.; Singh, J.; Westlin, W. F., Inhibition of Btk with CC-292 provides early pharmacodynamic assessment of activity in mice and humans. *J Pharmacol Exp Ther* **346** (2), 219-28.
46. Wu, H.; Wang, W.; Liu, F.; Weisberg, E. L.; Tian, B.; Chen, Y.; Li, B.; Wang, A.; Wang, B.; Zhao, Z.; McMillin, D. W.; Hu, C.; Li, H.; Wang, J.; Liang, Y.; Buhrlage, S. J.; Liang, J.; Liu, J.; Yang, G.; Brown, J. R.; Treon, S. P.; Mitsiades, C. S.; Griffin, J. D.; Liu, Q.; Gray, N. S., Discovery of a potent, covalent BTK inhibitor for B-cell lymphoma. *ACS Chem Biol* **2014**, *9* (5), 1086-91.
47. Zaffagnini, M.; Fermani, S.; Calvaresi, M.; Orru, R.; Iommarini, L.; Sparla, F.; Falini, G.; Bottoni, A.; Trost, P., Tuning Cysteine Reactivity and Sulfenic Acid Stability by Protein Microenvironment in Glyceraldehyde-3-Phosphate Dehydrogenases of Arabidopsis thaliana. *Antioxid Redox Signal* **2016**, *24* (9), 502-17.
48. Weerapana, E.; Wang, C.; Simon, G. M.; Richter, F.; Khare, S.; Dillon, M. B.; Bachovchin, D. A.; Mowen, K.; Baker, D.; Cravatt, B. F., Quantitative reactivity profiling predicts functional cysteines in proteomes. *Nature* **2010**, *468* (7325), 790-5.
49. Winterbourn, C. C.; Metodiewa, D., Reactivity of biologically important thiol compounds with superoxide and hydrogen peroxide. *Free Radic Biol Med* **1999**, *27* (3-4), 322-8.
50. Gould, N. S.; Evans, P.; Martinez-Acedo, P.; Marino, S. M.; Gladyshev, V. N.; Carroll, K. S.; Ischiropoulos, H., Site-Specific Proteomic Mapping Identifies Selectively Modified Regulatory Cysteine Residues in Functionally Distinct Protein Networks. *Chem Biol* **2015**, *22* (7), 965-75.
51. Abo, M.; Weerapana, E., A Caged Electrophilic Probe for Global Analysis of Cysteine Reactivity in Living Cells. *J Am Chem Soc* **2015**, *137* (22), 7087-90.
52. Arrhenius, S., Über die Dissociationswärme und den Einfluss der Temperatur auf den Dissociationsgrad der Elektrolyte. *Zeitschrift für physikalische Chemie* **1889**, *4* (1), 96-116.
53. Narayanan, A.; Jones, L. H., Sulfonyl fluorides as privileged warheads in chemical biology. *Chem Sci* **2015**, *6* (5), 2650-2659.
54. Chalker, J. M.; Bernardes, G. J.; Lin, Y. A.; Davis, B. G., Chemical modification of proteins at cysteine: opportunities in chemistry and biology. *Chem Asian J* **2009**, *4* (5), 630-40.
55. Masri, M. S.; Friedman, M., Protein reactions with methyl and ethyl vinyl sulfones. *J Protein Chem* **1988**, *7* (1), 49-54.
56. Harrington, B. K.; Gulrajani, M.; Covey, T.; Kaptein, A.; Van Lith, B.; Izumi, R.; Hamdy, A.; Ulrich, R. G.; Byrd, J. C.; Lannutti, B. J.; Johnson, A. J., ACP-196 Is a Second Generation Inhibitor of Bruton Tyrosine Kinase (BTK) with Enhanced Target Specificity. *Blood* **2015**, *126* (23), 2908-2908.
57. Buchanan, B. B.; Balmer, Y., Redox regulation: a broadening horizon. *Annu Rev Plant Biol* **2005**, *56*, 187-220.
58. Hendriks, R. W., Drug discovery: New Btk inhibitor holds promise. *Nat Chem Biol* **2011**, *7* (1), 4-5.
59. Bradshaw, J. M., The Src, Syk, and Tec family kinases: distinct types of molecular switches. *Cell Signal* **22** (8), 1175-84.
60. Pan, Z.; Scheerens, H.; Li, S. J.; Schultz, B. E.; Sprengeler, P. A.; Burrill, L. C.; Mendonca, R. V.; Sweeney, M. D.; Scott, K. C.; Grothaus, P. G.; Jeffery, D. A.; Spoerke, J. M.; Honigberg, L. A.; Young, P. R.; Dalrymple, S. A.; Palmer, J. T., Discovery of selective irreversible inhibitors for Bruton's tyrosine kinase. *ChemMedChem* **2007**, *2* (1), 58-61.

61. de Claro, R. A.; McGinn, K. M.; Verdun, N.; Lee, S. L.; Chiu, H. J.; Saber, H.; Brower, M. E.; Chang, C. J.; Pfuma, E.; Habtemariam, B.; Bullock, J.; Wang, Y.; Nie, L.; Chen, X. H.; Lu, D. R.; Al-Hakim, A.; Kane, R. C.; Kaminskis, E.; Justice, R.; Farrell, A. T.; Pazdur, R., FDA Approval: Ibrutinib for Patients with Previously Treated Mantle Cell Lymphoma and Previously Treated Chronic Lymphocytic Leukemia. *Clin Cancer Res* **2015**, *21* (16), 3586-90.
62. Byrd, J. C.; Harrington, B.; O'Brien, S.; Jones, J. A.; Schuh, A.; Devereux, S.; Chaves, J.; Wierda, W. G.; Awan, F. T.; Brown, J. R.; Hillmen, P.; Stephens, D. M.; Ghia, P.; Barrientos, J. C.; Pagel, J. M.; Woyach, J.; Johnson, D.; Huang, J.; Wang, X.; Kaptein, A.; Lannutti, B. J.; Covey, T.; Fardis, M.; McGreivy, J.; Hamdy, A.; Rothbaum, W.; Izumi, R.; Diacovo, T. G.; Johnson, A. J.; Furman, R. R., Acalabrutinib (ACP-196) in Relapsed Chronic Lymphocytic Leukemia. *N Engl J Med* **2016**, *374* (4), 323-32.
63. Wu, J.; Zhang, M.; Liu, D., Acalabrutinib (ACP-196): a selective second-generation BTK inhibitor. *J Hematol Oncol* **2016**, *9*, 21.
64. Covey, T.; Barf, T.; Gulrajani, M.; Krantz, F.; van Lith, B.; Bibikova, E.; van de Kar, B.; de Zwart, E.; Hamdy, A.; Izumi, R.; Kaptein, A., Abstract 2596: ACP-196: a novel covalent Bruton's tyrosine kinase (Btk) inhibitor with improved selectivity and in vivo target coverage in chronic lymphocytic leukemia (CLL) patients. *Cancer Research* **2015**, *75* (15 Supplement), 2596-2596.
65. Labenski, M.; Chaturvedi, P.; Evans, E.; Mazdiasni, H.; Sheets, M.; Aslanian, S.; Niu, D.; Nacht, M.; Petter, R.; Singh, J., In vitro reactivity assessment of covalent drugs targeting Bruton's tyrosine kinase. *17th North Am Meet Int Soc Study Xenobiot (ISSX)* **2011**.
66. Di Paolo, J. A.; Huang, T.; Balazs, M.; Barbosa, J.; Barck, K. H.; Bravo, B. J.; Carano, R. A. D.; Darrow, J.; Davies, D. R.; DeForge, L. E.; Diehl, L.; Ferrando, R.; Gallion, S. L.; Giannetti, A. M.; Gribbling, P.; Hurez, V.; Hymowitz, S. G.; Jones, R.; Kropf, J. E.; Lee, W. P.; Maciejewski, P. M.; Mitchell, S. A.; Rong, H.; Staker, B. L.; Whitney, J. A.; Yeh, S.; Young, W. B.; Yu, C.; Zhang, J.; Reif, K.; Currie, K. S., Specific Btk inhibition suppresses B cell- and myeloid cell-mediated arthritis. *Nat Chem Biol* **2011**, *7* (1), 41-50.
67. Herbst, R. S., Review of epidermal growth factor receptor biology. *Int J Radiat Oncol Biol Phys* **2004**, *59* (2 Suppl), 21-6.
68. Yarden, Y.; Sliwkowski, M. X., Untangling the ErbB signalling network. *Nat Rev Mol Cell Biol* **2001**, *2* (2), 127-37.
69. Okines, A.; Cunningham, D.; Chau, I., Targeting the human EGFR family in esophagogastric cancer. *Nat Rev Clin Oncol* **2011**, *8* (8), 492-503.
70. Reid, A.; Vidal, L.; Shaw, H.; de Bono, J., Dual inhibition of ErbB1 (EGFR/HER1) and ErbB2 (HER2/neu). *Eur J Cancer* **2007**, *43* (3), 481-9.
71. Wang, D. D.; Ma, L.; Wong, M. P.; Lee, V. H.; Yan, H., Contribution of EGFR and ErbB-3 Heterodimerization to the EGFR Mutation-Induced Gefitinib- and Erlotinib-Resistance in Non-Small-Cell Lung Carcinoma Treatments. *PLoS One* **2015**, *10* (5), e0128360.
72. Nelson, V.; Ziehr, J.; Agulnik, M.; Johnson, M., Afatinib: emerging next-generation tyrosine kinase inhibitor for NSCLC. *Onco Targets Ther* **2013**, *6*, 135-43.
73. Kobayashi, S.; Boggon, T. J.; Dayaram, T.; Janne, P. A.; Kocher, O.; Meyerson, M.; Johnson, B. E.; Eck, M. J.; Tenen, D. G.; Halmos, B., EGFR mutation and resistance of non-small-cell lung cancer to gefitinib. *N Engl J Med* **2005**, *352* (8), 786-92.
74. Stewart, E. L.; Tan, S. Z.; Liu, G.; Tsao, M. S., Known and putative mechanisms of resistance to EGFR targeted therapies in NSCLC patients with EGFR mutations-a review. *Transl Lung Cancer Res* **2015**, *4* (1), 67-81.
75. Taylor, D., The Pharmaceutical Industry and the Future of Drug Development. In *Pharmaceuticals in the Environment*, The Royal Society of Chemistry: **2016**; pp 1-33.
76. Paul, S. M.; Mytelka, D. S.; Dunwiddie, C. T.; Persinger, C. C.; Munos, B. H.; Lindborg, S. R.; Schacht, A. L., How to improve R&D productivity: the pharmaceutical industry's grand challenge. *Nat Rev Drug Discov* **2010**, *9* (3), 203-214.
77. DiMasi, J. A.; Grabowski, H. G.; Hansen, R. W., Innovation in the pharmaceutical industry: New estimates of R&D costs. *J Health Econ* **2016**, *47*, 20-33.
78. Morgan, P.; Van Der Graaf, P. H.; Arrowsmith, J.; Feltner, D. E.; Drummond, K. S.; Wegner, C. D.; Street, S. D., Can the flow of medicines be improved? Fundamental pharmacokinetic and

- pharmacological principles toward improving Phase II survival. *Drug Discov Today* **2012**, *17* (9-10), 419-24.
79. Bunnage, M. E.; Chekler, E. L.; Jones, L. H., Target validation using chemical probes. *Nat Chem Biol* **2013**, *9* (4), 195-9.
80. Martinez Molina, D.; Jafari, R.; Ignatushchenko, M.; Seki, T.; Larsson, E. A.; Dan, C.; Sreekumar, L.; Cao, Y.; Nordlund, P., Monitoring drug target engagement in cells and tissues using the cellular thermal shift assay. *Science* **2013**, *341* (6141), 84-7.
81. Simon, G. M.; Niphakis, M. J.; Cravatt, B. F., Determining target engagement in living systems. *Nat Chem Biol* **2013**, *9* (4), 200-5.
82. Bantscheff, M.; Eberhard, D.; Abraham, Y.; Bastuck, S.; Boesche, M.; Hobson, S.; Mathieson, T.; Perrin, J.; Raida, M.; Rau, C.; Reader, V.; Sweetman, G.; Bauer, A.; Bouwmeester, T.; Hopf, C.; Kruse, U.; Neubauer, G.; Ramsden, N.; Rick, J.; Kuster, B.; Drewes, G., Quantitative chemical proteomics reveals mechanisms of action of clinical ABL kinase inhibitors. *Nat Biotechnol* **2007**, *25* (9), 1035-44.
83. Duncan, J. S.; Gyenis, L.; Lenehan, J.; Bretner, M.; Graves, L. M.; Haystead, T. A.; Litchfield, D. W., An unbiased evaluation of CK2 inhibitors by chemoproteomics: characterization of inhibitor effects on CK2 and identification of novel inhibitor targets. *Mol Cell Proteomics* **2008**, *7* (6), 1077-88.
84. Kruse, U.; Pallasch, C. P.; Bantscheff, M.; Eberhard, D.; Frenzel, L.; Ghidelli, S.; Maier, S. K.; Werner, T.; Wendtner, C. M.; Drewes, G., Chemoproteomics-based kinome profiling and target deconvolution of clinical multi-kinase inhibitors in primary chronic lymphocytic leukemia cells. *Leukemia* **2011**, *25* (1), 89-100.
85. Sumi, N. J.; Kuenzi, B. M.; Knezevic, C. E.; Remsing Rix, L. L.; Rix, U., Chemoproteomics Reveals Novel Protein and Lipid Kinase Targets of Clinical CDK4/6 Inhibitors in Lung Cancer. *ACS Chem Biol* **2015**, *10* (12), 2680-6.
86. Bantscheff, M.; Drewes, G., Chemoproteomic approaches to drug target identification and drug profiling. *Bioorg Med Chem* **2012**, *20* (6), 1973-8.
87. Schürmann, M.; Janning, P.; Ziegler, S.; Waldmann, H., Small-Molecule Target Engagement in Cells. *Cell Chemical Biology* **23** (4), 435-441.
88. Schepers, E.; Glorieux, G.; Dhondt, A.; Leybaert, L.; Vanholder, R., Flow cytometric calcium flux assay: evaluation of cytoplasmic calcium kinetics in whole blood leukocytes. *J Immunol Methods* **2009**, *348* (1-2), 74-82.
89. Moellering, R. E.; Cravatt, B. F., How chemoproteomics can enable drug discovery and development. *Chem Biol* **2012**, *19* (1), 11-22.
90. Jung, H. J.; Kwon, H. J., Target deconvolution of bioactive small molecules: the heart of chemical biology and drug discovery. *Archives of Pharmacol Research* **2015**, *38* (9), 1627-1641.
91. Lee, J.; Bogoy, M., Target deconvolution techniques in modern phenotypic profiling. *Curr Opin Chem Biol* **2013**, *17* (1), 118-26.
92. Terstappen, G. C.; Schlupen, C.; Raggiaschi, R.; Gaviraghi, G., Target deconvolution strategies in drug discovery. *Nat Rev Drug Discov* **2007**, *6* (11), 891-903.
93. Medard, G.; Pachi, F.; Ruprecht, B.; Klaeger, S.; Heinzlmeir, S.; Helm, D.; Qiao, H.; Ku, X.; Wilhelm, M.; Kuehne, T.; Wu, Z.; Dittmann, A.; Hopf, C.; Kramer, K.; Kuster, B., Optimized chemical proteomics assay for kinase inhibitor profiling. *J Proteome Res* **2015**, *14* (3), 1574-86.
94. Bantscheff, M.; Hopf, C.; Savitski, M. M.; Dittmann, A.; Grandi, P.; Michon, A. M.; Schlegl, J.; Abraham, Y.; Becher, I.; Bergamini, G.; Boesche, M.; Delling, M.; Dumpelfeld, B.; Eberhard, D.; Huthmacher, C.; Mathieson, T.; PoECKel, D.; Reader, V.; Strunk, K.; Sweetman, G.; Kruse, U.; Neubauer, G.; Ramsden, N. G.; Drewes, G., Chemoproteomics profiling of HDAC inhibitors reveals selective targeting of HDAC complexes. *Nat Biotechnol* **2011**, *29* (3), 255-65.
95. Bantscheff, G. D. M., *Chemical Proteomics: Methods and Protocols*. Humana Press: 2012; Vol. 803.
96. Werner, T.; Becher, I.; Sweetman, G.; Doce, C.; Savitski, M. M.; Bantscheff, M., High-resolution enabled TMT 8-plexing. *Anal Chem* **2012**, *84* (16), 7188-94.
97. Bantscheff, M.; Hopf, C.; Savitski, M. M.; Dittmann, A.; Grandi, P.; Michon, A.-M.; Schlegl, J.; Abraham, Y.; Becher, I.; Bergamini, G.; Boesche, M.; Delling, M.; Dumpelfeld, B.; Eberhard, D.; Huthmacher, C.; Mathieson, T.; PoECKel, D.; Reader, V.; Strunk, K.; Sweetman, G.; Kruse, U.;

- Neubauer, G.; Ramsden, N. G.; Drewes, G., Chemoproteomics profiling of HDAC inhibitors reveals selective targeting of HDAC complexes. *Nat Biotech* **2011**, *29* (3), 255-265.
98. Lanning, B. R.; Whitby, L. R.; Dix, M. M.; Douhan, J.; Gilbert, A. M.; Hett, E. C.; Johnson, T. O.; Joslyn, C.; Kath, J. C.; Niessen, S.; Roberts, L. R.; Schnute, M. E.; Wang, C.; Hulce, J. J.; Wei, B.; Whiteley, L. O.; Hayward, M. M.; Cravatt, B. F., A road map to evaluate the proteome-wide selectivity of covalent kinase inhibitors. *Nat Chem Biol* **10** (9), 760-7.
99. Li, L.; Zhang, Z., Development and Applications of the Copper-Catalyzed Azide-Alkyne Cycloaddition (CuAAC) as a Bioorthogonal Reaction. *Molecules* **2016**, *21* (10).
100. Lim, R. K.; Lin, Q., Bioorthogonal chemistry: recent progress and future directions. *Chem Commun (Camb)* **2010**, *46* (10), 1589-600.
101. Liu, N.; Hoogendoorn, S.; van de Kar, B.; Kaptein, A.; Barf, T.; Driessen, C.; Filippov, D. V.; van der Marel, G. A.; van der Stelt, M.; Overkleeft, H. S., Direct and two-step bioorthogonal probes for Bruton's tyrosine kinase based on ibrutinib: a comparative study. *Org Biomol Chem* **2015**, *13* (18), 5147-57.
102. Ranjitkar, P.; Perera, B. G.; Swaney, D. L.; Hari, S. B.; Larson, E. T.; Krishnamurty, R.; Merritt, E. A.; Villen, J.; Maly, D. J., Affinity-based probes based on type II kinase inhibitors. *J Am Chem Soc* **2012**, *134* (46), 19017-25.
103. Sletten, E. M.; Bertozzi, C. R., From Mechanism to Mouse: A Tale of Two Bioorthogonal Reactions. *Accounts of Chemical Research* **2011**, *44* (9), 666-676.
104. Lang, K.; Chin, J. W., Bioorthogonal reactions for labeling proteins. *ACS Chem Biol* **2014**, *9* (1), 16-20.
105. Rostovtsev, V. V.; Green, L. G.; Fokin, V. V.; Sharpless, K. B., A stepwise Huisgen cycloaddition process: copper(I)-catalyzed regioselective "ligation" of azides and terminal alkynes. *Angew Chem Int Ed Engl* **2002**, *41* (14), 2596-9.
106. Tornøe, C. W.; Christensen, C.; Meldal, M., Peptidotriazoles on solid phase: [1,2,3]-triazoles by regioselective copper(I)-catalyzed 1,3-dipolar cycloadditions of terminal alkynes to azides. *J Org Chem* **2002**, *67* (9), 3057-64.
107. Agard, N. J.; Baskin, J. M.; Prescher, J. A.; Lo, A.; Bertozzi, C. R., A Comparative Study of Bioorthogonal Reactions with Azides. *ACS Chemical Biology* **2006**, *1* (10), 644-648.
108. Bodwell, G. J.; Pi, Z.; Pottie, I. R., Electron Deficient Dienes. 2. One Step Synthesis of a Coumarin-Fused Electron Deficient Diene and its Inverse Electron Demand Diels-Alder Reactions with Enamines. *Synlett* **1999**, *1999* (04), 477-479.
109. Patterson, D. M.; Nazarova, L. A.; Prescher, J. A., Finding the right (bioorthogonal) chemistry. *ACS Chem Biol* **2014**, *9* (3), 592-605.
110. Prescher, J. A.; Bertozzi, C. R., Chemistry in living systems. *Nat Chem Biol* **2005**, *1* (1), 13-21.
111. Huisgen, R., 1,3-Dipolar Cycloadditions. Past and Future. *Angewandte Chemie International Edition in English* **1963**, *2* (10), 565-598.
112. Carell, T.; Vrabl, M., Bioorthogonal Chemistry—Introduction and Overview. *Topics in Current Chemistry* **2016**, *374* (1), 9.
113. Rodionov, V. O.; Presolski, S. I.; Díaz Díaz, D.; Fokin, V. V.; Finn, M. G., Ligand-Accelerated Cu-Catalyzed Azide-Alkyne Cycloaddition: A Mechanistic Report. *Journal of the American Chemical Society* **2007**, *129* (42), 12705-12712.
114. Landgraf, P.; Antileo, E. R.; Schuman, E. M.; Dieterich, D. C., BONCAT: Metabolic Labeling, Click Chemistry, and Affinity Purification of Newly Synthesized Proteomes. In *Site-Specific Protein Labeling: Methods and Protocols*, Gautier, A.; Hinner, M. J., Eds. Springer New York: New York, NY, **2015**; pp 199-215.
115. Wright, M. H.; Sieber, S. A., Chemical proteomics approaches for identifying the cellular targets of natural products. *Nat Prod Rep* **2016**, *33* (5), 681-708.
116. Abegg, D.; Frei, R.; Cerato, L.; Prasad Hari, D.; Wang, C.; Waser, J.; Adibekian, A., Proteome-Wide Profiling of Targets of Cysteine reactive Small Molecules by Using Ethynyl Benziodoxolone Reagents. *Angewandte Chemie International Edition* **2015**, *54* (37), 10852-10857.
117. Griffin, R. J., The medicinal chemistry of the azido group. *Prog Med Chem* **1994**, *31*, 121-232.

118. Agard, N. J.; Prescher, J. A.; Bertozzi, C. R., A Strain-Promoted [3 + 2] Azide-Alkyne Cycloaddition for Covalent Modification of Biomolecules in Living Systems. *Journal of the American Chemical Society* **2004**, *126* (46), 15046-15047.
119. Baskin, J. M.; Prescher, J. A.; Laughlin, S. T.; Agard, N. J.; Chang, P. V.; Miller, I. A.; Lo, A.; Codelli, J. A.; Bertozzi, C. R., Copper-free click chemistry for dynamic in vivo imaging. *Proceedings of the National Academy of Sciences* **2007**, *104* (43), 16793-16797.
120. Laughlin, S. T.; Bertozzi, C. R., In Vivo Imaging of *Caenorhabditis elegans* Glycans. *ACS Chemical Biology* **2009**, *4* (12), 1068-1072.
121. Hudlikar, M. S.; Li, X.; Gagarinov, I. A.; Kolishetti, N.; Wolfert, M. A.; Boons, G.-J., Controlled Multi-functionalization Facilitates Targeted Delivery of Nanoparticles to Cancer Cells. *Chemistry (Weinheim an der Bergstrasse, Germany)* **2016**, *22* (4), 1415-1423.
122. Blackman, M. L.; Royzen, M.; Fox, J. M., Tetrazine ligation: fast bioconjugation based on inverse-electron-demand Diels-Alder reactivity. *J Am Chem Soc* **2008**, *130* (41), 13518-9.
123. Devaraj, N. K.; Weissleder, R.; Hilderbrand, S. A., Tetrazine-Based Cycloadditions: Application to Pretargeted Live Cell Imaging. *Bioconjugate Chemistry* **2008**, *19* (12), 2297-2299.
124. Kim, Y. R.; Kim, Y. H.; Kim, S. W.; Lee, Y. J.; Chae, D. E.; Kim, K. A.; Lee, Z. W.; Kim, N. D.; Choi, J. S.; Choi, I. S.; Lee, K. B., A bioorthogonal approach for imaging the binding between Dasatinib and its target proteins inside living cells. *Chem Commun (Camb)* **2016**, *52* (79), 11764-11767.
125. Rutkowska, A.; Thomson, D. W.; Vappiani, J.; Werner, T.; Mueller, K. M.; Dittus, L.; Krause, J.; Muelbaier, M.; Bergamini, G.; Bantscheff, M., A Modular Probe Strategy for Drug Localization, Target Identification and Target Occupancy Measurement on Single Cell Level. *ACS Chem Biol* **2016**, *11* (9), 2541-50.
126. Reiner, T.; Earley, S.; Turetsky, A.; Weissleder, R., Bioorthogonal Small-Molecule Ligands for PARP1 Imaging in Living Cells. *ChemBioChem* **2010**, *11* (17), 2374-2377.
127. Kurganov, B. I., Kinetics of protein aggregation. Quantitative estimation of the chaperone-like activity in test-systems based on suppression of protein aggregation. *Biochemistry (Mosc)* **2002**, *67* (4), 409-22.
128. Vedadi, M.; Niesen, F. H.; Allali-Hassani, A.; Fedorov, O. Y.; Finerty, P. J., Jr.; Wasney, G. A.; Yeung, R.; Arrowsmith, C.; Ball, L. J.; Berglund, H.; Hui, R.; Marsden, B. D.; Nordlund, P.; Sundstrom, M.; Weigelt, J.; Edwards, A. M., Chemical screening methods to identify ligands that promote protein stability, protein crystallization, and structure determination. *Proc Natl Acad Sci U S A* **2006**, *103* (43), 15835-40.
129. Pantoliano, M. W.; Bone, R. F.; Rhind, A. W.; Salemme, F. R., Microplate thermal shift assay apparatus for ligand development and multi-variable protein chemistry optimization. Google Patents: **2000**.
130. Fraser, J. A.; Madhumalar, A.; Blackburn, E.; Bramham, J.; Walkinshaw, M. D.; Verma, C.; Hupp, T. R., A novel p53 phosphorylation site within the MDM2 ubiquitination signal: II. a model in which phosphorylation at SER269 induces a mutant conformation to p53. *J Biol Chem* **2010**, *285* (48), 37773-86.
131. Martinez Molina, D.; Nordlund, P., The Cellular Thermal Shift Assay: A Novel Biophysical Assay for In Situ Drug Target Engagement and Mechanistic Biomarker Studies. *Annu Rev Pharmacol Toxicol* **2016**, *56*, 141-61.
132. Berger, A. B.; Vitorino, P. M.; Bogoy, M., Activity-based protein profiling: applications to biomarker discovery, in vivo imaging and drug discovery. *Am J Pharmacogenomics* **2004**, *4* (6), 371-81.
133. Liu, Y.; Patricelli, M. P.; Cravatt, B. F., Activity-based protein profiling: The serine hydrolases. *Proceedings of the National Academy of Sciences* **1999**, *96* (26), 14694-14699.
134. Saghatelian, A.; Jessani, N.; Joseph, A.; Humphrey, M.; Cravatt, B. F., Activity-based probes for the proteomic profiling of metalloproteases. *Proceedings of the National Academy of Sciences of the United States of America* **2004**, *101* (27), 10000-10005.
135. Cravatt, B. F.; Sorensen, E. J., Chemical strategies for the global analysis of protein function. *Curr Opin Chem Biol* **2000**, *4* (6), 663-8.

136. Adam, G. C.; Sorensen, E. J.; Cravatt, B. F., Chemical strategies for functional proteomics. *Mol Cell Proteomics* **2002**, *1* (10), 781-90.
137. Savitski, M. M.; Reinhard, F. B.; Franken, H.; Werner, T.; Savitski, M. F.; Eberhard, D.; Martinez Molina, D.; Jafari, R.; Dovega, R. B.; Klaeger, S., Tracking cancer drugs in living cells by thermal profiling of the proteome. *Science* **2014**, *346*.
138. Reinhard, F. B.; Eberhard, D.; Werner, T.; Franken, H.; Childs, D.; Doce, C.; Savitski, M. F.; Huber, W.; Bantscheff, M.; Savitski, M. M.; Drewes, G., Thermal proteome profiling monitors ligand interactions with cellular membrane proteins. *Nat Methods* **2015**, *12* (12), 1129-31.
139. Becher, I.; Werner, T.; Doce, C.; Zaal, E. A.; Togel, I.; Khan, C. A.; Rueger, A.; Muelbaier, M.; Salzer, E.; Berkers, C. R.; Fitzpatrick, P. F.; Bantscheff, M.; Savitski, M. M., Thermal profiling reveals phenylalanine hydroxylase as an off-target of panobinostat. *Nat Chem Biol* **2016**, *12* (11), 908-910.
140. Mateus, A.; Maatta, T. A.; Savitski, M. M., Thermal proteome profiling: unbiased assessment of protein state through heat-induced stability changes. *Proteome Sci* **2016**, *15*, 13.
141. Sakamoto, K. M.; Kim, K. B.; Kumagai, A.; Mercurio, F.; Crews, C. M.; Deshaies, R. J., Protacs: chimeric molecules that target proteins to the Skp1-Cullin-F box complex for ubiquitination and degradation. *Proc Natl Acad Sci U S A* **2001**, *98* (15), 8554-9.
142. Pagan, J.; Seto, T.; Pagano, M.; Cittadini, A., Role of the ubiquitin proteasome system in the heart. *Circ Res* **2013**, *112* (7), 1046-58.
143. Churcher, I., Protac-Induced Protein Degradation in Drug Discovery: Breaking the Rules or Just Making New Ones? *J Med Chem* **2017**.
144. Lee, H.; Puppala, D.; Choi, E. Y.; Swanson, H.; Kim, K. B., Targeted degradation of the aryl hydrocarbon receptor by the PROTAC approach: a useful chemical genetic tool. *Chembiochem* **2007**, *8* (17), 2058-62.
145. Lai, A. C.; Toure, M.; Hellerschmied, D.; Salami, J.; Jaime-Figueroa, S.; Ko, E.; Hines, J.; Crews, C. M., Modular PROTAC Design for the Degradation of Oncogenic BCR-ABL. *Angew Chem Int Ed Engl* **2016**, *55* (2), 807-10.
146. Huang, H. T.; Dobrovolsky, D.; Paulk, J.; Yang, G.; Weisberg, E. L.; Doctor, Z. M.; Buckley, D. L.; Cho, J. H.; Ko, E.; Jang, J.; Shi, K.; Choi, H. G.; Griffin, J. D.; Li, Y.; Treon, S. P.; Fischer, E. S.; Bradner, J. E.; Tan, L.; Gray, N. S., A Chemoproteomic Approach to Query the Degradable Kinome Using a Multi-kinase Degradator. *Cell Chem Biol* **2017**.
147. Ottis, P.; Crews, C. M., Proteolysis-Targeting Chimeras: Induced Protein Degradation as a Therapeutic Strategy. *ACS Chem Biol* **2017**, *12* (4), 892-898.
148. Ottis, P.; Toure, M.; Cromm, P. M.; Ko, E.; Gustafson, J. L.; Crews, C. M., Assessing Different E3 Ligases for Small Molecule Induced Protein Ubiquitination and Degradation. *ACS Chem Biol* **2017**, *12* (10), 2570-2578.
149. Savitski, M. M.; Zinn, N.; Faeltch-Savitski, M.; Poeckel, D.; Gade, S.; Becher, I.; Muelbaier, M.; Wagner, A. J.; Strohmmer, K.; Werner, T.; Melchert, S.; Petretich, M.; Rutkowska, A.; Vappiani, J.; Franken, H.; Steidel, M.; Sweetman, G. M.; Gilan, O.; Lam, E. Y. N.; Dawson, M. A.; Prinjha, R. K.; Grandi, P.; Bergamini, G.; Bantscheff, M., Multiplexed Proteome Dynamics Profiling Reveals Mechanisms Controlling Protein Homeostasis. *Cell* **2018**.
150. Domon, B.; Aebersold, R., Mass spectrometry and protein analysis. *Science* **2006**, *312* (5771), 212-7.
151. Zhang, Y.; Fonslow, B. R.; Shan, B.; Baek, M. C.; Yates, J. R., 3rd, Protein analysis by shotgun/bottom-up proteomics. *Chem Rev* **2013**, *113* (4), 2343-94.
152. Cravatt, B. F.; Simon, G. M.; Yates, J. R., 3rd, The biological impact of mass-spectrometry-based proteomics. *Nature* **2007**, *450* (7172), 991-1000.
153. Bagert, J. D.; Xie, Y. J.; Sweredoski, M. J.; Qi, Y.; Hess, S.; Schuman, E. M.; Tirrell, D. A., Quantitative, time-resolved proteomic analysis by combining bioorthogonal noncanonical amino acid tagging and pulsed stable isotope labeling by amino acids in cell culture. *Mol Cell Proteomics* **2014**, *13* (5), 1352-8.
154. Osinalde, N.; Aloria, K.; Omaetxebarria, M. J.; Kratchmarova, I., Targeted mass spectrometry: An emerging powerful approach to unblock the bottleneck in phosphoproteomics. *J Chromatogr B Analyt Technol Biomed Life Sci* **2017**, *1055-1056*, 29-38.

155. Murale, D. P.; Hong, S. C.; Haque, M. M.; Lee, J. S., Photo-affinity labeling (PAL) in chemical proteomics: a handy tool to investigate protein-protein interactions (PPIs). *Proteome Sci* **2016**, *15*, 14.
156. Savitski, M. M.; Reinhard, F. B.; Franken, H.; Werner, T.; Savitski, M. F.; Eberhard, D.; Martinez Molina, D.; Jafari, R.; Dovega, R. B.; Klaeger, S.; Kuster, B.; Nordlund, P.; Bantscheff, M.; Drewes, G., Tracking cancer drugs in living cells by thermal profiling of the proteome. *Science* **2014**, *346* (6205), 1255784.
157. Chait, B. T., Chemistry. Mass spectrometry: bottom-up or top-down? *Science* **2006**, *314* (5796), 65-6.
158. Steen, H.; Mann, M., The ABC's (and XYZ's) of peptide sequencing. *Nat Rev Mol Cell Biol* **2004**, *5* (9), 699-711.
159. Aebersold, R.; Mann, M., Mass spectrometry-based proteomics. *Nature* **2003**, *422* (6928), 198-207.
160. Yates, J. R.; Ruse, C. I.; Nakorchevsky, A., Proteomics by mass spectrometry: approaches, advances, and applications. *Annu Rev Biomed Eng* **2009**, *11*, 49-79.
161. Michalski, A.; Damoc, E.; Hauschild, J. P.; Lange, O.; Wieghaus, A.; Makarov, A.; Nagaraj, N.; Cox, J.; Mann, M.; Horning, S., Mass spectrometry-based proteomics using Q Exactive, a high-performance benchtop quadrupole Orbitrap mass spectrometer. *Mol Cell Proteomics* **2011**, *10* (9), M111 011015.
162. Fenn, J. B.; Mann, M.; Meng, C. K.; Wong, S. F.; Whitehouse, C. M., Electrospray ionization for mass spectrometry of large biomolecules. *Science* **1989**, *246* (4926), 64-71.
163. Wilm, M., Principles of electrospray ionization. *Mol Cell Proteomics* **2011**, *10* (7), M111 009407.
164. Chakraborty, A. B.; Berger, S. J., Optimization of reversed-phase peptide liquid chromatography ultraviolet mass spectrometry analyses using an automated blending methodology. *J Biomol Tech* **2005**, *16* (4), 327-35.
165. Delahunty, C.; Yates, J. R., 3rd, Protein identification using 2D-LC-MS/MS. *Methods* **2005**, *35* (3), 248-55.
166. Nägele, E.; Vollmer, M.; Hörth, P.; Vad, C., 2D-LC/MS techniques for the identification of proteins in highly complex mixtures. *Expert Review of Proteomics* **2004**, *1* (1), 37-46.
167. Taylor, G., Disintegration of Water Drops in an Electric Field. *Proceedings of the Royal Society of London. Series A. Mathematical and Physical Sciences* **1964**, *280* (1382), 383-397.
168. Rayleigh, L., XX. On the equilibrium of liquid conducting masses charged with electricity. *Philosophical Magazine* **1882**, *14* (87), 184-186.
169. Cech, N. B.; Enke, C. G., Practical implications of some recent studies in electrospray ionization fundamentals. *Mass Spectrom Rev* **2001**, *20* (6), 362-87.
170. Ho, C. S.; Lam, C. W.; Chan, M. H.; Cheung, R. C.; Law, L. K.; Lit, L. C.; Ng, K. F.; Suen, M. W.; Tai, H. L., Electrospray ionisation mass spectrometry: principles and clinical applications. *Clin Biochem Rev* **2003**, *24* (1), 3-12.
171. Gross, J. H., *Massenspektrometrie - Ein Lehrbuch*. Springer Berlin Heidelberg: **2013**.
172. Gates, P. Quadrupole Mass Analysis. <http://www.chm.bris.ac.uk/ms/images/quad-schematic.jpg> (accessed 10th July 2017).
173. Cox, J.; Mann, M., Computational principles of determining and improving mass precision and accuracy for proteome measurements in an Orbitrap. *J Am Soc Mass Spectrom* **2009**, *20* (8), 1477-85.
174. Cox, J.; Neuhauser, N.; Michalski, A.; Scheltema, R. A.; Olsen, J. V.; Mann, M., Andromeda: a peptide search engine integrated into the MaxQuant environment. *J Proteome Res* **2011**, *10* (4), 1794-805.
175. Perkins, D. N.; Pappin, D. J.; Creasy, D. M.; Cottrell, J. S., Probability-based protein identification by searching sequence databases using mass spectrometry data. *Electrophoresis* **1999**, *20* (18), 3551-67.
176. Scigelova, M.; Makarov, A., Orbitrap mass analyzer--overview and applications in proteomics. *Proteomics* **2006**, *6 Suppl 2*, 16-21.

177. Asara, J. M.; Christofk, H. R.; Freemark, L. M.; Cantley, L. C., A label-free quantification method by MS/MS TIC compared to SILAC and spectral counting in a proteomics screen. *Proteomics* **2008**, *8* (5), 994-9.
178. Desiderio, D. M.; Kai, M., Preparation of stable isotope-incorporated peptide internal standards for field desorption mass spectrometry quantification of peptides in biologic tissue. *Biomed Mass Spectrom* **1983**, *10* (8), 471-9.
179. Ong, S. E.; Kratchmarova, I.; Mann, M., Properties of ¹³C-substituted arginine in stable isotope labeling by amino acids in cell culture (SILAC). *J Proteome Res* **2003**, *2* (2), 173-81.
180. Ross, P. L.; Huang, Y. N.; Marchese, J. N.; Williamson, B.; Parker, K.; Hattan, S.; Khainovski, N.; Pillai, S.; Dey, S.; Daniels, S.; Purkayastha, S.; Juhasz, P.; Martin, S.; Bartlett-Jones, M.; He, F.; Jacobson, A.; Pappin, D. J., Multiplexed protein quantitation in *Saccharomyces cerevisiae* using amine-reactive isobaric tagging reagents. *Mol Cell Proteomics* **2004**, *3* (12), 1154-69.
181. Thompson, A.; Schafer, J.; Kuhn, K.; Kienle, S.; Schwarz, J.; Schmidt, G.; Neumann, T.; Johnstone, R.; Mohammed, A. K.; Hamon, C., Tandem mass tags: a novel quantification strategy for comparative analysis of complex protein mixtures by MS/MS. *Anal Chem* **2003**, *75* (8), 1895-904.
182. Bantscheff, M.; Lemeer, S.; Savitski, M. M.; Kuster, B., Quantitative mass spectrometry in proteomics: critical review update from 2007 to the present. *Anal Bioanal Chem* **2012**, *404* (4), 939-65.
183. Schwanhauser, B.; Gossen, M.; Dittmar, G.; Selbach, M., Global analysis of cellular protein translation by pulsed SILAC. *Proteomics* **2009**, *9* (1), 205-9.
184. Fierro-Monti, I.; Racle, J.; Hernandez, C.; Waridel, P.; Hatzimanikatis, V.; Quadroni, M., A novel pulse-chase SILAC strategy measures changes in protein decay and synthesis rates induced by perturbation of proteostasis with an Hsp90 inhibitor. *PLoS One* **2013**, *8* (11), e80423.
185. Zhang, G.; Bowling, H.; Hom, N.; Kirshenbaum, K.; Klann, E.; Chao, M. V.; Neubert, T. A., In-depth quantitative proteomic analysis of de novo protein synthesis induced by brain-derived neurotrophic factor. *J Proteome Res* **2014**, *13* (12), 5707-14.
186. Gygi, S. P.; Rist, B.; Gerber, S. A.; Turecek, F.; Gelb, M. H.; Aebersold, R., Quantitative analysis of complex protein mixtures using isotope-coded affinity tags. *Nat Biotechnol* **1999**, *17* (10), 994-9.
187. Werner, T.; Sweetman, G.; Savitski, M. F.; Mathieson, T.; Bantscheff, M.; Savitski, M. M., Ion coalescence of neutron encoded TMT 10-plex reporter ions. *Anal Chem* **2014**, *86* (7), 3594-601.
188. Ting, L.; Rad, R.; Gygi, S. P.; Haas, W., MS3 eliminates ratio distortion in isobaric multiplexed quantitative proteomics. *Nat Methods* **2011**, *8* (11), 937-40.
189. Rutkowska, A.; Thomson, D. W.; Vappiani, J.; Werner, T.; Mueller, K. M.; Dittus, L.; Krause, J.; Muelbaier, M.; Bergamini, G.; Bantscheff, M., A modular probe strategy for drug localization, target identification and target occupancy measurement on single cell level. *ACS Chem Biol* **2016**.
190. Kalxdorf, M.; Gade, S.; Eberl, H. C.; Bantscheff, M., Monitoring Cell-surface N-Glycoproteome Dynamics by Quantitative Proteomics Reveals Mechanistic Insights into Macrophage Differentiation. *Mol Cell Proteomics* **2017**, *16*.
191. Franken, H.; Mathieson, T.; Childs, D.; Sweetman, G. M.; Werner, T.; Togel, I.; Doce, C.; Gade, S.; Bantscheff, M.; Drewes, G.; Reinhard, F. B.; Huber, W.; Savitski, M. M., Thermal proteome profiling for unbiased identification of direct and indirect drug targets using multiplexed quantitative mass spectrometry. *Nat Protoc* **2015**, *10* (10), 1567-93.
192. Auchincloss, C. A.; Richardson, P.; McGuinness, C.; Mallikarjun, V.; Donaldson, K.; McNab, H.; Campbell, C. J., Monitoring intracellular redox potential changes using SERS nanosensors. *ACS Nano* **2012**, *6* (1), 888-96.
193. Sadler, N. C.; Melnicki, M. R.; Serres, M. H.; Merkley, E. D.; Chrisler, W. B.; Hill, E. A.; Romine, M. F.; Kim, S.; Zink, E. M.; Datta, S.; Smith, R. D.; Beliaev, A. S.; Konopka, A.; Wright, A. T., Live cell chemical profiling of temporal redox dynamics in a photoautotrophic cyanobacterium. *ACS Chem Biol* **2014**, *9* (1), 291-300.
194. Dittus, L.; Werner, T.; Muelbaier, M.; Bantscheff, M., Differential Kinobeads Profiling for Target Identification of Irreversible Kinase Inhibitors. *ACS Chem Biol* **2017**.
195. Gustafsson, M. O.; Hussain, A.; Mohammad, D. K.; Mohamed, A. J.; Nguyen, V.; Metalnikov, P.; Colwill, K.; Pawson, T.; Smith, C. I.; Nore, B. F., Regulation of nucleocytoplasmic shuttling of

- Bruton's tyrosine kinase (Btk) through a novel SH3-dependent interaction with ankyrin repeat domain 54 (ANKRD54). *Mol Cell Biol* **2012**, *32* (13), 2440-53.
196. Marcotte, D. J.; Liu, Y. T.; Arduini, R. M.; Hession, C. A.; Miatkowski, K.; Wildes, C. P.; Cullen, P. F.; Hong, V.; Hopkins, B. T.; Mertsching, E.; Jenkins, T. J.; Romanowski, M. J.; Baker, D. P.; Silvan, L. F., Structures of human Bruton's tyrosine kinase in active and inactive conformations suggest a mechanism of activation for TEC family kinases. *Protein Sci* **2010**, *19* (3), 429-39.
197. Mathea, S.; Abdul Azeez, K. R.; Salah, E.; Tallant, C.; Wolfreys, F.; Konietzny, R.; Fischer, R.; Lou, H. J.; Brennan, P. E.; Schnapp, G.; Pautsch, A.; Kessler, B. M.; Turk, B. E.; Knapp, S., Structure of the Human Protein Kinase ZAK in Complex with Vemurafenib. *ACS Chem Biol* **2016**, *11* (6), 1595-602.
198. Wilhelm, M.; Schlegl, J.; Hahne, H.; Gholami, A. M.; Lieberenz, M.; Savitski, M. M.; Ziegler, E.; Butzmann, L.; Gessulat, S.; Marx, H.; Mathieson, T.; Lemeer, S.; Schnatbaum, K.; Reimer, U.; Wenschuh, H.; Mollenhauer, M.; Slotta-Huspenina, J.; Boese, J. H.; Bantscheff, M.; Gerstmair, A.; Faerber, F.; Kuster, B., Mass-spectrometry-based draft of the human proteome. *Nature* **2014**, *509* (7502), 582-7.
199. Thul, P. J.; Akesson, L.; Wiking, M.; Mahdessian, D.; Geladaki, A.; Ait Blal, H.; Alm, T.; Asplund, A.; Bjork, L.; Breckels, L. M.; Backstrom, A.; Danielsson, F.; Fagerberg, L.; Fall, J.; Gatto, L.; Gnann, C.; Hober, S.; Hjelmare, M.; Johansson, F.; Lee, S.; Lindskog, C.; Mulder, J.; Mulvey, C. M.; Nilsson, P.; Oksvold, P.; Rockberg, J.; Schutten, R.; Schwenk, J. M.; Sivertsson, A.; Sjostedt, E.; Skogs, M.; Stadler, C.; Sullivan, D. P.; Tegel, H.; Winsnes, C.; Zhang, C.; Zwahlen, M.; Mardinoglu, A.; Ponten, F.; von Feilitzen, K.; Lilley, K. S.; Uhlen, M.; Lundberg, E., A subcellular map of the human proteome. *Science* **2017**, *356* (6340).
200. Ninomiya-Tsuji, J.; Kajino, T.; Ono, K.; Ohtomo, T.; Matsumoto, M.; Shiina, M.; Mihara, M.; Tsuchiya, M.; Matsumoto, K., A resorcylic acid lactone, 5Z-7-oxozeaenol, prevents inflammation by inhibiting the catalytic activity of TAK1 MAPK kinase kinase. *J Biol Chem* **2003**, *278* (20), 18485-90.
201. Sorrell, F. J.; Szklarz, M.; Abdul Azeez, K. R.; Elkins, J. M.; Knapp, S., Family-wide Structural Analysis of Human Numb-Associated Protein Kinases. *Structure* **2016**, *24* (3), 401-11.
202. Kim, E.; Hurtz, C.; Koehrer, S.; Wang, Z.; Balasubramanian, S.; Chang, B. Y.; Muschen, M.; Davis, R. E.; Burger, J. A., Ibrutinib inhibits pre-BCR+ B-cell acute lymphoblastic leukemia progression by targeting BTK and BLK. *Blood* **2017**, *129* (9), 1155-1165.
203. Dalton, S. E.; Dittus, L.; Thomas, D. A.; Convery, M. A.; Nunes, J.; Bush, J. T.; Evans, J. P.; Werner, T.; Bantscheff, M.; Murphy, J. A.; Campos, S., Selectively targeting the kinome-conserved lysine of PI3Kdelta as a general approach to covalent kinase inhibition. *J Am Chem Soc* **2017**.
204. Carmony, K. C.; Kim, K. B., PROTAC-induced proteolytic targeting. *Methods Mol Biol* **2012**, *832*, 627-38.
205. Brdicka, T.; Imrich, M.; Angelisova, P.; Brdickova, N.; Horvath, O.; Spicka, J.; Hilgert, I.; Luskova, P.; Draber, P.; Novak, P.; Engels, N.; Wienands, J.; Simeoni, L.; Osterreicher, J.; Aguado, E.; Malissen, M.; Schraven, B.; Horejsi, V., Non-T cell activation linker (NTAL): a transmembrane adaptor protein involved in immunoreceptor signaling. *J Exp Med* **2002**, *196* (12), 1617-26.
206. Callard, R. E.; Rigley, K. P.; Smith, S. H.; Thurstan, S.; Shields, J. G., CD19 regulation of human B cell responses. B cell proliferation and antibody secretion are inhibited or enhanced by ligation of the CD19 surface glycoprotein depending on the stimulating signal used. *J Immunol* **1992**, *148* (10), 2983-7.
207. Xu, Y.; Fairfax, K.; Light, A.; Huntington, N. D.; Tarlinton, D. M., CD19 differentially regulates BCR signalling through the recruitment of PI3K. *Autoimmunity* **2014**, *47* (7), 430-7.
208. Wisniewski, D.; Strife, A.; Swendeman, S.; Erdjument-Bromage, H.; Geromanos, S.; Kavanaugh, W. M.; Tempst, P.; Clarkson, B., A novel SH2-containing phosphatidylinositol 3,4,5-trisphosphate 5-phosphatase (SHIP2) is constitutively tyrosine phosphorylated and associated with src homologous and collagen gene (SHC) in chronic myelogenous leukemia progenitor cells. *Blood* **1999**, *93* (8), 2707-20.
209. Baran, C. P.; Tridandapani, S.; Helgason, C. D.; Humphries, R. K.; Krystal, G.; Marsh, C. B., The inositol 5'-phosphatase SHIP-1 and the Src kinase Lyn negatively regulate macrophage colony-stimulating factor-induced Akt activity. *J Biol Chem* **2003**, *278* (40), 38628-36.

210. Zhao, Q.; Ouyang, X.; Wan, X.; Gajiwala, K. S.; Kath, J. C.; Jones, L. H.; Burlingame, A. L.; Taunton, J., Broad-Spectrum Kinase Profiling in Live Cells with Lysine-Targeted Sulfonyl Fluoride Probes. *J Am Chem Soc* **2017**, *139* (2), 680-685.
211. Schwaid, A. G.; Cornella-Taracido, I., Causes and Significance of Increased Compound Potency in Cellular or Physiological Contexts. *J Med Chem* **2017**.
212. Miyahisa, I.; Sameshima, T.; Hixon, M. S., Rapid Determination of the Specificity Constant of Irreversible Inhibitors (kinact/KI) by Means of an Endpoint Competition Assay. *Angew Chem Int Ed Engl* **2015**, *54* (47), 14099-102.
213. Krippendorff, B. F.; Neuhaus, R.; Lienau, P.; Reichel, A.; Huisinga, W., Mechanism-based inhibition: deriving K(I) and k(inact) directly from time-dependent IC(50) values. *J Biomol Screen* **2009**, *14* (8), 913-23.
214. Médard, G.; Pachi, F.; Ruprecht, B.; Klaeger, S.; Heinzlmeir, S.; Helm, D.; Qiao, H.; Ku, X.; Wilhelm, M.; Kuehne, T.; Wu, Z.; Dittmann, A.; Hopf, C.; Kramer, K.; Kuster, B., Optimized Chemical Proteomics Assay for Kinase Inhibitor Profiling. *Journal of Proteome Research* **2015**, *14* (3), 1574-1586.
215. Klaeger, S.; Gohlke, B.; Perrin, J.; Gupta, V.; Heinzlmeir, S.; Helm, D.; Qiao, H.; Bergamini, G.; Handa, H.; Savitski, M. M.; Bantscheff, M.; Medard, G.; Preissner, R.; Kuster, B., Chemical Proteomics Reveals Ferrochelatase as a Common Off-target of Kinase Inhibitors. *ACS Chem Biol* **2016**, *11* (5), 1245-54.
216. Koch, H.; Busto, M. E.; Kramer, K.; Medard, G.; Kuster, B., Chemical Proteomics Uncovers EPHA2 as a Mechanism of Acquired Resistance to Small Molecule EGFR Kinase Inhibition. *J Proteome Res* **2015**, *14* (6), 2617-25.
217. Fadeyi, O. O.; Hoth, L. R.; Choi, C.; Feng, X.; Gopalsamy, A.; Hett, E. C.; Kyne, R. E., Jr.; Robinson, R. P.; Jones, L. H., Covalent Enzyme Inhibition through Fluorosulfate Modification of a Noncatalytic Serine Residue. *ACS Chem Biol* **2017**, *12* (8), 2015-2020.
218. Smith, E.; Collins, I., Photoaffinity labeling in target- and binding-site identification. *Future Med Chem* **2015**, *7* (2), 159-83.
219. Friedman Ohana, R.; Levin, S.; Wood, M. G.; Zimmerman, K.; Dart, M. L.; Schwinn, M. K.; Kirkland, T. A.; Hurst, R.; Uyeda, H. T.; Encell, L. P.; Wood, K. V., Improved Deconvolution of Protein Targets for Bioactive Compounds Using a Palladium Cleavable Chloroalkane Capture Tag. *ACS Chem Biol* **2016**, *11* (9), 2608-17.
220. Lebraud, H.; Heightman, T. D., Protein degradation: a validated therapeutic strategy with exciting prospects. *Essays Biochem* **2017**, *61* (5), 517-527.
221. Tejada-Munoz, N.; Robles-Flores, M., Glycogen synthase kinase 3 in Wnt signaling pathway and cancer. *IUBMB Life* **2015**, *67* (12), 914-22.
222. Cha, B.; Kim, W.; Kim, Y. K.; Hwang, B. N.; Park, S. Y.; Yoon, J. W.; Park, W. S.; Cho, J. W.; Bedford, M. T.; Jho, E. H., Methylation by protein arginine methyltransferase 1 increases stability of Axin, a negative regulator of Wnt signaling. *Oncogene* **2011**, *30* (20), 2379-89.
223. Dieterich, D. C.; Hodas, J. J.; Gouzer, G.; Shadrin, I. Y.; Ngo, J. T.; Triller, A.; Tirrell, D. A.; Schuman, E. M., In situ visualization and dynamics of newly synthesized proteins in rat hippocampal neurons. *Nat Neurosci* *13* (7), 897-905.
224. Dieterich, D. C.; Link, A. J.; Graumann, J.; Tirrell, D. A.; Schuman, E. M., Selective identification of newly synthesized proteins in mammalian cells using bioorthogonal noncanonical amino acid tagging (BONCAT). *Proc Natl Acad Sci U S A* **2006**, *103* (25), 9482-7.
225. Eichelbaum, K.; Krijgsveld, J., Rapid temporal dynamics of transcription, protein synthesis, and secretion during macrophage activation. *Mol Cell Proteomics* *13* (3), 792-810.
226. Picaud, S.; Strocchia, M.; Terracciano, S.; Lauro, G.; Mendez, J.; Daniels, D. L.; Riccio, R.; Bifulco, G.; Bruno, I.; Filippakopoulos, P., 9H-purine scaffold reveals induced-fit pocket plasticity of the BRD9 bromodomain. *J Med Chem* **2015**, *58* (6), 2718-36.
227. Copeland, R.A., Basavapathruni, A., Moyer, M., Scott M.P., Impact of enzyme concentration and residence time on apparent activity recovery in jump dilution analysis. *Anal Biochem* **2011**, *416* (2), 206-210.

Acknowledgment

First and foremost, I want to thank my wife **Meike** who supported me every single day during my PhD time. Without her, the frustrating moments would probably have made me quit long before writing these lines.

Thanks to my **mother** who always told me that every setback will finally turn out to be good for something, my **sister**, and my **father** who probably would be proud of me.

A big thank-you to my **friends** for their support and especially to **Tobi** who gave me some valuable feedback about this PhD thesis.

Of course I want to thank **Prof. Dr. Bernhard Kuester** who agreed on supervising this externally performed PhD thesis. Without his trust in my supervisors at Cellzome I would not have had the chance to graduate at the Technical University of Munich.

I want to express my greatest gratitude to all of my former **colleagues at Cellzome**. Without any of you this work would not be what it is. I am hesitant to highlight someone specific since I so much benefited from everybody in this company. But since they probably had the most work, I want to thank **Dr. Marcus Bantscheff** and **Dr. Marcel Muelbaier** for supervising my work, for discussing my data, for their constructive feedback and for working through my manuscripts. Last but not least, I want to thank **Johanna**, **Cecile** and **Mathias** from the 007 office. It was a pleasure to share an office with you.

Lea, this is for you.

Curriculum vitae

Personal data:

Name	Lars Thorsten Dittus
Date of birth, place	October 30 th , 1985, Boeblingen
Address	Berliner Strasse 27, 71093 Weil im Schoenbuch, Germany
E-Mail	lars-dittus@web.de
Nationality	German

Resume:

April 2014 – April 2018	Doctorate at the Technical University of Munich Chair: Proteomics and Bioanalytics Supervising professor: <i>Prof. Dr. Bernhard Kuester</i> , Work externally performed at Cellzome GmbH, a GSK company, Heidelberg, Germany Mentor: <i>Dr. Marcus Bantscheff (marcus.x.bantscheff@gsk.com)</i>
September 2012 – February 2014	University of Applied Sciences Mannheim, Master program: Biotechnology – Biomedical Science and Technology Degree: Master of Science (grade: 1.3) Master thesis performed at Cellzome GmbH, a GSK company, Heidelberg, Germany Reference: <i>Dr. Marcel Muelbaier (marcel.x.muelbaier@gsk.com)</i>
March 2009 – August 2012	University of Applied Sciences Esslingen, Studies: Biotechnology Degree: Bachelor of Science (grade: 1.7) Bachelor thesis performed at BioVersys AG, Basel, Switzerland Reference: <i>Dr. Marcel Tigges (marcel.tigges@gmail.com)</i>
September 2006 – October 2008	Baden-Wuerttemberg Cooperative State University in cooperation with Festo AG & Co.KG, Esslingen, Germany
October 2005 – June 2006	Civilian service: Residential care home for the elderly of the German Red Cross, Holzgerlingen, Germany
1996 – 2005	Schoenbuch-Gymnasium, Holzgerlingen, Germany Degree: Abitur (grade: 2.0)
1992 –1996	Primary school, Weil im Schoenbuch, Germany

Publications

Scientific papers:

- **Dittus, L.**, Werner, T., Muelbaier, M., and Bantscheff, M. (2017). Differential Kinobeads Profiling for Target Identification of Irreversible Kinase Inhibitors. *ACS Chem Biol* 12, 2515–2521.
- Dalton, S., **Dittus, L.**, Thomas, D., Convery, M., Nunes, J., Bush, J., Evans, J., Werner, T., Bantscheff, M., Murphy, J., and Campos, S. (2018). Selectively targeting the kinome-conserved lysine of PI3K δ as a general approach to covalent kinase inhibition. *J. Am. Chem. Soc.* 140 (3), 932–939
- Thomson, D. W., Wagner, A. J., Bantscheff, M., Benson, R. E., **Dittus, L.**, Duempelfeld, B., Drewes, G., Krause, J., Moore, J. T., Mueller, K., Poeckel, D., Rau, C., Salzer, E., Shewchuk, L. M., Hopf, C., Emery, J. G., and Muelbaier, M. (2017). Discovery of a Highly Selective Tankyrase Inhibitor Displaying Growth Inhibition Effects against a Diverse Range of Tumor Derived Cell Lines. *J. Med. Chem.* 60 (13), 5455–5471.
- Rutkowska, A., Thomson, D. W., Vappiani, J., Werner, T., Mueller, K. M., **Dittus, L.**, Krause, J., Muelbaier, M., Bergamini, G., and Bantscheff, M. (2016). A Modular Probe Strategy for Drug Localization, Target Identification and Target Occupancy Measurement on Single Cell Level. *ACS Chem Biol* 11, 2541-2550.

Presentations:

- Poster at “EMBL course: Quantitative Proteomics: Strategies and tools to probe biology” in Heidelberg, Germany
- Poster at “SLAS Nordic Chemical Biology Meeting 2017” in Copenhagen, Denmark
- Oral presentation and poster at “GSK’s First Annual Postdoctoral Symposium” in King of Prussia, Pennsylvania, USA